University College London
Department of Physics and Astronomy

DOCTORAL THESIS

Lukáš Gráf

Lepton Number Violation in the Nucleus and the Universe

Supervisor:	Dr. Frank F. Deppisch
Programme of Study:	Research Degree: Physics and Astronomy
Qualification:	Doctor of Philosophy

London 2018

Acknowledgements

First and foremost, I would like to express my gratitude to my supervisor, Frank Deppisch, who has always been very supportive during my Ph.D. studies. Not only I appreciate his professional erudition and pedagogical guidance, but also his patience, kindness and helpfulness in any situation.

My sincere thanks also go to Francesco Iachello for his mentorship and hospitality he provided me during my two long-term visits at Yale University. Working with him has been a wonderful experience, both professionally and personally.

At the same time, I would like to thank my dear friends and collaborators Tomás Gonzalo, Julia Harz, Wei-Chih Huang and Jenni Kotila, whose contribution to our common research projects has been important for successful completion of this thesis.

I also want to thank my parents, brother and grandparents for supporting me in many different ways throughout my studies. Especially, I am grateful to my grandfather, Václav Gráf, for his continuous availability to discuss any aspect of my work. Last but not least, I would like to thank my wife Tereza, without whose unwavering love, support and patience the path through my Ph.D. would have been much harder to follow.

I, Lukáš Gráf confirm that the work presented in this thesis is my own. Where information has been derived from other sources, I confirm that this has been indicated in the thesis.

September 2018, London Lukáš Gráf

"Look closely. The beautiful may be small."

IMMANUEL KANT

Abstract

Conservation of lepton number is an intriguing feature common for all particle interactions so far observed in Nature and it can be understood as a consequence of an anomalous abelian symmetry of the Standard Model. However, there are certain hints, most importantly the experimental evidence of non-zero neutrino masses, pointing at breaking of the lepton number symmetry at certain high energy scale. Although the new lepton number violating physics can generally lie beyond the reach of collider experiments, it is also possible to probe it at low energies. Most importantly, an observation of neutrinoless double beta decay would provide an evidence of non-conservation of lepton number, shedding light on the origin of non-zero neutrino mass at the same time. In this work we concentrate on the effective description of the non-standard mechanisms of this extremely rare nuclear process, drawing its connection to lepton number violation at high energies. Moreover, assuming its hypothetical observation we discuss some of the possible cosmological implications. Specifically, following a brief review of the long-range mechanisms triggered by 6-dimensional operators, we study in detail the short-range mechanisms contributing to neutrinoless double beta decay as 9-dimensional operators at Fermi scale. After deriving the nuclear matrix elements and phase-space factors involved, we determine limits on the respective particle physics parameters. Constraining these lepton number violating couplings allows to estimate the high-energy scale of the corresponding new physics. Unlike in the standard case, non-standard mechanisms yield energies of order of a few TeVs. Presence of lepton number violation at such low scales implies together with sphaleron transitions a potential washout of a primordial lepton and baryon asymmetry. Consequently, restrictions may be imposed on scenarios of the observed matter-antimatter asymmetry generation. We argue that certain models of high-scale baryogenesis can be generally excluded, if a non-standard neutrinoless double beta decay is observed.

Impact Statement

The research carried out in this thesis aims to help determine crucial neutrino properties as precisely and robustly as possible by interpreting experimental searches for so called neutrinoless double beta decay. At the same time, it correlates the results from these laboratory experiments with the early universe cosmology and related astrophysical measurements.

The hypothetical process of neutrinoless double beta decay involves the simultaneous transition of two neutrons into protons within an atomic nucleus, with two electrons being emitted. It has not been observed so far and the fact that there are no neutrinos in the final state requires new physics not present in the Standard Model of particle physics. More specifically, if the neutrino is identical to its anti-neutrino, the observation of neutrinoless double beta decay would allow to directly probe the neutrino mass. In this case, neutrinoless double beta decay is the most promising experimental approach to "weigh" neutrinos. On the other hand, there is a large variety of other possible mechanisms originating from yet undiscovered new physics that could lead to neutrinoless double beta decay, and these are the main subject of this work. Their accurate description and a robust determination of the process rates crucially require detailed nuclear physics calculations. As we show, this effort consequently allows to draw conclusions not only about new particle physics, but also about cosmological models explaining baryon asymmetry of the Universe. Therefore, the present study features interdisciplinary aspects, touching on and interconnecting theoretical and experimental particle physics, nuclear physics and cosmology. Since we directly aim to assess and sharpen the implications that can be deduced from the numerous current and upcoming searches for neutrinoless double beta decay, our analysis will increase their physics impact. Although the academic contribution of the publications based on this work lies primarily in the area of particle physics, the overlaps may have interesting consequences also in the other mentioned fields.

More generally, this work is part of basic, fundamental research and as such it does not have immediate technological use. On the other hand, it contributes to a natural endeavour that expands human knowledge, which has to inevitably precede any subsequent applications. As history has taught us, this kind of research also gives rise to a variety of side products that can find use in various areas of industry. Specifically, theoretical research drives experimental efforts which require the development of innovations and new technologies. Moreover, theoretical particle physics and phenomenology in general excites the interest of many, especially young, people, often leading them to pursue a career in the important economic sector of science and technology.

Contents

1

Introduction

The endeavour of particle physics to discover, describe and understand the elementary components of matter and their interplay is an integral part of fundamental physics. It sheds light on the deepest theoretical concepts governing the Universe and in the ideal case it is expected to pave the way towards an ultimate all-encompassing theory. Remarkably enough, our present comprehension of matter already contained in the Standard Model (SM) of Fundamental Particles and Interactions [1–7] provides a very detailed and accurate picture of subnuclear physics. It describes a large number of observed phenomena in a simple theory and with it we are able to make very precise predictions on particle properties and process rates, a vast majority of which agree with the experimental data to a great accuracy. Consequently, the SM represents one of the most successful physical theories.

Despite the immense success, for example in explaining the data from the Large Hadron Collider (LHC), the SM unfortunately does not capture completely the current experimental reality. Moreover, the presence of a considerable number of free parameters in the SM means it sometimes lacks predictivity and does not explain all the observed features in a satisfactory manner. As a consequence, the SM is generally considered to be an effective realization of a more complete high-scale theory, the search for which is the principal goal of Beyond the Standard Model (BSM) Physics. A major inconsistency of the SM with the current experimental data is the prediction of vanishing neutrino masses. This has clearly proven to be wrong by the observation of neutrino flavour oscillations [8–10]. Although these measurements cannot provide information on the absolute neutrino mass, they point to mass scales of order $m_\nu \sim 0.01 - 0.05$ eV obtained from solar and atmospheric neutrino oscillations, respectively. Cosmological data, on the other hand, constrain the sum of all active neutrino masses with the recent limit $\Sigma_{i=1}^{3} m_{\nu_i} \lesssim 0.17$ eV [11]. Therefore, the current state of knowledge implies that there are at least two neutrinos with masses within the range ~ 0.01 – 1 eV. In order to be more specific, the absolute neutrino mass has

to be probed, e.g. by the KATRIN experiment [12].

The small but non-vanishing neutrino masses naturally guide the direction to be followed when stepping beyond the SM. Neutrinos are generally very intriguing particles still evading our full understanding. Not only do they have very tiny masses, much smaller than the masses of other fermions, but they are also the only neutral fermions. As the SM incorporates only left-handed neutrinos, they cannot acquire Dirac masses like all the other fermions. The above features then rather suggest the concept of Majorana neutrinos, which is currently the most favoured way of explaining the light neutrino masses. It assumes that neutrinos are of Majorana nature (i.e. they should be represented rather by Majorana than Weyl spinors) and as such they can be identified with their antiparticles. Consequently, if this theoretical construction is indeed realized in Nature, we expect to observe lepton number violation (LNV). This would be in fact a very clear indication of new physics, as lepton number is conserved at the perturbative level within the SM, corresponding to an anomalous Abelian global symmetry. A prominent (hypothetical) LNV process that can test the hypothesis of Majorana neutrinos is neutrinoless double beta ($0\nu\beta\beta$) decay, which represents the central theme of this work. It is a simultaneous transition of two neutrons to two protons, two electrons and nothing else. As will be studied in detail, although the observation of this expectedly extremely rare nuclear process on its own would not be enough to pinpoint a particular neutrino mass scheme or track down the underlying BSM model, still, a number of interesting conclusions could be arrived at.

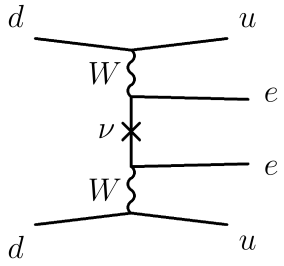

Figure 1.1: The standard mass mechanism of $0\nu\beta\beta$ decay.

Most commonly, $0\nu\beta\beta$ decay is considered to be triggered via the standard mass mechanism, which is simply given by two SM beta decay diagrams with the neutrino legs connected using the light Majorana neutrino mass insertion, see Fig. 1.1. The corresponding Majorana neutrino mass term can be written in the usual two-component spinor language as $m_\nu \nu_L \nu_L$, with m_ν denoting the light Majorana neutrino mass, and it clearly violates lepton number by two units.

This term cannot be added to the SM, since it violates its gauge symmetry. At the SM level it can be generally induced by the unique dimension-5 non-renormalizable effective Weinberg operator $\Lambda^{-1}(LLHH)$ [13], where L and H represent the $SU(2)_L$ doublets of the left-handed lepton and the Higgs fields, respectively, and Λ is a large new physics scale associated with breaking of the lepton number symmetry. Indeed, after the electroweak (EW) phase transition the Weinberg operator produces a small effective Majorana neutrino mass $m_\nu \sim v^2/\Lambda$ with v denoting the Higgs vacuum expectation value (VEV). At the tree level, the UV realization underlying the Weinberg operator typically incorporates the famous seesaw mechanism [14–18]. The most popular version (seesaw type I) is based on heavy right-handed neutrino singlets with mass $M \approx \Lambda$ yielding the light mass of the oscillating neutrinos $m_\nu = \frac{y_\nu^2 v^2}{M}$, where y_ν denotes the neutrino Yukawa coupling.

The above scenario, despite being the most popular, is not the only possibility to trigger $0\nu\beta\beta$ decay. One can think of a variety of other, non-standard $0\nu\beta\beta$ decay mechanisms. These can be described effectively, i.e. without specifying the underlying new physics. At the nuclear Fermi scale ~ 100 MeV, $0\nu\beta\beta$ decay is most generally represented by effective operators of dimension 9. In addition, operators of dimension 6 can also generate $0\nu\beta\beta$ decay, as they can substitute one (or even both, but that results in a strong suppression) SM vector currents in the standard mechanism. Like the neutrino mass term, all these other operators leading to $0\nu\beta\beta$ decay violate lepton number by two units. The effective couplings associated to each of the operators characterize the underlying UV physics and can be constrained employing a microscopic description of $0\nu\beta\beta$ decay together with the current experimental limits on its half life. This complex computation involves the determination of the nuclear matrix elements within a suitable nuclear structure model and the calculation of the corresponding phase space factors. In the same way as it is possible to map the neutrino mass term to the Weinberg operator; the other low-energy operators triggering $0\nu\beta\beta$ decay can be at the EW scale matched to SM effective operators of higher dimensions. Employing this connection, the scale of the new lepton number violating physics associated with each such operator can be determined assuming the hypothetical observation of $0\nu\beta\beta$ decay.

Along with lepton number L, baryon number B is another accidental symmetry in the SM at the perturbative level. Although the combination of these symmetries $(B+L)$ is violated by weak non-perturbative instanton and sphaleron

interactions through the chiral Adler-Bell-Jackiw anomaly [19, 20], the 'orthogonal' combination $(B-L)$ remains conserved. Consequently, apart from neutrino mass generation, another observation strongly hinting at BSM physics is the baryon asymmetry of the Universe (BAU). Quantified in terms of the baryon-to-photon number density it reads $\eta_B^{\text{obs}} = (6.20 \pm 0.15) \times 10^{-10}$ [21]. Intriguingly, a possible scheme for generation of this asymmetry is closely related to the simplest seesaw mechanism; leptogenesis [22] suggests that the heavy right-handed neutrino singlets living at the very high scale decay out of thermal equilibrium unevenly to leptons and antileptons; thus, a lepton asymmetry is produced, which is later translated into the desired baryon asymmetry by sphaleron effects. On the other hand, if the lepton number violating interactions are very efficient at lower energies, they have in connection with sphalerons the potential to erase a pre-existing lepton and baryon number asymmetry before it freezes in at the EW scale. Hence, if the $0\nu\beta\beta$ decay rate can be correlated with these washout processes, it would also allow to probe or rather falsify certain baryogenesis mechanisms. The investigation of this connection between LNV at low and high energies is the main topic of this work.

The thesis is structured as follows. After providing a brief overview of the SM and pointing out its successes as well as drawbacks hinting at possible solutions in Chapter 2, we focus specifically on neutrino physics in Chapter 3. Therein we review the basic concepts surrounding neutrinos such as mixing, oscillations and in particular aspects of neutrino mass describing several possible ways of its generation. In connection to Majorana neutrino masses we also introduce $0\nu\beta\beta$ decay focussing on the standard mechanism and discussing some features of its microscopic description as well as the related experimental efforts. In Chapter 4 we present the effective approach to $0\nu\beta\beta$ decay and we concentrate primarily on so called short-range $0\nu\beta\beta$ decay mechanisms. We provide a detailed derivation of the involved nuclear matrix elements as well as the phase space factors and assuming the current and future experimental sensitivities we estimate the bounds on the corresponding particle physics parameters. Chapter 5 contains a description of the SM effective operators violating lepton number and the way they can contribute to $0\nu\beta\beta$ decay. Employing these results we compute in Chapter 6 the washout of a primordial baryon asymmetry triggered by each of these effective operators. We compare the obtained results giving a detailed commentary and we discuss the implications of a discovery of $0\nu\beta\beta$ decay for high-scale baryogenesis mechanisms.

2

To the Standard Model and Beyond

Although this work focuses primarily on BSM physics, let us first discuss what is known to us and summarize the standard picture of matter we currently have together with a bit of background on how the well-known Standard Model of particle physics was developed. It is the proper understanding of this theory, what motivates best the steps beyond it, towards new theoretical concepts and possibly more complete particle physics models giving even more insight into the fundamental laws of Nature.

2.1 Beta Decay & Fermi Theory

Within the historical development of particle physics the construction of the SM was preceded by the attempts to understand and describe the weak interactions, some of which proved to be fairly successful. At the beginning of this path there was the desire to understand the physics behind the nuclear beta decay

$$n \to p + e^- + \bar{\nu}_e, \tag{2.1}$$

which, being experimentally observed for the first time at the turn of the 20th century, is the oldest and most notorious example of a process involving the weak interaction. Of course, at first, the only weakly interacting (anti)neutrinos were not observed in the process, but the existence of these elusive neutral particles was postulated by Pauli soon after on grounds of energy conservation. Neutrinos were detected much later, in 1956, in the Cowan-Reines experiment [23].

The first quantitative theoretical description of beta decay was proposed by Fermi in 1934 [24], who assumed a simple contact interaction of 4 fermionic quantum fields

$$\mathcal{L}_{\text{Fermi}} = -G\,(\bar{e}\gamma^\mu\nu)\,(\bar{p}\gamma_\mu n) + \text{h.c.}, \tag{2.2}$$

where G is a coupling constant, γ^μ are the Dirac gamma matrices and e, ν, p and n label the field corresponding to the electron, neutrino, proton and neutron, respectively. This interaction Lagrangian describes not only the decay in Eq. (2.1), but also related processes such as positron capture. Its effective form presuming a zero range of the nuclear weak force approximates the corresponding interactions well at low energies.

After the parity violation of weak interactions was experimentally discovered by Wu [25], the two-component neutrino theory developed earlier by Weyl [26] was revived. This hypothesis assumed that neutrinos are massless, left-handed fermions and as such they obey a two-component Weyl equation of the form

$$i\frac{\partial \nu_L}{\partial t} = i\boldsymbol{\sigma} \cdot \boldsymbol{\nabla} \nu_L, \tag{2.3}$$

where $\boldsymbol{\sigma}$ are the Pauli matrices. Despite the fact we nowadays know that this description is not realistic and that it cannot be perceived as the source of parity violation in weak interactions, it is a good approximation, which historically played an important role in the development of relevant theoretical model. It was the concept of a two-component neutrino that motivated Feynman and Gell-Mann [27] together with Cabbibo [28] to postulate the following Lagrangian of weak interactions

$$\mathcal{L}_{\text{weak}} = -\frac{G_F}{\sqrt{2}} J^\nu J^\dagger_\nu, \tag{2.4}$$

with G_F denoting the Fermi constant and the current J^ν being defined as

$$J^\nu = \bar{\nu_e}\gamma^\nu(1-\gamma_5)e + \bar{\nu_\mu}\gamma^\nu(1-\gamma_5)\mu + \bar{u}\gamma^\nu(1-\gamma_5)\left(d\cos\theta_C + s\sin\theta_C\right) \tag{2.5}$$

where the up, down and strange quarks u, d and s are introduced, ν^e and ν^μ denote electron and muon neutrinos and θ_C is the Cabbibo angle hinting at a rotation in the space of quark fields.

The above simple interaction Lagrangian was proven to be capable to successfully describe a lot of experimental data, including (although with less accuracy) the well-known scattering process

$$\bar{\nu} + p \to n + e^+, \tag{2.6}$$

which was used to detect neutrinos directly for the first time [23]. However, despite all the low energy accomplishments (back then all the predictions could be tested only within a limited kinematical region), the above Lagrangian possesses

one significant flaw, which becomes apparent when one starts thinking about higher energies - it is non-renormalizable. This is actually obvious already from the fact that one is dealing with four-fermion interactions, which are of mass dimension 6. Renormalizable quantum field theories are those with interaction Lagrangians containing terms of mass dimension $d \leq 4$ [29]. As a result, further theoretical development was needed in order to find a better-behaved theory at high energies. This theory was created soon after, in the late 1960s and early 1970s, and it is nothing but the electroweak Standard Model unifying weak and electromagnetic interactions.

2.2 Gauging the World

Although the notion of gauge symmetry appeared for the first time already in Maxwell's formulation of classical electrodynamics [30], it remained rather unnoticed until the introduction of quantum theory, when the real potential of this elegant theoretical framework was revealed in its full glory.

As first complete gauge theory one can consider the theory of Quantum Electrodynamics (QED), which was developed by Dirac [31] and others at the beginning of the 20th century, i.e., even earlier than the above discussed Fermi theory. QED is the simplest example of a gauge theory, an Abelian gauge theory, i.e., a quantum field theory with local internal symmetry corresponding to the Abelian Lie group $U(1)$. It describes the propagation and interaction of fermionic matter particles and photons, the gauge bosons of this theory, which mediate the electromagnetic force.

It was the extension of the beautiful concept of gauge theories to non-Abelian groups developed by Yang and Mills in 1954 [32], which allowed to describe the weak interactions in a similar way, and therefore, meant a major step forward towards the SM as we know it nowadays. This allowed to build a whole variety of new theories, from which those based on special unitary groups $SU(n)$ have been later proven to be especially useful for the purposes of particle physics. It is interesting to mention that the real potential of these theories remained initially unnoticed, because of the fact that on their own they require all the particles to be massles, which was obviously in clash with experiments. However, this issue was resolved by the introduction of the spontaneous symmetry breaking mechanism into particle physics by Anderson [33], Higgs [34], Englert and Brout [35] and others [36, 37] in the 1960s. At that point, the SM could start developing.

At first, the Fermi theory of the weak interactions described in the previous section was unified together with QED into the gauge theory of electroweak interactions, sometimes called the Electroweak Standard Model or also, after its fathers, the Glashow-Salam-Weinberg (GSW) Model [1–3], with the internal symmetries described by the semi-simple gauge group $SU(2) \otimes U(1)$. After the construction (contributed by many bright minds) of the parton model [4, 5] and Quantum Chromodynamics (QCD), an asymptotically free gauge theory with the $SU(3)$ symmetry group describing the strong nuclear force [6, 7], in 1970s, the theoretical framework of the SM was completed. In this way the quantum field description of the three fundamental interactions - electromagnetic, weak and strong - were incorporated in a single model.

2.3 The Very Standard Model

Following the rather historically themed previous paragraphs let us continue in more technical terms. The Standard Model of particle physics is a Quantum Field Theory (QFT) on a four-dimensional Minkowski spacetime including all renormalizable operators invariant under the local internal symmetries described by the semi-simple group

$$\mathcal{G}_{\mathrm{SM}} = SU(3)_C \otimes SU(2)_L \otimes U(1)_Y. \tag{2.7}$$

Here the subscripts C, L and Y remind us of the respective quantum numbers, i.e., they stand for colour, left-handed chirality and weak hypercharge, respectively. The fact that there is only the left-handed $SU(2)$ group reflects the experimentally confirmed parity violation [25] mentioned previously. As a result, the left-handed components of fermions transform non-trivially under the $SU(2)_L \otimes U(1)_Y$ group, while the right-handed only under the $U(1)_Y$. The fermionic fields of the SM are accommodated in the representations of the group $\mathcal{G}_{\mathrm{SM}}$ in the way captured in the upper part of Tab. 2.1. In this chapter, we describe fermions as four-spinors (unless otherwise stated) with appropriate chiral projections performed, i.e. $f_{R/L} = (1 \pm \gamma_5) f$ (where $f \in \{e, d, u\}$), corresponding to right-handed and left-handed four-component Weyl fields, respectively. We also define the conjugate left-handed four-component Weyl fields as $f^c = C \bar{f}_R^{\,T}$ with C being the charge conjugation matrix. In later chapters, in context of the SM effective field theory it will be often more convenient to describe chiral fermions in terms of two-component left-handed Weyl spinors. For a fermion f we will use the no-

Fermions		
Name	*Label*	*Representation*
left-handed lepton doublet	$L^\ell \equiv \begin{pmatrix} \nu_L^\ell \\ \ell_L \end{pmatrix}$	$\{\mathbf{1}, \mathbf{2}, -\frac{1}{2}\}$
right-handed lepton singlet	ℓ_R	$\{\mathbf{1}, \mathbf{1}, 1\}$
left-handed quark doublet	$Q^{a^i} \equiv \begin{pmatrix} u_L^r & u_L^g & u_L^b \\ d_L^r & d_L^g & d_L^b \end{pmatrix}^i$	$\{\mathbf{3}, \mathbf{2}, \frac{1}{6}\}$
right-handed up-quark singlet	$\left(u_R^r, u_R^g, u_R^b\right)^i$	$\{\overline{\mathbf{3}}, \mathbf{1}, -\frac{2}{3}\}$
right-handed down-quark singlet	$\left(d_R^r, d_R^g, d_R^b\right)^i$	$\{\overline{\mathbf{3}}, \mathbf{1}, \frac{1}{3}\}$
Vector Bosons		
Associated Charge − Group	*Label*	*Representation*
weak hypercharge − $U(1)_Y$	B	$\{\mathbf{1}, \mathbf{1}, 0\}$
weak isospin − $SU(2)_L$	W	$\{\mathbf{1}, \mathbf{3}, 0\}$
colour − $SU(3)_C$	G	$\{\mathbf{8}, \mathbf{1}, 0\}$
Scalar Bosons		
Name	*Label*	*Representation*
Higgs boson	$H = \begin{pmatrix} h^+ \\ h^0 \end{pmatrix}$	$\{\mathbf{1}, \mathbf{2}, \frac{1}{2}\}$

Table 2.1: The above table summarizes the particle content of the Standard Model. Labelling used later in the text is introduced and the representations accommodating the corresponding fields are specified in the usual form $\{SU(3)_C, SU(2)_L, U(1)_Y\}$. The representations $\mathbf{3}, \overline{\mathbf{3}}$ and $\mathbf{1}$ are fundamental colour triplet, conjugate colour triplet and colour singlet, respectively, while $\mathbf{2}$ and $\mathbf{1}$ are fundamental isospin doublet and isospin singlet, respectively. The weak hypercharge is given by $Y = Q - T_3$, where Q is the electric charge and T_3 the third component of isospin. In case of fermions the colour indices $\{r, g, b\}$ are explicitly shown here for clarity, later on they will be mostly suppressed to make expressions simple. The symbol ℓ denotes lepton flavour, i.e., $\ell \in \{e, \mu, \tau\}$. In case of quarks the three generations are captured by the index i, namely $u^i \in \{u, c, t\}$ and $d^i \in \{d, s, b\}$. The charge-conjugate fermion fields are defined as $f^c = C\bar{f}_R^T$ with C denoting the charge conjugation matrix.

tation f_L and f^c to capture both left-handed and right-handed components of the given fermion in terms of purely left-handed fields. Therefore, the same notation as the one we employ here for four-component Weyl spinors will be used for two-component Weyl spinors, but the meaning will be always easily inferable from the context. In some cases the standard four-component Dirac fermions f (without employing any projection) will be used. To distinguish their charge conjugates easily from the conjugates of the projected right-handed Weyl spinors, they will be denoted as f^C, i.e. with a capital C in the superscript. The four-component Dirac fermion can be written in terms of the two-component Weyl fields as $f = (f_L\ \bar{f^c})$, where the bar denotes Hermitian conjugation. The relation between the notations will be discussed later in connection to neutrinos' nature.

For a further discussion of the SM it is convenient to write the full SM Lagrangian as a sum of the following four terms,

$$\mathcal{L}_{\text{SM}} = \mathcal{L}_{\text{Gauge}} + \mathcal{L}_{\text{Fermion}} + \mathcal{L}_{\text{Higgs}} + \mathcal{L}_{\text{Yukawa}}. \tag{2.8}$$

The force mediators in the SM are the vector (gauge) bosons associated to the SM symmetry group in Eq. (2.7) and they are listed in the second part of Table 2.1. These fields ensure the gauge invariance of the theory. The first term of Eq. (2.8) contains the kinetic terms of the SM gauge fields

$$\mathcal{L}_{\text{Gauge}} = -\frac{1}{4}B_{\mu\nu}B^{\mu\nu} - \frac{1}{4}W^i_{\mu\nu}W^{i\mu\nu} - \frac{1}{4}G^a_{\mu\nu}G^{a\mu\nu}, \tag{2.9}$$

where

$$B_{\mu\nu} = \partial_\mu B_\nu - \partial_\nu B_\mu, \tag{2.10}$$
$$W^i_{\mu\nu} = \partial_\mu W^i_\nu - \partial_\nu W^i_\mu + g\varepsilon^{ijk}W^j_\mu W^k_\nu, \tag{2.11}$$
$$G^a_{\mu\nu} = \partial_\mu G^a_\nu - \partial_\nu G^a_\mu + g_s f^{abc}G^b_\mu G^c_\nu, \tag{2.12}$$

with g and g_s being the weak ($SU(2)_L$) and strong ($SU(3)_C$) gauge couplings, respectively. The $U(1)$ gauge coupling will be as usually denoted by g'. The structure constants ε^{ijk} and f^{abc} are defined through

$$\left[\tau^i, \tau^j\right] = i\varepsilon^{ijk}\tau^k, \tag{2.13}$$
$$\left[\lambda^a, \lambda^b\right] = if^{abc}\lambda^c, \tag{2.14}$$

where τ^i and λ^a are the generators of the $SU(2)_L$ and $SU(3)_C$ groups, respectively.

The second term of the Lagrangian (2.8) contains the fermionic kinetic terms and it can be written as

$$\mathcal{L}_{\text{Fermion}} = \sum_{\ell=e,\mu,\tau} i\bar{L}^{\ell}\gamma^{\mu}(\partial_{\mu} - ig'Y_L^{\ell}B_{\mu} - ig\frac{\tau^i}{2}W_{\mu}^i)L^{\ell} \tag{2.15}$$

$$+ \sum_{q=d,s,b} i\bar{Q}^{q}\gamma^{\mu}(\partial_{\mu} - ig'Y_L^{q}B_{\mu} - ig\frac{\tau^i}{2}W_{\mu}^i - ig_s\frac{\lambda^a}{2}G_{\mu}^a)Q^{q} \tag{2.16}$$

$$+ \sum_{\ell=e,\mu,\tau} i\bar{\ell_R}\gamma^{\mu}(\partial_{\mu} - iY_R^{\ell}g'B_{\mu})\ell_R \tag{2.17}$$

$$+ \sum_{q=d,u,s,c,b,t} i\bar{q_R}\gamma^{\mu}(\partial_{\mu} - iY_R^{q}g'B_{\mu})q_R, \tag{2.18}$$

where, of course, the terms in parentheses are the covariant derivatives and $Y_{\bullet}^{\circ}$ is the weak hypercharge of a corresponding particle.

Having written only the kinetic terms so far, all the particles are still massless and they preserve the SM symmetry. One cannot simply write Dirac mass terms of type $M_{\psi}\bar{\psi}_L\psi_R$, as the left-handed and right-handed fermions do not live in the same gauge representations; hence, the gauge symmetry would be explicitly broken. Since all the fermions are charged under $U(1)_Y$, Majorana mass terms are also out of the question. Mass terms for the gauge bosons are in an equivalent trouble, as terms of type $M_B B_{\mu}B^{\mu}$ are not invariant under gauge transformations.

This was the motivation for the development of the mechanism of spontaneous symmetry breaking of the SM gauge group to a smaller symmetry group of strong and electromagnetic interactions

$$SU(3)_C \otimes SU(2)_L \otimes U(1)_Y \to SU(3)_C \otimes U(1)_{em}, \tag{2.19}$$

which is a way the gauge bosons can acquire masses without spoiling the renormalizability of the theory as such. To achieve that, the SM particle content must be complemented by a Higgs doublet, a Lorentz scalar transforming as a doublet under $SU(2)_L$ (see the bottom of Tab. 2.1) that acquires a non-zero vacuum expectation value (VEV). The non-trivial transformation under the $SU(2)_L$ ensures that the non-zero VEV breaks this part of the gauge symmetry and gives mass to the corresponding vector bosons. Writing the potential of the underlying Goldstone-type model,

$$V_H = -\mu^2 H^{\dagger}H + \lambda\left(H^{\dagger}H\right)^2, \tag{2.20}$$

it can be observed that the corresponding ground state indeed breaks the gauge symmetry, as the vacuum expectation value reads

$$\langle H\rangle = \mu/\sqrt{\lambda}. \tag{2.21}$$

For the purpose of a more explicit description it is useful to introduce the following parametrization of the Higgs doublet

$$H = \begin{pmatrix} h^+ \\ \frac{1}{\sqrt{2}}\left(h + i\sigma + v\right) \end{pmatrix}, \tag{2.22}$$

where h^+, its conjugate h^- and σ are massless Nambu-Goldstone bosons [38, 39] corresponding to the three generators of $SU(2)_L$. These degrees of freedom are then "eaten" by the gauge fields, meaning they are transformed into the longitudinal components of the $SU(2)$ vector bosons, which, hence, become massive.

The gauge invariant Lagrangian of the Higgs sector can be written as

$$\begin{aligned} \mathcal{L}_{\text{Higgs}} = \; & H^\dagger \left(\partial_\mu + \frac{i}{2} g' B_\mu + i g W_\mu^a \frac{\tau^a}{2}\right) \left(\partial^\mu - \frac{i}{2} g' B^\mu - i g W^{b\mu} \frac{\tau^b}{2}\right) H \\ & - \lambda \left(H^\dagger H - \frac{v^2}{2}\right)^2 . \end{aligned} \tag{2.23}$$

Fixing the gauge such that the unphysical Nambu-Goldstone bosons are removed, i.e. "gauged away", one transforms into the so called U-gauge with the Higgs doublet taking the form

$$H_U = \begin{pmatrix} 0 \\ \frac{1}{\sqrt{2}}\left(h + v\right) \end{pmatrix}. \tag{2.24}$$

Hence, the Higgs Lagrangian (2.23) in the U-gauge can be written as

$$\begin{aligned} \mathcal{L}^U_{\text{Higgs}} = \; & \frac{1}{2}\partial_\mu h \partial^\mu h - \lambda v^2 h^2 - \lambda v h^3 - \frac{1}{4}\lambda h^4 + \frac{1}{8}(h+v)^2 \left[g^2 W_\mu^1 W^{1\mu} \right. \\ & \left. + g^2 W_\mu^2 W^{2\mu} + \left(g W_\mu^3 - 2 g' Y B_\mu\right) \left(g W^{3\mu} - 2 g' Y B^\mu\right) \right], \end{aligned} \tag{2.25}$$

where the terms quadratic in the gauge fields inside the square bracket were diagonalized. As a result, the part of the bracket proportional to v^2 gives the mass terms of the intermediate vector bosons, which can be identified as

$$W_\mu^\pm = \frac{1}{\sqrt{2}} \left(W_\mu^1 \mp W_\mu^2\right), \quad Z_\mu = \frac{1}{\sqrt{g^2 + g'^2}} \left(g W_\mu^3 - g' B_\mu\right), \tag{2.26}$$

with the masses

$$M_W = \frac{1}{2} g v, \quad M_Z = \frac{1}{2}\sqrt{g^2 + g'^2}\, v. \tag{2.27}$$

The combination of W_μ^3 and B_μ orthogonal to Z_μ gives the remaining gauge boson

$$A_\mu = \frac{1}{\sqrt{g^2 + g'^2}} \left(g' W_\mu^3 + g B_\mu\right), \tag{2.28}$$

which stays massless (it does not have a respective mass term) corresponding to the photon, i.e. the gauge boson of $U(1)_{em}$. The symmetry breaking affects only the electroweak sector; therefore the $SU(3)_C$ group stays untouched with all its eight gauge fields, gluons, remaining massless.

Breaking of the electroweak symmetry also allows to add fermion mass terms to the SM Lagrangian. Coupling the SM fermions to the Higgs doublet one can write down the Yukawa Lagrangian

$$\begin{aligned}\mathcal{L}_{\text{Yukawa}} = & -\sum_{\ell=e,\mu,\tau} \mathrm{y}_\ell \bar{L}^\ell H \ell_R - \sum_{\substack{q=d,s,b \\ q'=d,s,b}} \mathrm{y}^d_{qq'} \bar{Q}^q H q'_R \\ & - \sum_{\substack{q=d,s,b \\ q'=u,c,t}} \mathrm{y}^u_{qq'} \bar{Q}^q \tilde{H} q'_R + \text{h.c.}, \end{aligned} \tag{2.29}$$

where $\tilde{H} = i\tau_2 H^*$, with τ_2 being the second Pauli matrix, is the charge conjugate of H. The Yukawa couplings $\mathrm{y}_\ell, \mathrm{y}^d_{qq'}$ and $\mathrm{y}^u_{qq'}$ can be in principle arbitrary real numbers, the overall minus sign is conventional. Again, going to the U-gauge, the fermionic mass terms can be identified in Eq. 2.29

$$\begin{aligned}\mathcal{L}_{\text{Yukawa}} \supset & -\sum_{\ell=e,\mu,\tau} \frac{\mathrm{y}_\ell v}{\sqrt{2}} \bar{\ell}_L \ell_R - \sum_{\substack{q=d,s,b \\ q'=d,s,b}} \frac{\mathrm{y}^d_{qq'} v}{\sqrt{2}} \bar{q}_L q'_R \\ & - \sum_{\substack{q=u,c,t \\ q'=u,c,t}} \frac{\mathrm{y}^u_{qq'} v}{\sqrt{2}} \bar{q}_L q'_R + \text{h.c.}, \end{aligned} \tag{2.30}$$

where the leptonic masses are simply given as $\mathrm{m}_\ell = \frac{1}{\sqrt{2}} \mathrm{y}_\ell v$, as the corresponding terms are diagonal in flavour. On the other hand, the quark mass terms include (generally non-zero) off-diagonal terms, and therefore, form two different 3×3 mass matrices $\mathrm{M}^{d/u} = \frac{v}{\sqrt{2}} \mathrm{y}^{d/u}$, where $\mathrm{y}^{d/u}$ are matrices of quark Yukawa couplings with elements $\mathrm{y}^{d/u}_{qq'}$. These matrices can be diagonalized using a bi-unitary transformation, which allows for independent rotations of left-handed and right-handed quarks, explicitly

$$\mathrm{M}^{d/u} = (\mathrm{U}^{d/u}_L)^\dagger \mathrm{m}^{d/u} \mathrm{U}^{d/u}_R, \tag{2.31}$$

where $\mathrm{m}^{d/u}$ are real, diagonal matrices with diagonal elements given by the quark masses. Therefore, these are again proportional to the respective Yukawa couplings and the VEV as well, as in case of leptons. The unitary matrices (two for up-quarks and two for down-quarks) realizing this transformation thus effectively

rotate the weak interaction quark eigenstates q^i to the quark mass eigenstates q^m

$$u_L^i = \sum_{m=1,2,3} [\mathrm{U}_L^u]_{im} u_L^m, \quad d_L^i = \sum_{m=1,2,3} [\mathrm{U}_L^d]_{im} d_L^m, \tag{2.32}$$

$$u_R^i = \sum_{m=1,2,3} [\mathrm{U}_R^u]_{im} u_R^m, \quad d_R^i = \sum_{m=1,2,3} [\mathrm{U}_R^d]_{im} d_R^m. \tag{2.33}$$

Taking these redefinitions of fields and substituting them into the fermion-interaction part of the Lagrangian, the terms describing weak interaction of charged currents will give

$$\begin{aligned} \mathcal{L}_{\text{Fermion}} \supset & \frac{g}{\sqrt{2}} W_\mu^+ \bar{u}_L^i \gamma^\mu d_{L\,i} + \text{h.c.} \\ & = \frac{g}{\sqrt{2}} W_\mu^+ \left[\mathrm{U}_L^u \mathrm{U}_L^{d\dagger}\right]_{mm'} \bar{u}_L^m \gamma^\mu d_L^{m'} + \text{h.c.} \end{aligned} \tag{2.34}$$

where the Cabibbo-Kobayashi-Maskawa (CKM) mixing matrix given by the combination of the unitary transformation matrices arises,

$$V_{\text{CKM}} \equiv U_L^u U_L^{d\dagger} = \begin{pmatrix} V_{ud} & V_{us} & V_{ub} \\ V_{cd} & V_{cs} & V_{cb} \\ V_{td} & V_{ts} & V_{tb} \end{pmatrix}. \tag{2.35}$$

The phenomenon of quark mixing was first realized by Cabibbo [40] for two generations of quarks and later generalized for all three quark families by Kobayashi and Maskawa [41]. The neutral weak currents are flavour-diagonal by definition; hence, they are left intact by the considered bi-unitary transformations.

The CKM mixing matrix can be conveniently parametrized by four parameters: three quark mixing angles $\vartheta_{12}, \vartheta_{13}, \vartheta_{23} \in \left[0, \frac{\pi}{2}\right]$ and one complex phase $\alpha_{CP} \in [0, 2\pi]$, as five other phases can be absorbed by redefinitions of the quark fields. This parametrization is usually written in the form

$$V_{\text{CKM}} = \begin{pmatrix} c_{12}c_{13} & s_{12}c_{13} & s_{13}e^{-i\alpha_{CP}} \\ -s_{12}c_{23} - c_{12}s_{13}s_{23}e^{i\alpha_{CP}} & c_{12}c_{23} - s_{12}s_{13}s_{23}e^{i\alpha_{CP}} & c_{13}s_{23} \\ s_{12}s_{23} - c_{12}s_{13}c_{23}e^{i\alpha_{CP}} & -c_{12}s_{23} - s_{12}s_{13}c_{23}e^{i\alpha_{CP}} & c_{13}c_{23} \end{pmatrix}, \tag{2.36}$$

where the shorthand notation $s_{ij} \equiv \sin\vartheta_{ij}, c_{ij} \equiv \cos\vartheta_{ij}$ was used. The presence of the complex phase α_{CP} implies violation of CP symmetry (i.e. invariance under simultaneous charge conjugation C and space inversion P). This theoretical prediction is in agreement with the experimental observation of corresponding CP-violating processes.

How Well Does the SM Work? The fact that the SM is one of the most successful physical theories has already become common knowledge, as it describes the majority of particle physics phenomena. It is the most general theory consistent with general principles like Lorentz invariance and unitarity based on the assumptions of renormalizability and the given particle content. The SM allows us to make predictions about the behaviour of fundamental particles, some of which it had anticipated before their actual discovery. Moreover, the agreement between experimental data and theoretical calculations often reaches an incredible accuracy.

To be more specific, let us give a couple of concrete examples. Except for the photon, all the other gauge fields present in the SM were theoretically anticipated before their experimental discovery. The mediators of the weak force, $W^{\pm}$ and Z, were first theorized, as mentioned earlier, by Glashow, Salam and Weinberg and their existence was confirmed by the UA1 and UA2 collaborations at CERN in 1983 [42–45]. Similarly, the gluons as strong force mediators were anticipated [46] before their observation at DESY in 1978 [47, 48].

Furthermore, during the construction of the SM the existence of the charm quark [49] and the top and bottom quarks [50] was predicted. The charm quark was confirmed in 1974 through experimental observation of the J/ψ meson by teams of SLAC [51] and BNL [52], while the third quark generation was discovered by experiments at Tevatron at Fermilab - the bottom quark in 1977 [53] and the top quark in 1995 [54, 55].

One of the biggest successes of the SM is then, of course, the predicted discovery of Higgs boson. The implementation of the spontaneous symmetry breaking into the SM in 1960s implied the presence of a scalar boson in the SM spectrum, which was confirmed about 50 years later, in 2012, by the ATLAS [56] and CMS [57] collaborations at the LHC.

A great potential of testing the SM lies also in precision physics, i.e. theoretical predictions that can be calculated with great accuracy and which can be compared to very precise measurements. A famous example of a quantity that has been calculated extremely accurately is the anomalous magnetic dipole moment of the electron. The theoretical value $a_e^{\text{th}} = 1159652182.032(720) \times 10^{-12}$ [58] includes contributions up to the order α^5 (α is the fine structure constant) and it is in an amazing agreement with the experimental value $a_e^{\text{exp}} = 1159652180.73(28) \times 10^{-12}$ [59, 60].

So Where Is the Problem? After praising the SM as a remarkable theory and reviewing some of its big successes, it is time to look at the negatives and discuss the problems it is not able to deal with. Of course, when doing so, the length of the list of the shortcomings may depend on the initial expectations one has of the theory. For instance, it is often mentioned that the main flaw of the SM is the fact it cannot describe gravitational interactions. Despite the validity of such a statement, if one does not expect the SM to be the ultimate theory of everything, it is not such a big deal. The problem with the quantization of gravitational force is broader and the reality that the SM does not describe it is just a straightforward consequence of the impossibility to treat gravity as a quantum field theory. From this point of view, the exclusion of gravity is rather an ignorance than a failure of the SM.

Nevertheless, even if the question of gravity is set aside, there are still a number of other problems within the SM. Many of them are being paid a lot of attention, as their resolution would naturally lead towards a better and more complete particle physics model.

As mentioned earlier, the SM is consistent with most of the experimental data; nevertheless, it seems this comes to a certain degree at a price of predictivity, or, as some would say, elegance. The SM as such is often seen to be quite *ad hoc*, as its gauge group and particle content are very specific. This is reflected by the presence of 19 free physical parameters, which are not predicted by the model and must be determined experimentally: 3 gauge couplings, 2 scalar potential parameters, 6 quark masses, 3 charged lepton masses, 3 CKM angles, 1 CP-violating phase and 1 strong CP parameter. Already this may seem to be too many for an ultimate particle physics model plus one has to bear in mind that inclusion of neutrino masses further extends this list.

Similarly, the SM does not offer any explanation of the fairly non-trivial and rather surprising fact that the weak hypercharges (or, equivalently, the electric charges) of all elementary particles are in simple integral ratios. If a bigger group like $SU(2)$ is considered, the eigenvalues of its generators are quantized, as the algebra of such a group is non-trivial. This, however, is not the case for $U(1)$; therefore, from the theoretical point of view, the particles' charges could be anything. Nonetheless, they are observed to be quantized in nature.

Another completely arbitrary aspect of the SM is the pattern of fermions. There is no satisfactory reason for having three generations of leptons and quarks. Moreover, no light is shed on the parity violation in case of the weak interactions

in contrast to the parity of strong interactions, which is left intact.

A possible treatment for some of the above drawbacks can be found within the group-theoretical framework of Grand Unified Theories (GUTs), see Sec. 3.8.

The hierarchy problem [61] is another issue that is often mentioned along with the other shortcomings of the SM. It refers to the huge difference between the electroweak scale ($\Lambda_{EW} = 246$ GeV) and the Planck scale ($\Lambda_{Pl} = 10^{19}$ GeV), where gravity becomes important and thus must be taken into account. Specifically, what is mostly seen as problematic is the fact that if the SM is perceived as an effective theory, with Λ_{Pl} being its cut-off, the radiative corrections to the Higgs mass diverge quadratically with this very high energy scale. Although one can assume the bare mass to be of the same order and cancel these large contributions, this would require an extremely accurate cancellation, generally known as fine tuning, which is considered to be unnatural. This problem led to the belief there must be some kind of new physics involved just above the electroweak scale, which would avoid the big radiative corrections of the Higgs mass parameter. Low scale supersymmetric models have been the most popular solutions of the naturalness problem, within which the bosonic loop corrections are naturally cancelled by their fermionic versions. However, the existence of any new particles living in the vicinity of the electroweak scale has been disfavoured in recent years by the LHC.

A number of indications of incompleteness of the SM come from cosmology. The first of them is the simple fact of our own existence, because the SM does not address the origin of the observed asymmetry between matter and antimatter in our universe [62]. There is a variety of BSM mechanisms attempting to resolve this issue, which we will focus on later in Sec. 3.9.

The second important cosmological problem of the SM is the one of cosmological constant, which arises from the fact that the vacuum energy density measured in cosmology is very tiny [63, 64]. This is in clash with the value of this constant one would expect on grounds of quantum field theory and currently, there is not a generally accepted explanation of this issue.

The third big problem of the SM introduced by various cosmological and astrophysical observations is that it does not include particles that could play the role of Dark Matter. Although a number of particle physics experiments desperately search for this theorized form of matter, no firm signal hinting at the existence of such particles has been observed so far. There are a lot of particle physics models trying to explain the Dark Matter nature, origin and

behaviour. Typical candidates for Dark Matter are for instance axions [65, 66], sterile neutrinos [67] or neutralinos in supersymmetric scenarios [68].

As for other issues arising on the interface of particle physics and cosmology it is worth mentioning the flatness problem [69], the horizon problem [70] and (if one believes in GUTs) the monopole problem [71]. All these three puzzles can be solved by inflation [72–74], a period of an abrupt expansion in the early universe driven by a hypothesized scalar field called inflaton. Again, inclusion of such a field in the particle physics picture requires an extension of the SM.

For quite a long time in the history of modern particle physics neutrinos seemed to be massless. Nevertheless, the zero neutrino mass had been consistent with experiments (within their accuracy) until the turn of this century, when the existence of non-zero neutrino masses was confirmed by the observation of neutrino oscillations [8, 9]. As a consequence, one could then question the validity of the electroweak theory as such. However, despite the fact that absolute neutrino masses are not known, from cosmology it is already clear they must be very tiny, and thus they can be neglected in most processes. Hence, the fact that neutrinos are massive becomes crucial just and especially for phenomena that would not be possible with massless neutrinos. The origin, aspects and consequences of neutrino masses are in more detail discussed in the following chapter.

Regarding other experimental efforts manifesting certain deviations from the SM, let us mention the measurement of the muon $a_\mu \equiv (g_\mu - 2)/2$, i.e. the anomalous magnetic dipole moment of muon. The most recent results (2001) from a BNL experiment gave a 3.5 standard deviation discrepancy and an improved measurement of this quantity by the Muon $g - 2$ experiment is currently in progress at Fermilab [75].

More recently, intriguing anomalies have been observed in various meson decays [76], but it is too early to draw any definite conclusions.

All of the above listed problems support the broadly accepted consensus that the SM is an effective manifestation of a more complete theory living at some higher energy scale. However, the often miraculously accurate agreement with current experimental data hints this scale might be rather large, and therefore, hardly accessible by experiments. From the point of view of possible discoveries of new particle physics phenomena, neutrino physics and cosmology thus appear to be promising research areas.

2.4 Effective Point of View

If the SM is indeed just an Effective Field Theory (EFT), then it works very well when all renormalizable operators (i.e. operators up to dimension 4) are considered, as we could see in the previous section. Nonetheless, in the effective framework the SM can be extended by non-renormalizable operators originating from some high-scale physics, which are suppressed by a cut-off scale Λ. The success of the SM then implies smallness of couplings of such operators, and therefore large cut-off. In some cases the SM predictions agree with the experiments to such an accuracy that the corresponding scale Λ (characterizing a given effective operator) reaches values as high as 10^{15} GeV. The non-renormalizable SM effective operators violating lepton number will play an important part later in this work. Let us therefore give here a flavour of the effective approach and mention some other interesting operators.

The consistent EFT generalization of the SM commonly used for a model-independent parametrization of new, heavy physics is called Standard Model Effective Field Theory (SMEFT), for a review see e.g. Ref. [77]. The construction of SMEFT simply assumes that the possible UV completions of the SM contain particles heavier than the electroweak VEV $v_T \equiv \sqrt{2\langle H^\dagger H\rangle}$ characterizing the masses of the SM particle content. As a result, these heavy states can be integrated out at low energies yielding a series of higher-dimensional SM invariant[1] effective operators, which can be power counted in the ratio of scales v_T/Λ. It is further assumed that the observed Higgs boson is embedded in a $SU(2)_L$ scalar doublet with hypercharge 1/2 and that there are no hidden light states interacting with the SM particle content. Like the renormalizable SM, the SMEFT is invariant under $SU(3)_C \otimes SU(2)_L \otimes U(1)_Y$ and it has the Higgsed phase $SU(2)_L \otimes U(1)_Y \ \to \ U(1)_{\rm em}$. The SMEFT Lagrangian can be developed in the following way

$$\mathcal{L}_{\rm SMEFT} = \mathcal{L}_{\rm SM} + \mathcal{L}^{(5)} + \mathcal{L}^{(6)} + \mathcal{L}^{(7)} + \dots, \tag{2.37}$$

where $\mathcal{L}_{\rm SM}$ is the SM Lagrangian and

$$\mathcal{L}^{(D)} = \sum_{i=1}^{n_D} \frac{C_i^{(D)}}{\Lambda_i^{D-4}} \mathcal{O}_i^D \quad \text{with } D > 4. \tag{2.38}$$

Here, $\mathcal{O}_i^{(D)}$ denotes the i-th of n_D effective operators at dimension D, which is suppressed by $D-4$ powers of the corresponding cut-off (operator) scale Λ_i and

[1] By 'SM invariant' we mean invariant under the SM gauge group.

$C_i^{(D)}$ is its Wilson coefficient. The individual operators can generally consist of SM fields and covariant derivatives so as to be SM invariant.

Let us now discuss briefly the operators appearing at lowest dimensions in SMEFT concentrating on the implied beyond SM physics. An operator of the lowest possible dimension is clearly an arbitrary constant, which, as it does not depend on any fields or derivatives, corresponds to dimension 0. Such a term obviously respects all the symmetries of the SMEFT, and thus nothing prevents one from adding it to the Lagrangian. This constant can be interpreted as a vacuum energy density, which, despite having no measurable effect on particle physics, couples to gravity causing the accelerated expansion of the Universe. Therefore, it is possible to determine it from cosmology, where it plays the role of cosmological constant entering Einstein equations. Estimating the constant operator itself to be of order one, then the corresponding term in the Lagrangian is simply given by Λ^4 with Λ being the SM cut-off scale. Unfortunately, as the measured vacuum energy density is approximately of size $(10^{-3}\text{ eV})^4$, it would imply an extremely small (and obviously wrong) value of $\Lambda \approx 10^{-3}$ eV. As a result, the constant term in question must be very tiny, which either requires an extreme fine-tuning, or some kind of dynamical mechanism. This is the previously mentioned open problem of the cosmological constant.

The only term in the SM and SMEFT of dimension 2 is the quadratic term in the Higgs potential, which in the EFT approach can be written with the SM cut-off scale as $\Lambda^2 H^\dagger H$. The measured value of the Higgs VEV $v = 176$ GeV would then necessitate again a rather small Λ implying either new physics to be not far above the EW scale (which does not seem to be the case), or again certain fine-tuning. This is the above discussed hierarchy problem of the SM.

Four-dimensional operators form together with the operators of dimension 0 and 2 the SM Lagrangian described in Sec. 2.3.

As for non-renormalizable operators, one can construct only a single operator of dimension 5 in SMEFT, the so called Weinberg operator $LLHH$. It is of special importance, as it violates lepton number by two units and as such it can induce light Majorana neutrino masses. Hence, from the EFT point of view the fact that non-zero neutrino masses are the first evident inconsistency of the SM is not so surprising, as they should indeed represent the leading deviation. The current experimental limits on neutrino masses imply the cut-off scale of this operator to be roughly 10^{14} GeV. The Weinberg operator will be further discussed in connection to $0\nu\beta\beta$ decay in Sec. 3.5 and together with other lepton number

violating SM effective operators in Chap. 5.

At dimension 6 the number of independent SM effective operators jumps up to 63 [78] (for one generation of fermions only), 21 of which are fermionic, and thus also their hermitian conjugates can be considered. For example, schematically, the following 4 of the 63 operators violate both baryon and lepton number

$$QQQL,\ QQ\bar{u}^c\bar{e}^c,\ QL\bar{u}^c\bar{d}^c,\ \bar{u}^c\bar{d}^c\bar{u}^c\bar{e}^c. \tag{2.39}$$

Hence, they can trigger proton decay via the main mode $p \to e^+\pi^0$. These operators typically arise e.g. from Grand Unified Theories (GUTs) such as $SO(10)$-based GUT outlined in Sec. 3.8. Assuming the current experimental bounds on proton decay reaching approximately 10^{34} y the cut-off scale of these operators can be roughly estimated as 10^{16} GeV. Consequently, the new physics is again either very high, or it conserves baryon and lepton number.

Another interesting group of dimension-6 operators are those violating lepton flavour, i.e. those that conserve the total lepton number, but violate the individual lepton number of a given generation. Although lepton flavour violation (LFV) is present in the SM in the form of neutrino oscillations, an analogous process for charged leptons is highly suppressed. Therefore, searches for charged LFV can put constraints on new physics. The processes with the highest experimental sensitivities are the rare muon decays $\mu \to e\gamma$, $\mu \to eee$ and $\mu - e$ conversion in nuclei. Operators triggering these processes are of the form $\mathcal{O}_{\ell\ell\gamma} = \bar{L}_\ell \sigma^{\mu\nu} \bar{\ell}^c H F_{\mu\nu}$ and $\mathcal{O}_{\ell\ell qq} = (\bar{\ell}\,\Pi_1 \ell)(\bar{q}\,\Pi_2 q)$ (Π_i stand for possible Lorentz structures) with $\ell = e, \mu, \tau$. The corresponding cut-off scales lie in the range $10^4 - 10^6$ GeV. We discuss these operators briefly in the context of this work in Sec. 6.4.

Operators of higher dimensions can be of phenomenological interest as well. In Chap. 5 we concentrate on operators violating lepton number by two units, relevant for $0\nu\beta\beta$ decay and Majorana neutrino mass. Interestingly, they appear only at odd dimension in SMEFT, as has been proven in Ref. [79]. In this work we will study $\Delta L = 2$ SM effective operators of dimension 7, 9 and a selection of dimension-11 operators, which are listed in Tabs. 5.1, 5.2 and 5.3, respectively.

3

The ν Physics

As the above issues in contemporary particle physics problems suggest, physics beyond the Standard Model is a rich field with many interesting research topics that could be discussed in more detail. Considering the subject of this thesis, let us concentrate on possible ways in which neutrino physics can pave a path beyond the SM.

The key role in our current understanding of neutrinos has been played by the observation of neutrino oscillations. The neutrinos' flavour change was established by experiments studying the flux of low-energy electron neutrinos coming from the Sun and since then this phenomenon has been confirmed and further studied by a number of other collaborations [8–10]. As the SM predicts the electron, muon and tauon lepton numbers to be separately conserved, neutrino oscillations provide a clear and solid evidence of its failure. A different description of neutrinos is necessary - neutrino masses must be introduced.

3.1 Weyl: "Dirac or Majorana?"

The SM neutrinos are Weyl fermions by their nature, i.e. they can be represented by Weyl spinors. If the three known flavour states are labelled by $|\nu^\ell(\mathbf{p}, h)\rangle$ with $\mathbf{p}$ and h being their momentum and helicity, respectively, then only the states with $h = -\frac{1}{2}$ are possible in the SM, as existence of only left-handed neutrinos is assumed. Every local Lorentz-invariant quantum field theory must be invariant under the combined charge-parity-time (CPT) transformation. Therefore, the CPT-conjugates of the left-handed neutrinos,

$$|\bar{\nu}^\ell(\bar{\mathbf{p}}, \bar{h})\rangle = CPT|\nu^\ell(\mathbf{p}, h)\rangle, \tag{3.1}$$

exist in the SM and describe the right-handed antineutrinos with $\bar{\mathbf{p}} = \mathbf{p}$, $\bar{h} = -h$.

However, for massive neutrinos (and fermions in general) helicity is not a good quantum number for its dependence on the reference frame. Hence, the spin direction in the particle's rest frame is used to label the states in this case

instead $|\nu^\ell(\mathbf{p}, s)\rangle$ with both values $s = \pm\frac{1}{2}$ possible. The CPT conjugation still changes $s = \pm\frac{1}{2}$ to $s = \mp\frac{1}{2}$, but since the initial neutrino has both signs of s, one cannot distinguish it decisively from its CPT conjugate, unless there is an additional quantum number. This means that a given neutrino is its own antiparticle and it is represented by a Majorana spinor; hence, it is referred to as a Majorana neutrino.

On the other hand, if there exists an extra conserved $U(1)$ charge, it allows to distinguish the neutrino states from their CPT conjugates. In such a case it is convenient to represent neutrinos by Dirac spinors (and they are called Dirac neutrinos for simplicity) analogous to the other fermions. The only difference is that the role of electric charge allowing to distinguish between charged fermion and anti-fermion is for neutral neutrinos supplied by their non-zero lepton number.

In the four-component formalism, the free-field Lagrangian for a Majorana neutrino reads

$$\mathcal{L}_M = \frac{1}{2} i\bar{\nu}_M \gamma^\mu \partial_\mu \nu_M - \frac{1}{2} M \bar{\nu}_M \nu_M \tag{3.2}$$

and the fact that a Majorana neutrino is its own antiparticle is reflected by the Majorana condition $\nu_M = \nu_M^C$. The equation obeyed by ν_M is just the standard text-book Dirac equation

$$(i\gamma^\mu \partial_\mu - M)\nu_M = 0. \tag{3.3}$$

The four-component Majorana neutrino can be expressed in terms of the two-component Weyl field as $\nu_M = (\nu_L \ \bar{\nu}_L)^T$. Note that the bar above the Weyl field ν_L denotes a Hermitian conjugation, not the Dirac conjugation, as it is in the standard four-component notation. Hence, in the usual two-component spinor notation[1] the free-field Lagrangian (3.2) for a Majorana neutrino takes the form

$$\mathcal{L}_M = i\bar{\nu}_L \bar{\sigma}^\mu \partial_\mu \nu_L - \frac{1}{2} M(\nu_L \nu_L + \bar{\nu}_L \bar{\nu}_L), \tag{3.4}$$

[1] In this work we sometimes employ the two-component spinor notation described in depth in Ref. [80] with the difference that we use a bar instead of a dagger to denote the Hermitian-conjugated (right-handed) fields, which is often the case in related literature. The unbarred spinors from the left-handed representation $(\frac{1}{2}, 0)$ of the Lorentz group carry undotted indices $\alpha, \beta, \ldots$, while the barred right-handed spinors transforming under the $(0, \frac{1}{2})$ representation carry dotted indices $\dot{\alpha}, \dot{\beta}, \ldots$. A spinor with a lowered undotted index is treated as a column vector, while a spinor with a raised undotted index is regarded as a row vector. For spinors with dotted indices it is the other way around. The lowered indices must be always contracted with raised indices (of the same type). As a common convention, descending contracted undotted indices and ascending contracted dotted indices are suppressed.

where $\bar{\sigma}^{\mu} = (\mathbb{1}_{2\times 2}, -\boldsymbol{\sigma})$ and the corresponding two-component Dirac equation reads

$$i\bar{\sigma}^{\mu\dot{\alpha}\beta}\partial_{\mu}\nu_{L\beta} - M\bar{\nu}_{L}^{\dot{\alpha}} = 0. \tag{3.5}$$

If $M = 0$, then ν_L in the above expressions describe the SM left-handed massless Weyl neutrino.

For a Dirac neutrino, one needs to add two more degrees of freedom in the form of another Weyl spinor. In the four-component notation this new right-handed neutrino state is usually denoted by N. The corresponding left-handed conjugate field is given as $N^c = C\bar{N}^T$ with C being the charge conjugation matrix. If N^c is represented by a two-component Weyl spinor, then by combining it with the two-component Weyl field ν_L one can assemble the four-component Dirac neutrino $\nu_D \equiv (\nu_L \ \bar{N^c})^T$, where the bar above N^c denotes Hermitian conjugation. Hence, the Lagrangian acquires the familiar form

$$\mathcal{L}_D = i\bar{\nu}_D\gamma^{\mu}\partial_{\mu}\nu_D - m\bar{\nu}_D\nu_D, \tag{3.6}$$

where again the bar stands for the Dirac conjugation, not for Hermitian conjugation, as it is in the two-component notation. The above expression can be equivalently written in terms of the two two-component fermion fields ν_L and N^c,

$$\mathcal{L}_D = i\bar{\nu}_L\bar{\sigma}^{\mu}\partial_{\mu}\nu_L + i\bar{N^c}\bar{\sigma}^{\mu}\partial_{\mu}N^c - m(\nu_L N^c + \bar{N^c}\bar{\nu_L}). \tag{3.7}$$

The respective free-field Dirac equations then read

$$i\bar{\sigma}^{\mu\dot{\alpha}\beta}\partial_{\mu}\nu_{L\beta} - m\bar{N^c}^{\dot{\alpha}} = 0, \quad i\bar{\sigma}^{\mu\dot{\alpha}\beta}\partial_{\mu}N^c_{\beta} - m\bar{\nu}_L^{\dot{\alpha}} = 0. \tag{3.8}$$

3.2 Neutrinos Mix

In the synopsis of the SM presented in Sec. 2.3 neutrinos are simply presumed to have zero masses, since the SM was designed in the way reflecting the experimental evidence of purely left-handed neutrinos. By relaxing this assumption, a straightforward way to construct a model with massive neutrinos allowing for lepton flavour violation arises. One can simply mimic the quark sector and include the neutrinos' right-handed counterparts into the fermionic spectrum. Then, neutrinos can also obtain their masses through the respective Yukawa couplings after symmetry breaking.

Hence, adding three flavours of right-handed neutrino singlets N transforming under the fermionic representation $\{\mathbf{1},\mathbf{1},0\}$ to the SM particle content, the new Yukawa terms read

$$\mathcal{L}_{\text{Yukawa}} \supset -\sum_{\substack{\ell=e,\mu,\tau \\ I=1,2,3}} \mathrm{y}^{\nu}_{\ell I}\bar{L}^{\ell}\tilde{H}N^{I} + \text{h.c.} \tag{3.9}$$

where $\mathrm{y}^{\nu}_{\ell I}$ are the neutrino Yukawa couplings. After the symmetry is broken, these terms give the neutrino mass terms

$$\mathcal{L}^{(\text{broken})}_{\text{Yukawa}} \supset -\sum_{\substack{\ell=e,\mu,\tau \\ I=1,2,3}} \frac{\mathrm{y}^{\nu}_{\ell I}v}{\sqrt{2}}\bar{\nu}^{\ell}_{L}N^{I} + \text{h.c.} \tag{3.10}$$

Hence, the neutrino mass matrix is given by $\mathrm{M}_{\nu} = (\mathrm{y}^{\nu}v/\sqrt{2})$ with y^{ν} denoting the matrix of neutrino Yukawa couplings. To get the actual neutrino masses, this matrix must be diagonalized. Similarly to the quark sector, the left-handed and right-handed neutrinos and charged leptons do not have to be diagonalized by the same unitary transformation (a bi-unitary transformation is employed again), which results in lepton mixing. Therefore, following the same procedure as before, a unitary mixing matrix for leptons arises in the charged currents after they are expressed in the mass eigenbasis. This mixing matrix is known as Pontecorvo-Maki-Nakagawa-Sakata (PMNS) matrix and it relates the flavour neutrino eigenstates ν^{ℓ} ($\ell = e,\mu,\tau$) to the mass neutrino eigenstates ν^{i} ($i = 1,2,3$) as follows

$$\begin{pmatrix}\nu^{e}\\ \nu^{\mu}\\ \nu^{\tau}\end{pmatrix} = V_{\text{PMNS}}\begin{pmatrix}\nu^{1}\\ \nu^{2}\\ \nu^{3}\end{pmatrix} = \begin{pmatrix}V_{e1} & V_{e2} & V_{e3}\\ V_{\mu 1} & V_{\mu 2} & V_{\mu 3}\\ V_{\tau 1} & V_{\tau 2} & V_{\tau 3}\end{pmatrix}\begin{pmatrix}\nu^{1}\\ \nu^{2}\\ \nu^{3}\end{pmatrix}. \tag{3.11}$$

As a result, in the weak charged currents (CC), it is not the neutrino mass eigenstate, that interacts with the charged lepton of a specific flavour, but it is a superposition of neutrino mass eigenstates given by the PMNS matrix,

$$\mathcal{L}_{CC} \supset \frac{g}{\sqrt{2}}\sum_{\ell=e,\mu,\tau}\bar{\ell}_{L}\gamma^{\mu}W^{-}_{\mu}\nu^{\ell}_{L} + \text{h.c.} = \frac{g}{\sqrt{2}}\sum_{\substack{\ell=e,\mu,\tau \\ i=1,2,3}}\bar{\ell}_{L}\gamma^{\mu}W^{-}_{\mu}V_{\ell i}\nu^{i}_{L} + \text{h.c.}. \tag{3.12}$$

In analogy to the quark CKM matrix, thanks to the freedom given by arbitrary phase redefinitions of the lepton fields, the PMNS matrix can be conveniently parametrized by only four physical parameters - three mixing angles θ_{12},θ_{13},

$\theta_{23} \in [0, \frac{\pi}{2}]$ and one (Dirac) CP-violating phase $\delta^l_{CP} \in [0, 2\pi]$. Explicitly, the parametrization reads

$$V^{(\mathrm{Dirac})}_{\mathrm{PMNS}} = \begin{pmatrix} c_{12}c_{13} & s_{12}c_{13} & s_{13}e^{-i\delta^l_{CP}} \\ -s_{12}c_{23} - c_{12}s_{13}s_{23}e^{i\delta^l_{CP}} & c_{12}c_{23} - s_{12}s_{13}s_{23}e^{i\delta^l_{CP}} & c_{13}s_{23} \\ s_{12}s_{23} - c_{12}s_{13}c_{23}e^{i\delta^l_{CP}} & -c_{12}s_{23} - s_{12}s_{13}c_{23}e^{i\delta^l_{CP}} & c_{13}c_{23} \end{pmatrix}, \tag{3.13}$$

where the short-hand notation $s_{ij} \equiv \sin\theta_{ij}$ and $c_{ij} \equiv \cos\theta_{ij}$ is used.

Besides this straightforward approach of "copying the quark sector", one could also deal with neutrino masses in a very minimalistic way - without assuming any new neutrino states besides the three SM ones. If that is the case, the previous discussion implies neutrinos must be their own antiparticles; hence, they are Majorana fermions with a Majorana mass term.

If only this term is present, then neutrino masses are given by the corresponding Majorana mass matrix, which is symmetric. As implied before, the extension of the SM Lagrangian by this violates the lepton number. This is obvious considering that there is no way how to distinguish between neutrino and antineutrino; therefore, the corresponding lepton number cannot be defined.

The actual neutrino masses are again obtained by diagonalization of the mass matrix, which again results in lepton mixing and introduction of the PMNS matrix. Although the Majorana mass matrix is symmetric (thus, it has fewer independent components), more parameters are needed in the respective mixing matrix, because in this case only the charged lepton fields can be rephased. Rephasing Majorana neutrinos would make their masses complex. Consequently, in the Majorana case there are 3 physical CP-violating phases instead of a single one and the PMNS matrix can be parametrized as

$$V^{(\mathrm{Majorana})}_{\mathrm{PMNS}} = V^{(\mathrm{Dirac})}_{\mathrm{PMNS}} P = V^{(\mathrm{Dirac})}_{\mathrm{PMNS}} \begin{pmatrix} e^{i\rho} & 0 & 0 \\ 0 & 1 & 0 \\ 0 & 0 & e^{i\sigma} \end{pmatrix}, \tag{3.14}$$

where ρ and σ are the Majorana phases, but various conventions are used for P in literature [81]. Without loss of generality the range of these phases can be restricted to $\rho, \sigma \in [0, \pi]$.

3.3 Neutrinos Oscillate

The only experimental proof of the described lepton mixing are neutrino oscillations. The standard theoretical description of this phenomenon presented in the following text involves a number of simplifications, but it leads to the correct result. Starting at time $t = 0$ with a neutrino flavour eigenstate created in a charged current process, it can be expanded in terms of neutrino mass eigenstates using the above described PMNS mixing matrix, for which the short-hand notation $V \equiv V_{\mathrm{PMNS}}$ will be used in the following, i.e. one can write

$$|\nu(t=0)\rangle \equiv |\nu^\ell\rangle = \sum_i V^*_{\ell i}|\nu^i\rangle, \tag{3.15}$$

where the complex conjugation of the mixing matrix elements comes from the fact that the corresponding states are created by conjugate fields $\bar{\nu}^i$ acting on the vacuum. The mass eigenstates are also eigenstates of the Hamiltonian in vacuum (having definite energies) and as such they evolve in time as

$$|\nu(t)\rangle = \sum_i V^*_{\ell i} e^{-iE_i t}|\nu^i\rangle, \tag{3.16}$$

where $E_i = \sqrt{p^2 + m_i^2}$ is the energy of the eigenstate ν^i with m_i being the corresponding mass and p the momentum. Making the assumption of considering ultra-relativistic neutrinos, the energy can be well approximated by the expression

$$\sqrt{p^2 + m_i^2} \approx p + \frac{m_i^2}{2p} + p\,\mathcal{O}\left(\frac{m_i^4}{p^4}\right). \tag{3.17}$$

From the above it follows that at a given time t the evolved neutrino state can be expressed as a superposition of flavour eigenstates

$$|\nu(t)\rangle = \sum_i V^*_{\ell i} e^{-iE_i t} \sum_{\ell'} V_{\ell' i}|\nu^{\ell'}\rangle, \tag{3.18}$$

where ℓ' is the flavour of the neutrino detected after time t. Therefore, the probability of neutrino oscillation between flavour eigenstates ℓ and ℓ' reads

$$\begin{aligned} P(\nu^\ell \to \nu^{\ell'}) = |\langle\nu^{\ell'}|\nu(t)\rangle|^2 &= \left|\sum_i V^*_{\ell i} V_{\ell' i} e^{-iE_i t}\langle\nu^{\ell'}|\nu^{\ell'}\rangle\right|^2 \\ &= \sum_{i,j} V^*_{\ell i} V_{\ell' i} V_{\ell j} V^*_{\ell' j} e^{-i(E_i - E_j)t} \end{aligned} \tag{3.19}$$

and employing Eq. (3.17) the following result can be obtained

$$P(\nu^\ell \to \nu^{\ell'}) = \delta_{\ell\ell'} - 4\sum_{i<j} \mathrm{Re}\left[V^*_{\ell i} V_{\ell' i} V_{\ell j} V^*_{\ell' j}\right] \sin^2\left(\frac{\Delta m^2_{ij} L}{4E}\right) + 2\sum_{i<j} \mathrm{Im}\left[V^*_{\ell i} V_{\ell' i} V_{\ell j} V^*_{\ell' j}\right] \sin\left(\frac{\Delta m^2_{ij} L}{2E}\right), \tag{3.20}$$

where the approximation $p \approx E$ and $t \approx L$ valid for ultra-relativistic neutrinos was used - L is the distance between the two points of production and detection.

From Eq. (3.20) it is apparent that for oscillations to be possible neutrinos must have non-degenerate masses, which means that for three neutrinos there must be at least two with non-zero mass. At the same time, the flavour mixing must be non-trivial, i.e. $V \neq \mathbb{1}$. Although the oscillation probability depends on all three mixing angles $\theta_{12}, \theta_{13}, \theta_{23}$ and the Dirac CP-violating phase, it does not depend on the Majorana phases appearing in diagonal matrix P. This is due to the fact that the PMNS mixing matrix appears in Eq. (3.20) always in products of the form $V_{\ell j} V^*_{\ell' j}$. Consequently, the phenomenon of neutrino oscillations does not distinguish between the Dirac and Majorana nature of neutrinos, as the same probabilities are obtained for both options. A possible way how to distinguish, whether neutrinos are Dirac or Majorana fermions, would be an observation of a lepton number violating process, which will be discussed later on.

The combination of matrices $V^*_{\ell i} V_{\ell' i} V_{\ell j} V^*_{\ell' j}$ is real only in case that $\ell = \ell'$, which means that

$$P(\nu^\ell \to \nu^\ell) = 1 - 4\sum_{i<j} |V_{\ell i} V_{\ell j}|^2 \sin^2\left(\frac{\Delta m^2_{ij} L}{4E}\right) = P(\bar{\nu}^\ell \to \bar{\nu}^\ell). \tag{3.21}$$

Hence, CP symmetry is preserved in survival experiments, i.e. when the flavours of the produced neutrino and of the neutrino detected at distance L are the same. On the other hand, CP violation, i.e. a process, for which $P(\nu^\ell \to \nu^{\ell'}) \neq P(\bar{\nu}^\ell \to \bar{\nu}^{\ell'})$, can be observed in appearance channels (when $\ell \neq \ell'$).

The formula (3.20) describes neutrino oscillations for the case of three flavours and as such it includes subleading and CP-violation effects. However, for the effective description of this phenomenon consideration of only two-flavour scenario turns out to be substantial, as it gives a good description of many neutrino oscillation experiments. In case of two neutrino flavours, the corresponding mixing matrix is real (i.e. there is no CP-violating phase) and can be parametrized by a single mixing angle θ (an equivalent of the Cabibbo angle parametrizing the

mixing of two quark generations) as follows

$$V_{\mathrm{PMNS}}^{(N_f=2)} = \begin{pmatrix} \cos\theta & \sin\theta \\ -\sin\theta & \cos\theta \end{pmatrix}. \tag{3.22}$$

The resulting oscillation probability (for $\ell \neq \ell'$) then reads

$$P^{(N_f=2)}(\nu^\ell \to \nu^{\ell'}) = \sin^2(2\theta)\sin^2\left(\frac{\Delta m_{ij}^2 L}{2E}\right). \tag{3.23}$$

Since the mixing matrix in Eq. (3.22) is real, the CP-symmetry is clearly preserved in the 2-flavour case and $P^{(N_f=2)}(\nu^\ell \to \nu^{\ell'}) = P^{(N_f=2)}(\bar{\nu}^\ell \to \bar{\nu}^{\ell'})$.

Neutrinos propagating through a dense medium like the Sun or the Earth experience the coherent elastic forward scattering from the particles they meet, which can significantly impact the oscillation probability. The influence of matter on the neutrino flavour changes has been described by Mikhaev, Smirnov and Wolfenstein, and thus it is usually referred to as the MSW mechanism [82, 83]. The key feature behind this effect is that electron neutrinos and antineutrinos interact with matter in a different way than other flavours. Specifically, ν^μ and ν^τ scatter off electrons only via neutral currents, whereas ν^e can have both neutral and charged current interactions with electrons. This leads to an additional term in the corresponding potential, namely

$$V = \pm\sqrt{2}G_F n_e, \tag{3.24}$$

where G_F is the Fermi constant, n_e denotes the number density of electrons and the sign is positive for neutrinos, while negative for antineutrinos. Due to this sign, the oscillation probabilities for neutrinos and antineutrinos can differ as a result of the MSW effect.

Considering for simplicity again only two neutrino generations, ν^e and ν^μ, and a constant matter density, the resulting formula for the oscillation probability of neutrinos in matter has an analogous form as in vacuum

$$P(\nu^e \to \nu^\mu) = \sin^2(2\theta_m)\sin^2\left(\frac{\Delta m_m^2 L}{4E}\right), \tag{3.25}$$

but now it depends on the modified mass difference Δm_m^2 and mixing angle θ_m. Hence, observations over long-baselines (large L) should yield significant matter effects. Most importantly, for a particular setting of the parameters a resonance of the oscillation probability occurs in the matter case. Since its presence depends on the sign of Δm^2, this phenomenon can be used to determine the neutrino mass ordering discussed in the following section.

3.4 Probing Neutrino Mass and Mixing

At present, most of our knowledge of the neutrinos' comes from neutrino oscillation experiments. In the usual convention, the observations of neutrinos from the Sun yield the angle θ_{12} and the mass difference $\Delta m^2_{\rm sol} \equiv \Delta m^2_{21} = m^2_2 - m^2_1$. The angle θ_{23} and the relative mass $\Delta m^2_{\rm atm} \equiv |m^2_{23}| = |m^2_2 - m^2_3|$ then can be determined based on measurements of atmospheric neutrinos, or also long-baseline accelerator neutrinos. The complementing angle θ_{13} and mass scale Δm^2_{31} can be obtained from short-baseline reactor neutrino experiments, or from long-baseline $\nu_\mu \to \nu_e$ oscillations. Since 10^{-3} eV$^2 \approx \Delta m^2_{\rm sol} \equiv \Delta m^2_{21} \gg \Delta m^2_{31} \simeq |\Delta m^2_{32}| \equiv |\Delta m^2_{\rm atm}| \approx 10^{-5}$ eV^2, the full Eq. (3.20) can be indeed well-approximated by Eq. (3.23). The actual values of all mixing parameters can be found e.g. in Ref. [84], where a global fit of experimental oscillation data is performed. As the sign of $\Delta m^2_{\rm atm}$ is not measured, yet, two different orderings of the neutrino mass eigenstates can be thought of. If ν_1 denotes the neutrino having the largest ν_e component and ν_3 is the one with the smallest ν_e contribution (see Fig. 3.1), then the three masses can be ordered either as $m_1 < m_2 < m_3$, or as $m_3 < m_1 < m_2$. These two scenarios generally correspond to the existence of either one, or two heavier mass states, respectively, which would have important consequences for the neutrino models. The first mass ordering with $\Delta m^2_{\rm atm} > 0$ is usually referred to as *normal hierarchy* (NH), while $\Delta m^2_{\rm atm} < 0$ corresponds to *inverted hierarchy* (IH). Both possibilities are illustrated in Fig. 3.1, where the notation used for the atmospheric mass is $\Delta m^2_{\rm atm} = \Delta m^2_{32}({\rm NH}) = \Delta m^2_{13}({\rm IH})$ for the two orderings, respectively. Given the smallest neutrino mass is known, the other two larger masses can be for individual hierarchies determined as

$$m_2({\rm NH}) = \sqrt{m^2_1 + \Delta m^2_{\rm sol}}, \quad m_2({\rm IH}) = \sqrt{m^2_3 + \Delta m^2_{\rm sol} + \Delta m^2_{\rm atm}}, \tag{3.26}$$

$$m_3({\rm NH}) = \sqrt{m^2_1 + \Delta m^2_{\rm sol} + \Delta m^2_{\rm atm}}, \quad m_1({\rm IH}) = \sqrt{m^2_3 + \Delta m^2_{\rm atm}}. \tag{3.27}$$

The absolute neutrino mass scale remains unknown, which in the limit when all of the masses are relatively large leads to the quasi-degenerate scheme, i.e. for $m^2_1 \simeq m^2_2 \simeq m^2_3 \gg \Delta m^2_{\rm atm}$. On the other hand, if the lightest mass is very small the relative sizes of neutrino masses for the two hierarchies read

$$m_1({\rm NH}) \ll m_2({\rm NH}) \simeq \sqrt{m^2_{\rm sol}} \ll m_3({\rm NH}) \simeq \sqrt{m^2_{\rm atm}}, \tag{3.28}$$

$$m_3({\rm IH}) \ll m_1({\rm IH}) \simeq \sqrt{m^2_{\rm atm}} \simeq m_2({\rm IH}). \tag{3.29}$$

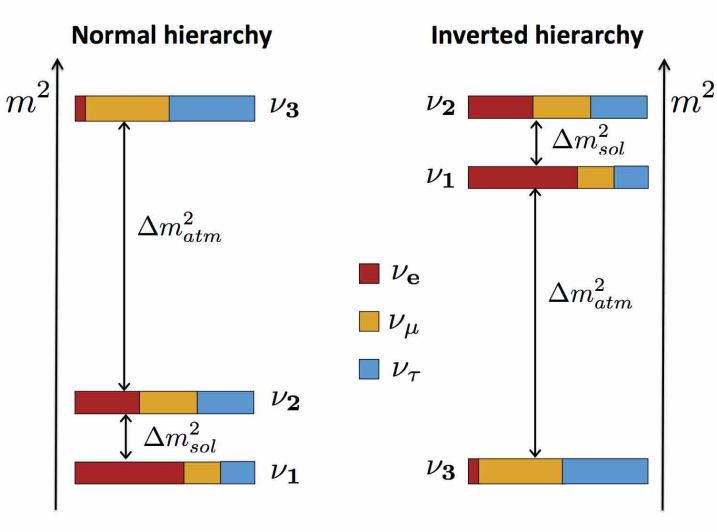

Figure 3.1: The normal (left) and inverted (right) hierarchy of neutrino mass eigenstates taken from [85]. The contributions of individual flavour eigenstates to particular mass eigenstates are represented by the colour bands.

The identification of the actual neutrino mass hierarchy realized in Nature should by achieved by current or upcoming neutrino oscillation experiments. Intriguingly, some of the oscillation measurements hint presence of additional, sterile neutrinos at low energies. Most recently, a 4.8σ excess has been reported by the MiniBooNE collaboration [86], which when combined with previous data from LSND experiment [87] yields 6.1σ deviation from the standard oscillation model. On the other hand, cosmological observations favour the existence of only three SM neutrino generations [88].

The absolute neutrino mass scale could be determined by measurements of the energy distribution of electrons in beta decay, as the non-zero neutrino mass would impact the kinematical endpoint of the spectrum. Namely, it would cause a downward deflection from the straight-line Kurie plot corresponding to vanishing neutrino mass. The functional dependence of the spectrum reads

$$\frac{\mathrm{d}N_e}{\mathrm{d}E_e} = (E_e - Q)\sqrt{(E_e - Q)^2 - m_\beta^2}, \tag{3.30}$$

where the Q-value of the decay appears, E_e is the electron energy and the neutrino mass parameter

$$m_\beta = \sqrt{\sum |V_{ei}|^2 m_i^2} \tag{3.31}$$

can be determined from the observed curve. The current upper limit on absolute

neutrino mass given by tritium decays is 2 eV at 95% C.L. [89]. The next generation experiment, KATRIN [12], is expected to reach the sensitivity of $m_\beta = 0.2$ eV at 90% C.L. and 5σ discovery potential of $m_\beta = 0.35$ eV.

Detectable imprints of neutrinos are left in a number of different astrophysical and cosmological observations, which can in consequence provide information on neutrino properties. Hence, another constraint on neutrino masses can be obtained from astrophysics and cosmology, particularly thanks to the neutrinos' effects in cosmic structure formation. The corresponding measurements are sensitive to the total sum of masses of all active neutrinos, $\sum m_i$. The currently best limits are based on Cosmic Microwave Background (CMB) data collected by the Planck collaboration [90]. However, apart from CMB experiments, upper bounds on $\sum m_i$ can be set for instance also from large scale structure surveys, Hubble constant measurements, high-redshift Type-I supernovae observations, or baryon acoustic oscillations measurements. A recent thorough analysis [11] combining a number of effects yields the upper limit $\sum m_i \lesssim 0.17$ eV.

Another possibility to probe neutrino masses (and not only that) is to search for neutrinoless double beta ($0\nu\beta\beta$) decay. As this work focuses mostly on aspects of this hypothetical nuclear process, we will review it in more detail in the next section.

3.5 Neutrinoless Double Beta Decay

Generally, a process of nuclear double beta decay can be considered

$$(A, Z) \to (A, Z+2) + 2e^- \text{ (+ missing energy)}, \tag{3.32}$$

in which a nucleus with A nucleons and Z protons transitions to another one with two more protons and the same nucleon number by emission of two electrons and possibly other light particles. In the most standard case, these light particles are two antineutrinos and the process is a simple 'double copy' of the standard beta decay, cf. Eq. 2.1, which is referred to as two-neutrino double beta ($2\nu\beta\beta$) decay. This process has been experimentally observed and the measured half-lives are in the range $10^{19} - 10^{21}$ y, depending on the isotope [91–93]. Alternatively, a nuclear double positron ($\beta^+\beta^+$) decay leading to a daughter nucleus $(A, Z-2)$ can be also thought of.

If there are no neutrinos on the right-hand side of Eq. (3.32), the process is

called neutrinoless double beta decay [94], which mostly[2] refers to

$$(A, Z) \rightarrow (A, Z + 2) + 2e^{-}. \tag{3.33}$$

Hence, from the particle physics perspective $0\nu\beta\beta$ decay is a simultaneous conversion of two neutrons to two protons, two electrons and no other particle, which makes it very interesting. Since there are only two leptons emitted and no antileptons, this process clearly violates lepton number by two units. Consequently, as will be argued in Subsec. 3.5.2, it requires the Majorana nature of neutrinos representing one of the best probes of this BSM hypothesis. As a result, a strong experimental effort is being made to observe this unique process. Unfortunately, even if $0\nu\beta\beta$ decay really exists in Nature, its observation will be very difficult, as it is predicted to be extremely rare - the current experimental lower limits on its half-life are around 10^{26} y. Moreover, it must be distinguished from the mentioned two-neutrino double beta decay, which is significantly more probable. Various aspects of $0\nu\beta\beta$ decay have been covered in detailed reviews [95, 96].

3.5.1 Experimental View

The construction of an experiment capable of detecting a nuclear process with such an extremely long half-life is a major challenge. In case of $0\nu\beta\beta$ decay there are several significant issues that must be dealt with. Primarily, as only specific nuclei can double beta decay, a large mass of a typically scarce isotope is needed. If the law of radioactive decay is used in the (in this case very well justified) approximation $T_{1/2} \gg t$, then the expected number of events N in a $0\nu\beta\beta$ decay experiment in time t reads

$$N = \log_e(2) \frac{\varepsilon N_A}{W} \, a \, M \, \frac{t}{T_{1/2}^{0\nu\beta\beta}}, \tag{3.34}$$

where ε is the experimental signal detection efficiency and N_A, a, W and M are the Avogadro's number, natural isotopic abundance of the parent nuclide, atomic weight of the given isotope and the isotope mass, respectively. Even if no background and perfect signal detection is assumed, then considering a $0\nu\beta\beta$ decay half-life $T_{1/2} \approx 10^{26}$-10^{27} y, hundreds of kilograms of the isotope are necessary in order to get only a single event a year. This is further complicated by $2\nu\beta\beta$ decay events representing an intrinsic background that can be discriminated

[2]Note that additional particles other than neutrinos can still be emitted. A typical example is the emission of Majoron.

Experiment	Isotope	Status	M [kg]	$T_{1/2}^{0\nu\beta\beta}$ limit [y]
CUORE	^{130}Te	running	200	(3.5×10^{26})
EXO-200	^{136}Xe	running	110	1.1×10^{25}
nEXO	^{136}Xe	R&D	5000	$(10^{27}$-$10^{28})$
GERDA	^{76}Ge	running	21.6	5.3×10^{25}
		in progress	40	$(\sim 10^{26})$
KamLAND-Zen	^{136}Xe	running	383	1.1×10^{26}
		in progress	600	(2×10^{26})
LEGEND	^{76}Ge	R&D	200	$(\sim 10^{27})$
		R&D	1000	$(\sim 10^{28})$
Majorana Dem.	^{76s}Ge	running	44.1	1.9×10^{25}
NEXT	^{136}Xe	in progress (demo)	100	(5.9×10^{25})
SNO+	^{130}Te	in progress	1300	(2×10^{26})
SuperNEMO	^{82}Se (^{150}Nd)	in progress (demo)	100	$(\sim 10^{26})$

Table 3.1: An overview of major $0\nu\beta\beta$ decay searches, both current and future. For each experiment the following information is shown: used isotope, operational status, the deployed mass M of the isotope in question and the measured or expected (for experiment in preparation these values are shown in parentheses) sensitivity $T_{1/2}^{0\nu\beta\beta}$. For some experiments (GERDA, KamLAND-Zen, LEGEND) characteristics of more stages of development are given. In case of SuperNEMO, the primary isotope to be tested is ^{82}Se and in future the measurement will be repeated with a ^{150}Nd source.

from the $0\nu\beta\beta$ decay events only by measurement of the energy of the emitted electrons, as the outgoing neutrinos are undetectable. Moreover, the narrow peak of $0\nu\beta\beta$ decay in the obtained energy spectrum can be overlapped by the tail of the peak corresponding to $2\nu\beta\beta$ decay, which places demands on the energy resolution of the experiment. Besides that, there are other factors that must be taken into account, when the convenient experimental approach is to be chosen. However, no optimal solution of all the related problems exists resulting in a variety of $0\nu\beta\beta$ decay experiments, some in operation, other being constructed or planned, see Tab. 3.1 for a list of the major collaborations.

One of the most important characterizations of each $0\nu\beta\beta$ decay search is the used isotope. In order to be able to study $0\nu\beta\beta$ decay experimentally, an even-even (i.e. nuclei with even proton and neutron numbers) isotope must be chosen,

for which single beta decay is energetically forbidden, or at least suppressed by respective selection rules. In Nature there are about thirty-five different even-even nuclei that can undergo a double beta decay. The experimentally most favourable ones for the $0\nu\beta\beta$ decay quest can be selected on a basis of a number of criteria.

Naturally, one is in particular interested in factors that can improve the resulting decay rate; the general formula can be written in a factorized form

$$\Gamma_{0\nu\beta\beta} = |\lambda\,\mathcal{M}(A,Z)|^2 G(Q,Z), \tag{3.35}$$

where the particle physics playing a role in the decay enters in form of the parameter λ, $\mathcal{M}(A,Z)$ is the nuclear matrix element (NME) and $G(Q,Z)$ is the corresponding phase-space factor (PSF). The NMEs as such differ for different nuclei (although not too dramatically) and mechanisms triggering the decay. Similarly, the involved PSF depends on the isotope and also on the particle physics involved. It can be also shown that it varies with the fifth power of the $Q_{\beta\beta}$ value,

$$Q_{\beta\beta} = E_I - E_F - 2m_e, \tag{3.36}$$

where m_e denotes the electron mass and E_I and E_F are the energies of the initial and final nuclei. Consequently, the decay rate is significantly enhanced in case of isotopes with high values of $Q_{\beta\beta}$, which makes them favourable for $0\nu\beta\beta$ decay searches. Usually, one of the eleven isotopes in Nature with $Q_{\beta\beta} > 2$ MeV is considered. A high value of $Q_{\beta\beta}$ is useful also for another reason - the background of natural radioactivity drops significantly above ~ 3 MeV, which makes it much easier to control. For a similar reason, isotopes with a slow two neutrino mode are desirable.

There are also other features favouring specific nuclei like natural abundance, price of enrichment or good understanding of the nuclear physics of the given isotope. Nonetheless, there is no ideal isotope, which would be convenient in every of the presented aspects. Different isotopes have different advantages and disadvantages, which is also why the isotopes employed in current or planned experiments vary. Most attention is paid to the eight nuclei

$$^{48}\mathrm{Ca}, ^{76}\mathrm{Ge}, ^{82}\mathrm{Se}, ^{100}\mathrm{Mo}, ^{116}\mathrm{Cd}, ^{130}\mathrm{Te}, ^{136}\mathrm{Xe}, ^{150}\mathrm{Nd} \tag{3.37}$$

and their characteristics are summarized in Tab. 3.2.

In the idealized case of no background, the sensitivity of a $0\nu\beta\beta$ experiment is proportional to

$$T_{1/2}^{-1} \propto \frac{N}{\varepsilon a M t}, \tag{3.38}$$

Isotope	a [%]	$Q_{\beta\beta}$ [keV]	G [10^{-15} y^{-1}]
^{48}Ca	0.187	4273.7	24.81
^{76}Ge	7.8	2039.1	2.363
^{82}Se	9.2	2995.5	10.16
^{100}Mo	9.6	3035.0	15.92
^{116}Cd	7.6	2809.1	16.70
^{130}Te	34.5	2530.3	14.22
^{136}Xe	8.9	2457.8	14.58
^{150}Nd	5.6	3367.3	63.03

Table 3.2: A list of the most commonly studied double beta decaying isotopes and their basic characteristics: natural abundance a, the $Q_{\beta\beta}$ value and the phase-space factor G (for the standard mechanism, see Sec. 3.5.4).

where the involved quantities were defined earlier. If no event has been observed within the time t, then for $N = 1$ the expression yields an upper limit on the decay rate. However, since the background of $0\nu\beta\beta$ decay is rather non-trivial, as discussed in the above paragraphs, it must be taken into account to get a more realistic formula [97]. The number of background events in time t is given by

$$N_b = bM\Delta Et, \tag{3.39}$$

where b denotes the background rate in counts/(keV·kg·y) and ΔE is is the energy window around $Q_{\beta\beta}$ in keV. It is assumed that the background is approximately constant over the interval ΔE, which is valid unless a large ΔE is considered, as then the two-neutrino events may enter. The expression for the inverse half-life sensitivity including background behaves as

$$T_{1/2}^{-1} \propto \frac{1}{\varepsilon a}\sqrt{\frac{b\Delta E}{Mt}}. \tag{3.40}$$

Consequently, the background significantly constrains the sensitivity, as the expression (3.40) improves slowly with exposure, as $(Mt)^{-\frac{1}{2}}$, while the background-free sensitivity (3.38) is proportional to $(Mt)^{-1}$.

An overview of current and planned $0\nu\beta\beta$ decay experiments is contained in Tab. 3.1, where also the used isotopes are specified. For the reasons described in previous paragraphs, a variety of experimental approaches trying to reach the highest possible sensitivity in different ways exists. Currently, major experimental

efforts focus on $0\nu\beta\beta$ decay detection in ^{76}Ge, ^{130}Te and ^{136}Xe, but very promising experiments are being designed also for several other isotopes [98].

The high-purity Germanium detectors have the best energy resolution of all techniques used for $0\nu\beta\beta$ decay detection, which helps to reduce the background. On the other hand, their fabrication costs are high and the value of $Q_{\beta\beta}$ is lower for Germanium than for other isotopes; therefore, the experiments must be well-shielded. Currently, the leading Germanium $0\nu\beta\beta$ search is the **Germanium Detector Array (GERDA)** [99], a successor of the International Germanium Experiment (IGEX) and the Heidelberg-Moscow Experiment. It began data-taking in 2011 and presently it provides the best bound for Germanium. Another $0\nu\beta\beta$ decay experiment using Germanium is the **Majorana Demonstrator** [100], which started acquiring data in 2016 and it is able to search also for other rare events, namely axions and light WIMPs. A joint collaboration of GERDA and Majorana Demonstrator called **LEGEND (The Large Enriched Germanium Experiment for Neutrinoless Double Beta Decay)** [101] combining their know-how and resulting in a tonne-scale $0\nu\beta\beta$ decay experiment has been recently established. The anticipated sensitivity of this project is an astonishing 10^{28} years.

The advantages of the ^{130}Te isotope are the highest natural abundance reaching 34.5% and relatively high value of $Q_{\beta\beta}$ ($\sim$ 2.5 MeV). Similarly as in case of Germanium, there are two major collaborations using Tellurium as the double-beta-decaying isotope. First, there is the **Cryogenic Underground Observatory for Rare Events (CUORE)** [102], which started searching for $0\nu\beta\beta$ decay signal in TeO_2 crystals in 2017 and its expected 10-year sensitivity is 3.5×10^{26} years with background level of 0.001 counts/(keV·kg·y) [102]. Naturally, it is also used to search for other rare events. The second large Tellurium experiment is **SNO+**, an upgrade of the **Sudbury Neutrino observatory (SNO)** detector [103]. It is currently under construction and the first phase of data-taking should start in 2019 [104, 105]. Despite a lower energy resolution, SNO+ will be able to compete with other experiments, as it will use an organic liquid scintilator, which can be loaded with large amounts of ^{130}Te.

Xenon differs from the other isotopes, since it is a scintilating noble gas and as such it allows for use of different experimental techniques. There exist three big collaborations with facilities focusing on detection of $0\nu\beta\beta$ decay in ^{136}Xe, which are in various stages of development. **KamLAND-Zen** [106] is one of them - it is an upgrade of the previous KamLAND experiment, which was designed to

measure reactor neutrino fluxes. It has the shape of a balloon containing ^{136}Xe dissolved in the liquid scintilator, which is shielded by another volume of the scintilator around it. Starting in 2011 it has completed two phases of measurement resulting in currently the best available limit on $0\nu\beta\beta$ decay and a new phase with bigger mass of the isotope is in progress [107]. The next experiment searching for $0\nu\beta\beta$ decay in ^{136}Xe is the **Enriched Xenon Observatory (EXO)** [108]. It uses pure enriched Xenon both as source and detector and the first phase called EXO-200 began in 2011. The proposed new version of this experiment, nEXO [109], seems to be very promising, as the recent report [110] quotes an expected discovery sensitivity at 3σ of $T^{\mathrm{Xe}}_{1/2} = 4.1 \times 10^{27}$ y. The third Xenon $0\nu\beta\beta$ search to mention is called **Neutrino Experiment with a Xenon TPC (NEXT)** [111]. As the name suggests, this experiment uses enriched gaseous Xenon in a high-pressure time projection chamber, which implies an excellent energy resolution (better than 0.5% at 2500 keV) and availability of a topological signature. Presently, the 10-kg demonstrator NEW is in operation and the second phase of the experiment, NEXT-100, will be deployed in 2019.

In all of the above described experiments the source plays the role of the detector at the same time (source = detector experiments). However, there are also $0\nu\beta\beta$ searches with separate source and detector, e.g. **SuperNEMO** [112], which is currently testing its first module, the SuperNEMO demonstrator. The biggest advantages of this experiment are the possibility of probing multiple isotopes and, similarly as in case of NEXT, the ability to track the emitted electrons using the track calorimeter technique, which was established by the preceding experiment, NEMO-3.

To sum up, the most stringent bounds on $0\nu\beta\beta$ decay are currently from ^{76}Ge [113] and ^{136}Xe [114], which read, respectively,

$$T^{\mathrm{Ge}}_{1/2} \equiv T_{1/2}\left({}^{76}_{44}\mathrm{Ge} \to {}^{76}_{42}\mathrm{Se} + e^- e^-\right) > 5.3 \times 10^{25}\ \mathrm{y}, \tag{3.41}$$

$$T^{\mathrm{Xe}}_{1/2} \equiv T_{1/2}\left({}^{136}_{54}\mathrm{Xe} \to {}^{136}_{56}\mathrm{Ba} + e^- e^-\right) > 1.1 \times 10^{26}\ \mathrm{y}, \tag{3.42}$$

at 90% confidence level (CL). The largest planned future experiments searching for $0\nu\beta\beta$ decay are expected to reach sensitivities of the order of $T_{1/2} \approx 10^{27}$ y.

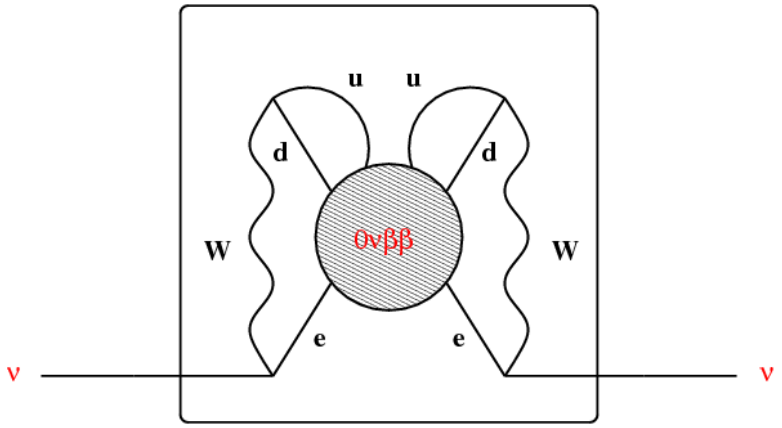

Figure 3.2: The black box theorem depicted diagrammatically, taken from Ref. [115].

3.5.2 Black Box Theorem

As mentioned above, $0\nu\beta\beta$ decay is tightly related to the Majorana nature of neutrinos. In fact, the equivalence

$$\text{Neutrinos have Majorana mass} \iff 0\nu\beta\beta \text{ decay exists} \tag{3.43}$$

holds and it can be very easily understood in effective terms. The implication that a nonzero Majorana neutrino mass automatically means that it is possible to trigger $0\nu\beta\beta$ decay can be verified from the fact that the effective Majorana mass dimension-3 operator (in the two-component formalism)

$$\mathcal{O}_\nu = \nu_L \nu_L \tag{3.44}$$

can be always extended to give the $0\nu\beta\beta$ decay diagram in Fig. 1.1 by attachment of the SM vertices. The converse of this statement then simply relies on the opposite use of the same SM rules to connect all the external legs of the effective $0\nu\beta\beta$ decay operator of dimension 9

$$\mathcal{O}_{0\nu\beta\beta} = \bar{e}^c \bar{e}^c d^c d^c \bar{u}^c \bar{u}^c \tag{3.45}$$

back together to give only neutrinos; thus, reconstructing the effective Majorana mass operator. The latter implication is known as Schechter-Valle, or black-box, theorem [116–118], which is graphically shown in Fig. (3.2). Consequently, if $0\nu\beta\beta$ decay is observed, this contribution to neutrino mass will always be induced. Nonetheless, it must be noted that it is highly suppressed by the four-loop factor and the W-boson propagators. A back-of-the-envelope estimate yields

the Majorana mass

$$m_{ee}^{\nu} \approx \left(\frac{1}{16\pi^2}\right)^4 \frac{1}{m_W^4} \text{ MeV}^5 \simeq 10^{-23} \text{ eV}, \tag{3.46}$$

where m_W is the mass of W boson and MeV is the typical energy of the fermions e, u, d taking part in the decay. The obtained number is obviously too tiny to be experimentally testable. Therefore, the experimental evidence of the $0\nu\beta\beta$ decay would not necessarily mean that it is related to the origin of the light neutrino mass. Although the possibility that $0\nu\beta\beta$ decay is triggered directly by the light neutrinos or their heavy counterparts entering the type-I seesaw mechanism is the best motivated one, the source of lepton number violation (LNV) can be completely different. It is even possible to imagine a situation, when the above black-box contribution is the only contribution to the light neutrino mass - e.g. a model with right-handed scalar triplet and no Dirac neutrino mass terms.

3.5.3 Discriminating among Different Mechanisms

The classification of different $0\nu\beta\beta$ decay interpretations usually cited in the literature simply distinguishes between the **standard mechanism**, i.e. $0\nu\beta\beta$ decay induced by the light neutrinos (while all other possible contributions are assumed to be negligible) and so called **non-standard mechanisms**. The latter corresponds to $0\nu\beta\beta$ decay triggered by some other underlying lepton number violating operator, typically by heavy neutrinos entering some kind of seesaw mechanism, as described in Sec. 3.6. In the following, a brief review of the standard $0\nu\beta\beta$ mechanism is given and later on the attention is paid to the effective approach to the non-standard $0\nu\beta\beta$ decay mechanisms, which is the main subject of the present work. As will be discussed in Chap. 4, one can generally distinguish between long-range and short-range non-standard $0\nu\beta\beta$ decay mechanisms. While for the former, the neutrino exchange between the two nucleons must be taken into account, in the latter case one deals with a contact interaction.

For our later arguments it will be important to discriminate among different $0\nu\beta\beta$ decay mechanisms, or at least, to distinguish between the standard and the non-standard mechanisms. There are several possibilities how to do so. One can e.g. measure the energy distribution and angular correlation of the emitted electrons. In the standard mass mechanism the two electrons are preferably emitted back-to-back, which is not always the case for exotic $0\nu\beta\beta$ decay contributions. In this regards, the long-range mechanisms have been studied in detail

in Refs. [119–124]. In Chap. 4, where we focus on the short-range mechanisms, we calculate, plot and comment also on the corresponding energy and angular correlation distributions. Experimentally, it is possible to probe these distributions e.g. in the SuperNEMO experiment [112, 125].

Another test distinguishing among different $0\nu\beta\beta$ mechanisms that could be performed is the search for $0\nu\beta\beta$ decay in multiple isotopes [126–128], which motivates the development of several experiments using different nuclei. At the same time, the comparison of $0\nu\beta\beta$ decay with electron capture or $0\nu\beta^+\beta^+$ decay [129], or the comparison of $0\nu\beta\beta$ decay to the ground state and an excited state [130] could suggest the mechanism responsible for $0\nu\beta\beta$ decay.

Further, inconsistencies between the experimental results from $0\nu\beta\beta$ decay and from the determination of the sum of neutrino masses using cosmological considerations could potentially also hint at the existence of non-standard $0\nu\beta\beta$ decay contributions [131]. On top of that, LNV could be also probed by other experimental means. For instance, searches for LNV in resonant processes at high energy colliders could determine the corresponding scale more directly [132, 133].

3.5.4 The Standard (Mass) Mechanism

The standard mechanism of $0\nu\beta\beta$ decay (often called 'mass mechanism') relies on presence of the Majorana neutrino mass term induced by the operator in Eq. (3.44) in the Lagrangian $\mathcal{L}$ of given theory. In the four-component Weyl-spinor formalism this mass term reads

$$\mathcal{L}_{\text{Majorana}} = \frac{1}{2} M_\nu \left(\nu_L^T C \nu_L \right) + \text{h.c.} \tag{3.47}$$

and it can be generated in numerous ways. Typically it originates from some new, high-energy physics living at a scale Λ via some kind of a seesaw mechanism, see Sec. 3.6. However, the mass term in Eq. (3.47) can be also understood as an effective operator without need of specifying the underlying high-energy physics. At the SM level, this mass term is induced by the unique five-dimensional Weinberg operator

$$\mathcal{L}^{(5)} = \frac{C_W}{\Lambda} \varepsilon_{ij} \varepsilon_{kl} {L^i}^T C L^k H^j H^l + \text{h.c.}, \tag{3.48}$$

where C_W is the corresponding Wilson coefficient. After the electroweak symmetry breaking one gets

$$\mathcal{L}^{(5)}_{(\text{broken})} = \frac{1}{2} \frac{C_W v^2}{\Lambda} \left(\nu_L^T C \nu_L \right) + \text{h.c.}, \tag{3.49}$$

and the small masses of neutrinos $M_\nu = \frac{C_W v^2}{2\Lambda}$ are obtained for big Λ and/or small C_W. Hence, as expected, the new physics responsible for light neutrino masses must lie at high energies or it must be weakly coupled to the SM.

Using this new vertex and two $V-A$ vertices of the SM, the standard $0\nu\beta\beta$ decay mechanism is obtained, see Fig. 1.1. The corresponding transition amplitude contains the expression

$$\sum_i V_{ei}^2 \bar{e}_2 \gamma_\nu P_L \frac{\not{q} + m_i}{q^2 + m_i^2} P_L \gamma_\mu e_1^C = \sum_i V_{ei}^2 \bar{e}_2 \gamma_\nu \frac{m_i}{q^2 + m_i^2} \gamma_\mu e_1^C, \tag{3.50}$$

where $P_L = \frac{1}{2}(\mathbb{1} - \gamma_5)$ is the left-handed projector, V_{ei} are elements of the first (electron) row of the neutrino mixing matrix, m_i denotes the mass of the i-th neutrino mass eigenstate, q is the neutrino four-momentum ($q \approx 100$ MeV) and $e_{1,2}$ are the two emitted electrons in the four-component Dirac-spinor notation. The $\not{q}$ in the numerator in Eq. (3.50) drops out due to the chiral projectors. For light neutrinos the m_i^2 term in the denominator can be safely neglected,

$$\sum_i V_{ei}^2 \bar{e}_2 \gamma_\nu \frac{m_i}{q^2} \gamma_\mu e_1^C, \tag{3.51}$$

and the Majorana neutrino propagator can be understood as a 'mass insertion' rule, which corresponds to the spin flip (outgoing left-handed Majorana neutrino can be reckoned for ingoing right-handed Majorana neutrino). Obviously, it is the ratio $\frac{m_i}{q^2} \lesssim \frac{0.5 \text{ eV}}{(10^8 \text{ eV})^2}$ that strongly suppresses the $0\nu\beta\beta$ decay rate in case of the standard mechanism.

Therefore, the standard mass mechanism of $0\nu\beta\beta$ decay is sensitive to the so-called effective Majorana neutrino mass,

$$m_{ee} \equiv \sum_i V_{ei}^2 m_i, \tag{3.52}$$

where the sum is over all light neutrinos with masses m_i, weighted by the square of the elements of the mixing matrix V_{PMNS}. This quantity is equal to the (ee) entry of the Majorana neutrino mass matrix. Assuming the standard picture with three light neutrinos and employing the parametrization of the PMNS matrix given in Eq. (3.14), the effective mass is given by

$$\begin{aligned} m_{ee} &= m_1 |V_{e1}|^2 e^{2i\rho} + m_2 |V_{e2}|^2 + m_3 |V_{e3}|^2 e^{2i\sigma} \\ &= m_1 c_{12}^2 c_{13}^2 e^{2i\rho} + m_2 s_{12}^2 c_{13}^2 + m_3 s_{13}^2 e^{2i\sigma}, \end{aligned} \tag{3.53}$$

where, as before, $c_{ij} \equiv \cos\theta_{ij}$, $s_{ij} \equiv \sin\theta_{ij}$ and θ_{12}, θ_{13} are the mixing angles and ρ, σ are the Majorana CP-violating phases. Note that the Dirac CP-violating phase δ_{CP} does not enter the above expression.

Decay Rate Derivation

Using the effective mass, the inverse $0\nu\beta\beta$ decay half life for the standard mass mechanism in a given isotope reads

$$T_{1/2}^{-1} = \left|\frac{m_{ee}}{m_e}\right|^2 G_\nu |\mathcal{M}_\nu|^2, \tag{3.54}$$

where, as in the general case, G_ν is the PSF and $\mathcal{M}_\nu$ the corresponding NME of the process. The normalization with respect to the electron mass m_e yields a small dimensionless parameter $\epsilon_\nu = m_{ee}/m_e$. The standard mechanism PSFs for various isotopes are calculated in Ref. [134] and some of them are shown in Table 3.2. The NMEs can be written as

$$\mathcal{M}_\nu = \left(g_A^2 \mathcal{M}_{GT} - g_V^2 \mathcal{M}_F + g_A^2 \mathcal{M}_T\right), \tag{3.55}$$

where $\mathcal{M}_F, \mathcal{M}_{GT}$ and $\mathcal{M}_T$ are the Fermi, Gamow-Teller and Tensor NMEs, respectively. These are defined as [135]

$$\mathcal{M}_F = \langle h^F(q^2) \rangle, \tag{3.56}$$

$$\mathcal{M}_{GT} = \langle h^{GT}(q^2)(\boldsymbol{\sigma}_a \cdot \boldsymbol{\sigma}_b) \rangle, \tag{3.57}$$

$$\mathcal{M}_T = \left\langle h^T(q^2) \left[3(\boldsymbol{\sigma}_a \cdot \hat{\mathbf{r}}_{ab})(\boldsymbol{\sigma}_b \cdot \hat{\mathbf{r}}_{ab}) - (\boldsymbol{\sigma}_a \cdot \boldsymbol{\sigma}_b)\right] \right\rangle, \tag{3.58}$$

where $\boldsymbol{\sigma} = (\sigma_1, \sigma_2, \sigma_2)^T$ denotes the vector of Pauli matrices operating on the nucleon spin space and $\hat{\mathbf{r}}_{ab} = \mathbf{r}_{ab}/|\mathbf{r}_{ab}|$ is the direction unit vector between two nucleons. Further, $h^F(q^2), h^{GT}(q^2)$ and $h^T(q^2)$ are functions of the square of the neutrino three-momentum given by a product of neutrino potential originating from the propagator of the exchanged neutrino and the relevant nuclear form factors describing the momentum-distance dependence of nuclear interaction [135].

The NMEs of the nuclear $0\nu\beta\beta$ transitions are notoriously difficult to calculate and limits derived from $0\nu\beta\beta$ decay are affected for any contribution. There are several distinct nuclear structure model approaches to the calculation of the $0\nu\beta\beta$ decay NMEs. The main ones are the following: Interacting Boson Model (IBM) [135–137], Quasi-particle Random Phase Approximation (QRPA) [138–141], Nuclear Shell Model (NSM) [142,143], Energy Density Functional (EDF) [144], Relativistic Energy Density Functional (REDF) [145] and the Projected Hartree Fock Bogoliubov (PHFB) [146] model. In case of QRPA and NSM there are more independent groups working on different variants of the computation. Nonetheless, despite all the tremendous efforts to improve the nuclear

theory calculations, the latest matrix elements obtained using various approaches differ in many cases by factors of $\sim(2-3)$. Every method has its strengths and weaknesses and the discussion, which approach should be used, is ongoing and far from its end [147].

For instance, the QRPA and related methods work in large configuration spaces with many single-particle orbits included. Opposite to that, the configuration space in the NSM is usually based just on a few single-particle orbitals. On the other hand, the advantage of NSM is that all correlations around the Fermi surface are included, while the set of correlations in the QRPA is restricted. The EDF-based approach together with so called generator coordinate method (GCM) treats carefully the collective correlations, which may not be described by the NSM and the QRPA. The IBM also captures the collective motion and, being an approximation of the NSM, it shares the advantage of a large number of correlations. The price for that may be seen in a bit more phenomenological approach to nuclear structure. Based on these facts, it may be surprising that the NMEs obtained by the IBM are similar to those calculated by QRPA, but rather different from the results provided by the NSM. The reason for that is so far unclear.

Phenomenological Implications

Assuming Majorana nature of neutrinos and using the bounds on $0\nu\beta\beta$ decay half-life together with the computed values of NMEs and PSFs one can, up to some uncertainty given by the nuclear-physics input, use Eq. (3.54) to get the upper limit on the effective neutrino mass. Since the effective mass incorporates neutrino mixing, the standard mechanism of $0\nu\beta\beta$ decay is directly related to phenomenology of neutrino oscillations. Employing the measured oscillation parameters a limit on absolute neutrino mass scale can be set, too, complementing constraints from cosmology and single beta decay experiments. Naturally, this limit will depend on the considered neutrino mass hierarchy, which can be, consequently, also probed in this way. When relating the effective and absolute neutrino masses, the uncertainties of the experimentally determined parameters must be taken into account. Another complication, which affects the calculation, are the unknown CP-violating phases.

In Fig. 3.3 the effective neutrino mass in dependence on the mass of the lightest neutrinos is depicted for both normal and inverted hierarchies. The regions

in colour thus represent the parametric space allowed by data from neutrino oscillation experiments. Cosmological observations and beta decay measurements constrain the graph from the right. Searches for $0\nu\beta\beta$ decay restrict this plot from the top, as they set an upper bound on effective neutrinos mass. Specifically, the current experimental results lead to the following limit on effective neutrino mass [114]

$$|m_{ee}| \lesssim 0.06 - 0.17 \text{ eV}, \tag{3.59}$$

with an uncertainty due to the different values for NMEs calculated by various nuclear structure models.

If one considers the lightest neutrino mass to be larger than Δm^2_{12} and Δm^2_{13}, which is a setting probed by current experiments, a quasi-degenerate scheme is obtained. In this regime the limit on absolute neutrino mass $m_\nu \lesssim 0.5$ eV can be obtained from effective neutrino mass using the current experimental data.

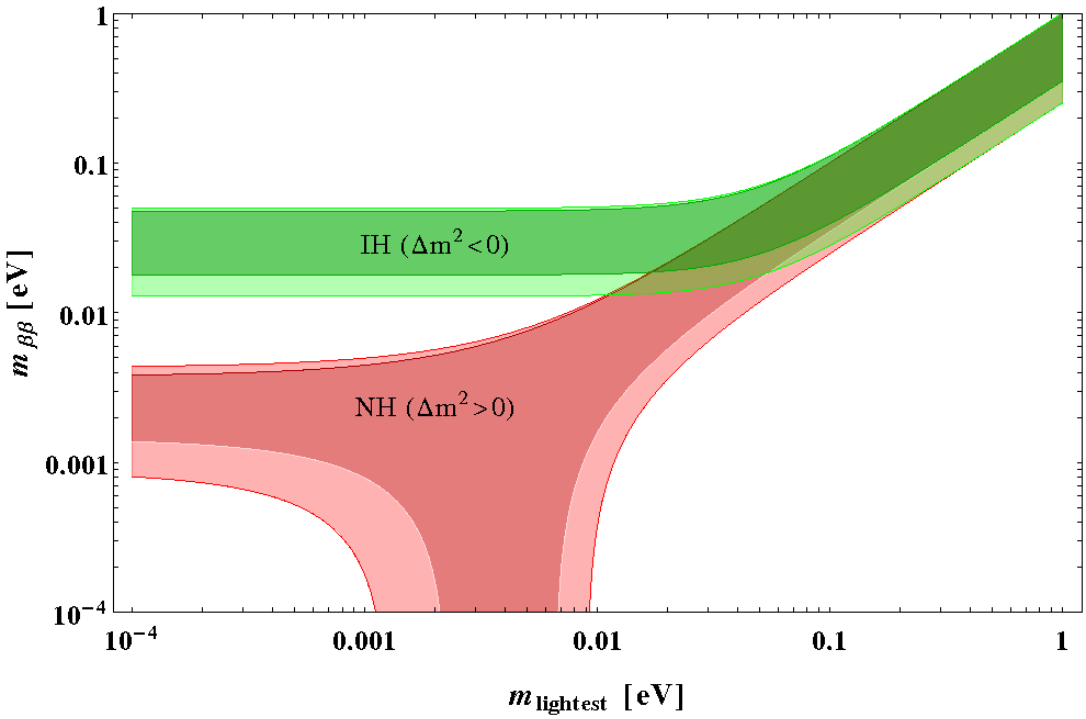

Figure 3.3: Effective neutrino mass as a function of the lightest neutrino mass shown in the logarithmic scale both for normal ($\Delta m^2 > 0$) and inverted ($\Delta m^2 < 0$) hierarchy. The 3σ regions due to error propagation are shaded. Taken from Ref. [148].

As can be seen from Fig. 3.3, in case of normal hierarchy the values of the parameters can conspire in such way that the effective neutrino mass vanishes. If this unfortunate possibility is realized in Nature, or even if the effective mass is non-zero, but very small ($m_{ee} < 10^{-4}$), observation of $0\nu\beta\beta$ decay would be practically impossible, unless certain non-standard mechanism contributes more significantly. In case that the absolute neutrino mass is determined (from cosmology or beta decay), then (considering the realistically reachable values of absolute neutrino mass) it would automatically mean that neutrinos are either 'inversely hierarchical', or 'normally hierarchical' and quasi-degenerate. In either case, the effective mass would have a non-zero value and the potential $0\nu\beta\beta$ decay signal would be fairly likely.

The important feature of the effective mass for the inverted hierarchy is that its minimal value is non-zero, see Fig. 3.3. Reaching this value is the long-term goal of $0\nu\beta\beta$ decay searches, because even non-observation of any signal would be useful. It would imply either that neutrino mass ordering is not inverted, or that neutrinos are not of Majorana nature (unless some kind of more complicated LNV physics causes the non-observation of $0\nu\beta\beta$ decay). Logically, if the inverted hierarchy is confirmed by a different measurement, the unsuccessful $0\nu\beta\beta$ quest would mean that neutrinos are not Majorana particles. Based on the current experimental data the minimal value of the effective neutrino mass in the inverted hierarchy corresponds to ≈ 0.02 eV. The respective half lives are of order 10^{27} y; therefore, the lower limit of inverted hierarchy could be probed by planned future experiments.

The information about Majorana CP-violating phases is also encoded in the effective neutrino mass and in principle it can be extracted, but it is a rather challenging issue. Naturally, only one phase (or their combination) can be obtained plus additional information about the absolute neutrino mass is needed. Realistically, the determination can be achieved either for the inverted mass ordering, or in the quasi-degenerate regime of normal ordering.

So far, the role of the $0\nu\beta\beta$ decay experiments in standard Majorana neutrino phenomenology including 'only' the three SM generations of neutrinos was discussed. Nonetheless, if neutrinos are Dirac particles (which is, after all, a fairly straightforward extension of the SM, as shown in Chap. 2), then, of course, no $0\nu\beta\beta$ decay can be observed and the effective mass is identically zero. If only a tiny Majorana mass parameter appears in the neutrino mass matrix, so called Pseudo-Dirac neutrinos [149] are obtained and the effective neutrino mass is non-

zero, although very small. Alternatively, the neutrino picture can be also bigger than assumed. A popular modification is through the inclusion of light sterile neutrinos with masses in the range from eV to MeV [150–153], in which case the half life is still given by Eq. (3.54), but with different masses m_i and couplings V_{ei} [131, 154–156].

3.6 Neutrinos May Seesaw

As discussed in the Sec. 3.1, there are two straightforward ways how to make neutrinos massive - one can either mimic the charged fermion sector and introduce Dirac neutrino mass terms, or the Majorana nature of neutrinos can be assumed, which allows for addition of Majorana mass terms to the SM Lagrangian. While the former possibility requires presence of sterile neutrinos, the latter one does not involve any new neutrino states. However, both options suffer from certain drawbacks. In order to get Dirac neutrino masses of correct size the corresponding Yukawa couplings must be very tiny - several orders of magnitude smaller than the Yukawa couplings of other fermions, which seems to be unnatural and fine-tuned. The same problem arises for Majorana masses. On top of that, the Majorana mass terms explicitly break the $SU(2)_L$ gauge symmetry.

The issue of artificially introduced small neutrino masses can be resolved employing the so called seesaw mechanism. This approach in general assumes the existence of heavy particles living at a high energy scale, which in turn makes the masses of the SM neutrinos very small in a rather natural way. Moreover, the involved heavy degrees of freedom are typically motivated by other BSM physics. There are a number of different set-ups, but only three types of seesaw mechanism can be constructed at tree level, if just one type of new particle is assumed to be added to the SM content [157]. Effectively, tiny neutrino masses can be obtained from the Weinberg operator introduced in Sec. 2.4 and further discussed in Sec. 3.5. This lowest-dimensional SM invariant effective operator naturally provides the strong suppression of neutrino masses given by a large cut-off scale $\Lambda \approx 10^{14}$ GeV derived from non-observation of $0\nu\beta\beta$ decay. Seesaw mechanisms described in the following text can then be understood as UV completions of the Weinberg operator.

Seesaw Type I The original construction of a seesaw mechanism [14–17] is based on the addition of right-handed neutrinos. Since these are SM singlets,

gauge invariance allows to write not only the Dirac mass term but also the Majorana mass term[3]

$$\mathcal{L}^{(N)}_{\text{Majorana}} = -\frac{1}{2}\sum_{\substack{I=1,2,3\\J=1,2,3}} [\mathrm{M}_M]_{IJ} N^{I^T} C N^J + \text{h.c.}, \tag{3.60}$$

which should be added to the SM Lagrangian. Defining

$$n_L = \begin{pmatrix} \nu_L^\ell \\ N^{I^c} \end{pmatrix} \tag{3.61}$$

the Dirac and Majorana mass terms

$$\mathcal{L}_N = -\sum_{\substack{\ell=e,\mu,\tau\\I=1,2,3}} \mathrm{y}^\nu_{\ell I} \bar{L}^\ell \tilde{H} N^I - \frac{1}{2}\sum_{\substack{I=1,2,3\\J=1,2,3}} [\mathrm{M}_M]_{IJ} N^{I^T} C N^J + \text{h.c.} \tag{3.62}$$

can be combined to give in the broken phase the expression

$$\mathcal{L}_N = \frac{1}{2} n_L^T C \mathsf{M} n_L + \text{h.c.}, \tag{3.63}$$

where the 6×6 mass matrix of the form

$$\mathsf{M} = \begin{pmatrix} 0 & \mathrm{m}_D \\ \mathrm{m}_D^T & \mathrm{M}_M \end{pmatrix} \tag{3.64}$$

was introduced. By block-diagonalizing this matrix,

$$\mathsf{M}_{\text{diag}} = U^T \mathsf{M} U \approx \begin{pmatrix} -\mathrm{m}_D \mathrm{M}_M^{-1} \mathrm{m}_D^T & 0 \\ 0 & \mathrm{M}_M \end{pmatrix}, \tag{3.65}$$

the masses of the eigenstates

$$U \begin{pmatrix} \nu_L^\ell \\ N^{I^c} \end{pmatrix} = \begin{pmatrix} 1 & \mathrm{m}_D^* \mathrm{M}_M^{*-1} \\ -\mathrm{M}_M^{-1} \mathrm{m}_D^T & 1 \end{pmatrix} \begin{pmatrix} \nu_L^\ell \\ N^{I^c} \end{pmatrix} = \begin{pmatrix} \nu_L^\ell + (\mathrm{m}_D^* \mathrm{M}_M^{*-1}) N^{I^c} \\ N^{I^c} - (\mathrm{M}_M^{-1} \mathrm{m}_D^T) \nu_L^\ell \end{pmatrix} \tag{3.66}$$

are obtained. As a result, the first diagonal element of the matrix in Eq. (3.65), which is proportional to the second power of Dirac mass matrix and inversely proportional to the right-handed Majorana mass matrix, effectively describes the mass of the light left-handed neutrinos

$$\mathrm{M}^{\mathrm{I}}_\nu = -\mathrm{m}_D \frac{1}{\mathrm{M}_M} \mathrm{m}_D^T. \tag{3.67}$$

[3]Although one right-handed neutrino singlet per generation is considered in the following text, it is actually not necessary. Current experiments demand at least two neutrinos to be massive; therefore it is in fact enough if two right-handed singlet neutrinos are added to the SM particle content.

The second diagonal element is simply the Majorana mass matrix giving effectively the masses of the new right-handed neutrinos. This setting allows for a naturally small mass of the SM neutrinos, as the Majorana mass parameter can be chosen to be arbitrarily large. If the neutrino Yukawa couplings are set to be of order one and the Majorana mass is taken to be of order 10^{14} GeV, the masses of the light left-handed neutrinos are of the desired order $m_\nu \approx 0.1$ eV.

Another interesting observation is that the additional neutrino states, despite being often called 'sterile', are not completely sterile in the mass eigenbasis - as apparent from Eq. (3.66), there is a small contribution from the light SM neutrinos. However, this contribution is negligible, as it is inversely proportional to the large Majorana mass parameter.

Seesaw Type II The introduction of additional neutrino states is not the only possibility to get naturally small neutrino masses. The SM neutrino masses do not have to be generated through the standard Yukawa couplings like all other SM fermions. The second type of seesaw mechanism [158–160] is based on the idea that the light neutrino masses are induced by a heavy scalar $SU(2)_L$-triplet,

$$\{\mathbf{1},\mathbf{3},2\} \equiv \Delta_L = \mathbf{\Delta}_L \cdot \boldsymbol{\tau} = \begin{pmatrix} \frac{1}{\sqrt{2}}\Delta^+ & \Delta^{++} \\ \Delta^0 & -\frac{1}{\sqrt{2}}\Delta^+ \end{pmatrix}, \tag{3.68}$$

which allows for new Yukawa couplings of the form

$$\mathcal{L}_{\Delta-\text{Yukawa}} = \sum_{\substack{\ell=e,\mu,\tau \\ \ell'=e,\mu,\tau}} \mathrm{y}^{\Delta}_{\ell\ell'} L^{\ell^T} C(i\tau^2)\Delta_L L^{\ell'} + \text{h.c.}. \tag{3.69}$$

Hence, when the scalar triplet acquires its VEV, the neutrino mass matrix reads $\mathrm{M}_\nu = \mathrm{y}^{\Delta}\langle\Delta_L\rangle$. The VEV $\langle\Delta_L\rangle$ can be expressed in terms of parameters appearing in the respective scalar potential

$$\mathcal{L}_{\Delta-\text{Scalar}} = M_\Delta^2 \mathrm{Tr}[\Delta\Delta^\dagger] + [\mu H^T (i\tau^2)\Delta_L^* H + \text{h.c.}] \tag{3.70}$$

as

$$\langle\Delta_L\rangle \simeq \begin{pmatrix} 0 & 0 \\ \frac{\mu v^2}{2M_\Delta^2} & 0 \end{pmatrix}, \tag{3.71}$$

where μ is expected to be of order M_Δ and v is the SM Higgs VEV. Therefore, in analogy to the first seesaw: if M_Δ is chosen to be large enough, i.e. $M_\Delta \gg v$, then small masses of the SM neutrinos are naturally achieved,

$$\mathrm{M}_\nu^{\mathrm{II}} = \frac{\mu v^2}{M_\Delta^2}\mathrm{y}^{\Delta}. \tag{3.72}$$

Seesaw Type III Another possibility to construct a seesaw mechanism is to assume the existence of new fermionic $SU(2)_L$ triplets $\mathbf{T}_F^I$[4] [161], which interact with the SM content in an analogous way to the right-handed neutrino singlets in Eq. (3.62), i.e.

$$\mathcal{L}_{T_F} = \sum_{\substack{\ell=e,\mu,\tau \\ J=1,2,3}} \mathrm{y}_{\ell J}^{T_F} L^{\ell^T} C(i\tau^2)(\mathbf{T}_F^J \cdot \boldsymbol{\tau}) H + \sum_{\substack{I=1,2,3 \\ J=1,2,3}} \mathrm{M}_{IJ}^{T_F} (\mathbf{T}_F^I)^T C \mathbf{T}_F^J + \mathrm{h.c.}. \tag{3.73}$$

As in the case of type I seesaw the neutrino mass matrix is obtained as

$$\mathrm{M}_\nu^{\mathrm{III}} = (\mathrm{y}^{T_F})^T v^2 \frac{1}{\mathrm{M}^{T_F}} \mathrm{y}^{T_F} \tag{3.74}$$

and for $\mathrm{M}^{T_F} \gg \mathrm{y}^{T_F} v$ the SM neutrinos become light.

Inverse Seesaw This type of seesaw mechanism motivated by string theories [162] represents a low-scale tree-level scheme for light neutrino mass production. It relies on the assumption of a non-minimal lepton content of a given model, namely, on the addition of extra singlet leptons. Generally, any number of such particles can be added to any gauge theory [18]. Minimally, an extension of the SM particle content by a pair of left-handed two-component lepton singlets N^c and S can be assumed [163]. Considering three generations of these new singlets, the 9×9 mass matrix of the neutral leptons in the basis $\{\nu_L^\ell, N^{Ic}, S^A\}$ (where $A = a, b, c$) reads

$$\mathsf{M}^{\mathrm{IS}} = \begin{pmatrix} 0 & \mathrm{m}_D & 0 \\ \mathrm{m}_D^T & 0 & \mathrm{M} \\ 0 & \mathrm{M}^T & \mu \end{pmatrix}, \tag{3.75}$$

where m_D is the Dirac neutrino mass matrix as usual, while M and μ are the mass matrices corresponding to the $SU(2)_L$ singlets. There are no Majorana mass terms corresponding to ν_L and N - the relevant entries of the matrix are zero, as predicted by some string models. The only Majorana mass matrix is the matrix μ corresponding to the extra singlet S. As such it is the source of lepton number violation and if $\mu = 0$, the $(B - L)$ symmetry is restored, the matrix M^{IS} degenerates and one is left with three massless neutrinos.

For μ nonzero and provided that $\mu \ll \mathrm{m}_D \ll \mathrm{M}$ the resulting mass matrix of the light neutrino eigenstates is given by the following expression

$$\mathrm{M}_\nu^{\mathrm{IS}} = \mathrm{m}_D \mathrm{M}^{-1} \mu [\mathrm{M}^T]^{-1} \mathrm{m}_D^T. \tag{3.76}$$

[4] Again, only two triplets are needed, although three (one for each flavour) are considered in this text.

While in the standard seesaw mechanisms the neutrino masses tend to zero with growing size of the involved Majorana mass matrix, in the present case neutrinos become light for $\mu \to 0$; hence, one talks about 'inverse' seesaw. The smallness of μ in this kind of SM inverse seesaw mechanism can be considered to be natural, as sending μ to zero enhances the symmetry of the theory [164, 165].

Linear Seesaw An interesting variant of the inverse seesaw mechanism can be realized within $SO(10)$ models (which will be briefly discussed in Sec. 3.8) with broken D-parity [166]. Although originally developed within the supersymmetric $SO(10)$ framework, it can be employed also in non-supersymmetric scenarios. The minimal fermionic content of the $SO(10)$ model contained by three copies of the $\mathbf{16}_F$ representation is extended by three gauge singlets S^A. Hence, the mass matrix for the neutral fermions in the basis $\{\nu_L^\ell, N^{Ic}, S^A\}$ reads

$$\mathsf{M}^{\rm LS} = \begin{pmatrix} 0 & \mathrm{m}_D & \mathrm{m}_L \\ \mathrm{m}_D^T & 0 & \mathrm{M} \\ \mathrm{m}_L^T & \mathrm{M}^T & 0 \end{pmatrix}, \tag{3.77}$$

where m_D is the Dirac neutrino mass, M denotes the heaviest Dirac neutrino mass term mixing N-S and m_L is the small term mixing ν-S, which is responsible for breaking of the $(B-L)$ symmetry. The resulting mass matrix of the light neutrinos generated by this seesaw is

$$\mathrm{M}_\nu^{\rm LS} \simeq \mathrm{m}_D^T \mathrm{M}^{-1} \mathrm{m}_L + (\mathrm{M}^{-1}\mathrm{m}_L)^T \mathrm{m}_D, \tag{3.78}$$

and the fact that this formula depends linearly on m_D (and therefore also on corresponding Yukawa couplings) gives the presented seesaw mechanism its name. Obviously, the small neutrino masses are ensured by the large unification scale M, which suppresses them independently of the $(B-L)$ symmetry breaking scale. This is a very interesting feature, as it allows for $(B-L)$ symmetry restoration/breaking at low energies (without spoiling the light neutrino masses or the unification), where the related phenomena can be probed experimentally.

Other Neutrino Mass Models Although the seesaw mechanisms are probably the most commonly quoted schemes of neutrino mass generation, there are a number of other alternatives. These can be phenomenologically even more interesting, as they often predict, unlike the standard seesaws, a low-energy origin of neutrino masses. The required smallness of the masses is either achieved by an

introduction of a small parameter violating lepton number (in the same way as in case of inverse or linear seesaw), or by a loop suppression, which can be combined with small Yukawa couplings. The former possibility is employed e.g. in supersymmetric models [167], where the violation of lepton number corresponds to R-parity breaking. The latter option refers to radiative models, where the tiny neutrino masses are generated by calculable radiative corrections [168], for instance at two loops [169].

3.7 Left-Right Symmetry

One of the minimal extensions of the SM is the so called left-right symmetric extension [170–174], which is appealing particularly for its automatic inclusion of non-zero neutrino masses and the seesaw mechanism. Consequently, it represents also a typical UV completion leading to $0\nu\beta\beta$ decay and as such it will be discussed in various contexts within this work. There were expectations that the typical scale at which the left-right symmetry is restored would lie at rather low energies, within the range of the LHC, which would then observe the related new physics. Nonetheless, these hopes have not been supported by the collected data, so far.

As mentioned earlier, parity P is explicitly broken within the SM model, but it seems to be rather suggestive to conjecture its restoration at higher energies and assume it is broken spontaneously via some type of Higgs mechanism. The minimal left-right symmetric extension of the Standard Model gauge group is the following

$$\mathcal{G}_{LR} = SU(3)_C \otimes SU(2)_L \otimes SU(2)_R \otimes U(1)_{B-L}, \tag{3.79}$$

where $B - L$ is the difference between baryon and lepton number and the electromagnetic charge is in the left-right symmetric case given by

$$Q = T_{3L} + T_{3R} + \frac{B-L}{2}. \tag{3.80}$$

The fermionic particle content of left-right symmetric models is given by a straightforward left-right symmetric extension of the SM content, i.e. the right-

handed doublets are introduced

$$L_R^\ell = \begin{pmatrix} N^\ell \\ \ell_R \end{pmatrix} \overset{P}{\leftrightarrow} \begin{pmatrix} \nu_L^\ell \\ \ell_L \end{pmatrix} = L^\ell, \tag{3.81}$$

$$Q_R^i = \begin{pmatrix} u_R^i \\ d_R^i \end{pmatrix} \overset{P}{\leftrightarrow} \begin{pmatrix} u_L^i \\ d_L^i \end{pmatrix} = Q^i. \tag{3.82}$$

As a result, the right-handed neutrinos are naturally included and neutrinos can acquire masses in the left-right symmetric models. The presence of the right-handed neutrino partners is also essential for cancellation of the $B - L$ gauge anomaly, as can be inferred from Eq. (3.80).

The Higgs sector of left-right symmetric models can vary. The minimal breaking scenarios mostly include a scalar bi-doublet[5]

$$\Phi \equiv \{\mathbf{1}, \mathbf{2}, \mathbf{2}, 0\} = \begin{pmatrix} \phi_1^0 & \phi_2^+ \\ \phi_1^- & \phi_2^0 \end{pmatrix}, \tag{3.83}$$

containing the SM Higgs, which subsequently gives masses to quarks and leptons. The corresponding VEV reads

$$\langle \Phi \rangle = \begin{pmatrix} v_{\Phi 1} & 0 \\ 0 & v_{\Phi 2} \end{pmatrix}, \tag{3.84}$$

where $v \equiv \sqrt{v_1^2 + v_2^2}$ and it mixes the left-handed and right-handed gauge bosons as described below.

On top of the bi-doublet, typically a pair of scalar triplets

$$\Delta_L \equiv \{\mathbf{1}, \mathbf{3}, \mathbf{1}, -2\}, \quad \Delta_R \equiv \{\mathbf{1}, \mathbf{1}, \mathbf{3}, -2\}, \tag{3.85}$$

or doublets

$$\chi_L \equiv \{\mathbf{1}, \mathbf{2}, \mathbf{1}, -1\}, \quad \chi_R \equiv \{\mathbf{1}, \mathbf{1}, \mathbf{2}, -1\}, \tag{3.86}$$

must be added to the Higgs sector in order to break the left-right gauge group down to the SM. In fact, the right-handed scalar is enough to do so, but inclusion of the left-handed triplet (or doublet) ensures that parity is preserved in the left-right phase (so called "manifest left-right symmetry"), i.e. the $SU(2)_L$ and $SU(2)_R$ gauge couplings are equal: $g_L = g_R$.

[5]Here, the representations are labelled in the usual way in the order $\{SU(3)_C, SU(2)_L, SU(2)_R, U(1)_{B-L}\}$.

It can be proven [175] that if no additional fermions besides the SM fermionic content are considered, at least two bi-doublets must be present in the scalar sector to account for the correct SM flavour physics. In case only a single bi-doublet is incorporated, the Yukawa Lagrangian implies that the up-quark mass matrix is proportional to the down-quark mass matrix (independently of the VEV structure); thus, the CKM matrix becomes trivial $V_{\mathrm{CKM}} = \mathbb{1}$.

Hence, the left-right symmetry is broken in two steps. At first, the neutral component of right-handed scalar triplet (or doublet) acquires the VEV v_R and breaks the left-right gauge group to the SM gauge group

$$SU(3)_C \otimes SU(2)_L \otimes SU(2)_R \otimes U(1)_{B-L} \xrightarrow{M_{LR}} SU(3)_C \otimes SU(2)_L \otimes U(1)_Y, \tag{3.87}$$

where M_{LR} is the energy scale of the phase transition and the weak hypercharge Y can be expressed as

$$Y = 2T_{3R} + (B - L). \tag{3.88}$$

In this step the parity symmetry is also broken. Subsequently, the bi-doublet acquires its VEV and breaks the SM gauge group to $SU(3)_C \otimes U(1)_Q$. The experimental data imply that $v_R \gg v_{\Phi 1}, v_{\Phi 2}$.

The gauge sector of the left-right symmetric models incorporates the extra three gauge fields of the $SU(2)_R$ group, which are usually denoted as W_R^i. Similarly as in the left-handed case it is convenient to define

$$W_{R\mu}^{\pm} \equiv \frac{W_{R\mu}^1 \mp W_{R\mu}^2}{\sqrt{2}}. \tag{3.89}$$

These vector bosons become massive after the left-right symmetry is broken and their masses are proportional to v_R. Therefore, they are expected to be much heavier than the $SU(2)_L$ vector bosons $W_\mu^{\pm}, Z_\mu$, which receive masses proportional to $v_{\Phi 1}$ and $v_{\Phi 2}$ in the second step of symmetry breaking.

The masses of the charged and neutral gauge bosons are described by corresponding mass matrices and their diagonalization leads to the mixing. Therefore, the mass eigenstates of the charged gauge bosons are given by the following mixture of the right-handed gauge bosons with their left-handed partners

$$W_{1\mu} = W_\mu \cos\zeta + W_{R\mu} \sin\zeta, \tag{3.90}$$

$$W_{2\mu} = -W_\mu \sin\zeta + W_{R\mu} \cos\zeta, \tag{3.91}$$

where

$$\tan\zeta = \frac{v_{\Phi 1} v_{\Phi 2}}{v_R^2 - v_L^2}, \tag{3.92}$$

and v_L is the VEV of the neutral component of the scalar triplet Δ_L which is assumed to be $v_L \ll v_{\Phi 1}, v_{\Phi 2}$. If the additional assumption $v_{\Phi 1} \gg v_{\Phi 2}$ is made, then the mixing angle ζ becomes small and W_1, W_2 can be well approximated by W_L, W_R. The corresponding masses then satisfy

$$M_{W_L}^2 \simeq M_{W_1}^2 \cos^2\zeta + M_{W_2}^2 \sin^2\zeta, \tag{3.93}$$

$$M_{W_R}^2 \simeq M_{W_1}^2 \sin^2\zeta + M_{W_2}^2 \cos^2\zeta. \tag{3.94}$$

Similarly as in the SM, the neutral vector bosons can be conveniently transformed into a new basis

$$Z_\mu = \cos\theta_W W_\mu^3 - \sin\theta_W \tan\theta_W W_{R\mu}^3 - \tan\theta_W \sqrt{\cos 2\theta_W} B_\mu, \tag{3.95}$$

$$Z'_\mu = \frac{\sqrt{\cos 2\theta_W}}{\cos\theta_W} W_{R\mu}^3 - \tan\theta_W B_\mu, \tag{3.96}$$

$$A_\mu = \sin\theta_W W_\mu^3 + \sin\theta_W W_{R\mu}^3 + \sqrt{\cos 2\theta_W} B_\mu, \tag{3.97}$$

where B_μ denotes the gauge field corresponding to $U(1)_{B-L}$, Z_μ and Z'_μ are the massive (after the symmetry breaking) neutral vector bosons, A_μ stands for the massless photon and θ_W is the weak mixing angle.

As in the case of the charged gauge bosons, the massive neutral gauge bosons mix and the mass eigenstates Z_1 and Z_2 are given by combinations

$$Z_{1\mu} = Z_\mu \cos\xi + Z'_\mu \sin\xi, \tag{3.98}$$

$$Z_{2\mu} = -Z_\mu \sin\xi + Z'_\mu \cos\xi, \tag{3.99}$$

and assuming $v_R^2 \gg v_{\Phi 1}^2 + v_{\Phi 2}^2 \gg v_L^2$, then

$$\tan 2\xi \simeq \frac{(\cos 2\theta_W)^{3/2}}{2\cos^4\theta_W} \frac{v_{\Phi 1}^2 + v_{\Phi 2}^2}{v_R^2}. \tag{3.100}$$

The masses of the neutral gauge bosons are given by

$$M_Z^2 = M_{Z_1}^2 \cos^2\xi + M_{Z_2}^2 \sin^2\xi, \tag{3.101}$$

$$M_{Z'}^2 = M_{Z_1}^2 \sin^2\xi + M_{Z_2}^2 \cos^2\xi. \tag{3.102}$$

If the phenomenological limit $v_R^2 \gg v_{\Phi 1}^2 + v_{\Phi 2}^2$ is assumed, then the left-handed and right-handed gauge bosons decouple and their masses are proportional to the

VEVs v and v_R, respectively. Expectedly, in the same limit the SM relations like $M_{W_1} = M_{Z_1} \cos\theta_W$ are reproduced.

The possibilities of the light neutrino mass generation are related to the scalar content of the left-right symmetric model. Typically, one of the above seesaw mechanisms are implemented, in order to ensure the experimentally required smallness of the masses. As there are right-handed neutrinos in the left-right symmetric models, the most general neutrino mass matrix takes the form

$$\mathsf{M}_\nu = \begin{pmatrix} \mathrm{M}_{M,L} & \mathrm{m}_D \\ \mathrm{m}_D^T & \mathrm{M}_{M,R} \end{pmatrix}, \tag{3.103}$$

where, as before, m_D stands for the Dirac mass matrix, while $\mathrm{M}_{M,L}$ and $\mathrm{M}_{M,R}$ are the Majorana mass matrices corresponding to the left-handed and right-handed neutrinos, respectively.

Depending on the included scalar fields, different mass terms can be generated within a given model. The Dirac mass term typically originates from Yukawa couplings involving the scalar bi-doublet,

$$\mathcal{L}^{\Phi}_{\text{Yukawa}} = \sum_{\substack{\ell=e,\mu,\tau \\ \ell'=e,\mu,\tau}} \mathrm{y}^{\Phi}_{\ell\ell'} L^{\ell^T} C \Phi L^{\ell'}_R + \tilde{\mathrm{y}}^{\Phi}_{\ell\ell'} L^{\ell^T} C \tilde{\Phi} L^{\ell'}_R + \text{h.c.}, \tag{3.104}$$

with $\tilde{\Phi} = \sigma^2 \Phi^* \sigma^2$. Hence, in the broken phase the Dirac neutrino mass matrix and the mass matrix of charged leptons are given by

$$\mathrm{m}_D = \mathrm{y}^{\Phi} v_{\Phi 1} + \tilde{\mathrm{y}}^{\Phi} v_{\Phi 2}, \tag{3.105}$$

$$\mathrm{m}_\ell = \mathrm{y}^{\Phi} v_{\Phi 2} + \tilde{\mathrm{y}}^{\Phi} v_{\Phi 1}. \tag{3.106}$$

Further, if the LR symmetry is broken by the right-handed scalar triplet Δ_R, then the Yukawa couplings for the right-handed lepton doublet can be written as

$$\mathcal{L}^{\Delta_R}_{\text{Yukawa}} = \frac{1}{2} \sum_{\substack{\ell=e,\mu,\tau \\ \ell'=e,\mu,\tau}} \mathrm{y}^{\Delta_R}_{\ell\ell'} (L^{\ell}_R)^T C (i\tau^2) \Delta_R L^{\ell'}_R + \text{h.c.}, \tag{3.107}$$

where the Higgs triplet is assumed in the adjoint representation $\Delta_R = \boldsymbol{\Delta}_R \cdot \boldsymbol{\tau}$ and its decomposition under the charge eigenstates is same as in Eq. (3.68). After acquiring the VEV

$$\langle \Delta_R \rangle = \begin{pmatrix} 0 & 0 \\ v_R & 0 \end{pmatrix}, \tag{3.108}$$

the LR symmetry is broken as well as parity and the right-handed neutrino receives the mass

$$\mathcal{L}^{\Delta_R}_{\text{Mass}} = \frac{1}{2} \sum_{\substack{\ell=e,\mu,\tau \\ \ell'=e,\mu,\tau}} \mathrm{y}^{\Delta_R}_{\ell\ell'} v_R N^{\ell^T} C N^{\ell'} + \text{h.c.}. \tag{3.109}$$

As a result, the mass matrix $\mathrm{M}_{M,R} = \mathrm{y}^{\Delta_R} v_R \gg v$ allows for the implementation of type-I seesaw mechanism.

If the left-handed scalar triplet Δ_L is present in the Higgs sector, then after acquiring the VEV

$$\langle \Delta_L \rangle = \begin{pmatrix} 0 & 0 \\ v_L & 0 \end{pmatrix} \tag{3.110}$$

it generates the left-handed Majorana mass matrix $\mathrm{M}_{M,L} = \mathrm{y}^{\Delta_L} v_L$ and the seesaw of type II can be constructed.

In principle, nothing prevents one from combining the type I and type II seesaws, which gives the 'full' seesaw matrix of the form (3.103). The resulting light neutrino mass matrix reads

$$\mathrm{M}^{\text{I+II}}_{\nu} = \mathrm{M}_{M,L} - \mathrm{m}_D \frac{1}{\mathrm{M}_{M,R}} \mathrm{m}^T_D. \tag{3.111}$$

Assuming for simplicity that $v_{\Phi 2} = 0$, then this combined seesaw formula can be easily expressed specifically for the left-right models as

$$\mathrm{M}^{\text{LR}}_{\nu} = \mathrm{y}^{\Delta_L} v_L - \frac{v^2_{\Phi 1}}{v_R} \mathrm{y}^{\Phi} [\mathrm{y}^{\Delta_R}]^{-1} \mathrm{y}^{\Phi T}, \tag{3.112}$$

and considering the hierarchy $v_R \gg v_{\Phi 1} \gg v_L$ the smallness of the obtained neutrino masses is ensured.

In models with the left-right symmetry breaking driven by the right-handed doublet χ_R instead of the triplet Δ_R, the small neutrino masses can be induced using the inverse [163] and/or linear [176–178] seesaw mechanisms, provided that a singlet fermion $\{\mathbf{1}, \mathbf{1}, \mathbf{1}, 0\}$ is available. Alternatively, with a left-handed or right-handed fermionic triplet at hand, the seesaw of type III can be implemented [179].

A number of different $0\nu\beta\beta$ decay mechanisms can be constructed in the left-right symmetric models [115]. Besides the earlier discussed standard mass mechanism based on the exchange of light neutrino (see Fig. 1.1), one can think of several non-standard mechanisms involving exchange of heavy neutrino as well

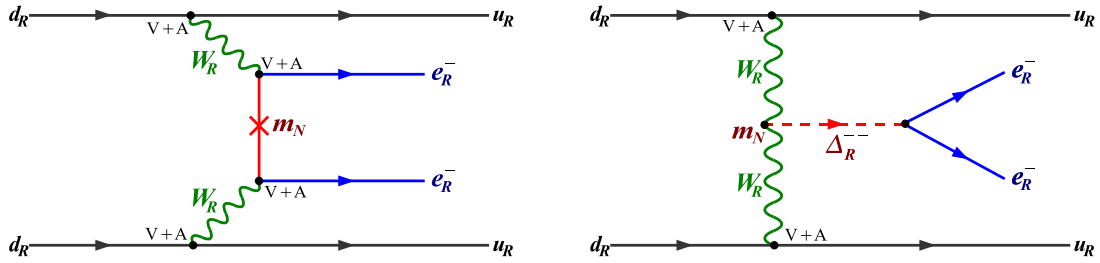

Figure 3.4: The exotic short-range $0\nu\beta\beta$ decay that can be constructed in the left-right symmetric models using either a heavy neutrino (left), or right-handed triplet Higgs (right). Taken from Ref. [115].

as light and heavy W vector bosons. In the simplest exotic case the light neutrino exchange is substituted by a heavy right-handed neutrino exchange, which means that the involved vector currents and emitted electrons must be also right-handed, see Fig. 3.4 (left). For a model with manifest left-right symmetry, $g_L \equiv g_R$, the corresponding contribution is proportional to the following combination of the model parameters

$$\frac{1}{\Lambda^5} = \sum_{i=1}^{3} U_{ei}^2 \frac{1}{m_{N_i}} \frac{1}{M_{W_R}^4}, \tag{3.113}$$

where m_{N_i} denotes the heavy neutrino mass, respectively, while U is the mixing matrix of heavy neutrino states. As the propagating neutrino is heavy, the interaction can be considered to be contact and we refer to this contribution as to short-range mechanism. The corresponding operator will be 9-dimensional and is thus suppressed by the fifth power of the cut-off scale Λ, as indicated. A model-independent approach to these mechanisms will be discussed in detail in Chap. 4. Another short-range contribution can be in the left-right symmetric framework obtained also using the right-handed triplet Higgs Δ_R. This contribution is then proportional to

$$\frac{1}{\Lambda^5} = \sum_{i=1}^{3} U_{ei}^2 \frac{m_{N_i}}{m_{\Delta_R}^2} \frac{1}{M_{W_R}^4}, \tag{3.114}$$

where m_{Δ_R} is the mass of Δ_R and the heavy neutrino mass originates from the couplings of the right-handed triplet. The corresponding diagram is shown in Fig. 3.4 (right).

As the right-handed currents are present in left-right symmetric models, one can also think of $0\nu\beta\beta$ decay mechanisms, in which the neutrino exchange does

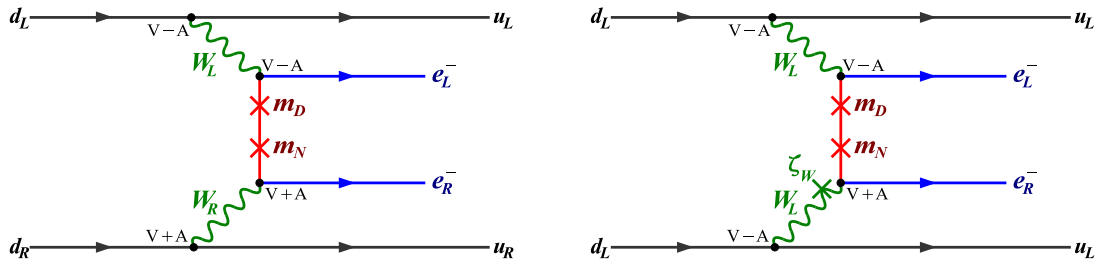

Figure 3.5: The exotic long-range $0\nu\beta\beta$ decay that can be constructed in the left-right symmetric models with vector currents of opposite (left), or same (right) chiralities. Taken from Ref. [115].

not violate chirality, i.e. the contribution is not proportional to the neutrino mass. In such cases the two outgoing electrons are of opposite chiralities. Two possible contributions of this type are depicted in Fig. 3.5. The left diagram involves vector currents of opposite chiralities, whereas the right diagram contains two left-handed currents, one of which is attached via the chirality-changing mixing angle ζ of the W bosons. The corresponding contributions are proportional to

$$\frac{1}{\Lambda^2} = \sum_{i=1}^{3} V_{ei} W_{ei} \frac{1}{M_{W_R}^2}, \tag{3.115}$$

$$\frac{1}{\Lambda^2} = \sum_{i=1}^{3} V_{ei} W_{ei} \frac{\tan\zeta}{M_{W_L}^2}, \tag{3.116}$$

for the left and right diagrams in Fig. 3.5, respectively. Here, W is the active-sterile neutrino mixing matrix and V is the PMNS matrix introduced earlier. This type of mechanisms is generally called long-range and they will be further discussed in effective terms in Chap. 4.

3.8 Going High - Do We Have the GUTs?

The left-right models can be understood as a step on path towards a Grand Unified Theory (GUT) with $SO(10)$ gauge group. GUTs as such are for a number of reasons very attractive extensions of the SM and the $SO(10)$ based GUT is one of the most favourable candidates for a unifying model. Generally, a GUT is a gauge theory based on a simple group $\mathcal{G}_{GUT}$ containing the SM gauge group as a subgroup. A simple gauge group means there is only a single gauge coupling

g_{GUT} unifying the three fundamental forces appearing in the SM. The idea of GUTs originated in 1974, when Glashow and Georgi suggested to embed the SM group into the $SU(5)$ gauge group [180]. Soon after, the $SO(10)$ based GUT was proposed [181]. Apart from that, exceptional Lie groups E_6 and E_8 can be used for the construction of the unification models. From the early nineties, along with the growing interest in low-energy supersymmetry (SUSY) also the supersymmetric versions of GUTs were developed and studied.

There is a fairly long list of features that make the idea of GUTs, and particularly $SO(10)$ unification, glamorous. The most obvious is, of course, the unification of the three SM couplings. The corresponding transition from the semi-simple Lie group of the SM to a greater symmetry described by a simple Lie group then promises a somewhat more constraining framework, which should be able to reduce the arbitrariness of the SM.

GUTs give several model-independent predictions. They always contain exotic particles coupling both to quarks and leptons; therefore, the lepton and baryon numbers are not conserved [17]. As a result, new phenomena like neutron-antineutron oscillations, lepton flavour violating processes and, particularly, proton decay are possible. Although baryon number can be violated also in different ways, GUTs provide a very suitable framework. The main proton decay mode is $p \to e^+ + \pi^0$ and the predicted proton decay half-life can be in a simple approximation estimated as [182]

$$\tau_p^{\text{theory}} \approx \frac{1}{\alpha_{GUT}^2} \frac{M_{GUT}^2}{m_p^5}, \tag{3.117}$$

where α_{GUT} is the gauge coupling fine structure constant given at the unification scale M_{GUT} and m_p is the proton mass. The current experimental bound determined by the Super-Kamiokande collaboration [183] reads

$$\tau_p^{\text{exp}} > 1.29 \times 10^{34} y, \tag{3.118}$$

therefore, one can write

$$\frac{\tau_p^{\text{theory}}}{\tau_p^{\text{exp}}} \approx \frac{1}{\alpha_{GUT}^2} \left(\frac{M_{GUT}}{2.6 \times 10^{16}\ \text{GeV}} \right)^4, \tag{3.119}$$

and the unification scale must lie above 10^{16} GeV.

As mentioned earlier, the SM cannot provide any explanation of the numerical values of particular hypercharges (or, equivalently, electromagnetic charges)

assigned to individual fermions. This drawback can be cured within the unification framework, where the fermion charges are quantized. Thus, quantization of charges is another remarkable model-independent prediction of GUTs. Furthermore, unifications generally predict the existence of topologically nontrivial configurations of the Higgs and gauge fields, so called magnetic monopoles [184,185]. These could be produced during the symmetry breaking in early universe via the Kibble mechanism [186].

3.8.1 $SO(10)$ Unification

A variety of $SO(10)$ based models with different symmetry breaking chains reproducing the SM gauge group at the EW scale can be constructed. For the context of this work it is particularly interesting that the left-right symmetric model discussed in the previous section can be taken to be an intermediate step of the $SO(10)$ symmetry breaking. The simplest example of such a scenario is the chain

$$SO(10) \xrightarrow{M_{GUT}} \mathcal{G}_{LR} \xrightarrow{M_{LR}} \mathcal{G}_{SM} \tag{3.120}$$

with the $\mathcal{G}_{LR}$ gauge group being the only intermediate symmetry. For the first breaking step either **45**, or **210** representation must be present in the Higgs sector of the assumed model and for the subsequent breaking inclusion of the rank-reducing scalar **126** is necessary. Moreover, in order to get the Standard Model Higgs the scalar representations **10** and $\overline{\mathbf{126}}$ must be added.

A very elegant feature of an $SO(10)$ GUT is the fact that an entire generation of fermions, including the right-handed neutrino, can be assigned to a single 16-dimensional spinor representation of $SO(10)$, which can be demostrated by its decomposition under the SM gauge group (as the intermediate step the decomposition into the submultiplets of the left-right symmetric group $\mathcal{G}_{LR}$ is shown)

$$\begin{aligned}
\mathbf{16}_F \xrightarrow{M_{GUT}} & \{\mathbf{3},\mathbf{2},\mathbf{1},+\tfrac{1}{3}\} \oplus \{\mathbf{1},\mathbf{2},\mathbf{1},-1\} \\
& \oplus \{\overline{\mathbf{3}},\mathbf{1},\mathbf{2},-\tfrac{1}{3}\} \oplus \{\mathbf{1},\mathbf{1},\mathbf{2},+1\} \\
\xrightarrow{M_{LR}} & \{\mathbf{3},\mathbf{2},+\tfrac{1}{6}\} \oplus \{\mathbf{1},\mathbf{2},-\tfrac{1}{2}\} \\
& \oplus \{\overline{\mathbf{3}},\mathbf{1},+\tfrac{1}{3}\} \oplus \{\overline{\mathbf{3}},\mathbf{1},-\tfrac{2}{3}\} \oplus \{\mathbf{1},\mathbf{1},+1\} \oplus \{\mathbf{1},\mathbf{1},0\}.
\end{aligned} \tag{3.121}$$

Since both left-handed fermions and their charge conjugates are located in the same representation, the left-right symmetry is within the $SO(10)$ GUT framework a finite gauge transformation in the form of charge conjugation.

The presence of the right-handed neutrino together with other fermions within a single representation supports the idea of a high-energy origin of light neutrino masses. The Yukawa couplings are within the $SO(10)$ models generally obtained by coupling of a pair of the fermionic representations $\mathbf{16}_F$ to the scalar representations **10**, **126** and **120**, i.e.

$$\mathcal{L}^{SO(10)}_{\text{Yukawa}} = \bar{\mathbf{16}}_F \left(\mathrm{Y}_{10}\mathbf{10} + \mathrm{Y}_{120}\mathbf{120} + \mathrm{Y}_{126}\overline{\mathbf{126}}\right) \mathbf{16}_F, \tag{3.122}$$

where Y_X are matrices of Yukawa couplings in fermion flavour space. After symmetry breaking the fermion masses are generated. The neutrino masses and mixings are in the $SO(10)$ GUTs related to those of charged fermions. The neutrino mass matrix has the same form as in the left-right symmetric case Eq. (3.103), leading to the seesaw formula of the type in Eq. (3.111). If a non-minimal fermionic content is assumed, then a linear seesaw described in Sec. 3.6, or a seesaw of type III can be employed.

Unfortunately, the $SO(10)$ unification in its purest form does not shed any extra light on the existence of three fermion families; therefore, to cover the SM particle content three copies of $\mathbf{16}_F$ representations must be put in by hand for a realistic model. In this regard, a possible way to reason the repetition of fermion families has been proposed and it is based on gauging the direct product of $SO(10)$ with a discrete family group, e.g. A_4 [187–189].

A variety of symmetry breaking scenarios of the $SO(10)$ gauge group reproducing the SM group at the electroweak scale exist and concrete possibilities depend on the assumed Higgs sector. In minimal scenarios, at least two Higgs representations are necessary [190–192] - the representation **45** is used to break $SO(10)$ to an intermediate symmetry of the same rank and either **16** or **126** reduces the rank and breaks the intermediate symmetry (rank 5) to the SM (rank 4).

The 45-dimensional representation is particularly important, as it is the adjoint representation of $SO(10)$ and as such it contains the gauge bosons of the theory. The decomposition of **45** under the groups $\mathcal{G}_{LR}$ and $\mathcal{G}_{SM}$ reads

$$\begin{aligned}
\mathbf{45} \xrightarrow{M_{GUT}} \; & \{\mathbf{3},\mathbf{2},\mathbf{2},\ \tfrac{1}{2}\} \oplus \{\bar{\mathbf{3}},\mathbf{2},\mathbf{2},\text{-}\tfrac{1}{2}\} \oplus \{\mathbf{8},\mathbf{1},\mathbf{1},\ 0\} \oplus \{\bar{\mathbf{3}},\mathbf{1},\mathbf{1},\ 1\} \\
& \oplus \{\mathbf{1},\mathbf{3},\mathbf{1},0\} \oplus \{\mathbf{3},\mathbf{1},\mathbf{1},\text{-}1\} \oplus \{\mathbf{1},\mathbf{1},\mathbf{3},\ 0\} \oplus \{\mathbf{1},\mathbf{1},\mathbf{1},\ 0\} \\
\xrightarrow{M_{LR}} \; & \{\mathbf{1},\mathbf{1},+1\} \oplus \{\mathbf{1},\mathbf{1},0\} \oplus \{\mathbf{1},\mathbf{1},-1\} \oplus \{\mathbf{3},\mathbf{2},+\tfrac{1}{6}\} \\
& \oplus \{\mathbf{3},\mathbf{2},-\tfrac{5}{6}\} \oplus \{\bar{\mathbf{3}},\mathbf{2},-\tfrac{1}{6}\} \oplus \{\bar{\mathbf{3}},\mathbf{2},+\tfrac{5}{6}\} \oplus \{\mathbf{3},\mathbf{1},+\tfrac{2}{3}\} \\
& \oplus \{\bar{\mathbf{3}},\mathbf{1},-\tfrac{2}{3}\} \oplus \{\mathbf{8},\mathbf{1},0\} \oplus \{\mathbf{1},\mathbf{3},0\} \oplus \{\mathbf{1},\mathbf{1},0\}.
\end{aligned} \tag{3.123}$$

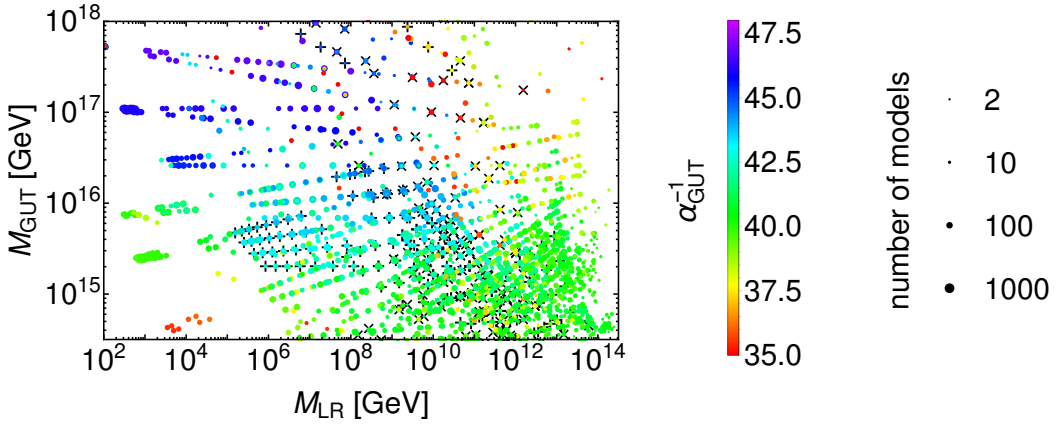

Figure 3.6: Solutions $(M_{GUT}, M_{LR}, \alpha_{GUT})$ to the unified RG running for the next-to-minimal models with the symmetry breaking chain (3.120). The value of $\alpha_{\rm GUT}$ is indicated by the colour of the dots, whereas the point sizes represent the multiplicity of individual models represented, as explained in the legend. The crosses identify models satisfying the CKM constraint (+) and models with manifest left-right symmetry (×).

Apart from the 12 SM gauge bosons residing in the last three SM submultiplets some of the extra 33 gauge bosons are charged both under $SU(3)_C$ and $SU(2)_L$, which means they can mediate lepton-quark transitions allowing e.g. proton decay. Hence, these fields must be assumed to live at high energies.

The scale of the left-right symmetry breaking M_{LR} can in principle lie anywhere between M_{GUT} and the electroweak scale. Although scenarios with the left-right scale close above the electroweak scale can be constructed (and they are of great interest for their testability at the LHC), the recent RGE analysis [193] of a large number of the next-to-minimal models with the above breaking chain has confirmed that in this case the preferred size of M_{LR} is much higher, above 10^{10} GeV. In Fig. 3.6 the models scattered in the $M_{GUT} - M_{LR}$ parameter space are displayed. As there are usually several different models giving the same predictions for the energy scales and observables, the size of each dot represents the multiplicity of the individual next-to-minimal left-right models. The colour of the dots indicates the value of the gauge coupling constant, ranging from $\approx 1/47$ (purple) to $\approx 1/33$ (red). The models that are manifestly left-right symmetric, i.e. they are invariant under the exchange $SU(2)_L \leftrightarrow SU(2)_R$, are indicated in Fig. 3.6 by a cross (×) underneath the corresponding dots. A specific set of representations must be contained by the model to reproduce the SM fermion masses

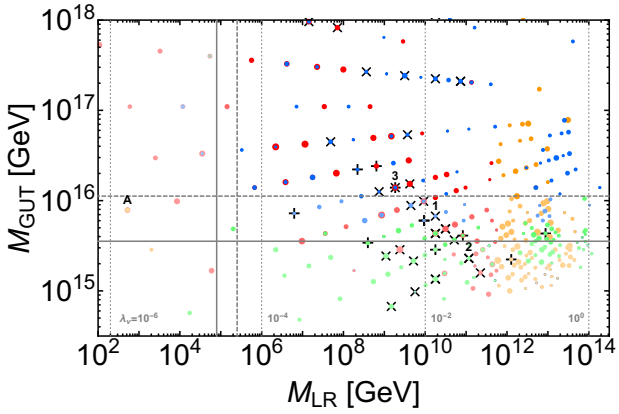

Figure 3.7: Combined effect of all observables on the solutions (M_{GUT}, M_{LR}) of the unified RG running for models with the SM content only at the EW scale. Here, the colours of the dots indicate the potential contribution of exotic scalar fields in the given model to proton decay or LFV interactions. While the vertical lines and corresponding shading represent the contribution to LFV from gauge interactions, the horizontal lines and the respective shading show the gauge contribution to proton decay. The point sizes represent the multiplicity of models, as in graph 3.6. The crosses again identify models that satisfy the CKM constraint (+) and models with manifest left-right symmetry (×).

and mixing. The models satisfying this constraint are denoted by a plus sign (+) underneath the dot. The Fig. 3.6 clearly shows a cumulation of models in the bottom right corner of the figure, around $M_{GUT} \approx 10^{15}$ GeV and $M_{LR} \approx 10^{13}$ GeV. This reflects the natural running of the SM gauge couplings, which get close to one another around 10^{15} GeV, in combination with a small number of exotic representations included in the studied models.

As can be seen from Fig. 3.7 a large portion of such scenarios is excluded by current experimental constraints, namely by proton decay (from the top) and LFV (from the right). The size of the dots again represents the number of models with given sizes of scales M_{GUT} and M_{LR}. However, the colour of the dots now indicates the potential contribution of exotic scalar fields to proton decay, or LFV. The blue dots are unconstrained, while green, orange and red dots denote dangerous contributions to either proton decay, or LFV, if the relevant couplings are of orders $10^{-2} - 1$, $10^{-4} - 10^{-2}$ and $10^{-6} - 10^{-4}$, respectively. The levels of saturation and the dashed and solid lines show the potentially dangerous gauge contributions to proton decay (horizontal lines) and LFV (vertical lines). The low saturation

to the left from the vertical solid line (LFV) and below the horizontal solid line (proton decay) indicates the models excluded by the current experimental limits. The mid level of shading used between the solid and dashed lines identifies the prospective exclusion by future experiments, assuming one order of magnitude improvement. The full saturation is clearly used for models unconstrained by gauge contributions. As apparent, using the current experimental limits the gauge contributions to proton decay disfavour values of M_{GUT} below $\approx 10^{15} - 10^{16}$ GeV, while the gauge contributions to LFV exclude models with the left-right scale $M_{LR} \lesssim 10^5$ GeV.

Besides the above observables, Fig. 3.7 captures also bounds that can be set by the current limits on neutrino masses. Considering left-right symmetric models with both type I and type II seesaw mechanisms implemented (see Sec. 3.7), let us denote the standard Dirac-type neutrino Yukawa coupling as y_ν and the Yukawa coupling corresponding to the left-handed triplet Higgs Δ_L as y^{Δ_L}. Since the VEV of Δ_L is given by $v_L \sim v^2/M_{LR}$ [174], the following conservative range of the masses can be imposed

$$0.16 < \frac{m_\nu}{m_\nu^{\text{exp}}} \approx \left| y^{\Delta_L} - y_\nu^2 \right| \left(\frac{2 \times 10^{14}\ \text{GeV}}{M_{LR}} \right) < 1. \tag{3.124}$$

Here, we have taken the conservative bound on the mass of neutrinos, namely $m_\nu^{\text{exp}} = \sum m_{\nu_i} \lesssim 0.3$ eV [90] and the lower limit provided by the atmospheric mass splitting $\sqrt{\Delta m^2_{\text{atm}}} \approx 0.05$ eV for normally ordered neutrinos. Note also that 10^{14} GeV is the familiar value of the seesaw scale. The thin dotted vertical lines in Fig. 3.7 then show the mass scales of the right-handed neutrino satisfying the constraint in Eq. 3.124 for values of the combined couplings $\sqrt{y^{\Delta_L} - y_\nu^2} \sim 1, 10^{-2}, 10^{-4}$ and 10^{-6} from right to left. As expected, a large left-right scale clearly leads to the correct neutrino masses even for a reasonable coupling of order $\lesssim 1$. On the other hand, a certain fine-tuning of the couplings is necessary for smaller M_{LR}. Taking into account all the maximal constraints, the parametric space of the energy scales is restricted to a rather small region with $10^{14} \gtrsim M_{LR} \gtrsim 10^5$ GeV and $M_{GUT} \gtrsim 10^{16}$ GeV.

3.9 Baryon Asymmetry of the Universe

Probably the most obvious observation requiring physics beyond the SM is the apparent baryon asymmetry of the Universe (BAU). Numerically it is usually

expressed as the baryon-to-photon number density ratio [90]

$$\eta_B^{obs} = \left(\frac{n_B - n_{\overline{B}}}{n_\gamma} \right) = (6.09 \pm 0.06) \times 10^{-10}, \tag{3.125}$$

which can be determined from the power spectrum of temperature fluctuations in the Cosmic Microwave Background (CMB), or from the abundancies of light elements in the intergalactic medium. There are a number of theories trying to explain how this value has been generated. Probably the most popular scenario of baryogenesis is the leptogenesis mechanism, which is based on the generation of a $(B - L)$ number density asymmetry at some high scale.

3.9.1 Conditions for Baryogenesis

As pointed out by Sakharov [62], there are generally three necessary conditions on a theory for baryogenesis to happen from a symmetric initial state:

1. Baryon number violation,

2. C and CP violation,

3. Departure from thermal equilibrium.

The first condition is quite obvious, as any theory of baryogenesis is to evolve a baryon symmetric to a baryon asymmetric Universe, which means that interactions violating baryon number are vital.

The second condition requires that C and CP are not exact symmetries. Indeed, if C was not violated, then the probability of the process $X \to B + Y$ would be equal to the probability of the conjugated process $\bar{X} \to \bar{B} + \bar{Y}$, where X, B and Y denote generic particles with B carrying a baryon number. Hence, the baryon number of products of these two interactions would be equal in absolute value and opposite in sign; thus, the net baryon number B would vanish. Moreover, because of the CPT theorem, CP symmetry would imply that the rate of the process $I(r_i, p_i, s_i) \to F(r_j, p_j, s_j)$ and the rate of its time-reversed version $F(r_j, -p_j, -s_j) \to I(r_i, -p_i, -s_i)$ must be equal. Here, the quantities r, p and s in the brackets denote position, momentum and spin characterizing a particular state. Therefore, even though a baryon asymmetry in certain region of the phase space can be created, after integration over all momenta and summing over all spins the baryon asymmetry would vanish.

Finally, the departure from thermal equilibrium is needed since if all particles remained in thermal equilibrium, no preferred direction of time could be defined and the CPT theorem would not allow for any baryon excess. Hence, any present CP violating interactions would be irrelevant. Since the baryon number B is odd under C and CP transformations, the need for the third Sakharov condition can be understood based on the calculation of the thermodynamic mean value of B at temperature $T = 1/\beta$ [194]

$$\begin{aligned}\langle B\rangle_T &= \mathrm{Tr}[e^{\frac{H}{T}}B] \\ &= \mathrm{Tr}[(CPT)^{-1}(CPT)e^{\frac{H}{T}}B] \\ &= \mathrm{Tr}[e^{\frac{H}{T}}(CPT)B(CPT)^{-1}] \\ &= -\langle B\rangle_T, \end{aligned} \tag{3.126}$$

where the Hamiltonian H is assumed to commute with CPT. Consequently, $\langle B\rangle = 0$, i.e. the average of baryon number in thermal equilibrium at temperature T vanishes.

3.9.2 Leptogenesis

One of the most popular mechanisms explaining the BAU is leptogenesis [22, 195–198]. The original formulation of this theory assumes that at a high energy scale there exist new heavy neutrino states N_i, which goes in hand with the type-I seesaw mechanism described in Sec. 3.6 and as such is very well motivated. These neutrinos are held in thermal equilibrium by processes of the type $N_i \leftrightarrow L^\ell + H$ as long as the temperature of the Universe satisfies $T \gtrsim M_1$, where M_1 is the mass of the lightest heavy neutrino N_1. However, as the Universe cools down, the decay of the heavy neutrinos starts to dominate and if their lifetime is long enough, then an important part of them decays out of equilibrium. Taking into account also the one-loop-level contributions it can be shown in general that the heavy neutrinos decay to leptons and antileptons unevenly. As a result, the second and third Sakharov conditions are satisfied.

The CP asymmetry generated by decays of the i-th heavy neutrino is given by expression

$$\varepsilon_i = \frac{\sum_\ell \Big(\Gamma(N_i \to L^\ell H) - \Gamma(N_i \to \bar{L}^\ell \bar{H})\Big)}{\sum_\ell \Big(\Gamma(N_i \to L^\ell H) + \Gamma(N_i \to \bar{L}^\ell \bar{H})\Big)}, \tag{3.127}$$

and the processes contributing to the above decay widths are depicted in Fig. 3.8. If the heavy neutrinos are hierarchical, i.e. $M_1 \ll M_2,\ M_3$, then ε_1 contributes

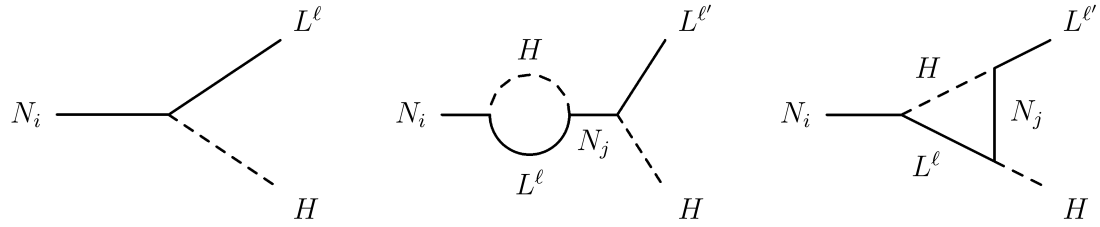

Figure 3.8: Diagrams of heavy neutrino decaying to a lepton and Higgs. The tree-level decay rate is CP-symmetric, and thus in order to generate a non-zero lepton asymmetry the loop-level diagrams must be taken into account. Specifically, the asymmetry originates from the interference of the tree-level and one-loop contributions.

dominantly to the total lepton asymmetry [22]. The non-zero contribution to Eq. (3.127) is generated at loop level, as it comes from interference terms between the tree-level and one-loop diagrams shown in Fig. 3.8 and the approximate resulting asymmetry written in terms of seesaw parameters reads [199]

$$\varepsilon_1 \simeq -\frac{1}{8\pi}\frac{1}{(\mathrm{y}_\nu \mathrm{y}_\nu^\dagger)_{11}}\sum_{j\neq 1}\mathrm{Im}\left[\left(\mathrm{y}_\nu \mathrm{y}_\nu^\dagger\right)_{1j}\left(\mathrm{y}_\nu \mathrm{y}_\nu^\dagger\right)_{1j}\right] f\left(\frac{M_j^2}{M_1^2}\right), \tag{3.128}$$

with

$$f(x) = \sqrt{x}\left(\frac{2}{x-1} + \log_e \frac{1+x}{x}\right). \tag{3.129}$$

Since $M_j^2/M_1^2 \gg 1$, $j \neq 1$, the formula in Eq. (3.128) can be simplified as

$$\varepsilon_1 \simeq -\frac{3}{8\pi}\frac{1}{(\mathrm{y}_\nu \mathrm{y}_\nu^\dagger)_{11}}\sum_{j\neq 1}\mathrm{Im}\left[\left(\mathrm{y}_\nu \mathrm{y}_\nu^\dagger\right)_{1j}\left(\mathrm{y}_\nu \mathrm{y}_\nu^\dagger\right)_{1j}\right]\frac{M_1}{M_j}. \tag{3.130}$$

The hierarchical heavy neutrino case can also lead to interesting predictions. Particularly, it is possible to derive the well-known Davidson-Ibarra upper bound on ϵ_1 [197],

$$|\epsilon_1| \lesssim \frac{3}{8\pi}\frac{M_1}{v^2}(m_3 - m_1), \tag{3.131}$$

where m_1 and m_3 denote masses of light neutrinos, the squared difference of which is known from oscillation experiments. As the above limit depends also on the smallest heavy neutrino mass, the lower bound

$$M_1 \geq 10^9 \text{ GeV} \tag{3.132}$$

can be obtained using the value of ϵ_1 required by the observed baryon asymmetry.

As outlined, the departure from thermal equilibrium is provided by the expansion of the Universe. The interaction rates which are slower than or similar to the Hubble expansion rate cannot equilibrate the particle distributions, as they are not fast enough. The non-equilibrium dynamics is generally described by Boltzmann equations. Assuming the single flavour scenario the evolutions of the N_1 number density and the lepton number density n_L are governed by [195, 200]

$$Hz\frac{\mathrm{d}n_{N_1}}{\mathrm{d}z} = -\left(\Gamma_D + \Gamma_S\right)\left(n_{N_1} - n_{N_1}^{\mathrm{eq}}\right), \tag{3.133}$$

$$Hz\frac{\mathrm{d}n_L}{\mathrm{d}z} = \varepsilon_1\Gamma_D\left(n_{N_1} - n_{N_1}^{\mathrm{eq}}\right) - \Gamma_W n_L, \tag{3.134}$$

respectively, where H is the Hubble expansion parameter and $z = M_1/T$ with T denoting temperature. The superscript 'eq' labels the values of the number densities in thermal equilibrium. Further, the rate Γ_D accounts for both decays and inverse decays of N_1, while the other decay rates take into account 2-2 scattering processes involving the heavy neutrino. There are scatterings of two types. First, Γ_S is the rate of $\Delta L = 1$ scattering processes mediated by Higgs, for which both s-channel

$$N_1 L^\ell \leftrightarrow t\bar{Q}, \quad N_1\bar{L}^\ell \leftrightarrow t\bar{Q} \tag{3.135}$$

and t-channel

$$N_1 t \leftrightarrow \bar{L}^\ell Q, \quad N_1\bar{t} \leftrightarrow L^\ell\bar{Q} \tag{3.136}$$

contributions must be taken into account, see Fig. 3.9. Here, t denotes top quark and Q and L are the SM quark and lepton doublets as before. The second type of scatterings violate lepton number by two units and together with the first type and the inverse decays of N_1 they contribute to the washout rate Γ_W. These $\Delta L = 2$ interactions mediated by the heavy neutrino N_1 read

$$L^\ell H \leftrightarrow \bar{L}^\ell\bar{H}, \quad L^\ell L^\ell \leftrightarrow \bar{H}\bar{H}, \quad \bar{L}^\ell\bar{L}^\ell \leftrightarrow HH \tag{3.137}$$

and are illustrated in Fig. 3.9.

From the right-hand side of the Eq. (3.134) one can readily infer that it is indeed the N_1 decay what produces the lepton number asymmetry (the first term), while all the other processes diminish it, as they contribute to Γ_W coming with a negative sign in front. By solving this set of Boltzmann equations the

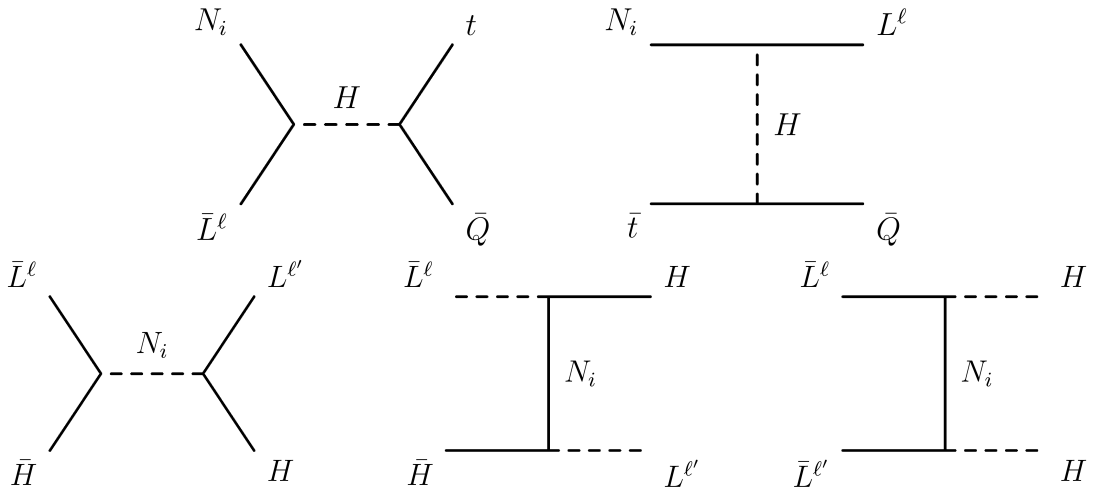

Figure 3.9: The $\Delta L = 1$ (top row) and $\Delta L = 2$ (bottom row) scattering processes in the thermal bath contributing to washout of lepton number asymmetry.

lepton number density $n_L(T_c)$ at the critical temperature T_c of the electroweak transition can be obtained.

To get a baryon number asymmetry one has to consider sphaleron processes violating baryon number [201] (thus, also the first Sakharov condition is fulfilled), or more precisely, the $(B+L)$ symmetry. These non-perturbative processes are described within the thermal field theory and they correspond to tunnelling between two topologically different energy minima (vacua) of the field configurations, which cannot be related by continuous gauge transformations. The sphaleron processes are effective within a wide range of energies from 100 to 10^{12} GeV, where they can convert the lepton number asymmetry generated at some high energy scale to the desired baryon number asymmetry [201]. This conversion is efficient down to the EW scale at the boundary between unbroken and broken phase, where the observed value of baryon asymmetry is frozen in. Defining the lepton and baryon number density normalized to the photon number density as $\eta_L = n_L/n_\gamma$ and $\eta_B = n_B/n_\gamma$, the conversion of the lepton asymmetry to the final baryon asymmetry is given by [202]

$$\eta_B = -d_{\rm rec}\frac{8N_f + 4N_H}{14N_f + 9N_H}\eta_L(T_c), \tag{3.138}$$

where N_f and N_H denote the number of fermion families and Higgs doublets, respectively, in a given theory. The parameter $d_{\rm rec}$ captures the increase of the photon density during the recombination epoch and T_c is the critical temperature of the electroweak phase transition. In the SM these quantities acquire values

$T_c \approx 135$ GeV and $d_{\rm rec} \approx 1/27$. The lepton asymmetry $\eta_L(T_c)$ then corresponds to the value at the sphaleron decoupling temperature [203].

In the above described vanilla scenario of leptogenesis, the hierarchy of heavy neutrino masses has been considered. The situation gets a bit more complicated, if the heavy neutrino states are mass degenerate. In such case resonance effects may occur [204]. To compute the resulting asymmetry in this scheme, one needs to take into account the decays of all the heavy neutrinos. Consequently, the upper bound on ϵ_1 generally depends also on masses M_2 and M_3 [205] and some of the heavy neutrino states can be as light as 100 GeV, while still providing the correct baryon asymmetry.

Generally, a variety of baryogenesis mechanisms have been proposed in the literature [206]. The earliest well-motivated implementations of baryogenesis were developed within the framework of GUTs, in which all three Sakharov conditions can be naturally fulfilled [207]. Unifications embed quarks and leptons in the same representations and as such they naturally incorporate the required baryon number violation. At the same time, they typically include a number of CP-violating complex phases on top of the SM one. Finally, the decays of the heavy particles living around GUT scale are slow in comparison to the expansion rate of the early Universe, which ensures the desired departure from thermal equilibrium. Since the $(B+L)$ number is violated within the SM by sphaleron transitions, the preexisting $(B+L)$ asymmetry would be erased. This is also the reason why minimal GUT baryogenesis producing $(B+L)$ asymmetry fails to work. The desired asymmetry must be therefore created in the $(B-L)$ number, which is conserved in the SM. Intriguingly, the $SO(10)$ GUT incorporates the $U(1)_{B-L}$ subgroup, breaking of which can consequently lead to production of baryon asymmetry via a mechanism akin leptogenesis. Unfortunately, the relevant breaking scales are often far above the electroweak scale making the related hypotheses hard to test.

Besides the GUT baryogenesis a lot of attention has been paid to the electroweak baryogenesis [201, 208–210]. This idea is particularly attractive, for it could be probed by collider experiments. As mentioned above, the baryon number is violated in the SM by sphaleron processes and CP violation is present in the CKM mixing matrix. Nonetheless, electroweak baryogenesis unfortunately cannot rely purely on the SM CP-violating phase, as an additional source of CP violation is necessary for generation of the observed baryon asymmetry. The required departure from thermal equilibrium is provided by the phase transition, if it is of first order. Since this is not the case of the SM symmetry breaking,

consideration of a BSM model, e.g. two Higgs doublet model, is necessary.

A number of other scenarios of baryogenesis also exist. For instance, within a supersymmetric framework the Affleck-Dine mechanism of baryogenesis [211] can be naturally incorporated.

The above discussion has been given to provide an example of particular baryon asymmetry generation mechanisms. In the context of this work we will discuss general washout processes associated with $0\nu\beta\beta$ decay that can erase preexisting $(B-L)$ asymmetry and endanger some of the baryogenesis scenarios. As we will see, the specific scheme generating the baryon asymmetry is not important for our argument. What matters is the energy scale, where baryogenesis happens.

4

Non-Standard $0\nu\beta\beta$ Decay Mechanisms

After reviewing the standard mass mechanism of $0\nu\beta\beta$ decay in previous chapter, let us now concentrate on the non-standard mechanisms basing our discussion on Ref. [212]. From a theoretical point of view, the non-standard $0\nu\beta\beta$ decay can be most generally (i.e. taking into account any other mechanism than the standard one) described by considering the new physics contributions parametrized in terms of all effective low-energy currents that are allowed by Lorentz invariance. Using this convenient approach the nuclear physics part of $0\nu\beta\beta$ decay can be clearly distinguished from the underlying particle physics model.

4.1 The Effective $0\nu\beta\beta$ Decay Lagrangian

The general $0\nu\beta\beta$ decay Lagrangian consists of long range and short range parts [122, 213]

$$\mathcal{L}_{0\nu\beta\beta} = \mathcal{L}_{LR} + \mathcal{L}_{SR}, \tag{4.1}$$

which corresponds to parametrization of different $0\nu\beta\beta$ decay contributions in terms of effective operators of dimension 6 and 9 (in the standard four-component notation),

$$\mathcal{L}_{LR}: \quad \frac{\epsilon_{LR} G_F}{\sqrt{2}} \left(\bar{u}\Pi_1 d\right)\left(\bar{e}\Pi_2 \nu\right) \sim \frac{1}{\Lambda_{LR}^2} \left(\bar{u}\Pi_1 d\right)\left(\bar{e}\Pi_2 \nu\right), \tag{4.2}$$

$$\mathcal{L}_{SR}: \quad \frac{\epsilon_{SR} G_F^2}{2m_p} \left(\bar{u}\Pi_1 d\right)\left(\bar{u}\Pi_2 d\right)\left(\bar{e}\Pi_3 e^C\right) \sim \frac{1}{\Lambda_{SR}^5} \left(\bar{u}\Pi_1 d\right)\left(\bar{u}\Pi_2 d\right)\left(\bar{e}\Pi_3 e^C\right). \tag{4.3}$$

Here, Π_i $(i = 1, 2, 3)$ denote symbolically the Lorentz structures involved and $\frac{\epsilon_{LR} G_F}{\sqrt{2}}$, $\frac{\epsilon_{SR} G_F^2}{2m_p}$ are general effective couplings, which are small as they implicitly incorporate the suppression by the powers of the corresponding cut-off scales Λ_{LR} and Λ_{SR}, to which they can be related. Further, G_F denotes Fermi constant and m_p is the proton mass.

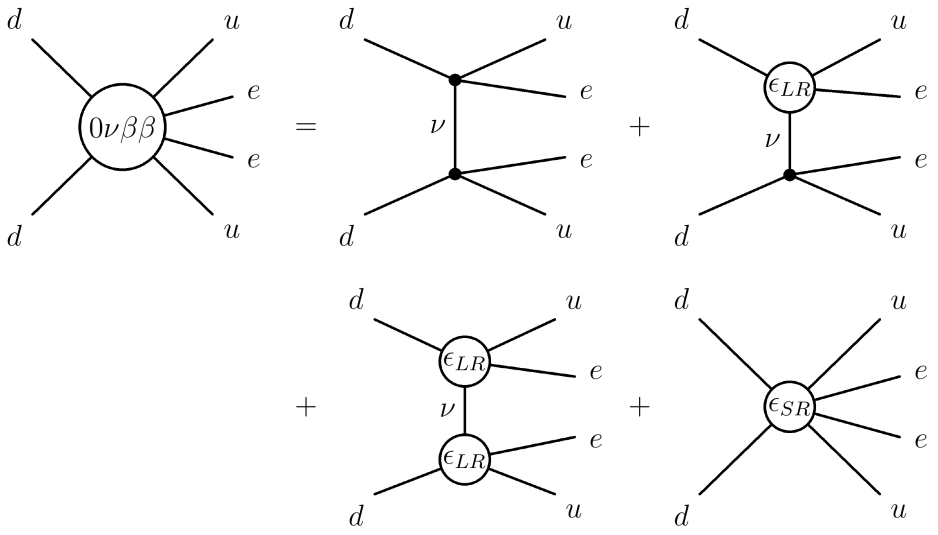

Figure 4.1: Effective low-energy contributions to $0\nu\beta\beta$ decay. The four different diagrams on the right-hand side correspond in the respective order to the standard mass mechanism, long-range mechanisms proportional to ϵ_{LR} and ϵ_{LR}^2 (this contribution is negligible, as ϵ is small) and short-range mechanisms proportional to ε_{SR}.

Graphically, the contributions to $0\nu\beta\beta$ decay including effective couplings ϵ are illustrated in Fig. 4.1. While the first three diagrams on the right-hand side of Fig. 4.1 correspond to the long-range part of the general $0\nu\beta\beta$ decay Lagrangian, the last diagram represents a short-range contribution. The first diagram on the right-hand side of Fig. 4.1 gives the $0\nu\beta\beta$ decay triggered via the standard mass mechanism. The contribution of the third diagram is proportional to ϵ_{LR}^2, and thus it can be neglected. Taking into account the low-energy scale of nuclear beta decays, the standard pointlike lepton number conserving electroweak vertices are in Fig. 4.1 depicted as effective four-fermion interactions.

Contributions to $0\nu\beta\beta$ decay can be constructed at various levels. While Fig. 4.1 illustrates effective $0\nu\beta\beta$ decay contributions at $E < 100$ MeV, in total six different types of diagrams can be drawn in the SM broken phase, i.e. right below the EW scale. These are shown in Fig. 4.2, where they are associated to the mechanisms from Fig. 4.1 they contribute to.

The blobs D_d represent in these diagrams the generated LNV operators of dimension d effective in the energy region under the electroweak scale and the fermion legs coming out of these blobs have origin in the interactions of the underlying UV physics; i.e., none of them is attached via additional SM vertices. The

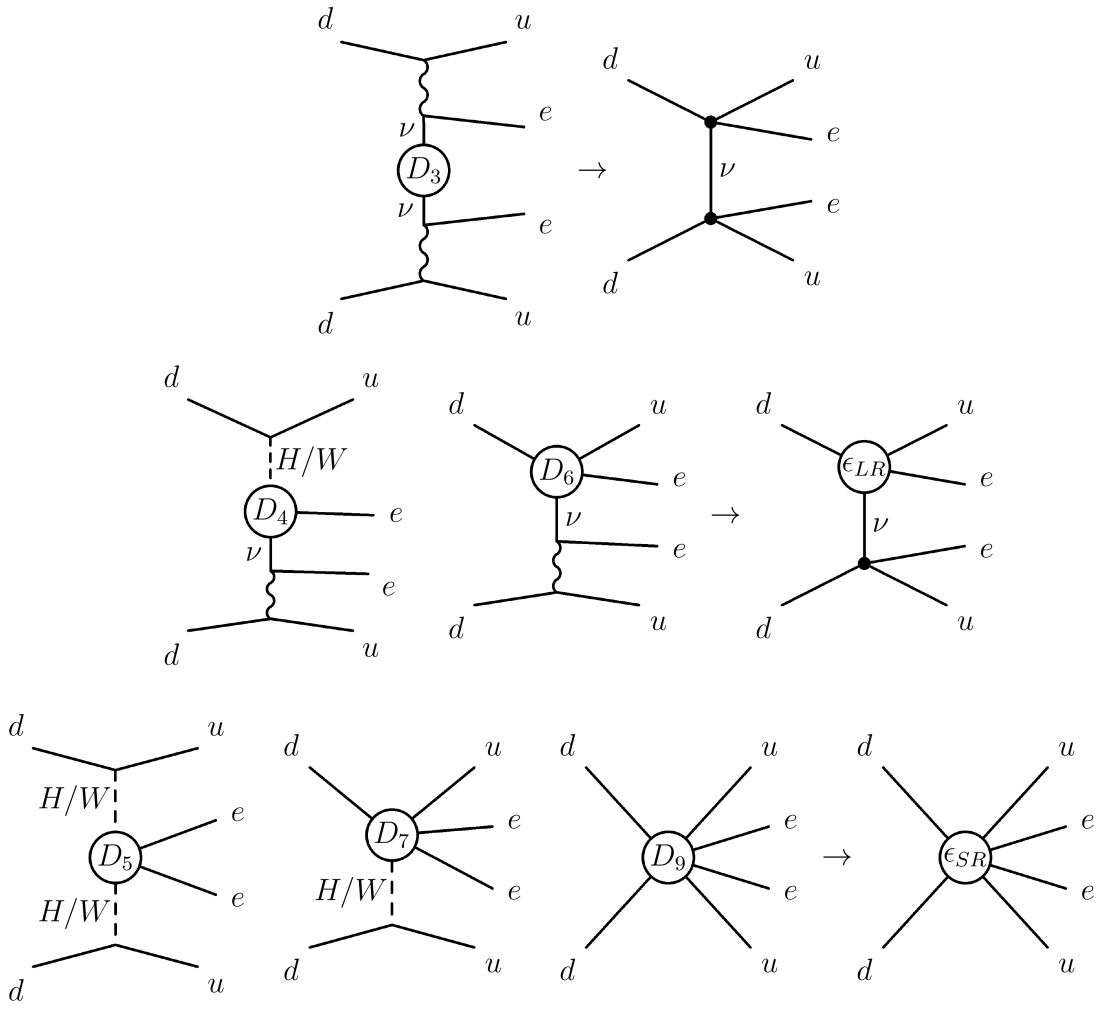

Figure 4.2: Contributions to $0\nu\beta\beta$ decay depicted in the SM broken phase. From top to bottom they correspond to the standard mass mechanism, long range mechanism and short-range mechanism, respectively. The underlying LNV physics is hidden in the effective $\Delta L = 2$ LNV operators D_d of dimension d [214].

blob D_3 in the top diagram is just the standard aforementioned neutrino mass operator. The operators D_4 and D_6 allow for a construction of $0\nu\beta\beta$ decay diagrams contributing to the long-range part of the general $0\nu\beta\beta$ decay Lagrangian. Finally, the remaining three diagrams incorporating D_5, D_7 and D_9 contribute to the short-range part of the general $0\nu\beta\beta$ decay Lagrangian. Each operator D_d will contribute to $0\nu\beta\beta$ decay via all six diagrams. However, it can be expected that there will always be one dominant contribution.

Long-Range Contributions The long-range part of the Lagrangian (represented by the last diagram on the first line in Fig. 4.1) in terms of effective couplings ϵ_β^α corresponding to the pointlike vertices at the Fermi scale ≈ 100 MeV (i.e., the Fierz rearrangement can be used) reads [122]

$$\mathcal{L}_{LR} = \frac{G_F}{\sqrt{2}}\left[J^\dagger_{V-A_\mu} j^\mu_{V-A} + \tilde{\sum_{\alpha,\beta}} \epsilon^\beta_\alpha J^\dagger_\alpha j_\beta\right], \tag{4.4}$$

where the tilde above the sum means that we sum over all contractions allowed by Lorentz invariance except for combination when $\alpha = \beta = (V-A)$, as this one is taken separately with coupling normalized to one The hadronic and leptonic Lorentz currents are defined as $J^\dagger_\alpha = \bar{u}\mathcal{O}_\alpha d$ and $j_\beta = \bar{e}\mathcal{O}_\beta \nu$ of given helicity, respectively. The fields u, d, e and ν are 4-component Dirac bispinors representing the up-quark, down-quark, electron and neutrino, respectively. The operators $\mathcal{O}_{\alpha,\beta}$ can take the forms

$$\mathcal{O}_{V\pm A} = \gamma^\mu(1 \pm \gamma_5), \tag{4.5}$$

$$\mathcal{O}_{S\pm P} = (1 \pm \gamma_5), \tag{4.6}$$

$$\mathcal{O}_{T_{R,L}} = \frac{i}{2}[\gamma_\mu, \gamma_\nu](1 \pm \gamma_5). \tag{4.7}$$

A very detailed and extensive description of the long-range $0\nu\beta\beta$ decay contributions was given by Ali et al. [124].

Short-Range Contributions In the present work most attention will be paid to the short-range contributions to $0\nu\beta\beta$ decay following the Ref. [212]. The short-range mechanisms are represented by the last diagram on the second line in Fig. 4.1 and the general effective Lagrangian can be schematically written as [213]

$$\mathcal{L}_{\rm SR} = \frac{G_F^2}{2m_p} \sum_{\text{chiralities}} \left[\epsilon^\bullet_1 J_\circ J_\circ j_\circ + \epsilon^\bullet_2 J^{\mu\nu}_\circ J_{\circ\mu\nu} j_\circ + \epsilon^\bullet_3 J^\mu_\circ J_{\circ\mu} j_\circ + \epsilon^\bullet_4 J^\mu_\circ J_{\circ\mu\nu} j^\nu + \epsilon^\bullet_5 J^\mu_\circ J_\circ j_\mu\right]. \tag{4.8}$$

Here the place holders $\circ$ and the sum indicate that the currents involved can have different chiralities and for every different combination there is a separate effective coupling $\epsilon^\bullet_i$. The possible hadronic and leptonic currents in Eq. (4.8) read

$$J_{R/L} = \bar{u}(1 \pm \gamma_5)d, \quad J^\mu_{R/L} = \bar{u}\gamma^\mu(1 \pm \gamma_5)d, \quad J^{\mu\nu}_{R/L} = \bar{u}\sigma_{\mu\nu}(1 \pm \gamma_5)d, \tag{4.9}$$

$$j_{R/L} = \bar{e}(1 \pm \gamma_5)e^c, \quad j^\mu = \bar{e}\gamma^\mu\gamma_5 e^c, \tag{4.10}$$

where the usual definition $\sigma_{\mu\nu} = \frac{i}{2}[\gamma_\mu, \gamma_\nu]$ is used. The presence of the charge-conjugated field $e^c = Ce$ in the lepton current means that the electron lepton number is violated by two units, as expected. Despite the fact that all possible combinations of chiralities from Eq. (4.9) can be considered in Eq. (4.8), a number of them will give the same results, thus only a few specific choices will have to be distinguished in the end.

The effective couplings $\epsilon_i^\bullet$ are dimensionless, as the Lagrangian in Eq. (4.8) is conventionally normalized by the factor $G_F^2/(2m_p)$, where m_p is the proton mass and G_F denotes the Fermi constant.

An independent basis of low-energy $0\nu\beta\beta$ decay effective operators of dimension 9 can be chosen in a number of ways and to avoid any confusion about the one considered in this text, we spell the individual operators explicitly out in Table 4.1. The labelling of these operators is analogous to the one used for the corresponding effective coupling in Eq. (4.8), i.e., $\mathcal{O}_i^\bullet \sim \epsilon_i^\bullet$ with the superscript specifying the chiralities of the particular bilinears in their respective order. The redundant or vanishing combinations of chiralities of the three currents are eliminated from this list. Specifically, we omit operators $\mathcal{O}_2^{RLL}$, $\mathcal{O}_2^{LRL}$, $\mathcal{O}_2^{RLR}$ and $\mathcal{O}_2^{LRR}$, which give trivially zero, because of the identity

$$[\bar{u}\sigma^{\mu\nu}(1+\gamma_5)d]\,[\bar{u}\sigma_{\mu\nu}(1-\gamma_5)d] \equiv [\bar{u}\sigma^{\mu\nu}(1-\gamma_5)d]\,[\bar{u}\sigma_{\mu\nu}(1+\gamma_5)d] = 0. \quad (4.11)$$

Note that no terms with vector, tensor or axial-tensor electron currents, $\bar{e}\gamma^\mu e^c = 0$ and $\bar{e}\sigma_{\mu\nu}(1\pm\gamma_5)e^c = 0$, are contained in the Lagrangian Eq. (4.8). This is a trivial consequence of the Pauli exclusion principle.

As a result, the operators listed in Tab. 4.1 form a complete basis of 24 linearly independent 9-dimensional effective operators invariant under the gauge group $SU(3)_C \otimes U(1)_Q$, which trigger $0\nu\beta\beta$ decay. To be explicit, we use the i, j indices to specify also the considered colour contractions. However, in the present basis these are rather trivial, as they always contract the quarks within the same Lorentz bilinear, thus forming colour singlets.

To make sure we have the correct total number of independent effective operators, we have used the Hilbert series method [78,215] as a consistency check. The result of 24 dimension-9 $0\nu\beta\beta$-decay-trigerring operators respecting the gauge group $SU(3)_C \otimes U(1)_Q$ agrees also with Ref. [216]. Nonetheless, it seems to us to be unnecessary to include operators with quark bilinears transforming as octets under $SU(3)_C$, because using Fierz transformations these can be traded for operators involving tensor Lorentz structure, which are included in Tab. 4.1. For

$\mathcal{O}_1^{RRR}$	$[\bar{u}^i(1+\gamma_5)d_i]\,[\bar{u}^j(1+\gamma_5)d_j]\,[\bar{e}(1+\gamma_5)e^c]$
$\mathcal{O}_1^{RRL}$	$[\bar{u}^i(1+\gamma_5)d_i]\,[\bar{u}^j(1+\gamma_5)d_j]\,[\bar{e}(1-\gamma_5)e^c]$
$\mathcal{O}_1^{LRR} \equiv \mathcal{O}_1^{RLR}$	$[\bar{u}^i(1-\gamma_5)d_i]\,[\bar{u}^j(1+\gamma_5)d_j]\,[\bar{e}(1+\gamma_5)e^c]$
$\mathcal{O}_1^{LRL} \equiv \mathcal{O}_1^{RLL}$	$[\bar{u}^i(1-\gamma_5)d_i]\,[\bar{u}^j(1+\gamma_5)d_j]\,[\bar{e}(1-\gamma_5)e^c]$
$\mathcal{O}_1^{LLR}$	$[\bar{u}^i(1-\gamma_5)d_i]\,[\bar{u}^j(1-\gamma_5)d_j]\,[\bar{e}(1+\gamma_5)e^c]$
$\mathcal{O}_1^{LLL}$	$[\bar{u}^i(1-\gamma_5)d_i]\,[\bar{u}^j(1-\gamma_5)d_j]\,[\bar{e}(1-\gamma_5)e^c]$
$\mathcal{O}_2^{RRR}$	$[\bar{u}^i\sigma^{\mu\nu}(1+\gamma_5)d_i]\,[\bar{u}^j\sigma_{\mu\nu}(1+\gamma_5)d_j]\,[\bar{e}(1+\gamma_5)e^c]$
$\mathcal{O}_2^{RRL}$	$[\bar{u}^i\sigma^{\mu\nu}(1+\gamma_5)d_i]\,[\bar{u}^j\sigma_{\mu\nu}(1+\gamma_5)d_j]\,[\bar{e}(1-\gamma_5)e^c]$
$\mathcal{O}_2^{LLR}$	$[\bar{u}^i\sigma^{\mu\nu}(1-\gamma_5)d_i]\,[\bar{u}^j\sigma_{\mu\nu}(1-\gamma_5)d_j]\,[\bar{e}(1+\gamma_5)e^c]$
$\mathcal{O}_2^{LLL}$	$[\bar{u}^i\sigma^{\mu\nu}(1-\gamma_5)d_i]\,[\bar{u}^j\sigma_{\mu\nu}(1-\gamma_5)d_j]\,[\bar{e}(1-\gamma_5)e^c]$
$\mathcal{O}_3^{RRR}$	$[\bar{u}^i\gamma^{\mu}(1+\gamma_5)d_i]\,[\bar{u}^j\gamma_{\mu}(1+\gamma_5)d_j]\,[\bar{e}(1+\gamma_5)e^c]$
$\mathcal{O}_3^{RRL}$	$[\bar{u}^i\gamma^{\mu}(1+\gamma_5)d_i]\,[\bar{u}^j\gamma_{\mu}(1+\gamma_5)d_j]\,[\bar{e}(1-\gamma_5)e^c]$
$\mathcal{O}_3^{LRR} \equiv \mathcal{O}_3^{RLR}$	$[\bar{u}^i\gamma^{\mu}(1-\gamma_5)d_i]\,[\bar{u}^j\gamma_{\mu}(1+\gamma_5)d_j]\,[\bar{e}(1+\gamma_5)e^c]$
$\mathcal{O}_3^{LRL} \equiv \mathcal{O}_3^{RLL}$	$[\bar{u}^i\gamma^{\mu}(1-\gamma_5)d_i]\,[\bar{u}^j\gamma_{\mu}(1+\gamma_5)d_j]\,[\bar{e}(1-\gamma_5)e^c]$
$\mathcal{O}_3^{LLR}$	$[\bar{u}^i\gamma^{\mu}(1-\gamma_5)d_i]\,[\bar{u}^j\gamma_{\mu}(1-\gamma_5)d_j]\,[\bar{e}(1+\gamma_5)e^c]$
$\mathcal{O}_3^{LLL}$	$[\bar{u}^i\gamma^{\mu}(1-\gamma_5)d_i]\,[\bar{u}^j\gamma_{\mu}(1-\gamma_5)d_j]\,[\bar{e}(1-\gamma_5)e^c]$
$\mathcal{O}_4^{RR}$	$[\bar{u}^i\gamma^{\mu}(1+\gamma_5)d_i]\,[\bar{u}^j\sigma_{\mu\nu}(1+\gamma_5)d_j]\,[\bar{e}\gamma^{\nu}\gamma_5 e^c]$
$\mathcal{O}_4^{RL}$	$[\bar{u}^i\gamma^{\mu}(1+\gamma_5)d_i]\,[\bar{u}^j\sigma_{\mu\nu}(1-\gamma_5)d_j]\,[\bar{e}\gamma^{\nu}\gamma_5 e^c]$
$\mathcal{O}_4^{LR}$	$[\bar{u}^i\gamma^{\mu}(1-\gamma_5)d_i]\,[\bar{u}^j\sigma_{\mu\nu}(1+\gamma_5)d_j]\,[\bar{e}\gamma^{\nu}\gamma_5 e^c]$
$\mathcal{O}_4^{LL}$	$[\bar{u}^i\gamma^{\mu}(1-\gamma_5)d_i]\,[\bar{u}^j\sigma_{\mu\nu}(1-\gamma_5)d_j]\,[\bar{e}\gamma^{\nu}\gamma_5 e^c]$
$\mathcal{O}_5^{RR}$	$[\bar{u}^i\gamma^{\mu}(1+\gamma_5)d_i]\,[\bar{u}^j(1+\gamma_5)d_j]\,[\bar{e}\gamma_{\mu}\gamma_5 e^c]$
$\mathcal{O}_5^{RL}$	$[\bar{u}^i\gamma^{\mu}(1+\gamma_5)d_i]\,[\bar{u}^j(1-\gamma_5)d_j]\,[\bar{e}\gamma_{\mu}\gamma_5 e^c]$
$\mathcal{O}_5^{LR}$	$[\bar{u}^i\gamma^{\mu}(1-\gamma_5)d_i]\,[\bar{u}^j(1+\gamma_5)d_j]\,[\bar{e}\gamma_{\mu}\gamma_5 e^c]$
$\mathcal{O}_5^{LL}$	$[\bar{u}^i\gamma^{\mu}(1-\gamma_5)d_i]\,[\bar{u}^j(1-\gamma_5)d_j]\,[\bar{e}\gamma_{\mu}\gamma_5 e^c]$

Table 4.1: Basis of low-energy, 9-dimensional $0\nu\beta\beta$ decay operators invariant under the $SU(3)_C \otimes U(1)_Q$ gauge group.

instance, the following Fierz identity holds for operator $\mathcal{O}_2^{LLL}$

$$\begin{aligned}\mathcal{O}_2^{LLL} &= \left[\bar{u}^i\sigma^{\mu\nu}(1-\gamma_5)d_i\right]\left[\bar{u}^j\sigma_{\mu\nu}(1-\gamma_5)d_j\right]j_L \\ &= 2\left[\bar{u}^i(1-\gamma_5)d_j\right]\left[\bar{u}^j(1-\gamma_5)d_i\right]j_L - \left[\bar{u}^i(1-\gamma_5)d_i\right]\left[\bar{u}^j(1-\gamma_5)d_j\right]j_L.\end{aligned} \tag{4.12}$$

Next, the well-known group-theoretic formula for the Gell-Mann matrices λ^a (where $a = 1, \ldots, 8$),

$$\delta_{ij}\delta_{kl} = \frac{1}{3}\delta_{il}\delta_{kj} + \frac{1}{2}(\lambda^a)_{il}(\lambda_a)_{kj}, \tag{4.13}$$

induces the $SU(3)_C$ Fierz identity, which can be applied on the first term on the right-hand side of Eq. (4.12) as

$$\begin{aligned}\mathcal{O}_2^{LLL} = &\left[\bar{u}^i(1-\gamma_5)(\lambda^a)_{ik}d^k\right]\left[\bar{u}^j(1-\gamma_5)(\lambda_a)_{jl}d^l\right]j_L \\ &-\frac{1}{3}\left[\bar{u}^i(1-\gamma_5)d_i\right]\left[\bar{u}^j(1-\gamma_5)d_j\right]j_L \\ \equiv &\left[\bar{u}^i(1-\gamma_5)(\lambda^a)_{ik}d^k\right]\left[\bar{u}^j(1-\gamma_5)(\lambda_a)_{jl}d^l\right]j_L - \frac{1}{3}\mathcal{O}_1^{LLL}.\end{aligned} \tag{4.14}$$

Consequently, if we neglect the first term on the right-hand side of Eq. (4.14), the operator $\mathcal{O}_2^{LLL}$ is identified with the operator $\mathcal{O}_1^{LLL}$ and as such it can be omitted. According to Ref. [217] this is well justified, as the operator containing colour octets does not contribute to $0\nu\beta\beta$ decay. The same procedure can be applied to all the other operators involving tensor quark currents. Hence, all of them can be exchanged for the operators with colour octets and after neglecting these the basis is reduced to colour-singlet operators consisting only of Lorentz scalar or vector bilinears. However, we will calculate also the direct limits on the operators $\mathcal{O}_2^\bullet$ including tensor bilinears for comparison with existing literature. Therefore, our approach is independent of the assumption that colour non-singlet currents do not contribute to $0\nu\beta\beta$ decay.

Effective Couplings From The Decay Rate Let us now briefly motivate the calculations contained by the rest of this chapter. As we will discuss later in more detail, the theoretical formula for the $0\nu\beta\beta$ decay half life $T_{1/2}$ can be written as

$$T_{1/2}^{-1} = (\epsilon_\bullet^\bullet)^2 G_i |M_i|^2, \tag{4.15}$$

where G_i are the relevant phase space factors (PSFs) and M_i stand for the nuclear matrix elements (NMEs) for a given isotope and operator, which is assumed

$\lvert\epsilon\rvert \times 10^8$	ϵ_ν	ϵ^{V+A}_{V-A}	ϵ^{V+A}_{V+A}	$\epsilon^{S+P}_{S\pm P}$	$\epsilon^{T_R}_{T_R}$	$\epsilon^{\bullet}_1$	$\epsilon^{\bullet}_2$	$\epsilon^{RR,LL}_3$	ϵ^{LR}_3	$\epsilon^{\bullet}_4$	$\epsilon^{\bullet}_5$
^{76}Ge	41	0.21	37	0.66	0.07	19	0.11	1.30	0.83	0.90	9.0
^{76}Xe	26	0.11	22	0.26	0.03	10	0.05	0.43	0.66	0.46	4.6

Table 4.2: Here, we summarize the upper limits on effective $0\nu\beta\beta$ interactions (in units of 10^{-8}), which were obtained by updating the limits given in Ref. [115] using the latest experimental bounds $T^{\rm Ge}_{1/2} \gtrsim 5.3\times10^{25}$ y and $T^{\rm Xe}_{1/2} \gtrsim 1.07\times10^{26}$ y. Only one contribution is assumed to be non-zero at a time. The coupling $\epsilon_\nu = m_\nu/m_e$ corresponds to the standard mechanism and as such it gives the limits of 0.21 eV (Ge) and 0.13 eV (Xe) on the effective $0\nu\beta\beta$ mass. The limit on ϵ_3 depends on the chirality of the hadronic currents: $\epsilon^{RR,LL}_3$ (hadronic currents have same chirality), ϵ^{LR}_3 (hadronic currents have opposite chirality).

to be dominant. The coefficient $\epsilon^{\bullet}_{\bullet}$ is the effective coupling of this specific operator. Considering the current experimental limits on $0\nu\beta\beta$ decay half life, the bounds on the effective couplings can be calculated using Eq.(4.15). In Tab. 4.2 we summarize the results for both the short-range and long-range parts of the Lagrangian, which were take from [115] and updated using the most recent experimental limits. The calculation performed in Ref. [115] uses the leading NMEs calculated by the QRPA method and approximate PSFs.

In the rest of this chapter a detailed derivation of the bounds on the effective couplings respective to the short-range operators is performed. The discussion is, however, kept fairly general and a significant part of the presented formulae as well as the overall approach can be applied to any $0\nu\beta\beta$ decay mechanism.

4.2 Neutrinoless Double Beta Decay Rate

In the following we calculate the $0\nu\beta\beta$ decay rate for SR effective operators. The starting point is the differential decay rate given by [218]

$$d\Gamma = 2\pi\overline{|\mathcal{R}|^2}\delta(E_1+E_2+E_F-E_I)\frac{d^3\mathbf{p}_1}{(2\pi)^3}\frac{d^3\mathbf{p}_2}{(2\pi)^3}, \tag{4.16}$$

with $\overline{|\mathcal{R}|^2}$ denoting the square of the full matrix element of the $0\nu\beta\beta$ decay process, which is summed over the spin projections s_1, s_2 of the electrons and the final nuclear state S_F. As already defined before, E_F and E_I stand for the energies of the final and initial nuclei, respectively, and the outgoing electrons have the

four momenta $(E_1, \mathbf{p}_1)$ and $(E_2, \mathbf{p}_2)$. The magnitudes of the electron 3-momenta are denoted as $p_i \equiv |\mathbf{p}_i| = \sqrt{E_i^2 - m_e^2}$, with the electron mass $m_e = 0.511$ MeV. The $Q_{\beta\beta}$ value of the transition, i.e. the kinetic energy release of the electrons, is determined by $Q_{\beta\beta} = E_I - E_F - 2m_e$. Note that the recoil energy of the final nucleus is neglected in the above formula, which is well justified, as for the isotope masses M_A of interest it can be estimated as $Q_{\beta\beta}^2/(2M_A) = \mathcal{O}(0.1 \text{ keV})$. The differential rate can be expressed (due to the energy conservation and the overall rotational invariance) in terms of the energy $E_1 \in (m_e, Q_{\beta\beta} + m_e)$ of one of the electrons and the angle $\theta \in [0, \pi]$ between the two electrons, defined by the relation $\cos\theta = \hat{\mathbf{p}}_1 \cdot \hat{\mathbf{p}}_2$.[1] Therefore, the energy of the second electron is then given by $E_2 = Q_{\beta\beta} + 2m_e - E_1$.

Formally, the full matrix element of the $0\nu\beta\beta$ decay process can be written as

$$\mathcal{R} = \left\langle \mathcal{O}_F^+ e_{\mathbf{p}_1 s_1} e_{\mathbf{p}_2 s_2} \right| \mathcal{L}_{\text{SR}} \left| \mathcal{O}_I^+ \right\rangle, \tag{4.17}$$

where $\left|\mathcal{O}_I^+\right\rangle$ denotes the initial nuclear state and $\left\langle \mathcal{O}_F^+ e_{\mathbf{p}_1 s_1} e_{\mathbf{p}_2 s_2} \right|$ is the final state composed of the 0^+ daughter nuclear state and the two emitted electrons. The wave functions of the $\mathcal{O}_I^+$ and $\mathcal{O}_F^+$ states in terms of their constituent nucleons and the wave function of the two electrons in Eq. (4.17) are understood to be anti-symmetrized. The quark level Lagrangian $\mathcal{L}_{\text{SR}}$ in Eq. (4.17) is considered in the most general form expressed in Eq. (4.8). Symbolically, the following short-hand notation can be used

$$\mathcal{L}_{\text{SR}} = \frac{G_F^2}{2m_p} \sum_{K,\Xi} \epsilon_K j_K^\Xi J_K^\Xi J_K'^\Xi, \tag{4.18}$$

where we sum over K and Ξ, which collectively label the different electron-quark-quark current combinations jJJ', including different chiralities, and the Lorentz contractions, respectively.

A detailed derivation for the specific long-range scenario combining the $(V-A)$ and $(V+A)$ currents was published by Doi et al. [219, 220] and Tomoda [218]. More recently, an extensive calculation for the general long-range Lagrangian was given by Ali et al. [124].

For every effective non-standard $0\nu\beta\beta$ decay contribution the hadronic part is given by a product of two quark currents. Therefore, one must perform a summation over a set of intermediate nuclear states $|\mathcal{N}\rangle$, which is a daunting task, because all states up to an energy $E \approx 100$ MeV must be taken into account.

[1] Throughout this text, unit vectors are denoted by $\hat{\mathbf{v}} \equiv \mathbf{v}/|\mathbf{v}|$.

For this reason, the summation is commonly treated in the so called *closure approximation*, which means that a sum over a complete set of states is performed,

$$\sum_{\mathcal{N}} \left\langle \mathcal{O}_F^+ \right| J_K^\Xi \left| \mathcal{N} \right\rangle \left\langle \mathcal{N} \right| J_K'^\Xi \left| \mathcal{O}_I^+ \right\rangle \approx \left\langle \mathcal{O}_F^+ \right| J_K^\Xi J_K'^\Xi \left| \mathcal{O}_I^+ \right\rangle . \tag{4.19}$$

For the short-range case the intermediate transition occurs at very high energies, $|\mathbf{q}| \approx 100$ MeV, corresponding to the inter-nucleon distance, compared to the nuclear transition itself at $Q_{\beta\beta} \approx 1$ MeV. Therefore, the closure approximation is very well justified.

What also complicates the calculation is the fact that the hadronic part is entangled with the leptonic one. To make the calculation feasible, an approximation is made wherein the electron wave functions are evaluated at the surface of the nucleus, i.e. at $r = R$ with R being the radius of the nucleus [134, 219]. As a result, the leptonic part can be separated from the hadronic one. It is possible to improve the approximation by using the simplified nucleon wave functions and calculating the weighted average electron position [134]. However, no sizeable error is introduced by the approximation employed in this text.

Using the outlined approach the overall $0\nu\beta\beta$ decay matrix element $\mathcal{R}$ can be factorized into the nuclear and atomic parts, which can be further treated separately. First, the product of the leptonic matrix elements must be integrated over the phase space of the two emitted electrons. Consequently, the so-called phase-space factor (PSF) is obtained, which depends only on the given leptonic current and the electron wave function at the surface of the nucleus.[2] Second, the nuclear matrix element (NME) must be computed. We start with a non-relativistic expansion of each nucleon current J_K^Ξ by means of a Foldy-Wouthuysen (FW) transformation taking terms to order $|\mathbf{q}|/m_p$. Subsequently, we calculate the product of the two currents and evaluate the matrix elements of the corresponding two-body operator in the nuclear many-body wave functions. The FW approximation works well for $0\nu\beta\beta$ decay, as the typical momentum transfer in the process is of order $|\mathbf{q}| \sim 100$ MeV, and therefore $|\mathbf{q}|/m_p \sim 0.1$. Although in the resulting products of hadronic currents we generally keep also only terms to order $|\mathbf{q}|/m_p$, in certain cases higher order terms are also taken into account because of a significant enhancement of the associated form factors.

[2]Naturally, the phase-space factors of the associated $2\nu\beta\beta$ decay will also depend on the outgoing neutrino wave functions.

Altogether, the full matrix element is given by

$$\mathcal{R} = \frac{G_F^2}{2m_p} \sum_{K,\Xi} \epsilon_K \left\langle e_{\mathbf{p}_1 s_1} \left| j_K^{\Xi} \right| e^c_{\mathbf{p}_2 s_2} \right\rangle \left\langle \mathcal{O}_F^+ \right| J_K^{\Xi} J_K'^{\Xi} \left| \mathcal{O}_I^+ \right\rangle . \tag{4.20}$$

A detailed evaluation of the leptonic matrix elements using the appropriate electron wave functions is given for the short-range case in Sec. 4.3 resulting in the corresponding PSFs. The short-range nucleon matrix elements are evaluated as outlined above, including appropriate $\mathbf{q}^2$-dependent form factors, in Sec. 4.5. The final nuclear matrix elements are derived in Sec. 4.7.

Combining the PSFs and NMEs, the fully differential rate for $0^+ \to 0^+$ $0\nu\beta\beta$ decay as expressed in [218–220] can be written in the form[3]

$$\frac{d^2\Gamma}{dE_1 d\cos\theta} = C\, w(E_1)\left(a(E_1) + b(E_1)\cos\theta\right), \tag{4.21}$$

where

$$C = \frac{G_F^4 m_e^2}{16\pi^5}, \tag{4.22}$$

$$w(E_1) = E_1 E_2 p_1 p_2, \tag{4.23}$$

with E_2, p_1 and p_2 given as functions of E_1.

As we stick to the notation of [218–220], the electron mass m_e is added in the numerator so that it cancels the mass m_e in the denominator of the so-called neutrino potential in the following Eq. (4.100). Similarly, the coefficient $1/m_p$ in Eq. (4.20) is included in the calculation of the nuclear matrix elements, see Eq. (4.100).

Consequently, the total decay rate Γ (and the inverse value of the decay half life $T_{1/2}$) reads

$$\Gamma = \frac{\ln 2}{T_{1/2}} = 2C \int_{m_e}^{Q_{\beta\beta}+m_e} dE_1 w(E_1) a(E_1). \tag{4.24}$$

The Eq. (4.21) yields the single electron energy distribution

$$\frac{d\Gamma}{dE_1} = 2C w(E_1) a(E_1), \tag{4.25}$$

and the energy-dependent angular correlation

$$\alpha(E_1) = \frac{b(E_1)}{a(E_1)}. \tag{4.26}$$

[3]Let us note that for $0^+ \to 2^+$ $0\nu\beta\beta$ decay, there is an additional term in Eq. (4.21) of the form $c(E_1)(\cos^2\theta - 1/3)$.

If we define the integrated quantities

$$A = \int_{m_e}^{Q_{\beta\beta}+m_e} dE_1 w(E_1) a(E_1), \quad B = \int_{m_e}^{Q_{\beta\beta}+m_e} dE_1 w(E_1) b(E_1), \tag{4.27}$$

and their ratio $K = B/A$, we obtain the angular distribution

$$\frac{d\Gamma}{d\cos\theta} = \frac{\Gamma}{2}\left(1 + K\cos\theta\right). \tag{4.28}$$

The single electron energy distribution and the angular correlation can be measured only by certain experimental setups like e.g. the SuperNEMO experiment mentioned earlier in Subsec. 3.5.1. Nevertheless, the calculation of these quantities is included in this work, as the contained information can be useful for distinguishing the underlying mechanism of $0\nu\beta\beta$ decay.

4.3 Leptonic Phase Space Factors

Let us first focus on the atomic part of the $0\nu\beta\beta$ decay, i.e. on the derivation of the leptonic phase-space factors quantifying the effect of the two relativistic electrons emitted in the process. First of all, the partial wave expansion can be applied to the position-dependent wave function of each electron. If we denote the asymptotic momentum at a far distance from the nucleus and the spin projection of the electron by $\mathbf{p}$ and s, respectively, then the electron wave function expands in terms of spherical waves as

$$e_{\mathbf{p}s}(\mathbf{r}) = e_{\mathbf{p}s}^{S_{1/2}}(\mathbf{r}) + e_{\mathbf{p}s}^{P_{1/2}}(\mathbf{r}) + \ldots, \tag{4.29}$$

where the $S_{1/2}$ and the $P_{1/2}$ waves are given by [218]

$$e_{\mathbf{p}s}^{S_{1/2}}(\mathbf{r}) = \begin{pmatrix} g_{-1}(E,r)\chi_s \\ f_1(E,r)(\boldsymbol{\sigma}\cdot\hat{\mathbf{p}})\chi_s \end{pmatrix}, \; e_{\mathbf{p}s}^{P_{1/2}}(\mathbf{r}) = i\begin{pmatrix} g_1(E,r)(\boldsymbol{\sigma}\cdot\hat{\mathbf{r}})(\boldsymbol{\sigma}\cdot\hat{\mathbf{p}})\chi_s \\ -f_{-1}(E,r)(\boldsymbol{\sigma}\cdot\hat{\mathbf{r}})\chi_s \end{pmatrix}. \tag{4.30}$$

Here, $g_\kappa(E,r)$ and $f_\kappa(E,r)$ denote the radial wave functions of the 'large' and 'small' components. Asymptotically, the electron energy goes to $E = \sqrt{\mathbf{p}^2 + m_e^2}$ and the electron spin state is described by the two-dimensional spinor χ_s. The Pauli matrices $\boldsymbol{\sigma}$ in the above formulae operate in the electron spin space.

The asymptotic boundary condition satisfied by the radial wave functions reads [218]

$$\begin{pmatrix} g_\kappa(E,r) \\ f_\kappa(E,r) \end{pmatrix} \xrightarrow{r\to\infty} \frac{e^{-i\Delta_\kappa^c}}{pr}\begin{pmatrix} \sqrt{\frac{E+m_e}{2E}}\sin\left(pr + y\ln(2pr) - \frac{1}{2}\pi l_\kappa + \Delta_\kappa^c\right) \\ \sqrt{\frac{E-m_e}{2E}}\cos\left(pr + y\ln(2pr) - \frac{1}{2}\pi l_\kappa + \Delta_\kappa^c\right) \end{pmatrix}, \tag{4.31}$$

with $\kappa = \pm(j + \frac{1}{2})$, $l_k = j \pm \frac{1}{2}$, $y = \alpha Z E/p$ and Δ_κ^c stands for a phase shift. Further, $p = |\mathbf{p}|$ is the magnitude of the electron momentum, j denotes the total angular momentum of the electron, Z stands for the atomic number of the daughter nucleus and α is the fine structure constant. The radial wave functions Eq. (4.30) can be approximated inside the nucleus by the leading terms of the expansion in r as follows

$$\begin{pmatrix} g_{-1}(E,r) \\ f_1(E,r) \end{pmatrix} \approx \begin{pmatrix} A_{-1} \\ A_{+1} \end{pmatrix}, \tag{4.32}$$

$$\begin{pmatrix} g_1(E,r) \\ -f_{-1}(E,r) \end{pmatrix} \approx \begin{pmatrix} A_{+1}\left[\frac{1}{2}\alpha Z + \frac{1}{3}(E+m_e)R_A\right]\frac{r}{R_A} \\ -A_{-1}\left[\frac{1}{2}\alpha Z + \frac{1}{3}(E-m_e)R_A\right]\frac{r}{R_A} \end{pmatrix}, \tag{4.33}$$

for $S_{1/2}$ and $P_{1/2}$ waves, respectively. Here, R_A is the radius of the daughter nucleus and A_κ are normalization constants. In the limit $Z \to 0$ the radial wave functions take the form of spherical Bessel functions and the normalization constants become

$$A_{\pm 1} \approx \sqrt{\frac{E \mp m_e}{2E}}. \tag{4.34}$$

Nonetheless, in the present work, instead of using the above approximations we derive the phase-space factors employing the numerically calculated radial wave functions as described in [134]. The performed numerical solution makes use of a piecewise exact power series expansion of the radial wave functions. Additionally, the nuclear size and electron cloud screening corrections are taken into account on top of the standard Coulomb potential of the daughter nucleus, $V(r) = -\alpha Z/r$, with charge Z.

The full potential we consider thus reads

$$V(r) = \begin{cases} -\alpha Z \frac{3-(r/R_A)^2}{2R_A} \times \varphi(r), & r < R, \\ -\frac{\alpha Z}{r} \times \varphi(r), & r \geq R, \end{cases} \tag{4.35}$$

with $\varphi(r)$ denoting the Thomas-Fermi function, which describes the electron screening. To incorporate the finite nuclear size a uniform charge distribution in a sphere of radius $R_A = R_0 A^{1/2}$ with $R_0 = 1.2$ fm is considered. As a result, the non-trivial r-dependence of the above potential for $r < R$ arises.

To calculate the electron currents involved in $0\nu\beta\beta$ decay we in principle need to evaluate the wave functions at the position of the corresponding transition. To do so exactly would require inclusion of the wave function of the nucleon undergoing the respective decay - either by employing a simplified harmonic oscillator

wave functions [134], or ideally, from the nuclear structure model used to calculate the NMEs (cf. Sec. 4.7). In the present work, we however follow [134] and adopt the approximation of evaluating the electron wave function at the nuclear radius $r = R_A$,

$$f_{\pm 1}(E) \equiv f_{\pm 1}(E, R_A), \tag{4.36}$$

$$g_{\pm 1}(E) \equiv g_{\pm 1}(E, R_A). \tag{4.37}$$

This choice reflects the fact that nucleons mostly decay at the surface of the nucleus due to Pauli-blocking of inner states.

In order to obtain $0^+ \to 0^+$ transitions, parity-even nucleon operators must be accompanied by $S_{1/2} - S_{1/2}$ and $P_{1/2} - P_{1/2}$ electron wave functions, while parity-odd operators need to be combined with $S_{1/2} - P_{1/2}$ wave functions. We do not take into account the $0^+ \to 2^+$ transitions, as it is relatively suppressed by the corresponding $Q_{\beta\beta}$ value. Also, in the following we will restrict ourselves to the case of $S_{1/2} - S_{1/2}$ wave functions providing the leading order contribution.

Terms 1, 2, 3 The Lorentz scalar electron current appearing in first three terms of the short-range Lagrangian (4.8) reads

$$j = \bar{e_1}(x)(1 \pm \gamma_5)e_2^C(x), \tag{4.38}$$

where the electron wave functions depend on the same coordinate variable, as a contact interaction is considered. In the $S_{1/2} - S_{1/2}$ wave approximation and using Tomoda's notation we obtain[4]

$$\begin{aligned}
&\bar{e_1}(1 \pm \gamma_5)e_2^C \left(\frac{1 - P_{e_1 e_2}}{2}\right) \\
&\approx (\bar{e}_{\mathbf{p}_1 s_1})^{S_{1/2}}(1 \pm \gamma_5)(e^C_{\mathbf{p}_2 s_2})^{S_{1/2}} \\
&= \left(e^{S_{1/2}}_{\mathbf{p}_1 s_1}\right)^\dagger \gamma_0(1 \pm \gamma_5) i\gamma_2 \left(e^{S_{1/2}}_{\mathbf{p}_2 s_2}\right)^* \\
&= \left(g_{-1}(\epsilon_1, r)\chi^\dagger_{s_1} \quad f_1(\epsilon_1, r)\chi^\dagger_{s_1}(\boldsymbol{\sigma}\cdot\hat{\mathbf{p}}_1)\right)\gamma_0\,(1 \pm \gamma_5)\, i\gamma_2 \begin{pmatrix} g_{-1}(\epsilon_2, r)\chi_{s_2} \\ f_1(\epsilon_2, r)(\boldsymbol{\sigma}\cdot\hat{\mathbf{p}}_2)\chi_{s_2} \end{pmatrix},
\end{aligned} \tag{4.39}$$

[4]Here, all the gamma matrices are considered in the standard Dirac representation, i.e.

$$\gamma_0 = \begin{pmatrix} 1 & 0 \\ 0 & -1 \end{pmatrix}, \quad \boldsymbol{\gamma} = \begin{pmatrix} 0 & \boldsymbol{\sigma} \\ -\boldsymbol{\sigma} & 0 \end{pmatrix}, \quad \gamma_5 = \begin{pmatrix} 0 & 1 \\ 1 & 0 \end{pmatrix}, \quad C = i\gamma_2\gamma_0 = \begin{pmatrix} 0 & -i\sigma_2 \\ -i\sigma_2 & 0 \end{pmatrix}.$$

where the operator $P_{e_1e_2}$ interchanges the electrons, and thus the expression is antisymmetrized under the exchange of the electrons. In this case the effect of antsymmetrization is trivial, but we show it explicitly to note that the current is antisymmetric, as it should due to the Pauli principle.

Next, we expand and square the Eq. (4.39). After summing over spins and using the properties of the spinors χ_s we get

$$\begin{aligned}
&\sum_{s_1,s_2} (\bar{e_1}(1+\gamma_5)e_2^C)(\bar{e_1}(1\pm\gamma_5)e_2^C)^\dagger \\
&= \sum_{s_1,s_2} \Big[\Big(f^{-1}{}_1\chi^\dagger_{s_1}(\boldsymbol{\sigma}\cdot\hat{\mathbf{p}}_2)\sigma_2\chi_{s_2} + f_1{}^{-1}\chi^\dagger_{s_1}(\boldsymbol{\sigma}\cdot\hat{\mathbf{p}}_1)\sigma_2\chi_{s_2}\Big) \\
&\quad \pm \Big(f^{-1-1}\chi^\dagger_{s_1}\sigma_2\chi_{s_2} + f_{11}\chi^\dagger_{s_1}(\boldsymbol{\sigma}\cdot\hat{\mathbf{p}}_1)(\boldsymbol{\sigma}\cdot\hat{\mathbf{p}}_2)\sigma_2\chi_{s_2}\Big)\Big]^2 \\
&= 2\left[f_{11}^{(0)} + f_{11+}^{(1)}(\hat{\mathbf{p}}_1\cdot\hat{\mathbf{p}}_2)\right],
\end{aligned} \tag{4.40}$$

where $f_{11}^{(0)}$, $f_{11+}^{(1)}$ are defined in Eq. (4.48) and $f^{-1-1}, f_{11}, f^{-1}{}_1, f_1{}^{-1}$ are introduced in Eqs. (4.51)-(4.54). For the interference term combining a left-handed with a right-handed electron current, the calculation is analogous to the procedure shown above, but the plus sign in the definition of $f_{11+}^{(1)}$ changes to a minus sign and the corresponding expression we denote as $f_{11-}^{(1)}$, see Eq. (4.48). If both the involved scalar currents are left-handed, the same result as for two right-handed currents holds.

Terms 4, 5 The vector electron current present in the fourth and fifth terms of the Lagrangian (4.8) reads

$$j^\mu = \bar{e_1}(x)\gamma^\mu\gamma_5 e_2^C(x), \tag{4.41}$$

and in the $S_{1/2} - S_{1/2}$ approximation it is obtained as

$$\begin{aligned}
&\bar{e_1}\gamma^\mu\gamma_5 e_2^C\left(\frac{1-P_{e_1e_2}}{2}\right) \\
&\approx (\bar{e}_{\mathbf{p}_1 s_1})^{S_{1/2}}\gamma_\mu\gamma_5(e^C_{\mathbf{p}_2 s_2})^{S_{1/2}} \\
&= \left(e^{S_{1/2}}_{\mathbf{p}_1 s_1}\right)^\dagger \gamma_0\gamma_\mu\gamma_5 i\gamma_2 \left(e^{S_{1/2}}_{\mathbf{p}_2 s_2}\right)^* \\
&= \begin{pmatrix} g_{-1}(\epsilon_1, r)\chi^\dagger_{s_1} & f_1(\epsilon_1, r)\chi^\dagger_{s_1}(\boldsymbol{\sigma}\cdot\hat{\mathbf{p}}_1)\end{pmatrix}\gamma_0\gamma_\mu\gamma_5 i\gamma_2 \begin{pmatrix} g_{-1}(\epsilon_2, r)\chi_{s_2} \\ f_1(\epsilon_2, r)(\boldsymbol{\sigma}\cdot\hat{\mathbf{p}}_2)\chi_{s_2}\end{pmatrix}.
\end{aligned} \tag{4.42}$$

For $\mu = 0$, after squaring, summing over spins and using the properties of the spinors χ_s, we have

$$\begin{aligned}
&\sum_{s_1,s_2} (\bar{e}_1\gamma_\mu\gamma_5 e_2^C)(\bar{e}_1\gamma_\nu\gamma_5 e_2^C)^\dagger\Big|_{\mu,\nu=0} \\
&= \sum_{s_1,s_2} \left[f^{-1-1}\chi_{s_1}^\dagger\sigma_2\chi_{s_2} + f_{11}\chi_{s_1}^\dagger(\boldsymbol{\sigma}\cdot\hat{\mathbf{p}}_1)(\boldsymbol{\sigma}\cdot\hat{\mathbf{p}}_2)\sigma_2\chi_{s_2}\right]^2 \\
&= \frac{1}{8}\left[f_{66}^{(0)} + f_{66}^{(1)}(\hat{\mathbf{p}}_1\cdot\hat{\mathbf{p}}_2)\right], \qquad (4.43)
\end{aligned}$$

where $f_{66}^{(0)}$ and $f_{66}^{(1)}$ are defined in Eq. (4.49) and f^{-1-1}, f_{11} are given by Eqs. (4.51) and (4.52). A similar derivation is possible for spatial $\mu = k$; however, it does not enter the contributions to $0^+ \to 0^+$ transition.

Interference terms 1, 2, 3 - 4, 5 Using the same procedure the PSFs for the interference between terms $1, 2, 3$ and terms $4, 5$ of Lagrangian (4.8) are received (in case of the vector electron current we take $\mu = 0$),

$$\begin{aligned}
&\sum_{s_1,s_2} (\bar{e}_1\gamma_\mu\gamma_5 e_2^C)(\bar{e}_1(1\pm\gamma_5) e_2^C)^\dagger\Big|_{\mu=0} \\
&= \sum_{s_1,s_2} \left[f^{-1-1}\chi_{s_1}^\dagger\sigma_2\chi_{s_2} + f_{11}\chi_{s_1}^\dagger(\boldsymbol{\sigma}\cdot\hat{\mathbf{p}}_1)(\boldsymbol{\sigma}\cdot\hat{\mathbf{p}}_2)\sigma_2\chi_{s_2}\right]^\dagger \\
&\quad\times\Big[\Big(f^{-1}{}_1\chi_{s_1}^\dagger(\boldsymbol{\sigma}\cdot\hat{\mathbf{p}}_2)\sigma_2\chi_{s_2} + f_1{}^{-1}\chi_{s_1}^\dagger(\boldsymbol{\sigma}\cdot\hat{\mathbf{p}}_1)\sigma_2\chi_{s_2}\Big) \\
&\qquad\pm\Big(f^{-1-1}\chi_{s_1}^\dagger\sigma_2\chi_{s_2} + f_{11}\chi_{s_1}^\dagger(\boldsymbol{\sigma}\cdot\hat{\mathbf{p}}_1)(\boldsymbol{\sigma}\cdot\hat{\mathbf{p}}_2)\sigma_2\chi_{s_2}\Big)\Big] \\
&= \mp\frac{1}{2}\left[f_{16}^{(0)} + f_{16}^{(1)}(\hat{\mathbf{p}}_1\cdot\hat{\mathbf{p}}_2)\right], \qquad (4.44)
\end{aligned}$$

where $f_{16}^{(0)}$ and $f_{16}^{(1)}$ are defined in Eq. (4.50) and $f^{-1-1}, f_{11}, f^{-1}{}_1, f_1{}^{-1}$ are introduced in Eqs. (4.51)-(4.54). As before, the phase space factor for $\mu = k$ does not enter the calculation of $0^+ \to 0^+$ transitions.

Hence, the resulting PSFs in the $S_{1/2} - S_{1/2}$ approximation for the short-range mechanisms can be summarized as

$$\sum_{s_1,s_2} (\bar{e}_1(1+\gamma_5) e_2^C)(\bar{e}_1(1\pm\gamma_5) e_2^C)^\dagger = 2\left[f_{11}^{(0)} + f_{11\pm}^{(1)}(\hat{\mathbf{p}}_1\cdot\hat{\mathbf{p}}_2)\right], \qquad (4.45)$$

$$\sum_{s_1,s_2} (\bar{e}_1\gamma_\mu\gamma_5 e_2^C)(\bar{e}_1\gamma_\nu\gamma_5 e_2^C)^\dagger\Big|_{\mu,\nu=0} = \frac{1}{8}\left[f_{66}^{(0)} + f_{66}^{(1)}(\hat{\mathbf{p}}_1\cdot\hat{\mathbf{p}}_2)\right], \qquad (4.46)$$

$$\sum_{s_1,s_2} (\bar{e}_1\gamma_\mu\gamma_5 e_2^C)(\bar{e}_1(1\pm\gamma_5) e_2^C)^\dagger\Big|_{\mu=0} = \mp\frac{1}{2} f_{16}^{(0)}, \qquad (4.47)$$

where the scalar product between the asymptotic momentum vectors of the two electrons appearing can be parametrized using the opening angle $0 \le \theta \le \pi$ as

$\hat{\mathbf{p}}_1 \cdot \hat{\mathbf{p}}_2 = \cos\theta$ and the quantities $f_{ij}^{(0)} = f_{ij}^{(0)}(E_1, E_2)$ and $f_{ij}^{(1)} = f_{ij}^{(1)}(E_1, E_2)$ are given by

$$f_{11}^{(0)} = |f^{-1-1}|^2 + |f_{11}|^2 + |f^{-1}{}_1|^2 + |f_1{}^{-1}|^2, \quad f_{11\pm}^{(1)} = -2\left[f^{-1}{}_1 f_1{}^{-1} \pm f^{-1-1} f_{11}\right], \tag{4.48}$$

$$f_{66}^{(0)} = 16\left[|f^{-1-1}|^2 + |f_{11}|^2\right], \qquad f_{66}^{(1)} = 32\left[f^{-1-1} f_{11}\right], \tag{4.49}$$

$$f_{16}^{(0)} = 4\left[|f_{11}|^2 - |f^{-1-1}|^2\right], \qquad f_{16}^{(1)} = 0. \tag{4.50}$$

All these phase space factors are defined in terms of the underlying energy-dependent wave functions of the two electrons, cf. Eq. (4.30),

$$f^{-1-1} = g_{-1}(E_1) g_{-1}(E_2), \tag{4.51}$$

$$f_{11} = f_1(E_1) f_1(E_2), \tag{4.52}$$

$$f^{-1}{}_1 = g_{-1}(E_1) f_1(E_2), \tag{4.53}$$

$$f_1{}^{-1} = f_1(E_1) g_{-1}(E_2). \tag{4.54}$$

The obtained results agree with those of Päs et al. [213] and Tomoda [218], except for the extra interference term $f_{11-}^{(1)}$ in Eq. (4.48) between the left-handed and right-handed scalar electron currents, and the fact that these authors use the notation of Doi [219, 220], while we have used that of Tomoda [218]. The phase space factors corresponding to $\mu = j$ or $\nu = j$ in Eqs. (4.46) and (4.47) are not shown, as their corresponding contributions to $0\nu\beta\beta$ decay do not trigger $0^+ \to 0^+$ transition, in the case of $S_{1/2} - S_{1/2}$ approximation, we are interested in (although they are relevant when general $0^+ \to J^+$ transitions are considered).

4.4 From Quarks to Nucleons

In order to determine the nuclear matrix elements generated by all the possible colour singlet quark currents present in the effective Lagrangian in Eq. (4.1), we first have to transition to the nucleon level. If we define the nucleon isodoublet

$$N = \begin{pmatrix} p \\ n \end{pmatrix}, \tag{4.55}$$

then the nucleon matrix elements of the both left-handed and right-handed scalar, vector and tensor quark currents are in the respective order given by [221]

$$\langle p|\, \bar{u}(1 \pm \gamma_5) d\, |n\rangle = \bar{N}\tau^+ \left[F_S(q^2) \pm F_{PS}(q^2)\gamma_5\right] N', \tag{4.56}$$

$$\langle p|\,\bar{u}\gamma^\mu(1\pm\gamma_5)d\,|n\rangle = \bar{N}\tau^+\left[F_V(q^2)\gamma^\mu - i\frac{F_W(q^2)}{2m_p}\sigma^{\mu\nu}q_\nu\right]N' \pm \bar{N}\tau^+\left[F_A(q^2)\gamma^\mu\gamma_5 - \frac{F_P(q^2)}{2m_p}\gamma_5 q^\mu\right]N', \tag{4.57}$$

$$\langle p|\,\bar{u}\sigma^{\mu\nu}(1\pm\gamma_5)d\,|n\rangle = \bar{N}\tau^+\left[J^{\mu\nu} \pm \frac{i}{2}\epsilon^{\mu\nu\rho\sigma}J_{\rho\sigma}\right]N', \tag{4.58}$$

where the prime denotes only that two different isodoublets are considered and we defined

$$J^{\mu\nu} = F_{T_1}(q^2)\sigma^{\mu\nu} + i\frac{F_{T_2}(q^2)}{m_p}(\gamma^\mu q^\nu - \gamma^\nu q^\mu) + \frac{F_{T_3}(q^2)}{m_p^2}(\sigma^{\mu\rho}q_\rho q^\nu - \sigma^{\nu\rho}q_\rho q^\mu), \tag{4.59}$$

and τ^+ is the isospin-raising operator, which transforms a neutron into a proton. As can be seen, the above matrix elements are functions of the momentum transfer defined as $q = p_p - p_n$, where $p_n = p_{N'}$ and $p_p = p_N$ are the neutron and proton momenta, respectively. All the form factors $F_X(q^2)$ with $X \in \{S, PS, V, W, A, P, T_1, T_2, T_3\}$ depend on the square of the transferred momentum. The scalar and axial-tensor terms are omitted from the Eq. (4.57), because the corresponding currents vanish in the isospin-symmetric limit [222]. In addition, they are suppressed by a factor $1/m_p$ without being enhanced by a pion resonance. For these reasons they can be safely neglected.

The nuclear form factors in Eqs. (4.56)-(4.58) are an important part of the discussed calculation, as they can enhance particular NMEs. Except for $F_{PS}(q^2)$ and $F_P(q^2)$ we parametrize their dependence on q^2 in the so-called dipole form,

$$F_X(q^2) = \frac{g_X}{\left(1 + q^2/m_X^2\right)^2}, \tag{4.60}$$

with the coupling constants g_X denoting the value of the form factor at zero momentum transfer, i.e. $g_X \equiv F_X(0)$.

For instance, using the electromagnetic form factor and the conserved vector current (CVC) hypothesis it is possible to determine the vector form factor from experiment as

$$F_V(q^2) = \frac{g_V}{\left(1 + q^2/m_V^2\right)^2}, \quad g_V = 1, \quad m_V = 0.84 \text{ GeV}. \tag{4.61}$$

This parametrization is typically chosen because it gives a good description of $F_V(q^2)$ for the values $|q| \in [0,\ 200]$ MeV, which are relevant in case of $0\nu\beta\beta$ decay. For large momentum transfer $q^2 \gtrsim 1$ GeV^2 a better parametrization given in [223] exists. Nevertheless, there is no reason to employ it in the present work.

In case of the induced form factor $F_W(q^2)$ its relation to the Pauli form factor $F_2(q^2)$ [223] and to the isovector anomalous magnetic moment of the nucleon allows to determine experimentally the following parametrization

$$F_W(q^2) = \frac{g_W}{(1+q^2/m_W^2)^2}, \quad g_W = \mu_p - \mu_n = 3.70, \quad m_W = m_V = 0.84 \text{ GeV}, \tag{4.62}$$

with μ_p and μ_n denoting the anomalous isovector magnetic moment of the proton and neutron, respectively.

The dipole form of parametrization can be used also for the axial vector form factor. The experiment yields

$$F_A(q^2) = \frac{g_A}{(1+q^2/m_A^2)^2}, \quad g_A = 1.269, \quad m_A = 1.09 \text{ GeV}, \tag{4.63}$$

where value of the coupling constant g_A comes from neutron decay [224], while m_A is determined in neutrino scattering [225].

Although the previous three form factors could be determined experimentally, in case of the induced pseudo-scalar form factor $F_P(q^2)$ it is not possible to proceed in the same way. Hence, in this case we stick to the parametrization based on the partially conserved axial-vector current (PCAC) hypothesis, which was suggested in [226], i.e.

$$F_P(q^2) = \frac{g_A}{(1+q^2/m_A^2)^2} \frac{1}{1+q^2/m_\pi^2} \frac{4m_p^2}{m_\pi^2} \left(1 - \frac{m_\pi^2}{m_A^2}\right), \tag{4.64}$$

where $m_\pi = 0.138$ GeV is the pion mass.

The value obtained from Eq. (4.64) reads $g_P \equiv F_P(0) = 231$, which is consistent with the analysis in chiral perturbation theory [227] claiming $g_P = 233$. Another confirmation is provided by recent muon capture measurements giving $F_P(q^2)\frac{|\mathbf{q}^2|}{2m_p}$ at $|\mathbf{q}| = 0.88 m_\mu$ with the muon mass $m_\mu = 0.105$ GeV. The experimental value 8.06 ± 0.55 [228] agrees with the calculated one, which is 8.0.

Recently, the zero momentum transfer values for the scalar $F_S(q^2)$ and pseudo-scalar $F_{PS}(q^2)$ form factors have been focussed in a lattice QCD study [229]. Therein quoted theoretically calculated values are $g_S = 1.02 \pm 0.11$ and $g_{PS} = 349 \pm 9$. However, there is not much information available about the corresponding q^2 dependence.

Hence, for the scalar form factor we use the following dipole-form parametrization

$$F_S(q^2) = \frac{g_S}{(1+q^2/m_S^2)^2}, \quad g_S = 1, \quad m_S = m_V = 0.84 \text{ GeV}, \tag{4.65}$$

while in case of the pseudo-scalar form factor we take

$$F_{PS}(q^2) = \frac{g_{PS}}{\left(1 + q^2/m_{PS}^2\right)^2} \frac{1}{1 + q^2/m_\pi^2}, \quad g_{PS} = 349 \quad m_{PS} = m_V = 0.84 \text{ GeV}. \tag{4.66}$$

Note that the lattice QCD calculation of g_{PS} depends on the extrapolation procedure, as the value of the pseudo-scalar form factor diverges in the chiral limit at $q^2 = 0$. It is beyond the scope of this work to verify the large enhancement of g_{PS} quoted by Ref. [229]. The parametrization (4.66) reduces to the simple monopole form $1/\left(1 + q^2/m_\pi^2\right)$ used in chiral perturbation theory; however, it includes the finite size of the nucleon.

Least is known about the tensor form factors. There is no information provided by experiments and the theoretical values usually quoted in literature are rather old. Only the value of $g_{T_1} \equiv F_{T_1}(0) = 0.987 \pm 0.055$ has been also determined in the recent Ref. [229]. The old calculation using the MIT bag model gives $g_{T_1} \equiv F_{T_1}(0) = 1.38$, $g_{T_2} \equiv F_{T_2}(0) = -3.30$ and $g_{T_3} \equiv F_{T_3}(0) = 1.34$. Nonetheless, the last two form factors $F_{T_2}(q^2)$ and $F_{T_3}(q^2)$ do not appear in our calculation; therefore, we will need only $F_{T_1}(q^2)$, for which we take

$$F_{T_i}(q^2) = \frac{g_{T_i}}{\left(1 + q^2/m_{T_i}^2\right)^2}, \quad g_{T_1} = 1, \quad m_{T_i} = m_V = 0.84 \text{ GeV}. \tag{4.67}$$

4.5 Non-Relativistic Expansion

As a next step towards the calculation of NMEs we need to expand non-relativistically the nucleon matrix elements from Sec. 4.4. Therefore, to obtain them we employ the Foldy-Wouthuysen transformation [230, 231], which corresponds to an expansion in powers of the velocity v/c or equivalently in powers of $|\mathbf{p}|/m_p$.

Let us therefore summarize here the non-relativistic expressions obtained for all the possible nucleon currents in Eqs. (4.56)-(4.58). As before we use the difference between the proton and neutron spatial momenta $\mathbf{q} = \mathbf{p}_p - \mathbf{p}_n$ and we also define the momentum sum $\mathbf{Q} = \mathbf{p}_p + \mathbf{p}_n$. Generally, we retain all terms to order $|\mathbf{q}|/m_p$ in the performed expansion. However, in case of terms accompanied by the enhanced form factors $F_P(q^2)$ and $F_{PS}(q^2)$ (see the earlier discussion) we keep expressions to order $\mathbf{q}^2/m_p^2$ and even higher.

Scalar Bilinears The right-handed (upper signs) and left-handed (lower signs) combinations of the scalar and pseudo-scalar nucleon currents are non-relativistically expanded as follows

$$J_{S\pm P} = F_S(q^2)I \pm \frac{F_{PS}(q^2)}{2m_p}\boldsymbol{\sigma}\cdot\mathbf{q} + \ldots, \tag{4.68}$$

where $\boldsymbol{\sigma} = (\sigma_1, \sigma_2, \sigma_2)^T$ and I denote the vector of Pauli matrices and the 2×2 identity matrix, respectively, both operating on the nucleon spin space.

Vector Bilinears In case of the nucleon current with a single Lorentz index there are four different components: vector, axial vector, induced pseudo-scalar and weak magnetism. The non-relativistic expansion of their right-handed (upper signs) and left-handed (lower signs) combinations can be written as

$$\begin{aligned} J^{\mu}_{V\pm A} = {} & g^{\mu 0}\left[F_V(q^2)I \pm \frac{F_A(q^2)}{2m_p}\boldsymbol{\sigma}\cdot\mathbf{Q} \mp \frac{F_P(q^2)}{4m_p^2}q_0\boldsymbol{\sigma}\cdot\mathbf{q}\right] \\ & + g^{\mu i}\left[-\frac{F_V(q^2)}{2m_p}\mathbf{Q}_i I + \frac{F_V(q^2)+F_W(q^2)}{2m_p}i(\boldsymbol{\sigma}\times\mathbf{q})_i \right. \\ & \left. \mp F_A(q^2)\sigma_i \pm \frac{F_P(q^2)}{4m_p^2}q_i\boldsymbol{\sigma}\cdot\mathbf{q}\right] + \ldots. \end{aligned} \tag{4.69}$$

Tensor Bilinears The non-zero nuclear components corresponding to the right-handed (upper signs) and left-handed (lower signs) combinations of the tensor and axial-tensor nucleon currents read

$$\begin{aligned} J^{\mu\nu}_{T\pm T_5} = {} & F_{T_1}(q^2)g^{\mu j}g^{\nu k}\varepsilon_{ijk}\sigma^i + (g^{\mu i}g^{\nu 0} - g^{\mu 0}g^{\nu i})T_i \\ & \pm \frac{i}{2}\varepsilon^{\mu\nu\rho\sigma}\left[(g_{\rho i}g_{\sigma 0} - g_{\rho 0}g_{\sigma i})T^i + F_{T_1}(q^2)g_{\rho m}g_{\sigma n}\varepsilon^{mni}\sigma_i\right] + \ldots, \end{aligned} \tag{4.70}$$

with the definition

$$T^i = \frac{i}{2m_p}\left[\left(F_{T_1}(q^2) - 2F_{T_2}(q^2)\right)q^i I + F_{T_1}(q^2)(\boldsymbol{\sigma}_a\times\mathbf{Q})^i\right]. \tag{4.71}$$

The terms with the momentum sum $\mathbf{Q}$ describe the nucleon recoil, and therefore they are commonly referred to as recoil terms [218].

As $0\nu\beta\beta$ decay involves a simultaneous transition of two neutrons, a combination of two of the above nucleon currents must be always considered. For the standard mechanism simply the product of two left-handed vector bilinears needs to be evaluated. In case of the long-range effective Lagrangian Eq. (4.4), combinations of a left-handed vector current with all the other possible currents must

be inspected. Finally, based on the effective Lagrangian Eq. (4.8) five different products of non-relativistically expanded nucleon currents have to be calculated to cover the short-range $0\nu\beta\beta$ decay mechanisms.

Let us now provide a detailed and explicit calculation of these products of the non-relativistically approximated hadronic currents for each of the five terms of the effective short-range Lagrangian Eq. (4.8) defined as

$$\Pi_{1,ab} \equiv \frac{1}{2}\left[J_{\circ,a}J_{\circ,b} + J_{\circ,b}J_{\circ,a}\right], \tag{4.72}$$

$$\Pi_{2,ab} \equiv \frac{1}{2}\left[J^{\mu\nu}_{\circ,a}J_{\circ\mu\nu,b} + J^{\mu\nu}_{\circ,b}J_{\circ\mu\nu,a}\right], \tag{4.73}$$

$$\Pi_{3,ab} \equiv \frac{1}{2}\left[J^{\mu}_{\circ,a}J_{\circ\mu,b} + J^{\mu}_{\circ,b}J_{\circ\mu,a}\right], \tag{4.74}$$

$$\Pi_{4\nu,ab} \equiv \frac{1}{2}\left[J^{\mu}_{\circ,a}J_{\circ\mu\nu,b} + J^{\mu}_{\circ,b}J_{\circ\mu\nu,a}\right], \tag{4.75}$$

$$\Pi^{\mu}_{5,ab} \equiv \frac{1}{2}\left[J^{\mu}_{\circ,a}J_{\circ,b} + J^{\mu}_{\circ,b}J_{\circ,a}\right]. \tag{4.76}$$

Each product is symmetrized in indices $a \leftrightarrow b$ that label two distinct neutrons in the decaying nucleus. The placeholders $\circ$ denote again that each current can be right-handed or left-handed. Different combinations of chiralities of the nucleon currents can generally lead to different signs of particular terms in the resulting expression for a given product. These will be worked out in detail below.

In the following we present the explicit expressions for the products shown in Eqs. (4.72)-(4.76). We generally include all the terms up to the linear order in $\mathbf{q}/m_p$. Higher order terms are retained only when they are enhanced by large form factors F_{PS} and/or F_P. All the products are written in terms of the nucleon momenta difference $\mathbf{q}$ and sum $\mathbf{Q}$, Pauli spin operators $\boldsymbol{\sigma}$ and the direction unit vector between two nucleons, $\hat{\mathbf{r}}_{ab} = \mathbf{r}_{ab}/|\mathbf{r}_{ab}|$. In this work we concentrate on $0^+ \to 0^+$ transitions. Hence, employing the angular momentum and parity selection rules all terms containing an odd number of $\boldsymbol{\sigma}$ and/or an odd number of $\mathbf{q}$, $\mathbf{Q}$ occurrences in each product vanish, provided that only $S_{1/2} - S_{1/2}$ wave approximation of the electron wave functions is assumed. On the right-hand side of every line we show the approximate order of magnitude of the given term and the corresponding approximation of the electron wave functions it must be combined with in order to contribute to the desired $0^+ \to 0^+$ transition. We also keep track of signs corresponding to different combinations of chiralities of the considered currents and we show them as a row vector in front of every single term of the expressions. For the first three products of hadronic currents given in Eqs. (4.72)-(4.74) there are three sign possibilities corresponding to the following

combinations of chiralities (in this ordering): RR, LL and $(1/2)\,(RL + LR)$. In case of the fourth and fifth product in Eqs. (4.75)-(4.76) a row of four signs is given, as in these cases the two hadronic currents have different Lorentz structures; hence, all the four possible combinations of chiralities have to be considered (in this ordering): RR, LL, RL and LR.

Term 1: JJj The product of currents JJ is

$$\begin{aligned}
\Pi_{1,ab} \equiv\ & \frac{1}{2}\left[J_{\circ,a}J_{\circ,b} + J_{\circ,b}J_{\circ,a}\right] && (4.77)\\
=\ & (+\ +\ +)\ F_S^2(q^2) I_a I_b && [\mathcal{O}(1)\ S-S]\\
& (+\ +\ -)\ \frac{F_{PS}^2(q^2)}{4m_p^2}(\boldsymbol{\sigma}_a\cdot\mathbf{q})(\boldsymbol{\sigma}_b\cdot\mathbf{q}) + \ldots, && [\mathcal{O}(100)\ S-S]
\end{aligned}$$

where the term proportional to $F_{PS}^2(q^2)$ can be re-coupled using the following relation [232]

$$(\boldsymbol{\sigma}_a\cdot\mathbf{q})(\boldsymbol{\sigma}_b\cdot\mathbf{q}) = \frac{1}{3}(\boldsymbol{\sigma}_a\cdot\boldsymbol{\sigma}_b)\mathbf{q}^2 - \frac{1}{3}\left[\mathbf{q}^2 - \frac{1}{3}(\mathbf{q}\cdot\hat{\mathbf{r}}_{ab})^2\right]\mathbf{S}_{ab}, \qquad (4.78)$$

with $\mathbf{S}_{ab} = 3(\boldsymbol{\sigma}_a\cdot\hat{\mathbf{r}}_{ab})(\boldsymbol{\sigma}_b\cdot\hat{\mathbf{r}}_{ab}) - (\boldsymbol{\sigma}_a\cdot\boldsymbol{\sigma}_b)$.

Term 2: $J^{\mu\nu}J_{\mu\nu}j$ For the second term of the short-range part of the Lagrangian we get the following approximation of the nuclear currents

$$\begin{aligned}
\Pi_{2,ab} \equiv\ & \frac{1}{2}\left[J^{\mu\nu}_{\circ,a}J_{\circ\mu\nu,b} + J^{\mu\nu}_{\circ,b}J_{\circ\mu\nu,a}\right] && (4.79)\\
=\ & (-\ -\ -)\ 2F_{T_1}^2(q^2)(\boldsymbol{\sigma}_a\cdot\boldsymbol{\sigma}_b) + \ldots. && [\mathcal{O}(1)\ S-S]
\end{aligned}$$

Term 3: $J^{\mu}J_{\mu}j$ Approximating the nuclear currents for the third term we obtain

$$\begin{aligned}
\Pi_{3,ab} \equiv\ & \frac{1}{2}\left[J^{\mu}_{\circ,a}J_{\circ\mu,b} + J^{\mu}_{\circ,b}J_{\circ\mu,a}\right] && (4.80)\\
=\ & (+\ +\ +)\ F_V^2(q^2) I_a I_b && [\mathcal{O}(1)\ S-S]\\
& (-\ -\ +)\ F_A^2(q^2)(\boldsymbol{\sigma}_a\cdot\boldsymbol{\sigma}_b) && [\mathcal{O}(1)\ S-S]\\
& (+\ +\ -)\ 2\frac{F_A(q^2)F_P(q^2)}{4m_p^2}(\boldsymbol{\sigma}_a\cdot\mathbf{q})(\boldsymbol{\sigma}_b\cdot\mathbf{q}) && [\mathcal{O}(1)\ S-S]\\
& (+\ +\ +)\ \frac{\left(F_V(q^2)+F_W(q^2)\right)^2}{4m_p^2}(\boldsymbol{\sigma}_a\times\mathbf{q})(\boldsymbol{\sigma}_b\times\mathbf{q}) && [\mathcal{O}(0.1)\ S-S]\\
& (-\ -\ +)\ \frac{F_P^2(q^2)}{16m_p^4}\mathbf{q}^2(\boldsymbol{\sigma}_a\cdot\mathbf{q})(\boldsymbol{\sigma}_b\cdot\mathbf{q}) + \ldots, && [\mathcal{O}(1)\ S-S]
\end{aligned}$$

where the term proportional to $\left(F_V(q^2)+F_W(q^2)\right)^2$ can be re-coupled as follows

$$(\boldsymbol{\sigma}_a\times\mathbf{q})(\boldsymbol{\sigma}_b\times\mathbf{q}) = -\frac{1}{3}(\boldsymbol{\sigma}_a\cdot\boldsymbol{\sigma}_b)\mathbf{q}^2 - \frac{1}{6}\left[\mathbf{q}^2-\frac{1}{3}(\mathbf{q}\cdot\hat{\mathbf{r}}_{ab})^2\right]\mathbf{S}_{ab}. \tag{4.81}$$

Term 4: $J^\mu J_{\mu\nu} j^\nu$ The product of tensor and vector nuclear current in the fourth term can be non-relativistically approximated as

$$\begin{aligned}
\Pi_{4\nu,ab} &\equiv \frac{1}{2}\left[J^\mu_{\circ,a}J_{\circ\mu\nu,b} + J^\mu_{\circ,b}J_{\circ\mu\nu,a}\right] && (4.82)\\
&\approx g_\nu{}^0\Bigg\{(-\ -\ +\ +)\ iF_A(q^2)F_{T_1}(q^2)\,(\boldsymbol{\sigma}_a\cdot\boldsymbol{\sigma}_b) && [\mathcal{O}(1)\ S-S]\\
&\qquad (+\ +\ -\ -)\ i\frac{F_P(q^2)F_{T_1}(q^2)}{4m_p^2}\,(\boldsymbol{\sigma}_a\cdot\mathbf{q})\,(\boldsymbol{\sigma}_b\cdot\mathbf{q})\Bigg\} && [\mathcal{O}(1)\ S-S]\\
&+ g_\nu{}^i\Bigg\{(+\ -\ -\ +)\ \frac{i}{2}F_V(q^2)F_{T_1}(q^2)\,(I_a\sigma_{bi}+I_b\sigma_{ai}) && [\mathcal{O}(1)\ S-P]\\
&\qquad (-\ -\ -\ -)\ i\frac{F_V(q^2)\,[F_{T_1}(q^2)-2F_{T_2}(q^2)]}{2m_p}q_iI_aI_b && [\mathcal{O}(0.1)\ S-P]\\
&\qquad (-\ -\ -\ -)\ \frac{F_V(q^2)F_{T_1}(q^2)}{4m_p}\\
&\qquad \times[I_a(\boldsymbol{\sigma}_b\times\mathbf{Q})_i + I_b(\boldsymbol{\sigma}_a\times\mathbf{Q})_i] && [\mathcal{O}(0.1)\ S-P]\\
&\qquad (-\ -\ -\ -)\ \frac{F_V(q^2)F_{T_1}(q^2)}{4m_p}\\
&\qquad \times[I_a(\boldsymbol{\sigma}_b\times\mathbf{Q})_i + I_b(\boldsymbol{\sigma}_a\times\mathbf{Q})_i] && [\mathcal{O}(0.1)\ S-P]\\
&\qquad (-\ -\ -\ -)\ i\frac{[F_V(q^2)+F_W(q^2)]\,F_{T_1}(q^2)}{4m_p}\\
&\qquad \times[2q_i(\boldsymbol{\sigma}_a\cdot\boldsymbol{\sigma}_b) - \sigma_{ai}(\mathbf{q}\cdot\boldsymbol{\sigma}_b) - \sigma_{bi}(\mathbf{q}\cdot\boldsymbol{\sigma}_a)] && [\mathcal{O}(0.1)\ S-P]\\
&\qquad (-\ -\ +\ +)\ \frac{F_A(q^2)F_{T_1}(q^2)}{4m_p}\,[(\boldsymbol{\sigma}_a\cdot\mathbf{Q})\sigma_{bi} + (\boldsymbol{\sigma}_b\cdot\mathbf{Q})\sigma_{ai}]\\
&\qquad && [\mathcal{O}(0.1)\ S-P]\\
&\qquad (+\ +\ -\ -)\ \frac{F_A(q^2)\,[F_{T_1}(q^2)-2F_{T_2}(q^2)]}{4m_p}\\
&\qquad \times[(\boldsymbol{\sigma}_a\times\mathbf{q})_iI_b + (\boldsymbol{\sigma}_b\times\mathbf{q})_iI_a] && [\mathcal{O}(0.1)\ S-P]\\
&\qquad (-\ -\ +\ +)\ i\frac{F_A(q^2)F_{T_1}(q^2)}{4m_p}\\
&\qquad \times[\sigma_{ai}(\mathbf{Q}\cdot\boldsymbol{\sigma}_b) + \sigma_{bi}(\mathbf{Q}\cdot\boldsymbol{\sigma}_a) - 2Q_i(\boldsymbol{\sigma}_a\cdot\boldsymbol{\sigma}_b)] && [\mathcal{O}(0.1)\ S-P]\\
&\qquad (-\ -\ +\ +)\ i\frac{F_P(q^2)F_{T_1}(q^2)}{8m_p^2}q^0
\end{aligned}$$

$$\times [(\boldsymbol{\sigma}_a \cdot \mathbf{q})\sigma_{bi} + (\boldsymbol{\sigma}_b \cdot \mathbf{q})\sigma_{ai}] \qquad [\mathcal{O}(0.1)\ S-P]$$

$$(+\ +\ -\ -)\ \frac{F_P(q^2)F_{T_1}(q^2)}{16m_p^3}\,[\sigma_{ai}(\mathbf{q}\cdot\mathbf{Q})(\mathbf{q}\cdot\boldsymbol{\sigma}_b)$$

$$+\sigma_{bi}(\mathbf{q}\cdot\mathbf{Q})(\mathbf{q}\cdot\boldsymbol{\sigma}_a) - 2Q_i(\mathbf{q}\cdot\boldsymbol{\sigma}_b)(\mathbf{q}\cdot\boldsymbol{\sigma}_b)]\Big\} + \dots.$$

$$[\mathcal{O}(0.1)\ S-P]$$

Term 5: $J^\mu J j_\mu$ Approximating the nuclear currents in this case we obtain

$$\Pi^\mu_{5,ab} \equiv \frac{1}{2}\left[J^\mu_{\circ,a}J_{\circ,b} + J^\mu_{\circ,b}J_{\circ,a}\right] \tag{4.83}$$

$$\approx g^\mu{}_0\Big\{(+\ +\ +\ +)\ F_S(q^2)F_V(q^2)I_aI_b \qquad [\mathcal{O}(1)\ S-S]$$

$$(+\ +\ -\ -)\ \frac{F_{PS}(q^2)F_A(q^2)}{8m_p^2}$$

$$\times [(\boldsymbol{\sigma}_a\cdot\mathbf{Q})(\boldsymbol{\sigma}_b\cdot\mathbf{q}) + (\boldsymbol{\sigma}_a\cdot\mathbf{q})(\boldsymbol{\sigma}_b\cdot\mathbf{Q})] \qquad [\mathcal{O}(1)\ S-S]$$

$$(-\ -\ +\ +)\ \frac{F_{PS}(q^2)F_P(q^2)}{8m_p^3}q^0(\boldsymbol{\sigma}_a\cdot\mathbf{q})(\boldsymbol{\sigma}_b\cdot\mathbf{q})\Big\} \qquad [\mathcal{O}(1)\ S-S]$$

$$+\ g^\mu{}_i\Big\{(-\ +\ -\ +)\ \frac{1}{2}F_S(q^2)F_A(q^2)\left(\sigma_a^iI_b + \sigma_b^iI_a\right) \qquad [\mathcal{O}(1)\ S-P]$$

$$(-\ -\ -\ -)\ \frac{F_S(q^2)F_V(q^2)}{2m_p}Q^iI_aI_b \qquad [\mathcal{O}(0.1)\ S-P]$$

$$(+\ +\ +\ +)\ i\frac{F_S(q^2)\,[F_V(q^2)+F_W(q^2)]}{4m_p}$$

$$\times\left[(\boldsymbol{\sigma}_a\times\mathbf{q})^iI_b + (\boldsymbol{\sigma}_b\times\mathbf{q})^iI_a\right] \qquad [\mathcal{O}(0.1)\ S-P]$$

$$(-\ -\ +\ +)\ \frac{F_{PS}(q^2)F_A(q^2)}{4m_p}\left[\sigma_a^i(\boldsymbol{\sigma}_b\cdot\mathbf{q}) + \sigma_b^i(\boldsymbol{\sigma}_a\cdot\mathbf{q})\right]$$

$$[\mathcal{O}(10)\ S-P]$$

$$(-\ +\ +\ -)\ \frac{F_{PS}(q^2)F_V(q^2)}{8m_p^2}Q^i\,[I_a(\boldsymbol{\sigma}_b\cdot\mathbf{q}) + I_b(\boldsymbol{\sigma}_a\cdot\mathbf{q})]$$

$$[\mathcal{O}(1)\ S-P]$$

$$(+\ -\ +\ -)\ \frac{F_S(q^2)F_P(q^2)}{8m_p^2}q^i\,[(\boldsymbol{\sigma}_a\cdot\mathbf{q})I_b + (\boldsymbol{\sigma}_b\cdot\mathbf{q})I_a] \quad [\mathcal{O}(1)\ S-P]$$

$$(+\ +\ -\ -)\ \frac{F_{PS}(q^2)F_P(q^2)}{8m_p^3}q^i(\boldsymbol{\sigma}_a\cdot\mathbf{q})(\boldsymbol{\sigma}_b\cdot\mathbf{q})\Big\} + \dots.$$

$$[\mathcal{O}(10)\ S-P]$$

4.6 From Nucleons to the Nucleus

Taking the Eqs. (4.68)-(4.71) to obtain the resulting nuclear currents we have to sum over all neutrons in the initial nucleus

$$\mathcal{J}_K^{\Xi}(\mathbf{x}) = \sum_a \tau_+^a \delta(\mathbf{x} - \mathbf{r}_a) J_{K,a}^{\Xi}, \tag{4.84}$$

where $\mathbf{r}_a$ denotes the positions of individual neutrons and $J_{K,a}^{\Xi}$ stands for any of the nucleon currents[5].

Hence, considering a product $\Pi_{K,ab}^{\Xi}$ of two non-relativistically expanded nucleon currents and summing over all neutrons in the initial nucleus the corresponding nuclear transition operators can be written as

$$\mathcal{H}_K(\mathbf{x}, \mathbf{y}) = \sum_{a \neq b} \tau_+^a \tau_+^b \delta(\mathbf{x} - \mathbf{r}_a) \delta(\mathbf{y} - \mathbf{r}_b) \Pi_{K,ab}^{\Xi}. \tag{4.85}$$

Using the five products in Eqs. (4.72)-(4.76) the nuclear transition operators for the short-range effective Lagrangian can be obtained. While those corresponding to the terms 1, 2 and 3 are Lorentz scalars and as such they completely decouple from the leptonic current, in case of terms 4 and 5 the nuclear part forms a Lorentz vector which is contracted with the vector electron current.

Having constructed the nuclear $0\nu\beta\beta$ decay transition operators using the general nucleon operators with their $\mathbf{q}^2$ and thus distance dependence parametrized by experimentally constrained form factors, we can now proceed towards the final and most challenging step, the determination of the $0\nu\beta\beta$ decay NMEs. The calculation of the matrix elements at the nuclear level requires an understanding of nuclear structure and given the highly complex nature of the many-body problem, it is not possible to solve it from first principles. Let us define the nuclear matrix elements as

$$\mathcal{M}_K \equiv \left\langle \mathcal{O}_F^+ \right| \mathcal{H}_K \left| \mathcal{O}_I^+ \right\rangle, \tag{4.86}$$

where $\left\langle \mathcal{O}_F^+ \right|$ and $\left\langle \mathcal{O}_I^+ \right|$ denote the wave functions of the final and initial nuclear state under consideration, respectively, and the transition operator is given in Eq. (4.85). To calculate the wave functions and thus also the transition operator in Eq. (4.86) one of the nuclear structure models briefly discussed within Subsec. 3.5.4 must be employed. In principle, transitions via the intermediate states

[5] In case of positron emission, the sum runs over protons and the operator τ_+ is replaced by operator τ_-.

formed by a single beta decay-like transitions from one nucleon current should be considered, which would require knowledge of the corresponding wave functions. However, it is customary to exploit the completeness of all intermediate states and make use of the *closure approximation* in directly calculating the above matrix element. For the short-range operators the intermediate transition occurs at very high energies $|q| \approx 100$ MeV, corresponding to the inter-nucleon distance, compared to the nuclear transition itself at $Q_{\beta\beta} \approx 1$ MeV. Therefore, the closure approximation is very well justified particularly in case of the contact interaction.

4.7 Know Your NMEs

Using Eqs. (4.85)-(4.86) and the five derived products in Eqs. (4.77), (4.79), (4.80), (4.82), (4.83) we obtain five matrix elements corresponding to the five terms of the short-range Lagrangian in Eq. (4.8). For the purpose of the following calculations it is enough to restrict ourselves only to terms that are of order 1 or higher[6] and that combine with the $S_{1/2} - S_{1/2}$ wave functions. The resulting simplified matrix elements for the five different short-range operators then read

$$\begin{aligned}
\mathcal{M}_1 = \; & (+\;+\;+)\; g_S^2 \mathcal{M}_F \\
& (+\;+\;-)\; \frac{g_{PS}^2}{12 m_p^2} \left(\mathcal{M}'^{PP}_{GT} - \mathcal{M}'^{PP}_{T} \right), \qquad (4.87) \\
\mathcal{M}_2 = \; & (-\;-\;-)\; 2 g_{T_1}^2 \mathcal{M}_{GT}, \qquad (4.88) \\
\mathcal{M}_3 = \; & (+\;+\;+)\; g_V^2 \mathcal{M}_F \\
& (-\;-\;+)\; g_A^2 \mathcal{M}^{AA}_{GT} \\
& (+\;+\;-)\; \frac{g_A g_P}{6 m_p^2} \left(\mathcal{M}'^{AP}_{GT} - \mathcal{M}'^{AP}_{T} \right) \\
& (+\;+\;+)\; \frac{(g_V + g_W)^2}{12 m_p^2} \left(\mathcal{M}'_{GT} + \frac{1}{2} \mathcal{M}'_{T} \right) \\
& (-\;-\;+)\; \frac{g_P^2}{24 m_p^4} \left(\mathcal{M}''^{PP}_{GT} - \mathcal{M}''^{PP}_{T} \right), \qquad (4.89) \\
\mathcal{M}^{\mu}_4 = \; & (-\;-\;+\;+)\; i g^{\mu 0} g_A g_{T_1} \mathcal{M}^{A}_{GT} \\
& (+\;+\;-\;-)\; i g^{\mu 0} \frac{g_P g_{T_1}}{12 m_p^2} \left(\mathcal{M}'^{P}_{GT} - \mathcal{M}'^{P}_{T} \right), \qquad (4.90)
\end{aligned}$$

[6]We will keep also the term in Eq. (4.80) proportional to $\left(F_V(q^2) + F_W(q^2)\right)^2$, which is slightly smaller; however, it is customary to retain it, as the corresponding contribution may be still important.

$$\begin{aligned}\mathcal{M}_5^{\mu} = \; & (+\;+\;+\;+)\; g^{\mu 0} g_S g_V \mathcal{M}_F \\ & (+\;+\;-\;-)\; g^{\mu 0} \frac{g_A g_{PS}}{12 m_p^2} \left(\tilde{\mathcal{M}}_{GT}^{AP} - \tilde{\mathcal{M}}_{T}^{AP} \right) \\ & (-\;-\;+\;+)\; g^{\mu 0} \frac{g_P g_{PS}}{24 m_p^3} \left(\mathcal{M}_{GT}^{\prime q_0 PP} - \mathcal{M}_{T}^{\prime q_0 PP} \right).\end{aligned} \tag{4.91}$$

Let us now explain the notation used above. The signs reflect the possible combinations of chiralities of the involved quark currents in the way explained above Eq. (4.77). Further, we have split the form functions $F_X(q^2)$ appearing in Eqs. (4.77), (4.79), (4.80), (4.82), (4.83) into the so-called charges, i.e. the values at $q^2 = 0$, $F_X(0) \equiv g_X$ and the q-dependence as

$$F_X(q^2) = F_X(0) \frac{1}{\left(1 + q^2/m_V^2\right)^2} \equiv g_X \frac{1}{\left(1 + q^2/m_V^2\right)^4}, \tag{4.92}$$

where $X \in \{S, V, W, T_1, T_2, T_3\}$. Since always products of two form factors appear, it is convenient to define the function

$$\tilde{h}(q^2) = \frac{F_X(q^2) F_Y(q^2)}{g_X g_Y} = \frac{1}{\left(1 + q^2/m_V^2\right)^4}, \tag{4.93}$$

which is subsequently absorbed into the definition of the accompanying nuclear matrix elements appearing on the right-hand sides of Eqs. (4.87)-(4.91), as described below. The A, P and PS form factors have a different q-dependence, and thus are treated separately. For products $F_A(q^2)F_X(q^2)$, $F_A(q^2)F_A(q^2)$ the combined q-dependence is given by

$$\tilde{h}_A(q^2) = \frac{1}{\left(1 + q^2/m_V^2\right)^2} \frac{1}{\left(1 + q^2/m_A^2\right)^2}, \tag{4.94}$$

$$\tilde{h}_{AA}(q^2) = \frac{1}{\left(1 + q^2/m_A^2\right)^4}, \tag{4.95}$$

respectively.

In case we have a product of one of the pseudoscalar couplings (P or PS) with the axial-vector coupling A or some other coupling X, then

$$\tilde{h}_{AP}(q^2) = \frac{1}{\left(1 + q^2/m_A^2\right)^4} \frac{1}{\left(1 + q^2/m_\pi^2\right)}, \tag{4.96}$$

$$\tilde{h}_P(q^2) = \frac{1}{\left(1 + q^2/m_V^2\right)^4} \frac{1}{\left(1 + q^2/m_\pi^2\right)}, \tag{4.97}$$

respectively. Finally, for a product of two pseudoscalar couplings the q-dependence is defined as

$$\tilde{h}_{PP}(q^2) = \frac{1}{\left(1 + q^2/m_V^2\right)^4} \frac{1}{\left(1 + q^2/m_\pi^2\right)^2}. \tag{4.98}$$

Having defined all these q-dependent functions we can proceed to definitions of all the NMEs on the right-hand sides of Eqs. (4.87)-(4.91). These NMEs can be generally calculated in any nuclear structure model [135, 138, 233]. Within this detailed treatment of the short-range $0\nu\beta\beta$ decay mechanisms we stick to the formulation of [226] and [135]. We start with introducing the notation

$$\langle H_{ab} \rangle = \left\langle \mathcal{O}_F^+ \right| \sum_{a \neq b} \tau_a^+ \tau_b^+ H_{ab} \left| \mathcal{O}_I^+ \right\rangle , \tag{4.99}$$

where H_{ab} represents any two-body transition operator. This two-body operator involves a function H, which, following [226] and [135], is constructed in momentum space as the product of the so-called neutrino potential, $v(q)$, times the above defined q-dependent parts of the form factors $\tilde{h}(q^2)$. Since we consider short-range mechanisms with a δ-function in configuration space, the Fourier transform is a constant, and the neutrino potential in momentum space is [135, 226]

$$v(q) = \frac{2}{\pi} \frac{1}{m_e m_p}, \tag{4.100}$$

where the standard normalization has been used.[7]

Let us now introduce functions

$$h_\circ(q^2) = \frac{2}{\pi} \frac{1}{m_e m_p} \tilde{h}_\circ(q^2), \tag{4.102}$$

where the placeholder $\circ$ notes that the same redefinition is used for all the above defined types of q-dependencies arising from the form factors. Then, for instance, we can write the Fermi, $\mathcal{M}_F$, and Gamow-Teller, $\mathcal{M}_{GT}$, matrix elements entering Eqs. (4.87)-(4.91) as

$$\mathcal{M}_F = \langle h(q^2) \rangle, \tag{4.103}$$

$$\mathcal{M}_{GT} = \langle h(q^2) (\boldsymbol{\sigma}_a \cdot \boldsymbol{\sigma}_b) \rangle, \tag{4.104}$$

[7] Incidentally, for the long-range mechanism the neutrino potential is

$$v(q) = \frac{2}{\pi} \frac{1}{q(q + \tilde{A})}, \tag{4.101}$$

with $\tilde{A}$ denoting the closure energy. Therefore, this formulation is convenient for calculating both short-range and long-range matrix elements, one just simply needs to specify the neutrino potential.

where[8]

$$h(q^2) = \frac{2}{\pi}\frac{1}{m_e m_p}\frac{1}{\left(1+q^2/m_V^2\right)^4}. \tag{4.106}$$

Let us now employ the introduced notation and present the definitions of other NMEs appearing in Eqs. (4.87)-(4.91). In case that the Gamow-Teller matrix element in Eq. (4.104) comes with one or two powers of the axial-vector coupling, we define

$$\mathcal{M}^{A}_{GT} = \langle h_A(q^2)(\boldsymbol{\sigma}_a \cdot \boldsymbol{\sigma}_b)\rangle, \tag{4.107}$$

$$\mathcal{M}^{AA}_{GT} = \langle h_{AA}(q^2)(\boldsymbol{\sigma}_a \cdot \boldsymbol{\sigma}_b)\rangle, \tag{4.108}$$

respectively.

Matrix elements $\mathcal{M}'_{GT}$ and $\mathcal{M}'_{T}$ appearing in the third short-range operator read

$$\frac{1}{m_p^2}\mathcal{M}'_{GT} = \left\langle \frac{\mathbf{q}^2}{m_p^2} h(q^2)(\boldsymbol{\sigma}_a \cdot \boldsymbol{\sigma}_b) \right\rangle, \tag{4.109}$$

$$\frac{1}{m_p^2}\mathcal{M}'_{T} = \left\langle \frac{1}{m_p^2}\left[\mathbf{q}^2 - \frac{1}{3}(\mathbf{q}\cdot\hat{\mathbf{r}}_{ab})^2\right] h(q^2)\mathbf{S}_{ab} \right\rangle. \tag{4.110}$$

Since $q \sim 100$ MeV in $0\nu\beta\beta$ decay, these contributions are suppressed by a factor of $\mathcal{O}(0.01)$ relative to the standard NMEs $\mathcal{M}_{GT}$ and $\mathcal{M}_T$. However, we include them because this suppression is partly compensated by the enhancement of the corresponding form factor. The calculation of these new matrix elements is straightforward, as the combination of neutrino potential and form factors gives simply a function of $\mathbf{q}^2$.

Similarly, the matrix elements $\mathcal{M}'^{P}_{GT}$, $\mathcal{M}'^{P}_{T}$ and $\mathcal{M}'^{AP}_{GT}$, $\mathcal{M}'^{AP}_{T}$ are defined as

$$\frac{1}{m_p^2}\mathcal{M}'^{P}_{GT} = \left\langle \frac{\mathbf{q}^2}{m_p^2} h_P(q^2)(\boldsymbol{\sigma}_a \cdot \boldsymbol{\sigma}_b) \right\rangle, \tag{4.111}$$

$$\frac{1}{m_p^2}\mathcal{M}'^{P}_{T} = \left\langle \frac{1}{m_p^2}\left[\mathbf{q}^2 - \frac{1}{3}(\mathbf{q}\cdot\hat{\mathbf{r}}_{ab})^2\right] h_P(q^2)\mathbf{S}_{ab} \right\rangle, \tag{4.112}$$

and

$$\frac{1}{m_p^2}\mathcal{M}'^{AP}_{GT} = \left\langle \frac{\mathbf{q}^2}{m_p^2} h_{AP}(q^2)(\boldsymbol{\sigma}_a \cdot \boldsymbol{\sigma}_b) \right\rangle, \tag{4.113}$$

[8] As aside, in order to do calculations in coordinate space, one simply takes the Fourier-Bessel transforms of the product of the neutrino potential v times the function $\tilde{h}$,

$$h(r) = \frac{2}{\pi}\int_0^\infty j_\lambda(q^2)\frac{1}{m_e m_p}\tilde{h}(q)q^2 \mathrm{d}q, \tag{4.105}$$

where $\lambda = 0$ for Fermi and Gamow-Teller contributions and $\lambda = 2$ for a tensor contribution.

$$\frac{1}{m_p^2}\mathcal{M}_T^{\prime AP} = \left\langle \frac{1}{m_p^2}\left[\mathbf{q}^2 - \frac{1}{3}(\mathbf{q}\cdot\hat{\mathbf{r}}_{ab})^2\right] h_{AP}(q^2)\mathbf{S}_{ab}\right\rangle, \tag{4.114}$$

respectively. As well as in the previous case, these terms are smaller by a factor of $\mathcal{O}(0.01)$ relative to the standard terms $\mathcal{M}_{GT}$ and $\mathcal{M}_T$. Nonetheless, the enhancement of the g_P coupling compensates for this suppression.

Next, the terms $\mathcal{M}_{GT}^{\prime PP}$, $\mathcal{M}_T^{\prime PP}$ induced by the first short-range operator, which are given as

$$\frac{1}{m_p^2}\mathcal{M}_{GT}^{\prime PP} = \left\langle \frac{\mathbf{q}^2}{m_p^2} h_{PP}(q^2)(\boldsymbol{\sigma}_a\cdot\boldsymbol{\sigma}_b)\right\rangle, \tag{4.115}$$

$$\frac{1}{m_p^2}\mathcal{M}_T^{\prime PP} = \left\langle \frac{1}{m_p^2}\left[\mathbf{q}^2 - \frac{1}{3}(\mathbf{q}\cdot\hat{\mathbf{r}}_{ab})^2\right] h_{PP}(q^2)\mathbf{S}_{ab}\right\rangle. \tag{4.116}$$

Although these matrix elements are also suppressed by a factor of $\mathcal{O}(0.01)$, if the pseudoscalar coupling g_{PS} is larger by two orders of magnitude as claimed in [229], then they become comparable with the standard Fermi and Gamow-Teller matrix elements $\mathcal{M}_F$ and $\mathcal{M}_{GT}$, or even larger.

The matrix elements $\mathcal{M}_{GT}^{\prime\prime PP}$ and $\mathcal{M}_T^{\prime\prime PP}$ present in the third short-range operator are defined

$$\frac{1}{m_p^4}\mathcal{M}_{GT}^{\prime\prime PP} = \left\langle \frac{\mathbf{q}^4}{m_p^4} h_{PP}(q^2)(\boldsymbol{\sigma}_a\cdot\boldsymbol{\sigma}_b)\right\rangle, \tag{4.117}$$

$$\frac{1}{m_p^4}\mathcal{M}_T^{\prime\prime PP} = \left\langle \frac{\mathbf{q}^2}{m_p^4}\left[\mathbf{q}^2 - \frac{1}{3}(\mathbf{q}\cdot\hat{\mathbf{r}}_{ab})^2\right] h_{PP}(q^2)\mathbf{S}_{ab}\right\rangle. \tag{4.118}$$

Considering again the values $q \sim 100$ MeV relevant for $0\nu\beta\beta$ decay, the above matrix elements are smaller by a factor of $\mathcal{O}(10^{-4})$ relative to the standard terms $\mathcal{M}_{GT}$ and $\mathcal{M}_T$. However, the enhanced pseudoscalar coupling g_P appears here in the second power and balances the suppression. Also these new terms can be easily calculated, because the neutrino potential is just a function of $\mathbf{q}^2$.

The matrix elements $\tilde{\mathcal{M}}_{GT}^{AP}$ and $\tilde{\mathcal{M}}_T^{AP}$, also called recoil terms, are defined as

$$\frac{1}{m_p^2}\tilde{\mathcal{M}}_{GT}^{AP} = \left\langle \frac{\mathbf{Q}\cdot\mathbf{q}}{m_p^2} h_{AP}(q^2)(\boldsymbol{\sigma}_a\cdot\boldsymbol{\sigma}_b)\right\rangle, \tag{4.119}$$

$$\frac{1}{m_p^2}\tilde{\mathcal{M}}_T^{AP} = \left\langle \frac{1}{m_p^2}\left[\mathbf{Q}\cdot\mathbf{q} - \frac{1}{3}(\mathbf{Q}\cdot\hat{\mathbf{r}}_{ab})(\mathbf{q}\cdot\hat{\mathbf{r}}_{ab})\right] h_{AP}(q^2)\mathbf{S}_{ab}\right\rangle. \tag{4.120}$$

Provided that the pseudoscalar coupling g_{PS} is larger by two orders of magnitude, these terms become important despite the overall suppression by the factor of $\mathcal{O}(0.01)$. However, since the operator $\mathbf{Q}$ is not simply a function of $\mathbf{q}^2$, these

matrix elements are difficult to calculate. A good estimate can be obtained by replacing $(\mathbf{Q}\cdot\mathbf{q})/m_p^2$ with the expectation value in the state $\left|O_I^+\right\rangle$, namely with $\left\langle \mathbf{Q}\cdot\mathbf{q}/m_p^2\right\rangle \sim 0.01$. In such a case we can write

$$\frac{1}{m_p^2}\tilde{\mathcal{M}}_{GT}^{AP} = \left\langle \frac{\mathbf{Q}\cdot\mathbf{q}}{m_p^2}\right\rangle \mathcal{M}_{GT}^{AP}, \tag{4.121}$$

etc.

Eventually, the fifth short-range operator contains the terms $\mathcal{M}_{GT}^{\prime q_0 PP}$, $\mathcal{M}_{T}^{\prime q_0 PP}$ that read

$$\frac{1}{m_p^3}\mathcal{M}_{GT}^{\prime q_0 PP} = \left\langle \frac{q_0\mathbf{q}^2}{m_p^3} h_{PP}(q^2)(\boldsymbol{\sigma}_a\cdot\boldsymbol{\sigma}_b)\right\rangle, \tag{4.122}$$

$$\frac{1}{m_p^3}\mathcal{M}_{T}^{\prime q_0 PP} = \left\langle \frac{q_0}{m_p^3}\left[\mathbf{q}^2 - \frac{1}{3}(\mathbf{q}\cdot\hat{\mathbf{r}}_{ab})^2\right] h_{PP}(q^2)\mathbf{S}_{ab}\right\rangle. \tag{4.123}$$

Similarly as for all the other terms involving the pseudoscalar form factors, the relative suppression is balanced by the enhancement of couplings g_P and g_{PS}.

It is important to remark that in case of the product $\Pi_{1,ab}$ in Eq. (4.77), the enhancement of the pseudoscalar form factor g_{PS} can make the third-order term of the non-relativistic expansion of the pseudoscalar nucleon current important. This term is anticipated to be of the order $F_{PS}(q^2)\mathcal{O}(\mathbf{q}^3/m_p^3)$, and therefore, its product with the first-order pseudoscalar term of the expansion would give a contribution $F_{PS}^2(q^2)\mathcal{O}(\mathbf{q}^4/m_p^4) \sim \mathcal{O}(1)$. This term is omitted in the above detailed discussion, as we consider only terms up to the order of $\mathbf{q}/m_p$ in the non-relativistic currents. However, we conjecture that the extra contribution in question will always be sub-dominant to the terms in Eqs. (4.115) and (4.116), as those should be larger by two orders of magnitude. Although the exact relative size of these contributions depends on the corresponding NMEs, there is no reason to believe that the NMEs arising from the third-order term of the non-relativistic expansion of the pseudoscalar current should be exceptionally large.

As mentioned earlier, different nuclear structure models can be used to compute the NMEs. In this work we employ the NMEs calculated in the Interacting Boson Model (IBM), specifically, the version IBM-2 [135–137]. It is important to emphasize that we do not calculate the exact values of all the above listed NMEs. Instead, we replace $(\mathbf{q}/m_p)^2 = 0.01$ as a rough average, and neglect the effect of differently-shaped $\mathbf{q}^2$-dependence of form factors. These approximations reduce all the NMEs to $\mathcal{M}_F, \mathcal{M}_{GT}$ and $\mathcal{M}_T$. Values of these basic NMEs we take from Ref. [137] and we list them in Tab. 4.3.

An improvement that is being made in the employed nuclear structure calculation is the introduction of short-range correlations (SRC), which are of crucial importance especially for the herein studied short-range mechanisms. They can be taken into account by multiplying the potential $v(r)$ in coordinate space by a square of a correlation function $f(r)$. Most commonly, the Jastrow function is used. It has the form

$$f_J(r) = 1 - ce^{-ar^2}(1 - br^2), \tag{4.124}$$

where $a = 1.1$ fm^{-2}, $b = 0.68$ fm^{-2} and $c = 1$ for the phenomenological Miller-Spencer parametrization [234], and $a = 1.59$ fm^{-2}, $b = 1.45$ fm^{-2} and $c = 0.92$ for the Argonne parametrization [235]. The above formulation is in momentum space, but in our case we can employ the Fourier-Bessel transform of $f_J(r)$ to take SRCs into account.

4.8 Decay Half-life and Angular Correlation

By combining the results derived for the leptonic and hadronic parts of the process, we can construct the coefficients $a(E_1)$ and $b(E_1)$ in the fully differential rate Eq. (4.21) for the short-range $0^+ \to 0^+$ $0\nu\beta\beta$ mechanisms as follows

$$a(E_1) = 2f_{11}^{(0)} \left| \sum_{I=1}^{3} \epsilon_I \mathcal{M}_I \right|^2 + \frac{1}{8} f_{66}^{(0)} \left| \sum_{I=4}^{5} \epsilon_I \mathcal{M}_I \right|^2 \mp f_{16}^{(0)} \mathrm{Re} \left[\left(\sum_{I=1}^{3} \epsilon_I \mathcal{M}_I \right) \left(\sum_{I=4}^{5} \epsilon_I \mathcal{M}_I \right)^* \right], \tag{4.125}$$

$$b(E_1) = 2f_{11\pm}^{(1)} \left| \sum_{I=1}^{3} \epsilon_I \mathcal{M}_I \right|_{\pm}^2 + \frac{1}{8} f_{66}^{(1)} \left| \sum_{I=4}^{5} \epsilon_I \mathcal{M}_I \right|^2 . \tag{4.126}$$

These expressions incorporate the NMEs from Eqs. (4.87)-(4.91) and the PSFs from Eqs. (4.48)-(4.50). The summations as indicated run over the different current types $i = 1, 2, 3, 4, 5$ including their different chiralities, $I = (i, XYZ)$ with $X, Y, Z \in \{L, R\}$. Further, the sign in front of $f_{16}^{(0)}$ in Eq. (4.125) is negative (positive) for R (L) chirality of the interfering electron scalar current. The $\pm$ in the subscript of the norm in Eq. (4.126) symbolically denotes that the terms containing ϵ_I and ϵ_J^* corresponding to the same electron chiralities combine with $f_{11+}^{(1)}$, while the relevant PSF for terms with opposite electron chiralities is $f_{11-}^{(1)}$. Note also that the interference term between currents $i = 1, 2, 3$ and $i = 4, 5$ does not contribute to $b(E_1)$ due to vanishing $f_{16}^{(1)}$ PSF, as given in Eq. (4.50).

	$\mathcal{M}_F$	$\mathcal{M}_{GT}$	$\mathcal{M}_T$
^{76}Ge	−42.8	104.0	−26.9
^{82}Se	−37.1	87.2	−27.3
^{100}Mo	−46.8	111.0	24.2
^{130}Te	−37.9	84.8	−16.6
^{136}Xe	−29.7	66.8	−12.7

Table 4.3: Nuclear matrix elements $\mathcal{M}_F$, $\mathcal{M}_{GT}$ and $\mathcal{M}_T$ for selected isotopes, adopted from [137].

Tab. 4.3 summarizes for selected isotopes the basic nuclear matrix elements $\mathcal{M}_F$, $\mathcal{M}_{GT}$ and $\mathcal{M}_T$ on which the short-range NMEs $\mathcal{M}_I$ are based. The values are taken from Tab. IV of [137]. These matrix elements are expressed in dimensionless units, which means that they are multiplied by the mass number dependent radius $R_A = R_0 A^{1/3}$ of the nucleus where $R_0 = 1.2$ fm.

Based on [134] and the description given in Sec. 4.3 we numerically calculate the radial electron wave functions. Using these and combining Eqs. (4.22), (4.23), (4.125), and (4.126), we then construct the single electron distribution $\mathrm{d}\Gamma/\mathrm{d}E_1$ and the angular correlation $\alpha(E_1)$ for the three relevant phase space factors that can occur under the presence of short-range operators, i.e. $f_{11}^{(a)}$ (for operators $i = 1, 2, 3$ with a scalar electron current), $f_{66}^{(a)}$ (for operators $i = 4, 5$ with an axial-vector electron current) and $f_{16}^{(0)}$ (for interference between the two classes). Note that the contribution $f_{16}^{(1)}$ to the angular coefficient $b(E_1)$ induced by the interference terms is identically zero. The electron phase space distribution f_{11} is the same one that is obtained for the standard mass mechanism (calculated also in the closure approximation).

The results for the $0\nu\beta\beta$ decay isotopes ^{76}Ge, ^{130}Te and ^{136}Xe are shown in Fig. 4.3. Therein we plot both the normalized single energy distributions and the angular correlation as functions of the kinetic energy $E_1^{\mathrm{kin}} = E_1 - m_e$ of one of the emitted electrons ranging from zero up to the $Q_{\beta\beta}$ value of the isotope in question. As one would expect, the available kinetic energy is preferably shared by the two electrons equally, which results in a *hill*-like shape of the single energy distribution $\mathrm{d}\Gamma/\mathrm{d}E_1^{\mathrm{kin}}$ in all three cases. The distributions corresponding to f_{11} and f_{66} are almost identical, and therefore hard to distinguish experimentally. The latter one has just a slightly flatter profile. The flatness of the profile is

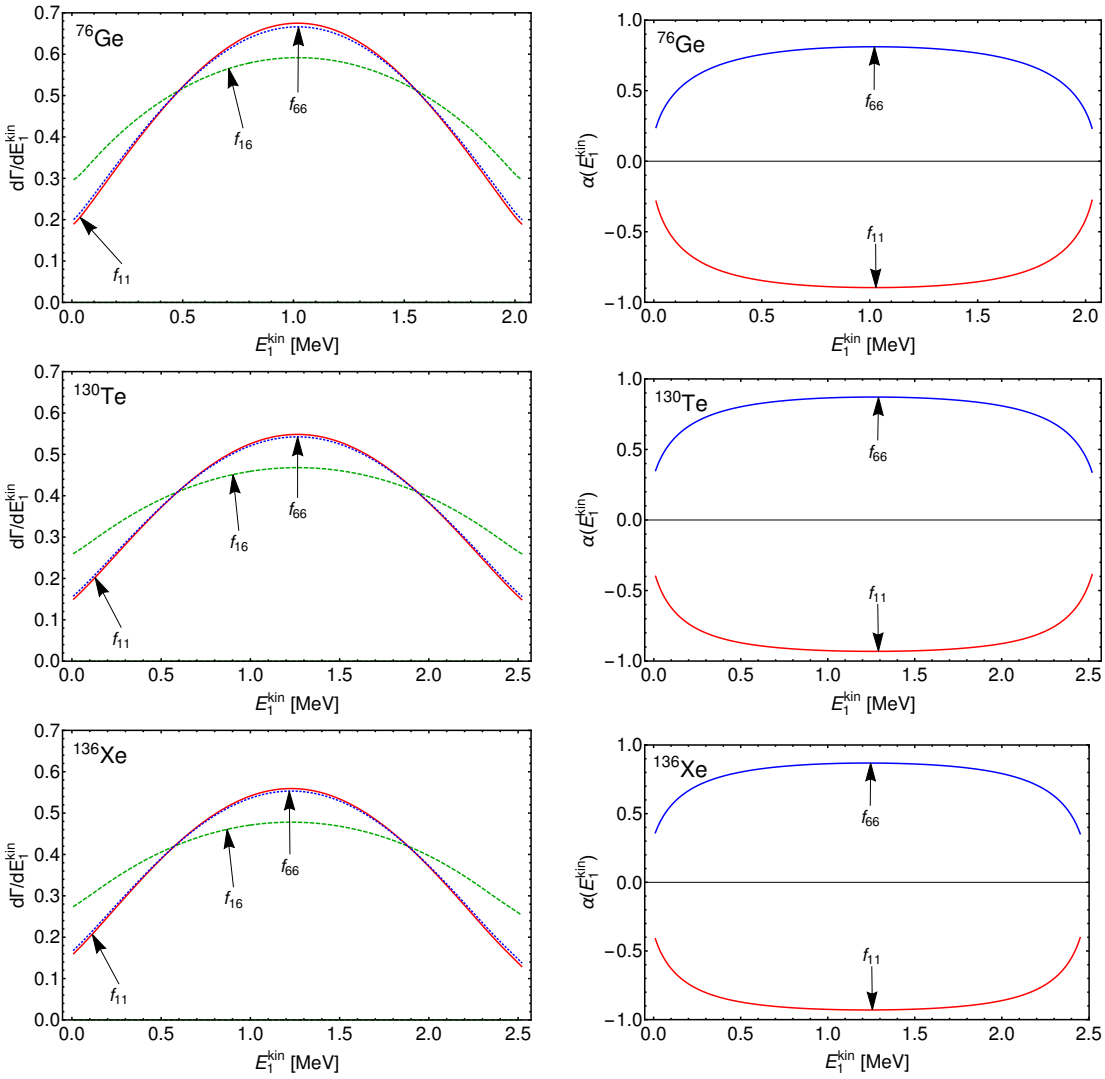

Figure 4.3: These plots show, from top to bottom, the results for the three selected $0\nu\beta\beta$ decay isotopes ^{76}Ge, ^{130}Te and ^{136}Xe. On the left-hand side we always show the single electron energy distribution $\mathrm{d}\Gamma/\mathrm{d}E_1^{\mathrm{kin}}$ as function of the kinetic energy $E_1^{\mathrm{kin}} = E_1 - m_e$ for the three different phase space factors in Eq. (4.125), namely f_{11}, f_{66} and f_{16}. On the right-hand side the energy-dependent angular correlation $\alpha(E_1^{\mathrm{kin}})$ between the two electrons as function of the kinetic energy E_1^{kin} for the phase space factors f_{11} and f_{66} (identically zero for f_{16}) is depicted for each nucleus.

more significant for the interference term f_{16}. The angular correlation $\alpha(E_1^{\mathrm{kin}})$ for f_{11} is always negative, which means that the electrons are preferably emitted back-to-back. On the other hand, for f_{66} the angular correlation is positive, thus reflecting the fact that the electrons in this case prefer to fly in a similar direction.

$G_{jk}^{(i)}$ [10^{-15} y^{-1}]	$G_{11}^{(0)}$	$G_{66}^{(0)}$	$G_{16}^{(0)}$	$G_{11+}^{(1)}$	$G_{11-}^{(1)}$	$G_{66}^{(1)}$	$G_{16}^{(1)}$	K_{11}	K_{66}
^{76}Ge	4.72	2.64	1.7	−3.90	0	1.95	0	−0.83	0.74
^{82}Se	20.4	10.8	5.9	−18.1	0	9.10	0	−0.89	0.84
^{100}Mo	31.8	17.0	8.4	−28.6	0	14.2	0	−0.90	0.84
^{130}Te	28.4	15.3	8.7	−24.8	0	12.4	0	−0.87	0.81
^{136}Xe	29.2	15.7	9.0	−25.4	0	12.7	0	−0.87	0.81

Table 4.4: Here, we summarize the phase space factors $G_{jk}^{(i)}$ and corresponding angular correlation factors K_{11} and K_{66} ($K_{16} = 0$ is always identically zero) calculated for selected isotopes in analogy with [134]. All the presented PSFs are given in units of 10^{-15} y^{-1}.

This difference potentially allows for distinguishing experimentally the scenarios with the f_{66} factor from the standard mass mechanism as well as from scenarios corresponding to f_{11}.

Following the definitions in [134], we calculate the integrated PSFs as

$$G_{ij}^{(a)} = \frac{2C}{\ln 2}\frac{g_{ij}^{(a)}}{4R_A^2}\int_{m_e}^{Q_{\beta\beta}+m_e} dE_1 w(E_1) f_{ij}^{(a)}(E_1, Q_{\beta\beta}+2m_e-E_1), \tag{4.127}$$

where $g_{11}^{(0)} = 2$, $g_{11}^{(1)} = 2$, $g_{66}^{(0)} = 1/8$, $g_{66}^{(1)} = 1/8$, $g_{16}^{(0)} = 1$, $g_{16}^{(1)} = 0$. The quantities C and $w(E_1)$ are defined in Eqs. (4.22) and (4.23), respectively, and the factor $1/R_A^2$ has been introduced in Eq. (4.127) to match the standard notation, in which it compensates for the corresponding factor in the NMEs as discussed above. The numerical values of the PSFs $G_{ij}^{(a)}$ were calculated in analogy with [134] and are provided in Tab. 4.4. As mentioned before, the PSF $G_{16}^{(1)}$ is identically zero. Moreover, the factor $G_{11-}^{(1)}$, which corresponds to the interference between a right-handed and left-handed scalar electron current, also vanishes.

Employing the above PSFs, the inverse $0\nu\beta\beta$ decay half-life can be written as

$$T_{1/2}^{-1} = G_{11}^{(0)}\left|\sum_{I=1}^{3}\epsilon_I\mathcal{M}_I\right|^2 + G_{66}^{(0)}\left|\sum_{I=4}^{5}\epsilon_I\mathcal{M}_I\right|^2 \mp G_{16}^{(0)}\mathrm{Re}\left[\left(\sum_{I=1}^{3}\epsilon_I\mathcal{M}_I\right)\left(\sum_{I=4}^{5}\epsilon_I\mathcal{M}_I\right)^*\right]. \tag{4.128}$$

Again, as in Eq. (4.125) the sign in front of the factor $G_{16}^{(0)}$ is negative (positive) for R (L) chirality of the electron scalar current involved in the interference term.

	$T_{1/2}^{\rm exp}$ [y]	$\lvert\epsilon_1^{XX}\rvert$	$\lvert\epsilon_1^{LR}\rvert$	$\lvert\epsilon_2^{XX}\rvert$	$\lvert\epsilon_3^{XX}\rvert$	$\lvert\epsilon_3^{LR}\rvert$	$\lvert\epsilon_4^{XX,LR}\rvert$	$\lvert\epsilon_5^{XX}\rvert$	$\lvert\epsilon_5^{RL,LR}\rvert$
^{76}Ge	5.3×10^{25}	1.5	1.5	190	110	220	250	60	50
^{130}Te	2.8×10^{24}	3.5	3.4	420	240	490	550	140	120
^{136}Xe	1.1×10^{26}	0.57	0.57	84	50	110	110	23	19

Table 4.5: Above we list the sensitivity estimates on the absolute values of the ϵ_I couplings (in units of 10^{-10}) from current experimental bounds. Only one given contribution is assumed to be non-zero at a time. We specify the chiralities of the involved quark currents, since the corresponding bounds differ. The label XX denotes the case when both chiralities are the same, i.e. $XX = RR$ or $XX = LL$, while the label LR stands for opposite chiralities of the two quark currents. We also include the used experimental bounds at 90% confidence level, reported by recent searches at KamLAND-Zen [236], GERDA [237] and CUORE [238].

The integrated angular correlation factors can be determined as

$$K_{jk} = \frac{B}{A} = \frac{G_{jk}^{(1)}}{G_{jk}^{(0)}}, \tag{4.129}$$

where $jk = 11,\ 66,\ 16$. Since $f_{16} = 0$, the factor K_{16} also trivially vanishes. The resulting numerical values of K_{11} and K_{66} are listed in Tab. 4.4. As already discussed, in view of their opposite sign, a discrimination of the two types of non-standard mechanisms will be possible in an eventual measurement of the angular correlation.

4.9 Bounds on Couplings

A particular underlying particle physics model may in principle generate several different contributions to $0\nu\beta\beta$ decay. Furthermore, the mixing among the corresponding Wilson coefficients can induce contributions through radiative effects from the scale of new physics, through the electroweak scale and down to the QCD scale. In the above presented formulae for the $0\nu\beta\beta$ decay rate we take into account all possible short-range contributions. The therein included ϵ_I factors are understood to be effective at the QCD scale. When determining the numerical limits on these effective couplings we make the customary simplifying assumption that only one term ϵ_I is different from zero, and hence only one mechanism contributes at a time.

	$T_{1/2}^{\text{exp}}$ [y]	$\lvert\epsilon_1^{XX}\rvert$	$\lvert\epsilon_1^{LR}\rvert$	$\lvert\epsilon_2^{XX}\rvert$	$\lvert\epsilon_3^{XX}\rvert$	$\lvert\epsilon_3^{LR}\rvert$	$\lvert\epsilon_4^{XX,LR}\rvert$	$\lvert\epsilon_5^{XX}\rvert$	$\lvert\epsilon_5^{RL,LR}\rvert$
^{76}Ge	10^{27}	0.35	0.35	44	26	50	58	14	11
^{82}Se	10^{27}	0.19	0.19	25	15	30	34	7.8	6.5
^{100}Mo	10^{27}	0.2	0.2	16	8.9	16	20	8.7	6.5
^{130}Te	10^{27}	0.18	0.18	22	13	26	29	7.5	6.1
^{136}Xe	10^{27}	0.19	0.19	28	17	35	38	7.6	6.4

Table 4.6: As Tab. 4.5, but using a prospective limit $T_{1/2}^{\text{future}} = 10^{27}$ y of future experiments.

Therefore, employing the above described calculation of the $0\nu\beta\beta$ decay half-life and considering the currently most stringent experimental bounds on $0\nu\beta\beta$ decay for the isotopes ^{76}Ge [237], ^{130}Te [238] and ^{136}Xe [236] we estimate the upper limits on the ϵ_I factors and the resulting numerical values are shown in Tab. 4.5. Moreover, we also provide the values of the effective couplings that could be reached assuming a common future experimental sensitivity of $T_{1/2}^{\text{future}} = 10^{27}$ y. In this case we include two additional potentially interesting isotopes, ^{82}Se and ^{100}Mo. In both tables, we show the upper bounds on the absolute values $|\epsilon_i^{XY}|$, where the superscript XY labels the chiralities of the involved quark currents. As before, ϵ_i^{XX} denotes the case of equal chiralities, i.e. $XX = LL$ and $XX = RR$. Note that the bound on ϵ_4 is independent of the choice of chiralities, which is not true for the other operators.

We stress again that for the calculation of the numerical results shown in Tabs. 4.5 and 4.6 we employed the values of $\mathcal{M}_F, \mathcal{M}_{GT}$ and $\mathcal{M}_T$ given in Tab. 4.3. The values of the other NMEs were estimated by replacing $(\mathbf{q}/m_p)^2 = 0.01$ as a rough average, and by neglecting the effect of differently-shaped $\mathbf{q}^2$-dependence of form factors.

The numerical limits on the effective couplings calculated using the current experimental sensitivity are between $\approx 10^{-10}$ and 10^{-8}. This range of orders of magnitude is, as expected, generally a bit more stringent than the one of the updated results from Ref. [115] shown in Tab. 4.2. Note that our results for ϵ_1 and ϵ_5 depend on the chiralities of the involved quark currents, while in Tab. 4.2 there is a single limit for each of these couplings. This is due to the additional NMEs we consider, as some of them come with signs dependent on the considered chiralities. The new bounds on these two couplings are also significantly more stringent,

which is primarily due to the large extra NMEs enhanced by the pseudoscalar form factors. We have checked that if we restrict ourselves only to the leading order NMEs used in Ref. [115], we receive values similar to those shown in Tab. 4.2. Other differences between our results and those from Ref. [115] have origin in the fact that we take NMEs calculated using different nuclear structure model and non-approximated PSFs. Clearly, when employing the prospective future limit on $0\nu\beta\beta$ decay half-life, all the limits (cf. Tab. 4.6) become more stringent ranging from 10^{-11} to 10^{-9}. Based on Eq. (4.3) we can see that the derived bounds on the effective couplings generally correspond to new physics scales in multi-TeV energy region.

4.10 QCD Running of Couplings

Above we estimated the limits on the effective couplings of exotic short-range mechanisms at the scale of QCD $\Lambda_{\rm QCD} \approx 1$ GeV making the assumption that only a single operator contributes at a time, and thus neglecting also the mixing of different Wilson coefficients. However, taking into account the Ref. [239] allows us to be more accurate. Employing the therein described procedure we can assume the effective couplings to be present at a certain new physics scale $\Lambda_{\rm NP} \approx 1$ TeV and run them down to $\Lambda_{\rm QCD}$, where we can set again the corresponding limits using the current experimental sensitivity to $0\nu\beta\beta$ decay half-life. The resulting numerical constraints then can be compared with results from collider experiments. Although this effect is not of a big importance in case of the long-range mechanisms, it can have an important impact on the herein focussed short-range operators [239].

For a set of coupled Wilson coefficients $\mathbf{c} = (c_1, c_2, \ldots, c_n)^T$ the Renormalization Group Equations (RGEs) are given by

$$\frac{\mathrm{d}\mathbf{c}(\mu)}{\mathrm{d}\log\mu} = \gamma^T \cdot \mathbf{c}(\mu). \tag{4.130}$$

Here, γ is the anomalous dimension matrix in the $\overline{\rm MS}$-scheme, which can be at one-loop level written as

$$\gamma = -2(b - 2C_F\mathbb{1}), \tag{4.131}$$

where b is a μ-independent constant matrix and C_F stands for the colour factor. The solution to Eq. (4.130) reads (in matrix form)

$$\mathbf{c}(\mu) = U(\mu, \Lambda_{\rm NP}) \cdot \mathbf{c}(\Lambda_{\rm NP}), \tag{4.132}$$

	$T_{1/2}^{\text{exp}}$ [y]	$\lvert c_1^{XX}\rvert$	$\lvert c_1^{LR}\rvert$	$\lvert c_2^{XX}\rvert$	$\lvert c_3^{XX}\rvert$	$\lvert c_3^{LR}\rvert$	$\lvert c_4^{XX}\rvert$	$\lvert c_4^{LR}\rvert$	$\lvert c_5^{XX}\rvert$	$\lvert c_5^{LR}\rvert$
^{76}Ge	5.3×10^{25}	0.62	0.36	88	160	260	580	400	25	12
^{130}Te	2.8×10^{24}	1.4	0.83	200	350	580	1300	880	59	28
^{136}Xe	1.1×10^{26}	0.24	0.14	32	72	130	250	190	9.6	4.7

Table 4.7: This table is analogous to Tab. 4.5, but for the effective couplings defined at the average new physics scale $\Lambda_{\text{NP}} = 1$ TeV.

with matrix U describing the evolution of the coefficients $\mathbf{c}$ between the low and high energy scales denoted by μ and Λ_{NP}, respectively.

In our case we are interested in evolving the effective couplings $c_I \equiv \epsilon_I(1\text{ TeV})$ of the short-range operators triggering $0\nu\beta\beta$ decay at the scale $\Lambda_{\text{NP}} = 1$ TeV down to the QCD scale, where it can be confronted with experimental data. The corresponding evolution matrix $U = U(\Lambda_{\text{QCD}}, \Lambda_{\text{NP}})$ of Wilson coefficients between Λ_{NP} and Λ_{QCD} is rather sparse. Its only non-zero elements are the following [239]

$$U_{(12)}^{XX} = \begin{pmatrix} 2.39 & 0.02 \\ -3.83 & 0.35 \end{pmatrix}, \quad U_{(31)}^{LR} = \begin{pmatrix} 0.84 & -2.19 \\ 0 & 4.13 \end{pmatrix}, \quad U_{(45)}^{XX} = \begin{pmatrix} 0.35 & 0.96i \\ -0.06i & 2.39 \end{pmatrix},$$
$$U_{(3)}^{XX} = 0.70, \quad U_{(4)}^{LR} = 0.62, \quad U_{(5)}^{LR} = 4.13. \tag{4.133}$$

Here, the subscripts label the respective short-range operator(s) and the superscripts the chiralities of the quark currents involved. Hence, for instance, the matrix $U_{(12)}^{XX}$ gives the mixing between the first and second short-range operators involving quark currents with the same chiralities. If we employ Eq. (4.133) and the approximated values of NMEs Eqs. (4.87)-(4.91), we get the bounds on couplings c_I displayed in Tab. 4.7. Although we assume here again only one effective coupling to be non-zero at a time, now we make this assumption at the new physics scale Λ_{NP} and using the above solution of the Wilson RGEs we evolve the couplings to Λ_{QCD} to calculate the $0\nu\beta\beta$ decay rate, potentially with more than one coupling active due to mixing.

If we compare the numerical results presented in Tab. 4.7 with the previously calculated bounds in Tab. 4.5, no common trend is apparent - some of the new limits are weaker and some more stringent than before. Note that now we have two different limits concerning the fourth short-range operator. As the corresponding QCD-running depends on the assumed quark current chiralities, the bound on $|\epsilon_4|$ is split into two different values c_4^{XX} and c_4^{LR}. Due to the fact that

the corresponding RG evolution matrix elements are smaller than 1, both the resulting limits on $|c_4|$ are less stringent. When it comes to the mixing between $\mathcal{O}_1^{XX}$ and $\mathcal{O}_2^{XX}$, one would expect the limit on $|c_2^{XX}|$ to be more stringent because of the expectedly strong contribution from $\mathcal{O}_1^{XX}$ (large NMEs). However, this effect is suppressed by smallness of the relevant element of the evolution matrix, $[U_{(12)}^{XX}]_{12} = 0.02$. Hence, to sum up, despite the strong variation in sensitivity to the couplings ϵ_i the bounds in Tab. 4.7 do not differ drastically from those shown in Tab. 4.5.

5

$0\nu\beta\beta$ Decay From SMEFT

While in the previous chapter the general effective approach to $0\nu\beta\beta$ decay at low energies (Fermi scale) was described, in the present chapter the SM-invariant effective operators generating the low-energy $0\nu\beta\beta$ decay effective operators after EW symmetry breaking will be discussed based on Ref. [240]. In Chap. 3 this correspondence has been already outlined in the case of the standard mass mechanism and it can be summarized as follows. Since the light neutrinos are electrically neutral fundamental fermions with tiny masses, one typically considers neutrino masses to be generated at certain high scale Λ, where the $U(1)_{B-L}$, the only non-anomalous global symmetry of the SM, is broken. This then allows neutrinos to acquire nonzero Majorana masses after EW symmetry breaking. However, since the renormalizable SM respects $U(1)_{B-L}$ symmetry, all the manifestations of this symmetry breaking at low energy scales are described by operators of some higher dimension. Consequently, the neutrino masses are suppressed by certain power of the cut-off scale Λ.

If we further assume that all the new physics lives high above the EW scale, then regardless of the details of the new high-scale theory all the new phenomena occurring below the EW scale are described by higher-dimensional operators. Hence, observable low scale manifestations of all high-energy models leading to small Majorana neutrino masses are just consequences of effective operators that break the $B-L$ number. The LNV processes, which are most relevant for $0\nu\beta\beta$, are those with $\Delta L = 2$ and $\Delta B = 0$, and thus in the following we focus on these.

5.1 $\Delta L = 2$ SM Effective Operators

Listing all the effective operators that respect particular symmetries is a rather tricky and tedious task. To our knowledge, there are two main references focusing on the SM-invariant operators violating lepton number by two units. The first enumeration by Babu and Leung [241] was later reviewed and extended by de Gouvea and Jenkins [214]. The latter study thus provides so far the most

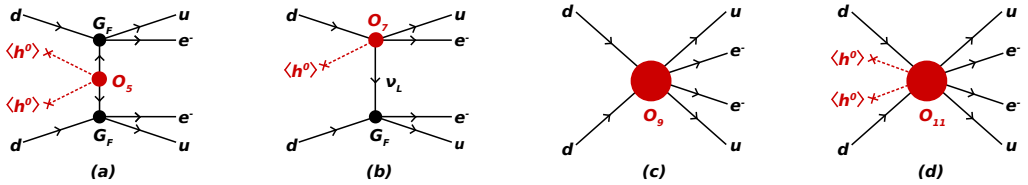

Figure 5.1: Diagrams illustrating the $0\nu\beta\beta$ decay contributions from $\Delta L = 2$ SM effective operators: (a) 5-dimensional Weinberg operator (standard mass mechanism), (b) 7-dimensional operator leading to long–range contribution, (c, d) operators of dimensions 9 and 11 leading to short–range contributions.

exhaustive, although by no means complete, list of the $\Delta L = 2$ SM invariant effective operators. In this work we will discuss operators up to dimension 9 and a representative fraction of dimension-11 operators. Our aim is to describe the contribution of these operators to the effective low-energy $0\nu\beta\beta$ interactions, as shown in Fig. 5.1. Most of them will not contribute directly at tree level, but rather at various loop levels.

In the following discussion we are using a list of $\Delta L = 2$ SM effective operators that is mostly based on Ref. [214]. We further make use of the Hilbert Series method [78, 215] to check that no important effective operators are omitted. Specifically, running the code accompanying Ref. [78] we obtain all possible independent operator patterns that can be constructed from the given set of fields and that violate lepton number by two units. By operator patterns we mean the field content of particular operators without specified gauge and Lorentz structure. Each such pattern comes in the series with the corresponding multiplicity factor denoting the number of possible independent contractions (both Lorentz and gauge) of that particular field content, which lead to independent effective operators invariant under given symmetries. Hence, comparing the series with our list ensures that we capture all possible types of $\Delta L = 2$ operators made of SM fermions and the Higgs at dimensions of our interest.

Similarly to Ref. [214] we do not cover operators involving gauge fields and derivatives, as these are expected to be more difficult to be generated at tree level from an underlying renormalizable theory [241]. Moreover, we specify only the possible $SU(2)_L$ contractions and we are not interested in various possible Lorentz and $SU(3)_C$ structures. The labels f_L and f^c refer to left-handed Weyl spinors with f denoting a fermion according to Tab. 2.1 and f^c being the charge-conjugate of the $SU(2)_L$ singlet right-handed charged fermions. As has been

proved in Ref. [79], the $\Delta L = 2$ SM-invariant effective operators are always of odd dimension. In addition to the single Weinberg operator of dimension-5 in Eq. (5.2), we show the resulting sets of operators of dimensions 7, 9 and 11 in Tabs. 5.1, 5.2 and 5.3, respectively. All the therein listed operators are written in terms of the first generation of fermions, although some may be non-trivial only if more generations are considered, as indicated.

The resulting Lagrangian summarizing all the considered interactions thus reads

$$\mathcal{L} = \mathcal{L}_{SM} + \frac{1}{\Lambda_5}\mathcal{O}_5 + \sum_i \frac{1}{\Lambda_{7_i}^3}\mathcal{O}_7^i + \sum_i \frac{1}{\Lambda_{9_i}^5}\mathcal{O}_9^i + \sum_i \frac{1}{\Lambda_{11_i}^7}\mathcal{O}_{11}^i. \tag{5.1}$$

Here, $\mathcal{L}_{SM}$ is the SM Lagrangian, $\mathcal{O}_5$ stands for the dimension-5 Weinberg operator suppressed by the corresponding typical energy scale Λ_5. The SM-invariant effective operators of higher dimensions are denoted as $\mathcal{O}_D^i$ with $D = 7,\ 9,\ 11$. The corresponding suppression is always given by $\Lambda_{D_i}^{D-4}$, where the energy scale Λ_{D_i} subsumes any mass scales and couplings of an underlying UV-complete theory. It is important to remark again that, as well as before, in all the following calculations we will always assume only a single $\Delta L = 2$ SM-invariant effective operator on top of the SM Lagrangian is present at a time.

5.1.1 Dimension 5

It is a well-known fact that there is just a single $\Delta L = 2$ SM effective operator (modulo generations) at dimension 5. This is confirmed by Hilbert series having the trivial form

$$\mathcal{H}_5^{\Delta L=2} = L^2H^2 + \text{h.c.}. \tag{5.2}$$

As mentioned, the Hilbert series is merely a polynomial in the given fields, hence it does not provide any information on the actual gauge and Lorentz contractions involved. The Weinberg operator reads

$$\mathcal{O}_1 = L^iL^jH^kH^l\epsilon_{ik}\epsilon_{jl}, \tag{5.3}$$

where the fields are defined in Tab. 2.1 and the indices i, j, k, l together with the corresponding ϵ-contractions define the $SU(2)_L$ structure of the operator. As we have mentioned earlier, it generates the light Majorana neutrino masses after EW symmetry breaking. As a result, it contributes to $0\nu\beta\beta$ decay through the effective neutrino mass of the order $m_\nu = \frac{v^2}{\Lambda_5}$.

$\mathcal{O}$	Operator	m_ν	LR	ϵ_{LR}
1^{H^2}	$L^iL^jH^kH^l\overline{H}^tH_t\epsilon_{ik}\epsilon_{jl}$	$\frac{v^2}{\Lambda}f\left(\frac{v}{\Lambda}\right)$	–	–
2	$L^iL^jL^ke^cH^l\epsilon_{ij}\epsilon_{kl}$	$\frac{y_e}{16\pi^2}\frac{v^2}{\Lambda}$	–	–
3_a	$L^iL^jQ^kd^cH^l\epsilon_{ij}\epsilon_{kl}$	$\frac{y_dg^2}{(16\pi^2)^2}\frac{v^2}{\Lambda}$	$\frac{v}{\Lambda^3}$	$\epsilon^{T_R}_{T_R}$
3_b	$L^iL^jQ^kd^cH^l\epsilon_{ik}\epsilon_{jl}$	$\frac{y_d}{16\pi^2}\frac{v^2}{\Lambda}$	$\frac{v}{\Lambda^3}$	ϵ^{S+P}_{S+P}
4_a	$L^iL^j\overline{Q}_i\bar{u}^cH^k\epsilon_{jk}$	$\frac{y_u}{16\pi^2}\frac{v^2}{\Lambda}$	$\frac{v}{\Lambda^3}$	ϵ^{S+P}_{S-P}
$4_b^\dagger$	$L^iL^j\overline{Q}_k\bar{u}^cH^k\epsilon_{ij}$	$\frac{y_ug^2}{(16\pi^2)^2}\frac{v^2}{\Lambda}$	$\frac{v}{\Lambda^3}$	ϵ^{S+P}_{S-P}
8	$L^i\bar{e}^c\bar{u}^cd^cH^j\epsilon_{ij}$	$\frac{y_e^{\text{ex}}y_dy_u}{(16\pi^2)^2}\frac{v^2}{\Lambda}$	$\frac{v}{\Lambda^3}$	$2\epsilon^{V+A}_{V+A}$

Table 5.1: Dimension-7 $\Delta L = 2$ SM-invariant effective operators. In each case the dominant contributions to $0\nu\beta\beta$ decay via the effective neutrino mass (m_ν) and long-range (LR) mechanisms are displayed. In column ϵ_{LR} the $0\nu\beta\beta$ long-range interaction triggered by a particular operator is shown. The notation used for labelling different contributions is explained in Sec. 5.2.3.

5.1.2 Dimension 7

The Hilbert series for $\Delta L = 2$ SM effective operators of dimension 7 reads

$$\mathcal{H}_7^{\Delta L=2} = d\bar{e}^cHL\bar{u}^c + 2d^cHL^2Q + e^cHL^3 + H^3\bar{H}L^2 + HL^2Q^\dagger\bar{u}^c + \text{h.c.}, \quad (5.4)$$

where the integer coefficient in front of the second term indicates the multiplicity of the given pattern. Indeed, requiring the Lorentz and SM invariance, there are two independent ways how to contract the fields in question. Specifically, there are two independent operators corresponding to the second term, $\mathcal{O}_{3a}$ and $\mathcal{O}_{3b}$, which differ by their $SU(2)_L$ structure, see Tab. 5.1.

The resulting set of operators, including explicitly specified $SU(2)_L$ contractions, is shown in Tab. 5.1. In general, we do not discuss in detail the operators given by a product of invariant operators of lower dimension; however, we list them here for completeness. This is the case of the operator $\mathcal{O}_{1^{H^2}}$ highlighted in italic. As one can immediately observe, this operator is simply the Weinberg operator multiplied by the singlet combination $H\bar{H}$. Next, we mark operator $\mathcal{O}_{4_b}$ by a dagger, since it is a Fierz transformation of operator $\mathcal{O}_{4_a}$, and thus it is not an independent operator. In addition, the existence of this operator requires more than a single fermion generation, otherwise it trivially vanishes. Therefore, it does not contribute to $0\nu\beta\beta$ decay on its own. However, the same reason means that this operator cannot be solely responsible for the observed neutrino oscillations. Therefore, in the minimal case there would have to be a misalignment between

the operator flavour structure and the charged-current mixing. Assuming so, $\mathcal{O}_{4_a}$ may still contribute to $0\nu\beta\beta$ decay with only a $\mathcal{O}(1)$ suppression; hence, it is retained in our results.

5.1.3 Dimension 9

At dimension 9 the Hilbert series covering the operator terms of our interest is given by

$$\begin{aligned}\mathcal{H}_9^{\Delta L=2} = &\left(d^c\right)^2 \bar{d^c} L^2 \bar{u^c} + \left(d^c\right)^2 \bar{e^c}^2 \bar{u^c}^2 + 2\left(d^c\right)^2 \bar{e^c} L Q \bar{u^c} + 4\left(d^c\right)^2 L^2 Q^2 \\ &+ d^c e^c \bar{e^c} L^2 \bar{u^c} + 2 d^c e^c L^3 Q + d^c \bar{e^c} H^2 \overline{H} L \bar{u^c} + 2 d^c \bar{e^c} L \overline{Q} \bar{u^c}^2 \\ &+ 3 d^c H^2 \overline{H} L^2 Q + d^c L^3 \overline{L} \bar{u^c} + 4 d^c L^2 Q \overline{Q} \bar{u^c} + d^c L^2 u^c \bar{u^c}^2 + \bar{d^c} H^3 L^2 \overline{Q} \\ &+ \left(e^c\right)^2 L^4 + e^c H^2 \overline{H} L^3 + e^c L^3 \overline{Q} \bar{u^c} + \bar{e^c} H^3 L^2 \overline{L} + \bar{e^c} H^3 L Q \overline{Q} \\ &+ H^4 \overline{H}^2 L^2 + H^3 L^2 Q u^c + 2 H^2 \overline{H} L^2 \overline{Q} \bar{u^c} + 2 L^2 \overline{Q}^2 \bar{u^c}^2 + \text{h.c.}, \end{aligned} \tag{5.5}$$

and the corresponding effective operators are displayed in Tab. 5.2. The operators 'derived' from lower-dimensional ones are again included just to provide a complete list. For instance, operator $\mathcal{O}_{1^{H^4}}$ is a product of Weinberg operator and two singlet combinations $H\bar{H}$. Similarly, operator $\mathcal{O}_{1^{ye}}$ is the Weinberg operator with the $\bar{L}H\bar{e^c}$ singlet combination attached. The asterisk in case of operator $\mathcal{O}_{12_b}$ marks that it vanishes for a single generation of fermions; therefore, it does not contribute to $0\nu\beta\beta$ decay. Analogous to operator $\mathcal{O}_{4_a}$, one needs to include another source of lepton flavour violation in order to reproduce the observed neutrino oscillations. In such a case, $\mathcal{O}_{12_b}$ may also contribute to $0\nu\beta\beta$ decay. Unlike $\mathcal{O}_{4_a}$, operator $\mathcal{O}_{12_b}$ cannot be Fierz-transformed to any of the other listed operators. Finally, note that operator $\mathcal{O}_{76}$ does not appear in [214].

5.1.4 Dimension 11

The number of $\Delta L = 2$ SM effective operators of dimension 11 is relatively large. However, many of them manifest a fairly similar behaviour, when contributions to $0\nu\beta\beta$ decay are studied. Therefore, we concentrate here only on a restricted selection of 11-dimensional operators displayed in Tab. 5.3. We include all operators that trigger $0\nu\beta\beta$ decay at tree level, but we skip e.g. operators that do not appreciably contribute to $0\nu\beta\beta$ decay through long-range or short-range interactions. All products of invariant sub-operators are omitted.

$\mathcal{O}$	Operator	m_ν	LR	$\epsilon_{\rm LR}$	SR	$\epsilon_{\rm SR}$
1^{H^4}	$L^iL^jH^kH^l\overline{H}^tH_t\overline{H}^uH_u\epsilon_{ik}\epsilon_{jl}$	$\frac{v^2}{\Lambda}f^2\left(\frac{v}{\Lambda}\right)$	–	–	–	–
1^{y_e}	$L^iL^jH^kH^l(\overline{L}^tH_t\bar{e}^c)\epsilon_{ik}\epsilon_{jl}$	$\frac{y_e}{(16\pi^2)^2}\frac{v^2}{\Lambda}$	–	–	–	–
1^{y_d}	$L^iL^jH^kH^l(\overline{Q}^tH_t\bar{d}^c)\epsilon_{ik}\epsilon_{jl}$	$\frac{y_d}{(16\pi^2)^2}\frac{v^2}{\Lambda}$	$\frac{y_d y^{\rm ex}_{d\|u}}{16\pi^2}\frac{v}{\Lambda^3}f\left(\frac{v}{\Lambda}\right)$	$\epsilon^{S+P}_{S\pm P}$	–	–
2^{H^2}	$L^iL^jL^ke^cH^l\overline{H}^tH_t\varepsilon_{ij}\varepsilon_{kl}$	$\frac{y_e}{16\pi^2}\frac{v^2}{\Lambda}f\left(\frac{v}{\Lambda}\right)$	–	–	–	–
$3^{H^2}_a$	$L^iL^jQ^kd^cH^l\overline{H}^tH_t\epsilon_{ij}\epsilon_{kl}$	$\frac{y_d g^2}{(16\pi^2)^2}\frac{v^2}{\Lambda}f\left(\frac{v}{\Lambda}\right)$	$\frac{v}{\Lambda^3}f\left(\frac{v}{\Lambda}\right)$	$\epsilon^{T_R}_{T_R}$	–	–
$3^{H^2}_b$	$L^iL^jQ^kd^cH^l\overline{H}^tH_t\epsilon_{ik}\epsilon_{jl}$	$\frac{y_d}{16\pi^2}\frac{v^2}{\Lambda}f\left(\frac{v}{\Lambda}\right)$	$\frac{v}{\Lambda^3}f\left(\frac{v}{\Lambda}\right)$	ϵ^{S+P}_{S+P}	–	–
$4^{H^2}_a$	$L^iL^j\overline{Q}_i\bar{u}^cH^k\overline{H}^tH_t\epsilon_{jk}$	$\frac{y_u}{16\pi^2}\frac{v^2}{\Lambda}f\left(\frac{v}{\Lambda}\right)$	$\frac{v}{\Lambda^3}f\left(\frac{v}{\Lambda}\right)$	ϵ^{S+P}_{S-P}	–	–
5	$L^iL^jQ^kd^cH^lH^m\overline{H}_i\epsilon_{jl}\epsilon_{km}$	$\frac{y_d}{(16\pi^2)^2}\frac{v^2}{\Lambda}$	$\frac{v}{\Lambda^3}f\left(\frac{v}{\Lambda}\right)$	ϵ^{S+P}_{S+P}	–	–
6	$L^iL^j\overline{Q}_k\bar{u}^cH^lH^k\overline{H}_i\epsilon_{jl}$	$\frac{y_u}{(16\pi^2)^2}\frac{v^2}{\Lambda}$	$\frac{v}{\Lambda^3}f\left(\frac{v}{\Lambda}\right)$	ϵ^{S+P}_{S-P}	–	–
7	$L^iQ^j\bar{e}^c\overline{Q}_kH^kH^lH^m\epsilon_{il}\epsilon_{jm}$	$\frac{y^{\rm ex}_e g^2}{(16\pi^2)^2}\frac{v^2}{\Lambda}f\left(\frac{v}{\Lambda}\right)$	$\frac{v^3}{\Lambda^5}$	$2\epsilon^{V+A}_{V-A}$	–	–
8^{H^2}	$L^i\bar{e}^c\bar{u}^cd^cH^j\overline{H}^tH_t\epsilon_{ij}$	$\frac{y^{\rm ex}_e y_d y_u}{(16\pi^2)^2}\frac{v^2}{\Lambda}f\left(\frac{v}{\Lambda}\right)$	$\frac{v}{\Lambda^3}f\left(\frac{v}{\Lambda}\right)$	$2\epsilon^{V+A}_{V+A}$	–	–
9	$L^iL^jL^ke^cL^le^c\epsilon_{ij}\epsilon_{kl}$	$\frac{y_e^2}{(16\pi^2)^2}\frac{v^2}{\Lambda}$	–	–	–	–
10	$L^iL^jL^ke^cQ^ld^c\epsilon_{ij}\epsilon_{kl}$	$\frac{y_e y_d}{(16\pi^2)^2}\frac{v^2}{\Lambda}$	$\frac{y_e}{16\pi^2}\frac{v}{\Lambda^3}$	ϵ^{S+P}_{S+P}	–	–
11_a	$L^iL^jQ^kd^cQ^ld^c\epsilon_{ij}\epsilon_{kl}$	$\frac{y_d^2 g^2}{(16\pi^2)^3}\frac{v^2}{\Lambda}$	$\frac{y_d}{16\pi^2}\frac{v}{\Lambda^3}$	$\epsilon^{T_R}_{T_R}$	$\frac{g^2}{16\pi^2}\frac{1}{\Lambda^5}$	ϵ_1
11_b	$L^iL^jQ^kd^cQ^ld^c\epsilon_{ik}\epsilon_{jl}$	$\frac{y_d^2}{(16\pi^2)^2}\frac{v^2}{\Lambda}$	$\frac{y_d}{16\pi^2}\frac{v}{\Lambda^3}$	ϵ^{S+P}_{S+P}	$\frac{1}{\Lambda^5}$	ϵ_1
12_a	$L^iL^j\overline{Q}_i\bar{u}^c\overline{Q}_j\bar{u}^c$	$\frac{y_u^2}{(16\pi^2)^2}\frac{v^2}{\Lambda}$	$\frac{y_u}{16\pi^2}\frac{v}{\Lambda^3}$	ϵ^{S+P}_{S-P}	$\frac{1}{\Lambda^5}$	ϵ_1
12^*_b	$L^iL^j\overline{Q}_k\bar{u}^c\overline{Q}_l\bar{u}^c\epsilon_{ij}\epsilon^{kl}$	$\frac{y_u^2 g^2}{(16\pi^2)^3}\frac{v^2}{\Lambda}$	$\frac{y_u}{16\pi^2}\frac{v}{\Lambda^3}$	ϵ^{S+P}_{S-P}	$\frac{g^2 y^{\rm ex}_d y^{\rm ex}_u}{(16\pi^2)^2}\frac{1}{\Lambda^5}$	ϵ_1
13	$L^iL^j\overline{Q}_i\bar{u}^cL^le^c\epsilon_{jl}$	$\frac{y_e y_u}{(16\pi^2)^2}\frac{v^2}{\Lambda}$	$\frac{y_e}{16\pi^2}\frac{v}{\Lambda^3}$	ϵ^{S+P}_{S-P}	–	–
14_a	$L^iL^j\overline{Q}_k\bar{u}^cQ^kd^c\epsilon_{ij}$	$\frac{y_d y_u g^2}{(16\pi^2)^3}\frac{v^2}{\Lambda}$	$\frac{y_{u\|d}}{16\pi^2}\frac{v}{\Lambda^3}$	$\epsilon^{T_R}_{T_R}$	$\frac{g^2}{(16\pi^2)^2}\frac{1}{\Lambda^5}$	ϵ_1
14_b	$L^iL^j\overline{Q}_i\bar{u}^cQ^ld^c\epsilon_{jl}$	$\frac{y_d y_u}{(16\pi^2)^2}\frac{v^2}{\Lambda}$	$\frac{y_{u\|d}}{16\pi^2}\frac{v}{\Lambda^3}$	$\epsilon^{S+P}_{S\pm P}$	$\frac{1}{\Lambda^5}$	ϵ_1
15	$L^iL^jL^kd^c\overline{L}_i\bar{u}^c\epsilon_{jk}$	$\frac{y_d y_u g^2}{(16\pi^2)^3}\frac{v^2}{\Lambda}$	$\frac{g^2 y^{\rm ex}_{u\|d\|e}}{(16\pi^2)^2}\frac{v}{\Lambda^3}$	$\epsilon^{S+P}_{S\pm P}\|2\epsilon^{V+A}_{V+A}$	–	–
16	$L^iL^je^cd^c\bar{e}^c\bar{u}^c\epsilon_{ij}$	$\frac{y_d y_u g^4}{(16\pi^2)^4}\frac{v^2}{\Lambda}$	$\frac{y_e}{16\pi^2}\frac{v}{\Lambda^3}$	$2\epsilon^{V+A}_{V+A}$	–	–
17	$L^iL^jd^cd^c\bar{d}^c\bar{u}^c\epsilon_{ij}$	$\frac{y_d y_u g^4}{(16\pi^2)^4}\frac{v^2}{\Lambda}$	$\frac{g^2 y^{\rm ex}_{u\|d\|e}}{(16\pi^2)^2}\frac{v}{\Lambda^3}$	$\epsilon^{T_R}_{T_R}\|2\epsilon^{V+A}_{V+A}$	$\frac{y^{\rm ex}_d y^{\rm ex}_e}{16\pi^2}\frac{1}{\Lambda^5}$	$2\epsilon_5$
18	$L^iL^jd^cu^c\bar{u}^c\bar{u}^c\epsilon_{ij}$	$\frac{y_d y_u g^4}{(16\pi^2)^4}\frac{v^2}{\Lambda}$	$\frac{g^2 y^{\rm ex}_{u\|d\|e}}{(16\pi^2)^2}\frac{v}{\Lambda^3}$	$\epsilon^{T_R}_{T_R}\|2\epsilon^{V+A}_{V+A}$	$\frac{y^{\rm ex}_e y^{\rm ex}_u}{16\pi^2}\frac{1}{\Lambda^5}$	$2\epsilon_5$
19	$L^iQ^jd^cd^c\bar{e}^c\bar{u}^c\epsilon_{ij}$	$\frac{y^{\rm ex}_e y_d^2 y_u}{(16\pi^2)^3}\frac{v^2}{\Lambda}$	$\frac{y_d}{16\pi^2}\frac{v}{\Lambda^3}$	$2\epsilon^{V+A}_{V+A}$	$\frac{1}{\Lambda^5}$	$2\epsilon_5$
20	$L^id^c\overline{Q}_i\bar{u}^c\bar{e}^c\bar{u}^c$	$\frac{y^{\rm ex}_e y_d y_u^2}{(16\pi^2)^3}\frac{v^2}{\Lambda}$	$\frac{y_u}{16\pi^2}\frac{v}{\Lambda^3}$	$2\epsilon^{V+A}_{V+A}$	$\frac{1}{\Lambda^5}$	$2\epsilon_5$
61	$L^iL^jH^kH^lL^re^c\overline{H}_r\epsilon_{ik}\epsilon_{jl}$	$\frac{y_e}{16\pi^2}\frac{v^2}{\Lambda}f\left(\frac{v}{\Lambda}\right)$	–	–	–	–
66	$L^iL^jH^kH^l\epsilon_{ik}Q^rd^c\overline{H}_r\epsilon_{jl}$	$\frac{y_d}{16\pi^2}\frac{v^2}{\Lambda}f\left(\frac{v}{\Lambda}\right)$	$\frac{1}{16\pi^2}\frac{v}{\Lambda^3}$	ϵ^{S+P}_{S+P}	–	–
71	$L^iL^jH^kH^lQ^ru^cH^s\epsilon_{rs}\epsilon_{ik}\epsilon_{jl}$	$\frac{y_u}{16\pi^2}\frac{v^2}{\Lambda}f\left(\frac{v}{\Lambda}\right)$	$\frac{y_u y^{\rm ex}_{d\|u}}{16\pi^2}\frac{v}{\Lambda^3}f\left(\frac{v}{\Lambda}\right)$	$\epsilon^{S+P}_{S\pm P}$	–	–
76	$\bar{e}^c\bar{e}^cd^cd^c\bar{u}^c\bar{u}^c$	$\frac{y^{\rm ex2}_e y_d^2 y_u^2}{(16\pi^2)^4}\frac{v^2}{\Lambda}$	$\frac{y_d y_u y^{\rm ex}_e}{(16\pi^2)^2}\frac{v}{\Lambda^3}$	$2\epsilon^{V+A}_{V+A}$	$\frac{1}{\Lambda^5}$	$2\tilde{\epsilon}_3$

Table 5.2: List of $\Delta L = 2$ SM-invariant effective operators at dimension 9. Next to the dominant contributions to $0\nu\beta\beta$ decay via the effective neutrino mass (m_ν) we provide also the dominant contributions triggered by long-range (LR) and short-range (SR) mechanisms. In columns $\epsilon_{\rm LR}$ and $\epsilon_{\rm SR}$ we show the types of $0\nu\beta\beta$ long-range and short-range interactions excited by a particular operator, using here the definition $\tilde{\epsilon}_3 \equiv \epsilon_3^{LL,RR}$ to keep the table more compact. To specify different contributions we use the notation explained in Sec. 5.2.3.

$\mathcal{O}$	Operator	m_ν	LR	$\epsilon_{\rm LR}$	SR	$\epsilon_{\rm SR}$
21_a	$L^iL^jL^ke^cQ^lu^cH^mH^n\epsilon_{ij}\epsilon_{km}\epsilon_{ln}$	$\frac{y_e y_u}{(16\pi^2)^2}\frac{v^2}{\Lambda}f\left(\frac{v}{\Lambda}\right)$	$\frac{y_e y_e^{\rm ex} y_u^{\rm ex}}{(16\pi^2)^2}\frac{v^3}{\Lambda^5}$	$2\epsilon_{V-A}^{V+A}$	–	–
21_b	$L^iL^jL^ke^cQ^lu^cH^mH^n\epsilon_{il}\epsilon_{jm}\epsilon_{kn}$	$\frac{y_e y_u}{(16\pi^2)^2}\frac{v^2}{\Lambda}f\left(\frac{v}{\Lambda}\right)$	$\frac{y_e y_e^{\rm ex} y_u^{\rm ex}}{(16\pi^2)^2}\frac{v^3}{\Lambda^5}$	$2\epsilon_{V-A}^{V+A}$	–	–
23	$L^iL^jL^ke^c\overline{Q}_k\bar{d}^cH^lH^m\epsilon_{il}\epsilon_{jm}$	$\frac{y_e y_d}{(16\pi^2)^2}\frac{v^2}{\Lambda}f\left(\frac{v}{\Lambda}\right)$	$\frac{y_{d(e)}^{\rm ex} y_d^{\rm ex} y_e}{(16\pi^2)^2}\frac{v}{\Lambda^3}f\left(\frac{v}{\Lambda}\right)$	$\epsilon_{S-P}^{S+P}\vert\epsilon_{V+A}^{V+A}$	–	–
24_a	$L^iL^jQ^kd^cQ^ld^cH^m\overline{H}_i\epsilon_{jk}\epsilon_{lm}$	$\frac{y_d^2}{(16\pi^2)^3}\frac{v^2}{\Lambda}$	$\frac{y_d}{16\pi^2}\frac{v}{\Lambda^3}f\left(\frac{v}{\Lambda}\right)$	ϵ_{S+P}^{S+P}	$\frac{1}{\Lambda^5}f\left(\frac{v}{\Lambda}\right)$	ϵ_1
24_b	$L^iL^jQ^kd^cQ^ld^cH^m\overline{H}_i\epsilon_{jm}\epsilon_{kl}$	$\frac{y_d^2}{(16\pi^2)^3}\frac{v^2}{\Lambda}$	$\frac{y_d}{16\pi^2}\frac{v}{\Lambda^3}f\left(\frac{v}{\Lambda}\right)$	ϵ_{S+P}^{S+P}	$\frac{g^2}{(16\pi^2)}\frac{1}{\Lambda^5}f\left(\frac{v}{\Lambda}\right)$	ϵ_1
25	$L^iL^jQ^kd^cQ^lu^cH^mH^n\epsilon_{im}\epsilon_{jn}\epsilon_{kl}$	$\frac{y_d y_u}{(16\pi^2)^2}\frac{v^2}{\Lambda}f\left(\frac{v}{\Lambda}\right)$	$\frac{y_u}{(16\pi^2)^2}\frac{v}{\Lambda^3}$	ϵ_{S+P}^{S+P}	$\frac{y_u^{\rm ex2}}{(16\pi^2)^2}\frac{1}{\Lambda^5}$	ϵ_1
26_a	$L^iL^jQ^kd^c\overline{L}_i\bar{e}^cH^lH^m\epsilon_{jl}\epsilon_{km}$	$\frac{y_e y_d}{(16\pi^2)^3}\frac{v^2}{\Lambda}$	$\frac{y_e}{16\pi^2}\frac{v}{\Lambda^3}f\left(\frac{v}{\Lambda}\right)$	ϵ_{S+P}^{S+P}	–	–
26_b	$L^iL^jQ^kd^c\overline{L}_k\bar{e}^cH^lH^m\epsilon_{il}\epsilon_{jm}$	$\frac{y_e y_d}{(16\pi^2)^2}\frac{v^2}{\Lambda}f\left(\frac{v}{\Lambda}\right)$	$\frac{y_e}{(16\pi^2)^2}\frac{v}{\Lambda^3}$	ϵ_{S+P}^{S+P}	–	–
27_a	$L^iL^jQ^kd^c\overline{Q}_i\bar{d}^cH^lH^m\epsilon_{jl}\epsilon_{km}$	$\frac{g^2}{(16\pi^2)^3}\frac{v^2}{\Lambda}$	$\frac{y_d}{16\pi^2}\frac{v}{\Lambda^3}f\left(\frac{v}{\Lambda}\right)$	ϵ_{S+P}^{S+P}	$\frac{y_d^{\rm ex2}}{(16\pi^2)^2}\frac{1}{\Lambda^5}$	ϵ_1
27_b	$L^iL^jQ^kd^c\overline{Q}_k\bar{d}^cH^lH^m\epsilon_{il}\epsilon_{jm}$	$\frac{g^2}{(16\pi^2)^3}\frac{v^2}{\Lambda}$	$\frac{y_d}{(16\pi^2)^2}\frac{v}{\Lambda^3}$	ϵ_{S+P}^{S+P}	$\frac{y_d^{\rm ex2}}{(16\pi^2)^2}\frac{1}{\Lambda^5}$	ϵ_1
28_a	$L^iL^jQ^kd^c\overline{Q}_j\bar{u}^cH^l\overline{H}_i\epsilon_{kl}$	$\frac{y_d y_u}{(16\pi^2)^3}\frac{v^2}{\Lambda}$	$\frac{y_u}{16\pi^2}\frac{v}{\Lambda^3}f\left(\frac{v}{\Lambda}\right)$	ϵ_{S+P}^{S+P}	$\frac{v^2}{\Lambda^7}$	ϵ_1
28_b	$L^iL^jQ^kd^c\overline{Q}_k\bar{u}^cH^l\overline{H}_i\epsilon_{jl}$	$\frac{y_d y_u}{(16\pi^2)^3}\frac{v^2}{\Lambda}$	$\frac{y_{u\vert d}}{16\pi^2}\frac{v}{\Lambda^3}f\left(\frac{v}{\Lambda}\right)$	$\epsilon_{S\pm P}^{S+P}$	$\frac{g^2}{(16\pi^2)}\frac{1}{\Lambda^5}f\left(\frac{v}{\Lambda}\right)$	ϵ_1
28_c	$L^iL^jQ^kd^c\overline{Q}_l\bar{u}^cH^l\overline{H}_i\epsilon_{jk}$	$\frac{y_d y_u}{(16\pi^2)^3}\frac{v^2}{\Lambda}$	$\frac{y_d}{16\pi^2}\frac{v}{\Lambda^3}f\left(\frac{v}{\Lambda}\right)$	ϵ_{S-P}^{S+P}	$\frac{1}{\Lambda^5}f\left(\frac{v}{\Lambda}\right)$	ϵ_1
29_a	$L^iL^jQ^ku^c\overline{Q}_k\bar{u}^cH^lH^m\epsilon_{il}\epsilon_{jm}$	$\frac{g^2}{(16\pi^2)^3}\frac{v^2}{\Lambda}$	$\frac{y_u}{(16\pi^2)^2}\frac{v}{\Lambda^3}$	ϵ_{S-P}^{S+P}	$\frac{y_d^{\rm ex}y_u^{\rm ex}}{(16\pi^2)^2}\frac{1}{\Lambda^5}$	ϵ_1
29_b	$L^iL^jQ^ku^c\overline{Q}_l\bar{u}^cH^lH^m\epsilon_{ik}\epsilon_{jm}$	$\frac{g^2}{(16\pi^2)^3}\frac{v^2}{\Lambda}$	$\frac{y_u}{16\pi^2}\frac{v}{\Lambda^3}f\left(\frac{v}{\Lambda}\right)$	ϵ_{S-P}^{S+P}	$\frac{y_d^{\rm ex}y_u^{\rm ex}}{(16\pi^2)^2}\frac{1}{\Lambda^5}$	ϵ_1
30_a	$L^iL^j\overline{L}_ie^c\overline{Q}_k\bar{u}^cH^kH^l\epsilon_{jl}$	$\frac{y_e y_u}{(16\pi^2)^3}\frac{v^2}{\Lambda}$	$\frac{y_e}{16\pi^2}\frac{v}{\Lambda^3}f\left(\frac{v}{\Lambda}\right)$	ϵ_{S-P}^{S+P}	–	–
30_b	$L^iL^j\overline{L}_me^c\overline{Q}_nu^cH^kH^l\epsilon_{ik}\epsilon_{jl}\epsilon^{mn}$	$\frac{y_e y_u}{(16\pi^2)^2}\frac{v^2}{\Lambda}f\left(\frac{v}{\Lambda}\right)$	$\frac{y_e}{(16\pi^2)^2}\frac{v}{\Lambda^3}$	ϵ_{S-P}^{S+P}	–	–
31_a	$L^iL^j\overline{Q}_i\bar{d}^c\overline{Q}_k\bar{u}^cH^kH^l\epsilon_{jl}$	$\frac{y_d y_u}{(16\pi^2)^2}\frac{v^2}{\Lambda}f\left(\frac{v}{\Lambda}\right)$	$\frac{y_d}{16\pi^2}\frac{v}{\Lambda^3}f\left(\frac{v}{\Lambda}\right)$	ϵ_{S-P}^{S+P}	$\frac{y_d^{\rm ex2}}{(16\pi^2)^2}\frac{1}{\Lambda^5}$	ϵ_1
31_b	$L^iL^j\overline{Q}_m\bar{d}^c\overline{Q}_nu^cH^kH^l\epsilon_{ik}\epsilon_{jl}\epsilon^{mn}$	$\frac{y_d y_u}{(16\pi^2)^2}\frac{v^2}{\Lambda}f\left(\frac{v}{\Lambda}\right)$	$\frac{y_d}{(16\pi^2)^2}\frac{v}{\Lambda^3}$	ϵ_{S-P}^{S+P}	$\frac{y_d^{\rm ex2}}{(16\pi^2)^2}\frac{1}{\Lambda^5}$	ϵ_1
32_a	$L^iL^j\overline{Q}_j\bar{u}^c\overline{Q}_k\bar{u}^cH^k\overline{H}_i$	$\frac{y_u^2}{(16\pi^2)^3}\frac{v^2}{\Lambda}$	$\frac{y_u}{16\pi^2}\frac{v}{\Lambda^3}f\left(\frac{v}{\Lambda}\right)$	ϵ_{S-P}^{S+P}	$\frac{1}{\Lambda^5}f\left(\frac{v}{\Lambda}\right)$	ϵ_1
32_b	$L^iL^j\overline{Q}_m\bar{u}^c\overline{Q}_n\bar{u}^cH^k\overline{H}_i\epsilon_{jk}\epsilon^{mn}$	$\frac{y_u^2}{(16\pi^2)^3}\frac{v^2}{\Lambda}$	$\frac{y_u}{16\pi^2}\frac{v}{\Lambda^3}f\left(\frac{v}{\Lambda}\right)$	ϵ_{S-P}^{S+P}	$\frac{y_d^{\rm ex2}}{(16\pi^2)^2}\frac{1}{\Lambda^5}$	ϵ_1
34	$\bar{e}^c\bar{e}^cL^iQ^je^cd^cH^kH^l\epsilon_{ik}\epsilon_{jl}$	$\frac{y_e^{\rm ex}y_d g^2}{(16\pi^2)^4}\frac{v^2}{\Lambda}$	$\frac{g^2 y_{e\vert u\vert (d)}^{\rm ex}}{(16\pi^2)^2}\frac{v}{\Lambda^3}f\left(\frac{v}{\Lambda}\right)$	$\epsilon_{S+P}^{S+P}\vert 2\epsilon_{V\pm A}^{V+A}$	–	–
35	$\bar{e}^c\bar{e}^cL^ie^c\overline{Q}_j\bar{u}^cH^jH^k\epsilon_{ik}$	$\frac{y_e^{\rm ex}y_u g^2}{(16\pi^2)^4}\frac{v^2}{\Lambda}$	$\frac{g^2 y_{e\vert d\vert (u)}^{\rm ex}}{(16\pi^2)^2}\frac{v}{\Lambda^3}f\left(\frac{v}{\Lambda}\right)$	$\epsilon_{S-P}^{S+P}\vert 2\epsilon_{V\pm A}^{V+A}$	–	–
36	$\bar{e}^c\bar{e}^cQ^id^cQ^jd^cH^kH^l\epsilon_{ik}\epsilon_{jl}$	$\frac{y_e^{\rm ex2}y_d^2 g^2}{(16\pi^2)^5}\frac{v^2}{\Lambda}$	$\frac{y_d y_e^{\rm ex}y_{e\vert u\vert (d)}^{\rm ex}}{(16\pi^2)^2}\frac{v}{\Lambda^3}f\left(\frac{v}{\Lambda}\right)$	$\epsilon_{S+P}^{S+P}\vert 2\epsilon_{V\pm A}^{V+A}$	$\frac{1}{\Lambda^5}f\left(\frac{v}{\Lambda}\right)$	ϵ_1
37	$\bar{e}^c\bar{e}^cQ^id^c\overline{Q}_j\bar{u}^cH^jH^k\epsilon_{ik}$	$\frac{y_e^{\rm ex2}y_d y_u g^2}{(16\pi^2)^5}\frac{v^2}{\Lambda}$	$\frac{g^2 y_e^{\rm ex}}{(16\pi^2)^2}\frac{v^3}{\Lambda^5}$	$2\epsilon_{V+A}^{V+A}$	$\frac{1}{\Lambda^5}f\left(\frac{v}{\Lambda}\right)$	ϵ_1
38	$\bar{e}^c\bar{e}^c\overline{Q}_i\bar{u}^c\overline{Q}_j\bar{u}^cH^iH^j$	$\frac{y_e^{\rm ex2}y_u^2 g^2}{(16\pi^2)^5}\frac{v^2}{\Lambda}$	$\frac{y_{e\vert d\vert (u)}^{\rm ex}y_u}{(16\pi^2)^2}\frac{v}{\Lambda^3}f\left(\frac{v}{\Lambda}\right)$	$\epsilon_{S-P}^{S+P}\vert 2\epsilon_{V\pm A}^{V+A}$	$\frac{1}{\Lambda^5}f\left(\frac{v}{\Lambda}\right)$	ϵ_1
40_a	$L^iL^jL^kQ^l\overline{L}_i\overline{Q}_jH^mH^n\epsilon_{km}\epsilon_{ln}$	$\frac{g^2}{(16\pi^2)^3}\frac{v^2}{\Lambda}$	$\frac{g^2 y_{d\vert u\vert u\vert e}^{\rm ex}}{(16\pi^2)^2}\frac{v}{\Lambda^3}f\left(\frac{v}{\Lambda}\right)$	$\epsilon_{S\pm P}^{S+P}\vert 2\epsilon_{V\pm A}^{V+A}$	–	–
43_a	$L^iL^jL^kd^c\overline{L}_l\bar{u}^cH^l\overline{H}_i\epsilon_{jk}$	$\frac{y_d y_u g^2}{(16\pi^2)^4}\frac{v^2}{\Lambda}$	$\frac{g^2 y_{u\vert d\vert e}^{\rm ex}}{(16\pi^2)^2}\frac{v}{\Lambda^3}f\left(\frac{v}{\Lambda}\right)$	$\epsilon_{S\pm P}^{S+P}\vert 2\epsilon_{V+A}^{V+A}$	–	–
44_c	$L^iL^jQ^ke^c\overline{Q}_l\bar{e}^cH^lH^m\epsilon_{ij}\epsilon_{km}$	$\frac{g^4}{(16\pi^2)^4}\frac{v^2}{\Lambda}$	$\frac{y_e}{16\pi^2}\frac{v^3}{\Lambda^5}$	ϵ_{V-A}^{V+A}	–	–
47_a	$L^iL^jQ^kQ^l\overline{Q}_i\overline{Q}_jH^mH^n\epsilon_{km}\epsilon_{ln}$	$\frac{g^2}{(16\pi^2)^3}\frac{v^2}{\Lambda}$	$\frac{g^2 y_{d\vert u\vert (e)}^{\rm ex}}{(16\pi^2)^2}\frac{v}{\Lambda^3}f\left(\frac{v}{\Lambda}\right)$	$\epsilon_{S\pm P}^{S+P}\vert 2\epsilon_{V-A}^{V+A}$	$\frac{v^2}{\Lambda^7}$	$2\tilde{\epsilon}_3$
47_d	$L^iL^jQ^kQ^l\overline{Q}_i\overline{Q}_mH^mH^nH^n\epsilon_{jk}\epsilon_{ln}$	$\frac{g^2}{(16\pi^2)^3}\frac{v^2}{\Lambda}$	$\frac{g^2 y_{d\vert u\vert (e)}^{\rm ex}}{(16\pi^2)^2}\frac{v}{\Lambda^3}f\left(\frac{v}{\Lambda}\right)$	$\epsilon_{S\pm P}^{S+P}\vert 2\epsilon_{V-A}^{V+A}$	$\frac{v^2}{\Lambda^7}$	$2\tilde{\epsilon}_3$
53	$L^iL^jd^cd^c\bar{u}^c\bar{u}^c\overline{H}_i\overline{H}_j$	$\frac{y_d^2y_u^2g^2}{(16\pi^2)^5}\frac{v^2}{\Lambda}$	$\frac{y_d y_u y_{u\vert d\vert e}^{\rm ex}}{(16\pi^2)^2}\frac{v}{\Lambda^3}f\left(\frac{v}{\Lambda}\right)$	$\epsilon_{S\pm P}^{S+P}\vert 2\epsilon_{V+A}^{V+A}$	$\frac{v^2}{\Lambda^7}$	$2\tilde{\epsilon}_3$
54_a	$L^iQ^jQ^kd^c\overline{Q}_i\bar{e}^cH^lH^m\epsilon_{jl}\epsilon_{km}$	$\frac{y_e^{\rm ex}y_d g^2}{(16\pi^2)^4}\frac{v^2}{\Lambda}$	$\frac{g^2 y_{e\vert (d)\vert u}^{\rm ex}}{(16\pi^2)^2}\frac{v}{\Lambda^3}f\left(\frac{v}{\Lambda}\right)$	$\epsilon_{S+P}^{S+P}\vert 2\epsilon_{V\mp A}^{V+A}$	–	–
54_d	$L^iQ^jQ^kd^c\overline{Q}_l\bar{e}^cH^lH^m\epsilon_{ij}\epsilon_{km}$	$\frac{y_e^{\rm ex}y_d g^2}{(16\pi^2)^4}\frac{v^2}{\Lambda}$	$\frac{y_d}{16\pi^2}\frac{v^3}{\Lambda^5}$	ϵ_{V-A}^{V+A}	$\frac{v^2}{\Lambda^7}$	$2\epsilon_5$
55_a	$L^iQ^j\overline{Q}_i\overline{Q}_k\bar{e}^c\bar{u}^cH^kH^l\epsilon_{jl}$	$\frac{y_e^{\rm ex}y_u g^2}{(16\pi^2)^4}\frac{v^2}{\Lambda}$	$\frac{y_u}{16\pi^2}\frac{v^3}{\Lambda^5}$	ϵ_{V-A}^{V+A}	$\frac{v^2}{\Lambda^7}$	$2\epsilon_5$
59	$L^iQ^jd^cd^c\bar{e}^c\bar{u}^cH^k\overline{H}_i\epsilon_{jk}$	$\frac{y_e^{\rm ex}y_d^2y_u}{(16\pi^2)^4}\frac{v^2}{\Lambda}$	$\frac{y_d}{(16\pi^2)^2}\frac{v}{\Lambda^3}$	ϵ_{V+A}^{V+A}	$\frac{1}{\Lambda^5}f\left(\frac{v}{\Lambda}\right)$	$2\epsilon_5$
60	$L^id^c\overline{Q}_j\bar{u}^c\bar{e}^c\bar{u}^cH^j\overline{H}_i$	$\frac{y_e^{\rm ex}y_d y_u^2}{(16\pi^2)^4}\frac{v^2}{\Lambda}$	$\frac{y_u}{(16\pi^2)^2}\frac{v}{\Lambda^3}$	ϵ_{V+A}^{V+A}	$\frac{1}{\Lambda^5}f\left(\frac{v}{\Lambda}\right)$	$2\epsilon_5$

Table 5.3: As Tab. 5.2, but showing selected effective $\Delta L = 2$ SM-invariant operators of dimension 11.

5.2 Relation to the Low-Scale Operators

Now we will take all the above listed SM effective operators and determine how they contribute to $0\nu\beta\beta$ decay, i.e. in other words, how they relate to the low-energy $0\nu\beta\beta$ decay Lagrangian discussed in Chap. 4. At first, we identify operators triggering $0\nu\beta\beta$ decay directly at tree level. Naturally, the Weinberg operator $\mathcal{O}_1$ does so through the effective neutrino mass, cf. Fig. 5.1 (a). As for higher-dimensional operators, the following contribute to $0\nu\beta\beta$ decay at tree level after EW symmetry breaking,

$$\text{Dimension-7} : \mathcal{O}_{3a},\ \mathcal{O}_{3b},\ \mathcal{O}_{4a},\ \mathcal{O}_{8}; \tag{5.6}$$

$$\text{Dimension-9} : \mathcal{O}_{5},\ \mathcal{O}_{6},\ \mathcal{O}_{7},\ \mathcal{O}_{11b},\ \mathcal{O}_{12a},\ \mathcal{O}_{14b},\ \mathcal{O}_{19},\ \mathcal{O}_{20},\ \mathcal{O}_{76}; \tag{5.7}$$

$$\begin{aligned}\text{Dimension-11:}\ &\mathcal{O}_{24a},\ \mathcal{O}_{28a},\ \mathcal{O}_{28c},\ \mathcal{O}_{32a},\ \mathcal{O}_{36},\ \mathcal{O}_{37},\ \mathcal{O}_{47a},\ \mathcal{O}_{47d},\\ &\mathcal{O}_{53},\ \mathcal{O}_{54a},\ \mathcal{O}_{54d},\ \mathcal{O}_{55a},\ \mathcal{O}_{59},\ \mathcal{O}_{60}.\end{aligned} \tag{5.8}$$

These operators of dimension 7, 9 and 11 trigger $0\nu\beta\beta$ decay, respectively, via diagrams (b), (c) and (d) in Fig. 5.1. The only exceptions are the dimension-9 operators $\mathcal{O}_5$, $\mathcal{O}_6$ and $\mathcal{O}_7$ contributing at tree level to the long-range mechanism (otherwise typically contributed by dimension-7 operators) after all three Higgs fields, which they contain, acquire their VEVs. Since we want to estimate the dominant contribution of a single D-dimensional operator to $0\nu\beta\beta$ decay, we derive its radiative corrections to all other LNV operators of the same and lower dimension. Clearly, this leads to numerous possible contributions, which we handle utilizing an algorithm outlined below.

5.2.1 $SU(2)_L$ Decomposition and Effective $0\nu\beta\beta$ Couplings

When constructing all possible $0\nu\beta\beta$ decay contributions of a given $\Delta L = 2$ SM effective operator we first decompose it into its $SU(2)_L$ components, and subsequently, we apply the same procedure to each of them. For an operator with d number of $SU(2)_L$ doublets there are $2^{d/2}$ components. Hence, for instance $\mathcal{O}_{3a}$ has 4 different $SU(2)_L$ components,

$$\begin{aligned}\mathcal{O}_{3a} &= L^i L^j Q^k d^c H^l \epsilon_{ij}\epsilon_{kl}\\ &= \nu_L e_L u_L h^0 d^c - e_L \nu_L u_L h^0 d^c - \nu_L e_L d_L h^+ d^c + e_L \nu_L d_L h^+ d^c.\end{aligned} \tag{5.9}$$

The earlier identified operators triggering $0\nu\beta\beta$ decay directly at tree level must, after the EW symmetry breaking, give straightforwardly one of the terms of the low-energy $0\nu\beta\beta$ decay Lagrangian discussed in previous chapter. Consequently, e.g. the $SU(2)_L$ components on the right-hand side of Eq. (5.9) including h^0 give (up to an overall factor) one of the terms in Eq. (4.4) after the Higgs acquires its VEV. All the other $\Delta L = 2$ SM effective operators contribute to $0\nu\beta\beta$ decay at certain loop level, as radiative corrections to the tree level contributing operators. Therefore, the appropriate loop contractions relating different $\Delta L = 2$ SM effective operators must be constructed, estimated and compared. To do so we employ the algorithmic approach described below. In this way a dominant contribution triggered by each of the $\Delta L = 2$ SM effective operators (unbroken phase) can be related to a corresponding term of the low-energy $0\nu\beta\beta$ Lagrangian (broken phase). This results in relations among the new physics scales Λ_i of the SM effective operators and the effective couplings $\epsilon^{\bullet}_{\bullet}$ appearing in Lagrangians (4.4) and (4.8). As we have discussed in great detail in Chap. 4, bounds on these effective couplings can be determined using the current experimental limits on the $0\nu\beta\beta$ decay half-life. Hence, in principle, limits on scales Λ_i can be also set. We start here with a derivation of the relations between unbroken-phase and broken-phase contributions.

6D Long-Range Contributions

In the broken phase there are four distinct 6-dimensional operators, with the desired particle content u, d, e and ν, giving long-range $0\nu\beta\beta$ decay contributions. In the above list of $\Delta L = 2$ SM effective operators we can identify seven of them, which after the $SU(2)_L$ decomposition and EW symmetry breaking reproduce one of these four low-energy long-range terms directly at tree level. The obtained correspondence can be summarized as

$$\mathcal{O}_{3a}, \mathcal{O}_{3b}, \mathcal{O}_5 \to \bar{e_L}\bar{\nu_L}\bar{u_L}\bar{d^c}, \tag{5.10}$$

$$\mathcal{O}_{4a}, \mathcal{O}_6 \to \bar{e_L}\bar{\nu_L}u^c d_L, \tag{5.11}$$

$$\mathcal{O}_7 \to \bar{u_L}\bar{\nu_L}e^c d_L, \tag{5.12}$$

$$\mathcal{O}_8 \to \bar{d^c}\bar{\nu_L}e^c u^c. \tag{5.13}$$

While operators $3a$, $3b$, $4a$ and 8 are 7-dimensional and induce $0\nu\beta\beta$ decay contributions containing a single power of the EW VEV v, operators 5, 6 and 7, on the other hand, appear at dimension 9 and contribute with the third pow-

er of v. Therefore, the 9-dimensional operators become relevant only when the respective contributions are comparable with the leading-order contribution generated by a competing operator of dimension 7.[1] Contributions proportional to v^3 can be also induced by the compound operators of dimension-9 formed by products of 7-dimensional operators with the singlet $H\bar{H}$, as shown in Tab. 5.2. If a given operator of dimension 7 contributes at second or higher loop level, even v^5-dependent contributions produced by a 9-dimensional operator multiplied by $H\bar{H}$ may become relevant. For instance, let us consider that the leading contributions generated by operators $3a$ and $3b$ are suppressed by two loops. Then the resulting general contribution to the 6-dimensional $0\nu\beta\beta$ decay operator in Eq. (5.10) can be (before EW symmetry breaking) written as follows

$$\begin{aligned}\mathcal{L}_{7+9+11} = &\frac{1}{(16\pi^2)^2}\frac{\mathcal{O}_{3a}}{\Lambda^3} + \frac{1}{(16\pi^2)^2}\frac{\mathcal{O}_{3b}}{\Lambda^3} + \frac{1}{16\pi^2}\frac{\mathcal{O}_5}{\Lambda^5} \\ &+ \frac{1}{16\pi^2}\frac{\mathcal{O}_{3a}(H\bar{H})}{\Lambda^5} + \frac{1}{16\pi^2}\frac{\mathcal{O}_{3b}(H\bar{H})}{\Lambda^5} + \frac{\mathcal{O}_5(H\bar{H})}{\Lambda^7}. \end{aligned} \tag{5.14}$$

As a next step we relate the above 7 different $\Delta L = 2$ SM effective operators triggering $0\nu\beta\beta$ decay at tree level to the low-energy $0\nu\beta\beta$ decay Lagrangian (4.4). Taking the four operators of dimension 6 from the right-hand sides of Eqs. (5.10 - 5.13) and rewriting them using four-spinor notation we have

$$\bar{e_L}\bar{\nu_L}\bar{u_L}\bar{d^c} \leftrightarrow \overline{e}\,(1+\gamma_5)\,\nu\;\overline{u}\,(1+\gamma_5)\,d, \tag{5.15}$$

$$\bar{e_L}\bar{\nu_L}u^c d_L \leftrightarrow \overline{e}\,(1+\gamma_5)\,\nu\;\overline{u}\,(1-\gamma_5)\,d, \tag{5.16}$$

$$\bar{u_L}\bar{\nu_L}e^c d_L \leftrightarrow \overline{u}\,(1+\gamma_5)\,\nu\;\overline{e}\,(1-\gamma_5)\,d, \tag{5.17}$$

$$\bar{d^c}\bar{\nu_L}e^c u^c \leftrightarrow \overline{d}\,(1+\gamma_5)\,\nu\;\overline{e}\,(1-\gamma_5)\,u. \tag{5.18}$$

Employing appropriate Fierz transformations we can rewrite the right-hand sides of Eqs. (5.17) and (5.18) in the conventional field ordering prescribed by Eq. (4.4); hence, we get

$$\overline{e}\,(1-\gamma_5)\,d\;\overline{u}\,(1+\gamma_5)\,\nu = \frac{1}{2}\overline{e}\gamma^\mu\,(1+\gamma_5)\,\nu\;\overline{u}\gamma_\mu\,(1-\gamma_5)\,d, \tag{5.19}$$

$$\overline{e}\,(1-\gamma_5)\,u\;\overline{d}\,(1+\gamma_5)\,\nu = \frac{1}{2}\overline{e}\gamma^\mu\,(1+\gamma_5)\,\nu\;\overline{u}\gamma_\mu\,(1+\gamma_5)\,d. \tag{5.20}$$

[1] However, there is not always a desired operator at dimension 7. Obviously, there is no 7-dimensional SM effective operator generating the low-energy contribution given in Eq. (5.12). Hence, this type of long-range contribution will be always proportional to v^3, as can be also inferred from considerations of possible UV completions of this operator.

From these equalities the relations between the scales of the SM effective operators on the left-hand sides of Eqs. (5.10 - 5.13) and the effective couplings ϵ_α^β can be obtained as

$$\mathcal{O}_{3a} : \frac{\lambda_{BSM}^3 v}{\Lambda_{3a}^3} = \frac{G_F \epsilon_{T_R}^{T_R}}{\sqrt{2}}, \tag{5.21}$$

$$\left.\begin{array}{l} \mathcal{O}_{3b} : \dfrac{\lambda_{BSM}^3 v}{\Lambda_{3b}^3} \\ \mathcal{O}_5 : \dfrac{\lambda_{BSM}^4 v^3}{\Lambda_5^5} \end{array}\right\} = \frac{G_F \epsilon_{S+P}^{S+P}}{\sqrt{2}}, \qquad \left.\begin{array}{l} \mathcal{O}_{4a} : \dfrac{\lambda_{BSM}^3 v}{\Lambda_{4a}^3} \\ \mathcal{O}_6 : \dfrac{\lambda_{BSM}^4 v^3}{\Lambda_6^5} \end{array}\right\} = \frac{G_F \epsilon_{S-P}^{S+P}}{\sqrt{2}}, \tag{5.22}$$

$$\mathcal{O}_7 : \frac{\lambda_{BSM}^4 v^3}{\Lambda_7^5} = 2\frac{G_F \epsilon_{V-A}^{V+A}}{\sqrt{2}}, \qquad \mathcal{O}_8 : \frac{\lambda_{BSM}^3 v}{\Lambda_8^3} = 2\frac{G_F \epsilon_{V+A}^{V+A}}{\sqrt{2}}, \tag{5.23}$$

where the contributions of the SM effective operators appearing on the left-hand side have always the form v^{N_H}/Λ^{D-4} with N_H being the number of Higgs fields present in a given operator and Λ denoting the typical energy scale of a considered operator of dimension D. To illustrate the scaling generated by a typical tree level UV completion of each operator we include the powers of a generic new physics coupling λ_{BSM}. We take the third power of this coupling for the 7-dimensional operators, as the typical UV diagram looks like those in Fig. 6.13, and thus incorporates three BSM vertices. For the 9-dimensional operators including three Higgses one additional BSM coupling is assumed. In all the following calculations we simply set $\lambda_{BSM} = 1$.

9D Short-Range Contributions

An analogous procedure must be followed in case of the $\Delta L = 2$ SM effective operators generating the short-range $0\nu\beta\beta$ decay contributions at tree level. The situation is simple for the term in Eq. (4.8) proportional to $\epsilon_1^\bullet$. Since it consists only of scalar Lorentz bilinears by definition, it can be easily identified with the appropriate SM effective operators. However, the terms of the short-range Lagrangian proportional to the other four epsilons involve γ-matrices, and thus must be Fierz-transformed to acquire a scalar form. The Fierz transformation applied to some of the long-range contributions can be used also in case of the short-range terms with couplings $\epsilon_3^\bullet$ and $\epsilon_5^\bullet$ containing just vector bilinears. To transform the second term of Eq. (4.8) with $\epsilon_2^\bullet$ the following identity can be

employed

$$\begin{aligned}&\left[\overline{u}_a \tfrac{i}{2}[\gamma^\mu,\gamma^\nu](1\pm\gamma_5)d^a\right]\left[\overline{u}_b \tfrac{i}{2}[\gamma_\mu,\gamma_\nu](1\pm\gamma_5)d^b\right]\\&= -2\left[\overline{u}_a(1\pm\gamma_5)d^b\right]\left[\overline{d}^a(1\pm\gamma_5)u_b\right] - \left[\overline{u}_a(1\pm\gamma_5)d^a\right]\left[\overline{u}_b(1\pm\gamma_5)d^b\right].\end{aligned} \tag{5.24}$$

Since the two terms on the right-hand side have different $SU(3)_C$ structures (represented by indices a, b), they cannot be combined into a single one and both of them must be considered in order to excite the effective coupling $\epsilon_2^\bullet$. This kind of contributions will not be discussed in the following, as we always assume just a single $\Delta L = 2$ effective operator to be present at a time. Similarly, considering a specific choice of chiralities in the fourth term of Eq. (4.8) (the one proportional to $\epsilon_4^\bullet$), it can be Fierz-transformed as

$$\begin{aligned}&\overline{u}_a\gamma_\mu(1+\gamma_5)d^a\left[\overline{u}_b\tfrac{i}{2}[\gamma^\mu,\gamma^\nu](1-\gamma_5)d^b\right]\overline{e}\gamma_\nu(1+\gamma_5)e^c\\&= -2i\overline{u}_a(1-\gamma_5)d^b\left[\overline{u}_b(1-\gamma_5)e^c\right]\overline{e}(1+\gamma_5)d^a\\&\quad - i\overline{u}_a(1-\gamma_5)e^c\left[\overline{u}_b(1-\gamma_5)d^b\right]\overline{e}(1+\gamma_5)d^a,\end{aligned} \tag{5.25}$$

and the conclusion is the same as in case of $\epsilon_2^\bullet$.

As in the long-range case, we can now relate the contributions of the relevant SM effective operators to the effective couplings $\epsilon_1^\bullet$, $\epsilon_3^\bullet$ or $\epsilon_5^\bullet$. The operators that excite $\epsilon_2^\bullet$ or $\epsilon_4^\bullet$ contribute also to the terms of Eq. (4.8) with effective couplings $\epsilon_1^\bullet$ and $\epsilon_5^\bullet$, respectively. Hence, due to the fact there are no operators contributing uniquely to $\epsilon_2^\bullet$ and $\epsilon_4^\bullet$, these can be indeed omitted. As a result, the equations connecting the effective scales to the respective operators listed in Eq. (5.6) with the three effective couplings $\epsilon_1^\bullet$, $\epsilon_3^{LL,RR}$ and $\epsilon_5^\bullet$ in Tab. 4.2 read

$$\left.\begin{aligned}\mathcal{O}_{11b},\mathcal{O}_{12a},\mathcal{O}_{14b} &: \frac{\lambda_{BSM}^4}{\Lambda_i^5}\\ \mathcal{O}_{24a},\mathcal{O}_{28a},\mathcal{O}_{28c},\mathcal{O}_{32a},\mathcal{O}_{36},\mathcal{O}_{37},\mathcal{O}_{38} &: \frac{\lambda_{BSM}^6 v^2}{\Lambda_i^7}\end{aligned}\right\} = \frac{G_F^2\epsilon_1^\bullet}{2m_p}, \tag{5.26}$$

$$\left.\begin{aligned}\mathcal{O}_{47a},\mathcal{O}_{47d},\mathcal{O}_{53} &: \frac{\lambda_{BSM}^6 v^2}{\Lambda_i^7}\\ \mathcal{O}_{76} &: \frac{\lambda_{BSM}^4}{\Lambda_i^5}\end{aligned}\right\} = 2\frac{G_F^2\epsilon_3^{LL,RR}}{2m_p}, \tag{5.27}$$

$$\left.\begin{aligned}\mathcal{O}_{19},\mathcal{O}_{20} &: \frac{\lambda_{BSM}^4}{\Lambda_i^5}\\ \mathcal{O}_{54a},\mathcal{O}_{54d},\mathcal{O}_{55a},\mathcal{O}_{59},\mathcal{O}_{60} &: \frac{\lambda_{BSM}^6 v^2}{\Lambda_i^7}\end{aligned}\right\} = 2\frac{G_F^2\epsilon_5^\bullet}{2m_p}. \tag{5.28}$$

Again, for illustration of the scaling generated by a typical tree level UV completion of each operator we include the powers of a generic new physics coupling λ_{BSM}. Adding an extra particle to the typical UV completion of a 7-dimensional operator depicted in Fig. 6.13 one clearly has to add also one additional vertex; therefore, the operators of dimension 9 scale with the fourth power of λ_{BSM}. The 11-dimensional operators have two extra Higgses compared to the dimension-9 operators, and thus two additional BSM couplings are necessary, resulting in the sixth power of λ_{BSM}. In all the following calculations the value $\lambda_{BSM} = 1$ is set.

5.2.2 Estimation of Wilson Coefficients

In general, our aim is to estimate for each of the above listed SM effective operators the value of same- and lower-dimensional Wilson coefficients induced by radiative effects. We achieve so by constructing all possible loop diagrams leading to the corresponding operators. Since each such radiative correction would be absorbed by the respective Wilson coefficient in the matching procedure, it provides an estimate of the size of the given contribution. Here, we should stress that this approach implicitly imposes certain requirements on the underlying UV theory. Since we estimate the Wilson coefficients by closing loops of heavy particles, it must be assumed that the resulting contributions are determined by the heavy mass of new physics, i.e. that the underlying theory is 'natural'. A straightforward 'counterexample' to this approach is e.g. the supersymmetric treatment of the SM hierarchy problem, i.e. a UV model featuring cancellations between different loop contributions. In such case our estimation would not work. Nonetheless, there are several examples in history of particle physics, for which this guiding principle proved to be successful - for instance, in case of hadronic resonances or the charm quark [242]. Therefore, bearing in mind its limitations the use of this approach seems to be well justified and the Wilson coefficients can be estimated as follows:

1. We begin with specifying both the $SU(2)_L$ component of the SM effective operator (A) that we want to study and the $SU(2)_L$ component of the operator (B) it should be reduced to. We will apply our algorithm to each $SU(2)_L$ component of every SM effective operator (A) and reduce it to all operators (B) of lower or same dimension that contribute to $0\nu\beta\beta$ decay at tree level.

f_L	$\bar{f}_L$	Z	$g/(16\pi^2)$
f_L	$\bar{f}'_L$	W^-	$g/(16\pi^2)$
$\bar{f}^c$	$\bar{f}'_L$	H^-	$y_f/(16\pi^2)$
$\bar{f}^c$	$\bar{f}_L$	h^0	$y_f/(16\pi^2)$
Z	$\bar{f}_L$	$\bar{f}_L$	$g/(16\pi^2)$
W^-	$\bar{f}_L$	$\bar{f}'_L$	$g/(16\pi^2)$
H^-	f^c	$\bar{f}'_L$	$y_f/(16\pi^2)$
h^0	$\bar{f}_L$	f^c	$y_f/(16\pi^2)$
$\langle h \rangle$	$\bar{f}_L$	f^c	$vy_f/(16\pi^2)$
$h^0\|W^-\|H^-$	$\bar{h}^0\|W^+\|H^+$	$-$	$1/(16\pi^2)$

Table 5.4: Effective Feynman rules - contraction of the fields given in the first two columns via a loop lead to radiation of the field shown in the third column. On the right-hand side the coefficient indicating the corresponding contribution is displayed. Here, f_L and f^c are left-handed Weyl spinors with f denoting a fermion according to Tab. 2.1 and f^c being the charge-conjugate of the $SU(2)_L$ singlet right-handed charged fermions.

2. When closing the loops to match the lower-dimensional operators (B), we make use of any SM Feynman rule that keeps or reduces the dimension of the initial operator. The employed Feynman rules leading to one-loop and two-loop contractions are explicitly listed in Tab. 5.4 and Tab. 5.5, respectively. All of these rules need to be considered in order to obtain all possible $0\nu\beta\beta$ decay contributions (see Fig. 5.1) and in what follows they will be discussed in detail.

3. We consider that every closed loop gives a factor $1/(16\pi^2)$ and all the loops are regulated via a momentum cut-off Λ - each integral over a fermionic propagator introduces one power. Let us emphasize that this approach would fail if we were to estimate the loop corrections within a pure EFT approach. In such case dimensional regularization involving only SM masses should be used. As stressed earlier, in this work we approximate the size by the assumption of a 'natural' UV theory rather than using a pure EFT. Consequently, we can introduce heavy masses (or a cut-off scale Λ) that would be integrated out in a pure EFT approach, where the Appelquist-Carazzone decoupling theorem [243] applies.

f_L	f^c	h^0	$y_f/(16\pi^2)^2$
f^c	f'_L	H^+	$y_f/(16\pi^2)^2$
f_L	$\bar{f}'_L$	W^+	$g/(16\pi^2)^2$
f_L	$\bar{f}_L$	Z	$g/(16\pi^2)^2$
h	Z $\|W^+$	Z $\|W^-$	$vg^2/(16\pi^2)^2$
Z	$H^+\|W^+$	$W^-\|H^-$	$2vg^2/(16\pi^2)^2$

Table 5.5: Effective Feynman rules - contraction of the fields in the three columns on the left gives a double loop. On the right-hand side the coefficient indicating the corresponding contribution is displayed. Here, f_L and f^c are left-handed Weyl spinors with f denoting a fermion according to Tab. 2.1 and f^c being the charge-conjugate of the $SU(2)_L$ singlet right-handed charged fermions.

4. Three examples of the application of the rules given in Tab. 5.4 are diagrammatically depicted in Fig. 5.2. All of them capture a reduction of a higher-dimensional operator to the neutrino mass operator (the Weinberg operator after the EW symmetry breaking). A contribution induced by two contractions from the 9-dimensional operator $\mathcal{O}_{12a} = L^i L^j \bar{Q}_i \bar{u^c} \bar{Q}_j \bar{u^c}$ is shown on the left. The diagrams in the middle and on the right then represent the contributions from the 11-dimensional operators $\mathcal{O}_{24a} = L^i L^j \bar{Q}_i \bar{u^c} \bar{Q}_j \bar{u^c}$ and $\mathcal{O}_{27a} = L^i L^j Q^k d^c \bar{Q}_i \bar{d^c} H^l H^m \epsilon_{jl} \epsilon_{km}$, respectively. When constructing the left and centre diagrams the algorithm first merges the fermions into loops and the radiated neutral Higgs bosons are in the following iteration assigned their VEVs. The charged Higgs bosons in the middle diagram are simply connected to form a loop. In case of the diagram on the right, two pairs

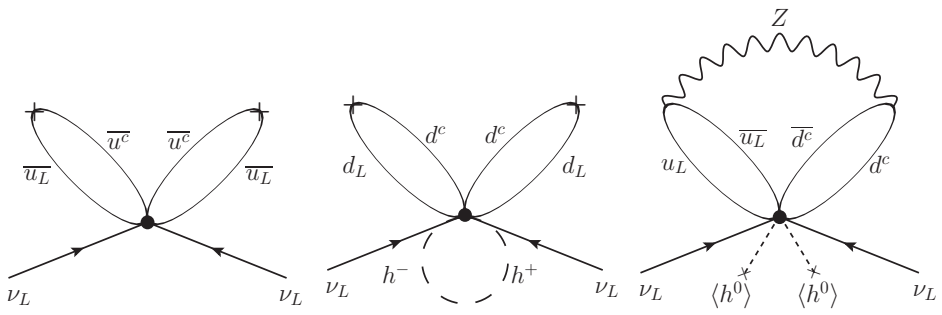

Figure 5.2: Diagrams illustrating the reduction of $\mathcal{O}_{12a}$ (left), $\mathcal{O}_{24a}$ (centre) and $\mathcal{O}_{27a}$ (right) to the neutrino mass.

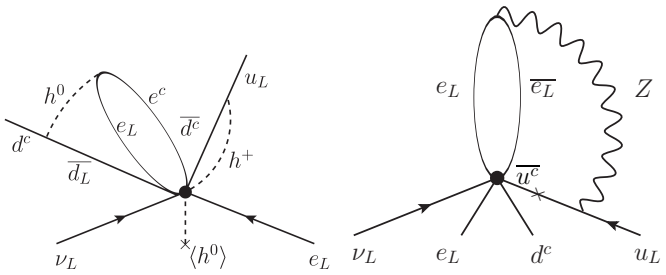

Figure 5.3: Depicted here is the reduction of operators $\mathcal{O}_{23}$ (left) and $\mathcal{O}_{15}$ (right) to a long-range $0\nu\beta\beta$ decay contribution.

of fermions are merged into neutral vector bosons, which are subsequently joined to create the third loop. These diagrams lead to the following neutrino mass contributions

$$m_\nu^{12a} = \frac{y_u^2 v^2}{(16\pi^2)^2 \Lambda}, \quad m_\nu^{24a} = \frac{y_d^2 v^2}{(16\pi^2)^3 \Lambda}, \quad m_\nu^{27a} = \frac{g^2 v^2}{(16\pi^2)^3 \Lambda}. \tag{5.29}$$

Generally, the algorithm in *every* iteration tests *all* n-rules (with n indicating the number of legs on which the given rule acts) for their applicability to *all* possible combinations of n legs of the diagram within total m legs.

5. There are operators that can be reduced to a compound operator consisting of a certain tree level contributing operator and an $\bar{H}H$ pair, as we have pointed out earlier. This decoupled Higgs boson and its hermitian conjugate can either acquire their VEVs giving a factor of $\frac{v^2}{\Lambda^2}$, or can be contracted to each other, forming a loop and producing a factor $\frac{1}{16\pi^2}$. Hence, the corresponding $0\nu\beta\beta$ decay contribution is proportional to $f\left(\frac{v}{\Lambda}\right) \equiv \left(\frac{1}{16\pi^2} + \frac{v^2}{\Lambda^2}\right)$. In some cases even more different ways how to reduce a given SM effective operator to the required low-energy $0\nu\beta\beta$ decay operator exist and one may need to consider sums of various contributions like in the example in Eq. (5.14). Nevertheless, these multiplicities are neglected in the herein presented results, as we concentrate only on a description and comparison of qualitatively distinct $0\nu\beta\beta$ decay contributions.

6. The next set of Feynman rules incorporated in our code is depicted in Fig. 5.3. There we show a reduction of the 9-dimensional operator $\mathcal{O}_{23} = L^i L^j L^k e^c \bar{Q}_k \bar{d}^c H^l H^m \epsilon_{il} \epsilon_{jm}$ (on the left) and the 11-dimensional operator $\mathcal{O}_{15} = L^i L^j L^k d^c \bar{L}_i \bar{u}^c \epsilon_{jk}$ (on the right) to a long-range $0\nu\beta\beta$ decay contribution. In the left diagram the rule merging one fermion with a Higgs boson is used in order to generate the fermion needed. Similarly, in the

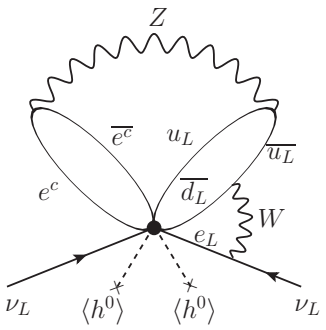

Figure 5.4: Diagram showing the reduction of $\mathcal{O}_{44c}$ to the neutrino mass.

right diagram we have to merge a fermion with a vector boson to create the correct quark. However, before doing so a Higgs VEV must be used to flip the helicity of the fermion. This rule is included explicitly among other Feynman rules, but to ensure convergence of our algorithm, up to three additional Higgs VEV insertions are allowed per diagram. The resulting contributions thus read

$$\frac{G_F \epsilon_7^{15}}{\sqrt{2}} = \frac{y_u^{\text{ex}} g^2 v}{(16\pi^2)^2 \Lambda^3}, \quad \frac{G_F \epsilon_7^{23}}{\sqrt{2}} = \frac{y_e (y_d^{\text{ex}})^2 v^2}{(16\pi^2)^3 \Lambda^3}, \tag{5.30}$$

with $\epsilon_7^{15} = \epsilon_{S+P}^{S+P}$ and $\epsilon_7^{23} = \epsilon_{S+P}^{S-P}$.

7. Note that in the above contributions corresponding to Fig. 5.3 we distinguish between the internal (default notation) and external (denoted by $y_\bullet^{\text{ex}}$) Yukawa couplings. We do so because the flavour of the external ones is fixed to the first generation in order to get a $0\nu\beta\beta$ decay contribution, while for the internal Yukawa couplings one can in principle sum over all flavours. This is an important feature, which can significantly influence the results of our calculation, as we will discuss later.

8. The following three features that must be taken care of is demonstrated in Fig. 5.4 depicting the reduction of the 11-dimensional operator $\mathcal{O}_{44c} = L^i L^j Q^k e^c \bar{Q}_l \bar{e^c} H^l H^m \epsilon_{ij} \epsilon_{km}$ to the neutrino mass. Because of the $SU(2)_L$ structure $L^i L^j \epsilon_{ij}$, one first has to convert the electron into a neutrino, which requires the introduction of 't-channel' rules. In the present case we employ an exchange of a W boson between two fermion legs resulting in an additional loop. Since this rule does not reduce the dimension of the operator, it must be treated separately, otherwise (if treated naively in the same way as all the other rules) it would lead to an infinite number of

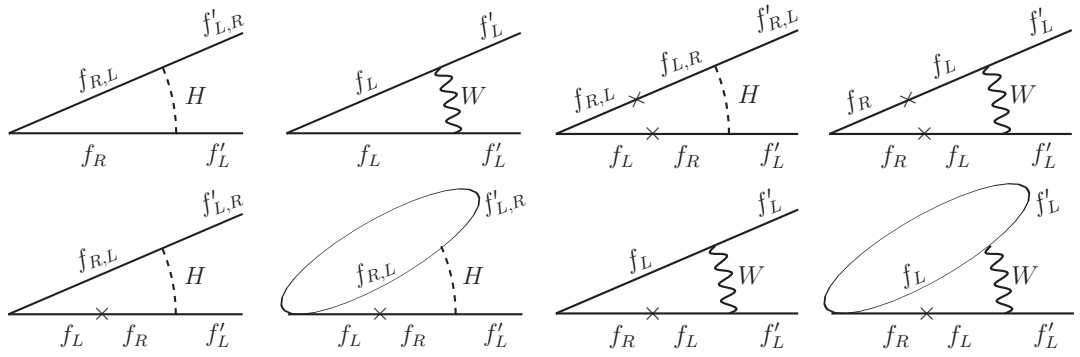

Figure 5.5: Diagrams depicting the additional 't-channel' rules that have to be considered separately so that a converging algorithm is obtained.

iterations. Diagrams corresponding to this and other considered 't-channel' rules are displayed in Fig. 5.5. Specific cases requiring introduction of very rare rules we treat manually.

9. The next feature that the automate algorithm must take into account is the fact that only contributions containing loops with an even number of fermions are valid. If an odd number of fermions appears in a loop then the diagram will be proportional to the external neutrino momentum and/or will vanish. For this reason the number of fermions in every loop contribution is tracked in each iteration step. If loops with an odd number of fermions appear in the final diagram, an extra neutral gauge boson exchange must be added. This has to be taken into account also in the previous step. Each diagram in the upper row of Fig. 5.5 contains always an even number of fermions generated in the t-channel, whereas the number is odd for the diagrams in the lower row. In the latter case one of the outgoing fermions can be therefore contracted with another fermion leg of the initial operator (without radiation of any other particle).

10. In some cases one ends up with three free legs, which have to be merged together to close a multi-loop. Consequently, the corresponding Feynman rules treating these cases are necessary in the algorithm. An example illustrating this feature can be found in Fig. 5.4, where after closing two fermion legs by radiating a Z boson and applying the t-channel rule one is left with three fields (two fermions and the neutral gauge boson) that must be connected into loops. In Tab. 5.5 we list the corresponding three-field rules included in our algorithm and the resulting contribution obtained for

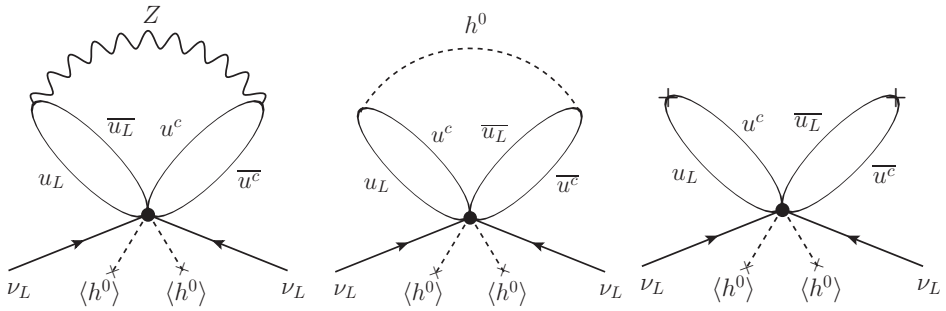

Figure 5.6: Three different neutrino-mass contributions of operator $\mathcal{O}_{29}$ are shown. On the left, we depict the contribution involving gauge couplings that is dominant, when first-generation internal Yukawa couplings are considered. The center and right diagrams represent the contributions dominant for third-generation internal Yukawa couplings.

the example $\mathcal{O}_{44c}$ is

$$m_\nu^{44c} = \frac{g^4 v^2}{(16\pi^2)^4 \Lambda}. \tag{5.31}$$

11. To summarize, we apply the algorithm described in the above paragraphs to every $SU(2)_L$-decomposed $\Delta L = 2$ SM effective operator reducing it via all possible loop contractions to all possible lower-dimensional or equal-dimensional operators contributing to $0\nu\beta\beta$ decay directly at tree level. The last step that is left is the identification of the most dominant $0\nu\beta\beta$ decay contribution generated by a given operator; this is described below.

When comparing our results for contributions to the standard mass mechanism with those derived in Ref. [214], several discrepancies can be found. For instance, in case of operator $\mathcal{O}_{29a}$, the neutrino mass in Tab. 5.3 recovered by our algorithm reads

$$m_\nu^{29a,1st} = \frac{g^2}{(16\pi^2)^3} \frac{v^2}{\Lambda}, \tag{5.32}$$

while Ref. [214] gives

$$m_\nu^{29a,3rd} = \frac{y_u^2}{(16\pi^2)^2} \frac{v^2}{\Lambda} f\left(\frac{v}{\Lambda}\right). \tag{5.33}$$

The origin of this mismatch lies in the way the dominant contribution is determined. The contribution in Eq. (5.32) is the dominant one only when first-generation internal Yukawa couplings are considered, cf. Fig. 5.6. On the other

y_e	y_τ	y_d	y_b	y_u	y_t	g
2.1×10^{-6}	0.01	2.0×10^{-5}	2.4×10^{-2}	9.4×10^{-6}	0.99	0.46

Table 5.6: A summary of the values of SM couplings used in the numerical evaluation of the contributions to $0\nu\beta\beta$ decay.

hand, for internal Yukawa couplings of the third generation, the contribution in Eq. (5.33) becomes dominant, cf. Fig. 5.6 (center and right). Since in our approach we store all the contributions and compare all of them in each case, the conclusion we arrive at depends on the considered generation of the internal Yukawa couplings. The same discussion applies to the mass contributions of operators $\mathcal{O}_{74a}$, $\mathcal{O}_{74b}$ and $\mathcal{O}_{75}$.

5.2.3 Determination of the Operator Scale

After gathering all the possible $0\nu\beta\beta$ contributions triggered by a given operator, we can compare them using the numerical values for the couplings listed in Tab. 5.6 and identify the dominant one. When doing so, we consider all fermions to be of first generation. The energy scale Λ characterizing each operator is purely for the purpose of comparison set to the value $\Lambda = 2186$ GeV derived from the equality $\frac{1}{16\pi^2} = \frac{v^2}{\Lambda^2}$. The reason we pick this particular value is that many operators can be reduced to a compound operator involving an $H\bar{H}$ pair, which can be contracted either to the vacuum, or into a loop. Therefore, it induces both a contribution with the factor $\frac{v^2}{\Lambda^2}$ and a contribution with the factor $\frac{1}{16\pi^2}$. Since in such cases we always want to retain both these contributions, it is convenient to assume the value of Λ ensuring their equality.

For every $\Delta L = 2$ SM effective operator we find its dominant contributions to the standard mass mechanism, long-range mechanism and short-range mechanism of $0\nu\beta\beta$ decay. All the results are listed in Tabs. 5.1, 5.2 and 5.3. We show there also the corresponding effective couplings $\epsilon^{\bullet}_{\bullet}$ excited by a particular $0\nu\beta\beta$ decay contribution. Always, a specific convenient scalar Lorentz structure (i.e. consisting only of scalar bilinears) of a given operator is assumed in order to relate it to the low-energy $0\nu\beta\beta$ decay operators, and thus to the effective couplings $\epsilon^{\bullet}_{\bullet}$. Taking into account other Lorentz structures of the initial operator could lead to excitation of other $\epsilon^{\bullet}_{\bullet}$ couplings.

In what follows we will for simplicity consider only the dominant contributions

of a given operator as listed in Tabs. 5.1, 5.2 and 5.3, i.e. we will not sum over all possible contributions. Moreover, as previously mentioned, we do not account for the multiplicity of particular contributions either (although different reductions of a specific operator can lead to the same tree level contributing $0\nu\beta\beta$ decay operator).

Let us at this point comment a bit on Tabs. 5.1, 5.2 and 5.3. When specifying the $0\nu\beta\beta$ decay contributions we employ the following short-hand notation $f\left(\frac{v}{\Lambda}\right) \equiv \left(\frac{1}{16\pi^2} + \frac{v^2}{\Lambda^2}\right)$. Some operators allow for more than a single independent Lorentz or $SU(3)_C$ contraction, but these we do not specify. If a dash is shown instead of one of the contributions, then the corresponding reduction of the operator cannot be achieved in our approach. What we call 's-channel' rules would have to be included to obtain these contributions, as will be further discussed at the end of the following chapter. In a number of cases the operators induce several qualitatively different (although quantitatively fairly similar) long-range contributions differing only by a flavour of one Yukawa coupling. Hence, we show the possible flavours separated by vertical lines in the superscript of the given Yukawa coupling. The $\epsilon^{\bullet}_{\bullet}$ couplings excited by these multiple contributions are presented in the same ordering as the flavour labels of the Yukawa coupling. On top of that, for some of these operators one of the Yukawa flavour labels is written in brackets, which denotes that the corresponding contribution includes only the factor $\frac{v^2}{\Lambda^2}$ and not the loop factor $\frac{1}{16\pi^2}$ in $f\left(\frac{v}{\Lambda}\right)$. A good example clarifying the used notation is the operator 34 with the long-range contributions $\frac{y^{\rm ex}_{e|u|(d)}}{(16\pi^2)^2 g^2}\frac{v}{\Lambda^3} f\left(\frac{v}{\Lambda}\right)$ and the corresponding excited couplings $\epsilon^{S+P}_{S+P}|2\epsilon^{V+A}_{V\pm A}$. Here, we in fact deal with 3 individual contributions $\frac{y^{\rm ex}_{e}}{(16\pi^2)^2 g^2}\frac{v}{\Lambda^3} f\left(\frac{v}{\Lambda}\right)$, $\frac{y^{\rm ex}_{u}}{(16\pi^2)^2 g^2}\frac{v}{\Lambda^3} f\left(\frac{v}{\Lambda}\right)$ and $\frac{y^{\rm ex}_{d}}{(16\pi^2)^2 g^2}\frac{v^3}{\Lambda^5}$ exciting the couplings ϵ^{S+P}_{S+P}, ϵ^{V+A}_{V+A} and ϵ^{V+A}_{V-A}, respectively.

In the following calculations, only a single dominant contribution of a given operator will be always considered. Assuming a hypothetical observation of $0\nu\beta\beta$ decay with a value of the half-life $T^{\rm Xe}_{1/2} = 10^{27}$ y, the operator scale Λ can be easily determined and further used as a basis for calculation of the lepton number asymmetry washout in the early Universe. In practice, we proceed as follows: after collecting all contributions of a given operator we fix the couplings according to Tab. 5.6 (choosing either first, or third generation for the internal Yukawas - see our later discussion) and express the inverse $0\nu\beta\beta$ decay half-life in dependence on the operator scale Λ, which we define as the maximum among all contributions. This is because the inverse half-life is proportional to Λ^{4-D}, and thus the dominant contribution corresponds to biggest Λ (for a lower operator scale the

dominant contribution would give a faster decay). Within the described approach any enhancement given by other contributions of similar size is neglected, which, however, will not affect the obtained results significantly. Besides that, this approximation also disregards any potential interference effects. In presence of more than one contribution their mutual cancellation is possible, but since we always assume, at the moment hypothetical, observation of $0\nu\beta\beta$ decay, it would actually strengthen our argument, implying even stronger washout of lepton number asymmetry.

6

Falsifying Baryogenesis

The observation of a baryon asymmetry in the Universe is one of the most significant evidences for BSM physics and any new theory of particle physics must be at least consistent with this phenomenon. However, an observation of new physics in the form of LNV at relatively low energies can also provide important implications on the origin of baryon number prevalence. As we will show in this chapter, which we base on Ref. [240], this interesting interplay between LNV at low and high energy scales provides a great motivation for an intensive search for $0\nu\beta\beta$ decay.

6.1 Effective Washout

We will now focus on the study of the washout effects of $\Delta L = 2$ SM effective operators on a pre-existing net lepton asymmetry. Although we will discuss all the operators in Tabs. 5.1, 5.2 and 5.3, only a single one will be assumed to be active at a time.

6.1.1 Boltzmann Equations

The net lepton density in the early Universe can be determined from the classic Boltzmann equation formalism. For a particle species N the generic Boltzmann equation reads[1]

$$zHn_\gamma \frac{\mathrm{d}\eta_N}{\mathrm{d}z} = -\sum_{a,i,j,\cdots} [Na\cdots \leftrightarrow ij\cdots]. \tag{6.1}$$

Here, $z = m_N/T$ with m_N referring to the mass of particle N and T to temperature; $\eta_N \equiv n_N/n_\gamma$ denotes the number density n_N of particle N normalized to the equilibrium photon number density $n_\gamma \approx 2.4T^3/\pi^2$, the Hubble parameter

[1] More detailed discussion on the Boltzmann equation formalism can be found e.g. in Refs. [244–246].

is given by $H \approx 1.66\sqrt{g_*}T^2/\Lambda_{\rm Pl}$ with $g_* \approx 107$ being the effective number of relativistic degrees of freedom in the SM and $\Lambda_{\rm Pl} = 1.2 \times 10^{19}$ GeV the Planck scale. Further, the short-hand notation

$$\begin{aligned}[Na\cdots \leftrightarrow ij\cdots] = &\frac{n_N n_a \cdots}{n_N^{\rm eq} n_a^{\rm eq} \cdots}\gamma^{\rm eq}(Na\cdots \to ij\cdots) \\ &- \frac{n_i n_j}{n_i^{\rm eq} n_j^{\rm eq} \cdots}\gamma^{\rm eq}\left(ij\cdots \to Na\cdots\right)\end{aligned} \tag{6.2}$$

is used, where a, N and i, j are the initial and final state particles, respectively, with the corresponding number densities n_N, n_a and n_i, n_j. The superscript 'eq' then labels values of these densities in thermal equilibrium. The thermally equilibrated space-time scattering density in $\gamma^{\rm eq}$ is given by

$$\begin{aligned}\gamma^{\rm eq}(Na\cdots \to ij\cdots) = &\int \frac{{\rm d}^3 p_N}{2E_N(2\pi)^3} e^{-\frac{E_N}{T}} \times \prod_{a=1}^{n-1}\left[\int \frac{{\rm d}^3 p_a}{2E_a(2\pi)^3} e^{-\frac{E_a}{T}}\right] \\ &\times \prod_{i=1}^{m}\left[\int \frac{{\rm d}^3 p_i}{2E_i(2\pi)^3}\right] \times (2\pi)^4 \delta^4\left(p_N + \sum_{a=1}^{n-1} p_a - \sum_{i=1}^{m} p_i\right)|M|^2,\end{aligned} \tag{6.3}$$

where n and m is the initial and final number of particles, respectively, and $|M|^2$ denotes the squared amplitude of the process summed over initial and final spins. The momentum and energy of the particle N is denoted by p_N and E_N, while momenta and energies with subscripts a and i correspond to other particles in the initial and final state, respectively. Now it would be convenient to express the products of integrations over momenta of individual particles as a single integration over the total momentum $P = (P_0, \vec{P})$. Following Ref. [246], we make use of the expression

$$\begin{aligned}1 &= \int {\rm d}^4 P \delta^4\left(P - p_N - \sum_{a=1}^{n-1} p_a\right) \\ &= \int \frac{1}{2}\sqrt{P_0^2 - s}\ \delta^4\left(P - p_N - \sum_{a=1}^{n-1} p_a\right)\ {\rm d}s\ {\rm d}P_0\ {\rm d}\Omega,\end{aligned} \tag{6.4}$$

with $s = P_0^2 - |\vec{P}|^2$ and Ω denoting the two-dimensional solid angle of the three-momentum $\vec{P}$. By inserting the above unity into the scattering density we can

rewrite the Eq. 6.3 as

$$\begin{aligned}\gamma^{\rm eq}(Na\cdots\to ij\cdots) &= \frac{1}{2}\frac{1}{(2\pi)^4}\int {\rm d}s\int {\rm d}\Omega\int {\rm d}P_0\sqrt{\frac{P_0^2}{s}-1}\,\sqrt{s}\;e^{-P_0/T}\\ &\times\int\frac{{\rm d}^3p_N}{2E_N(2\pi)^3}\times\prod_{a=1}^{n-1}\left[\int\frac{{\rm d}^3p_a}{2E_a(2\pi)^3}\right](2\pi)^4\delta^4\left(P-p_N-\sum_{a=1}^{n-1}p_a\right)\\ &\times\prod_{i=1}^{m}\left[\int\frac{{\rm d}^3p_i}{2E_i(2\pi)^3}\right](2\pi)^4\delta^4\left(P-\sum_{i=1}^{m}p_i\right)\times|M|^2\\ &=\frac{1}{2(2\pi)^4}\int {\rm d}s\sqrt{s}\int {\rm d}P_0\sqrt{P_0^2/s-1}e^{-P_0/T}\int {\rm d}\Omega{\rm d}PS^n{\rm d}PS^m\times|M|^2,\end{aligned}\tag{6.5}$$

where $\int {\rm d}PS^n$ and $\int {\rm d}PS^m$ are the initial and final state phase space integrals, respectively.

Under the assumption that $|M|^2$ does not depend on the relative motion of particles with respect to the thermal plasma and using $\int {\rm d}\Omega = 4\pi$ the integration over P_0 and Ω yields

$$\gamma^{\rm eq}(Na\cdots\to ij\cdots) = \frac{1}{(2\pi)^3}\int {\rm d}s\;\sqrt{s}K_1\left(\frac{\sqrt{s}}{T}\right){\rm d}PS^n{\rm d}PS^m\times|M|^2,\tag{6.6}$$

with K_n denoting the modified Bessel functions of the second kind.

Let us consider that this kind of process is mediated by an effective contact interaction of all $N = n + m$ particles. If it is further assumed that all the involved particles are scalars, then $|M|^2 \propto 1/\Lambda^{2(N-4)}$ with Λ denoting the cut-off scale of the effective operator in question. Moreover, $|M|^2$ does not depend on the variables of the phase space integral; therefore, the calculation of $\gamma^{\rm eq}$ is rather straightforward and we can write

$$\gamma^{\rm eq} = \frac{1}{2^2(2\pi)^{2N-3}}\times\frac{\Gamma(N-2)\Gamma(N-3)}{\Gamma(n)\Gamma(n-1)\Gamma(N-n)\Gamma(N-n-1)}\times\frac{T^{2N-4}}{\Lambda^{2N-8}},\tag{6.7}$$

where the following expression

$$PS^n = \int {\rm d}PS^n = \frac{1}{2(4\pi)^{2n-3}}\frac{s^{n-2}}{\Gamma(n)\Gamma(n-1)}.\tag{6.8}$$

for the phase space integration in the limit $\sqrt{s}\gg m_i$ $(i = 1,\cdots,n)$, in which all particles are massless, has been employed.

6.1.2 Approximated Scattering Density

The situation becomes less trivial for effective interaction involving fermions, as in such a case the matrix element of the process will generally depend on their

energies. Based on a naive dimensional analysis, the squared amplitude will for each fermion include an additional factor of E compared to the case involving only scalars. The quantity E with a dimension of energy can be determined from the details of interaction kinematics. The phase-space integration of $|M|^2$ for an interaction of a large number of particles is fairly complex, if fermions are present. However, a reasonable approximation can be obtained. We perform the integration in two simplified scenarios, for which the energy E of each fermion is replaced by

1. the centre-of-mass energy $\sqrt{s}$,
2. the average energy $\sqrt{s}/n$ ($\sqrt{s}/m$) for an initial (final) state fermion.

The calculation of the integral is in both these schemes analogous to the case involving only scalar particles. We have compared the results obtained in this way with the exact integration for a few selected operators concluding that the scattering rate is well-approximated by the geometric mean of the two results obtained for the above scenarios.

Specifically, we can assume a presence of n_f fermions within the n-particle initial state and m_f fermions within the m-particle final state.[2] Then the first scheme gives the following expression for the square of the matrix element

$$|M_1|^2 = \frac{\sqrt{s}^{N_f/2}}{\Lambda^{N-4+N_f/2}}, \tag{6.9}$$

with $N_f \equiv n_f + m_f$, while the second one yields

$$|M_2|^2 = \frac{(\sqrt{s}/n)^{n_f/2}(\sqrt{s}/m)^{m_f/2}}{\Lambda^{N-4+N_f/2}}. \tag{6.10}$$

Consequently, we get

$$\begin{aligned}\gamma^{\mathrm{eq}}_{1(2)}(Na\cdots \to ij\cdots) = {} & \frac{2^{N_f-2}}{(2\pi)^{2N-3}} \times \overline{c}_{1(2)} \\ & \times \frac{\Gamma(N+N_f/2-3)\Gamma(N+N_f/2-2)}{\Gamma(n)\Gamma(n-1)\Gamma(N-n)\Gamma(N-n-1)} \times \frac{T^{2N+N_f-4}}{\Lambda^{2N+N_f-8}},\end{aligned} \tag{6.11}$$

where

$$\overline{c}_1 = 1 \qquad \text{and} \qquad \overline{c}_2 = \frac{1}{n^{n_f}(N-n)^{N_f-n_f}}, \tag{6.12}$$

[2]The dimension D of the effective operator is related to the number of particles contained by the operator as $N + N_f/2 = D$.

for the two different simplifying scenarios.

In addition, if identical particles appear in the initial and final state, one has to take into account the corresponding symmetry factor due to the phase space integral as well as the numerical factor reflecting the number of possible ways the states can be created or annihilated. Moreover, interchanging particles in the initial and final states of each operator leads to physically distinguishable lepton number washout processes. Therefore, a sum over all contributions given by different permutations must be taken. The resulting estimation of the thermal rate $\gamma^{\rm eq}$ reads

$$\gamma^{\rm eq} = \sqrt{(\Sigma\gamma_1^{\rm eq}) \times (\Sigma\gamma_2^{\rm eq})}, \tag{6.13}$$

where the sums cover both the permutations and the symmetry factors. Based on our explicit checks the above approximation agrees with the exact results up to a 10% discrepancy obtained for some of the 7-dimensional operators.

6.1.3 The Minimal Washout Temperature

To provide an example of application of the above derived formulae we will now demonstrate the calculation of the lepton number washout rate from the operator $\mathcal{O}_8 = L^i \bar{e^c} \bar{u^c} d^c H^j \epsilon_{ij}$. One of the processes triggered by this operator is $L\bar{e^c} \to u^c \bar{d^c} \bar{H}$ (symbols denote particles) and the inverse process is induced by the complex conjugate of $\mathcal{O}_8$. On top of that, permutations of the field operators must be also included; hence, the operator $\mathcal{O}_8$ gives also a physically different process $\bar{u^c} d^c H \to \bar{L} e^c$ (and again, the inverse process $\bar{u^c} d^c H \leftarrow \bar{L} e^c$ is induced by $\mathcal{O}_8^\dagger$). As operator $\mathcal{O}_8$ contains 5 fields, it can trigger processes of type $3 \leftrightarrow 2$ and $1 \leftrightarrow 4$. However, due to the phase space integral (see Eq. (6.8)) the processes $1 \leftrightarrow 4$ are suppressed with respect to the $3 \leftrightarrow 2$ processes. The total lepton number washout rate from operator $\mathcal{O}_8$ is then given by the sum of all thirty distinguishable permutations - twenty of them arise from $3 \leftrightarrow 2$ and $2 \leftrightarrow 3$ processes, while ten correspond to $1 \leftrightarrow 4$ and $4 \leftrightarrow 1$ processes. It is important to note that $3 \leftrightarrow 2$ and $2 \leftrightarrow 3$ are physically different processes; for example, $\bar{u^c} d^c H \leftrightarrow \bar{L} e^c$ is not equivalent to $L\bar{e^c} \leftrightarrow u^c \bar{d^c} \bar{H}$.

Making the assumption that the SM Yukawa interactions and the sphalerons are in thermal equilibrium allows expressing all relevant chemical potentials in

terms of the chemical potential of the lepton doublet L^ℓ ($\ell = e, \mu, \tau$) [247][3], namely

$$\mu_H = \frac{4}{21}\sum_\ell \mu_{L^\ell}, \;\; \mu_{e^{\bar{c}}_\ell} = \mu_{L^\ell} - \frac{4}{21}\sum_\ell \mu_{L^\ell},$$
$$\mu_{\bar{u^c}} = \frac{5}{63}\sum_\ell \mu_{L^\ell}, \;\; \mu_{\bar{d^c}} = -\frac{19}{63}\sum_\ell \mu_{L^\ell}. \tag{6.14}$$

In the limit of a small asymmetry $|n - \bar{n}| \ll n^{\rm eq}$ we can write the relation between chemical potential and the normalized density η as

$$\frac{n}{n^{\rm eq}} = \frac{\eta}{\eta^{\rm eq}} \approx e^{\mu/T} \approx 1 + \frac{\mu}{T} \;\text{ and }\; \frac{\bar{n}}{n^{\rm eq}} = \frac{\bar{\eta}}{\eta^{\rm eq}} \approx 1 - \frac{\mu}{T}$$
$$\Rightarrow \;\; \frac{\eta_\Delta}{\eta^{\rm eq}} \equiv \frac{\eta - \bar{\eta}}{\eta^{\rm eq}} = 2\frac{\mu}{T}. \tag{6.15}$$

Here, $\eta^{\rm eq} \equiv n^{\rm eq}/n^{\rm eq}_\gamma = 1/2$ for e^c_ℓ and $\eta^{\rm eq} = 3/2$ for u^c and d^c due to the colour factor. In case of the doublets L^ℓ and H we take $\eta^{\rm eq} = 1$. Since all the chemical potentials can be related to the chemical potential of the lepton doublet, it is now enough to calculate the time evolution of the lepton doublet density. The densities of other particles can be obtained from η_L using Eqs. (6.14) and (6.15). The Boltzmann equation corresponding to L^e has the form[4]

$$\begin{aligned} zHn_\gamma \frac{{\rm d}\eta_{L_e}}{{\rm d}z} &= -\left[L_e\bar{e^c} \leftrightarrow u^c\bar{d^c}\bar{H}\right] + (\text{other permutations}) \\ &= -\left(\frac{n_{L_e}n_{\bar{e^c}}}{n^{\rm eq}_{L_e}n^{\rm eq}_{\bar{e^c}}} - \frac{n_{u^c}n_{\bar{d^c}}n_{\bar{H}}}{n^{\rm eq}_{u^c}n^{\rm eq}_{\bar{d^c}}n^{\rm eq}_{\bar{H}}}\right)\gamma^{\rm eq}(L_e\bar{e^c} \to u^c\bar{d^c}\bar{H}) + \cdots \\ &= -\frac{22}{7}\frac{\mu_{L_e}}{T}\gamma^{\rm eq}(L_e\bar{e^c} \to u^c\bar{d^c}\bar{H}) + \cdots \\ &= -\frac{11}{7}\eta_{\Delta L_e}\gamma^{\rm eq}(L_e\bar{e^c} \to u^c\bar{d^c}\bar{H}) + \cdots, \end{aligned} \tag{6.16}$$

where in the last two equalities we used Eqs. (6.14) and (6.15). Further, we consider the fermions of first generation and a universal chemical potential among three lepton flavours. As mentioned before, one should include all the possible

[3]To be precise, we should note that the charged lepton Yukawa interactions for the three generations e, μ, τ are not in thermal equilibrium above temperatures $T \gtrsim 10^5$ GeV, 10^9 GeV and 10^{12} GeV, respectively. Nevertheless, except for the Weinberg operator the cut-off scales of all other operators we study lie around or below 10^5 GeV. Consequently, the assumption that all the EW sphalerons and all SM Yukawa interactions are in thermal equilibrium in the given temperature interval is valid.

[4]To obtain the correct symmetry factor when more identical doublets are present in the operator (e.g. LL or HH), the operator should be decomposed in terms of the $SU(2)_L$ components. For the $SU(2)_L$ doublet components $\eta^{eq} = 1/2$ (and 3/2 for the coloured ones).

permutations of the $2 \leftrightarrow 3$ and $1 \leftrightarrow 4$ processes. For the antiparticle, i.e. for $\bar{L}_e$, an analogous Boltzmann equations could be written. Eventually, employing Eq. (6.13) it is possible to calculate the thermal rate $\gamma^{\rm eq}$ and inserting it into the Eq. 6.16 we obtain the total washout effect induced by the operator $\mathcal{O}_8$

$$zHn_\gamma \frac{\mathrm{d}\eta_{\Delta L_e}}{\mathrm{d}z} = -\frac{11\sqrt{195}\,T^{10}}{7\pi^7\Lambda^6}\eta_{\Delta L_e}. \tag{6.17}$$

The performed computation can be generalized to describe the washout effect from a dimension-D operator as

$$zHn_\gamma \frac{\mathrm{d}\eta_{\Delta L_e}}{\mathrm{d}z} = -c_D \frac{T^{2D-4}}{\Lambda_D^{2D-8}}\eta_{\Delta L_e}. \tag{6.18}$$

We can regard the washout processes to be in equilibrium if their interaction rate Γ_W is large in comparison with the expansion rate of the Universe, i.e.

$$\frac{\Gamma_W}{H} \equiv \frac{c_D}{n_\gamma H}\frac{T^{2D-4}}{\Lambda_D^{2D-8}} = c'_D \frac{\Lambda_{\rm Pl}}{\Lambda_D}\left(\frac{T}{\Lambda_D}\right)^{2D-9} \gtrsim 1, \tag{6.19}$$

with $c'_D = \pi^2 c_D/(3.3\sqrt{g_*}) \approx 0.3\, c_D$. Hence, to certain approximation, the washout is effective within the following temperature interval

$$\Lambda_D \left(\frac{\Lambda_D}{c'_D \Lambda_{\rm Pl}}\right)^{\frac{1}{2D-9}} \equiv \lambda_D \lesssim T \lesssim \Lambda_D. \tag{6.20}$$

We set here the upper limit $T \lesssim \Lambda_D$ on the washout imposed by the validity of the effective operator approach. However, as will be discussed later, the lepton number can be further washed out above Λ_D within an underlying UV theory. Clearly, a precise value of the lower bound of the temperature interval can be computed by solving the Boltzmann Eq. (6.18) from the baryogenesis scale down to the EW scale, where the value of the observed baryon asymmetry has to be reproduced. For the translation between the lepton and baryon number asymmetries the Eq. (3.138) can be employed. The resulting more stringent lower limit on the efficient washout effects reads

$$\hat{\lambda}_D \approx \left[(2D-9)\ln\left(\frac{10^{-2}}{\eta_B^{\rm obs}}\right)\lambda_D^{2D-9} + v^{2D-9}\right]^{\frac{1}{2D-9}} \tag{6.21}$$

where the primordial asymmetry (generated probably in a non-thermal fashion) has been conservatively assumed to be of order one and v denotes the EW VEV as earlier. As expected, this lower bound is larger than λ_D obtained simply based on $\Gamma_W > H$.

As for the 5-dimensional Weinberg operator, it has been already shown [248] that Majorana masses of neutrinos would imply an upper bound on the scale of baryogenesis $T \lesssim 10^{12}$ GeV $(1\text{ eV}/m_\nu)^2$. The reason is that the underlying LNV interactions allowing for the generation of the masses would together with sphaleron processes erase both the lepton and baryon asymmetries. The constraint induced by current limits on $0\nu\beta\beta$ decay is $T \lesssim 2 \times 10^{12}$ GeV as argued in Ref. [133]. In this work we will primarily concentrate on higher-dimensional LNV operators, studying the corresponding correlation of the washout effects with the triggered $0\nu\beta\beta$ decay rate.

6.2 Falsification of High-Scale Baryogenesis

In Chap. 5 we have listed all the dominant contributions of $\Delta L = 2$ SM effective operators to the long-range and short-range mechanisms of $0\nu\beta\beta$ decay induced either at tree, or any higher loop level. We will now study how these exotic contributions correlate with mechanisms erasing the baryon asymmetry.

We assume one $\Delta L = 2$ SM effective operator, with given operator scale Λ, to be active at a time. This operator then has the following two effects:

1. It induces the lepton number asymmetry washout, which is efficient within a certain temperature range with Λ being the upper limit. The approach to calculate this effect has been described above. We assume a lepton asymmetry of $\mathcal{O}(1)$ is injected at a certain temperature T and the Boltzmann equation then allows to compute the surviving baryon asymmetry at the current temperature. In this way we determine the minimal temperature $\hat{\lambda}_D$, for which the surviving asymmetry still equals the observed asymmetry. As a result, if the lepton number asymmetry is injected above $\hat{\lambda}_D$, then the washout processes erase it below the observed value.

2. It induces $0\nu\beta\beta$ decay triggered via neutrino mass, long-range and short-range mechanisms. We calculate the $0\nu\beta\beta$ decay rate as function of Λ. For a given experimental sensitivity to $0\nu\beta\beta$ decay we then obtain the corresponding Λ and determine the temperature range in which the lepton number asymmetry is strongly washed out.

The main results of our computation are summarized in Figs. 6.1, 6.4 and 6.5, which show the temperature ranges of highly effective washout for all the studied

operators. Different colours indicate operators of different dimensions; namely, the bars for operators of dimension 7, 9 and 11 are purple, green and magenta, respectively. The scale Λ of the given operator sets the upper bound of each temperature range using limits on effective couplings $\epsilon^{\bullet}_{\bullet}$ from Tab. 4.2 derived assuming an observation of $0\nu\beta\beta$ decay at the future sensitivity $T^{\mathrm{Xe}}_{1/2} = 10^{27} y$. The particular contribution used in the calculation varies with the figure. All the dominant contributions are considered in some cases, in others only long-range, or short-range contributions are taken into account leading to an effective scale Λ_{long} or Λ_{short}, respectively. The effective operator approach does not allow us to determine the washout above the typical operator scale Λ, which thus must be interpreted as the upper limit of validity of this treatment.

Note that there are always two lower limits shown for each bar. The dark bar segments depict the interval $[\hat{\lambda}, \Lambda]$ of strong washout mentioned above with $\hat{\lambda}$ denoting the temperature, at which an asymmetry of order one can be injected to yield the observed baryon asymmetry down at the EW scale, cf. Eq. (6.21). On the other hand, the smaller lower limit corresponding to the light bar segments is given by temperature λ, for which $\Gamma_W/H = 1$, see Eq. (6.20).

Based on Figs. 6.1, 6.4 and 6.5 a general observation can be made that all the temperature ranges lie much lower than the well-known cut-off scale of the Weinberg operator reaching roughly 10^{14} GeV. Further, the ranges corresponding to higher-dimensional operators lie lower. While the temperature intervals of dimension-7 operators reach as high as $10^5 - 10^6$ GeV, the operators of dimensions 9 and 11 typically wash the lepton number asymmetry out closer or even right above the EW scale. This behaviour is given by the derived sizes of the operator cut-off scales, as those determine the position of the washout ranges. To determine Λ we always use a dominant non-standard (long-range or short-range) contribution of particular effective operator to $0\nu\beta\beta$ decay. Nonetheless, we calculate also the contributions to the standard $0\nu\beta\beta$ decay mechanism, from which the scales of neutrino mass generation are determined and marked in our figures by orange diamonds and arrows. Whenever this orange indicator is shown above the corresponding temperature range (i.e. above Λ), the neutrino mass contribution to $0\nu\beta\beta$ decay dominates.

6.2.1 Long-Range Contributions

First we will focus on the operators contributing dominantly to one of the long-range mechanisms. In our discussion we will detail various aspects one has to take into account when constraining the scale of the operators using $0\nu\beta\beta$ decay and that can influence the identified washout intervals.

Impact of Sensitivity on $0\nu\beta\beta$ Couplings Although the operators $\mathcal{O}_{3a,3b,4a}$ yield the same scaling as $\mathcal{O}_8$ (discussed in Ref. [132]),

$$\frac{G_F \epsilon_7^{3a,3b,4a,8}}{\sqrt{2}} = \frac{v}{\Lambda^3}, \tag{6.22}$$

their specific hadronic and leptonic current structure, which we derived in Sec. 5.2.1, causes that they excite different effective couplings,

$$\epsilon_7^{3a} = \epsilon_{T_R}^{T_R}, \quad \epsilon_7^{3b} = \epsilon_{S+P}^{S+P}, \quad \epsilon_7^{4a} = \epsilon_{S-P}^{S+P}, \quad \epsilon_7^{8} = 2\epsilon_{V+A}^{V+A}, \tag{6.23}$$

cf. Eq. 5.22 and Eq. 5.23. The nuclear matrix elements for distinct long-range mechanisms (characterized by the effective couplings) vary, which leads to different sensitivities, see Tab. 4.2. As a result, the corresponding operator scales differ significantly: $\Lambda_{3a} = 6.6 \times 10^5$ GeV vs. $\Lambda_{3b,4a} = 3.3 \times 10^5$ GeV vs. $\Lambda_8 = 7.5 \times 10^4$ GeV, see Fig. 6.1.

The bounds on $\epsilon_{T_R}^{T_R}$ and $\epsilon_{S\pm P}^{S+P}$ for $\mathcal{O}_{3a}$ and $\mathcal{O}_{3b,4a}$, respectively, are more stringent, which results in a higher operator scale. Consequently, the washout rate induced by these operators is suppressed when compared to the one of $\mathcal{O}_8$. To be more concrete, if $0\nu\beta\beta$ decay is observed at the future sensitivity $T_{1/2}^{\mathrm{Xe}} = 10^{27} y$, a dominant contribution of $\mathcal{O}_8$ would imply exclusion of baryogenesis models above $\hat{\lambda}_8 \approx 900$ GeV. On the other hand, for operators $\mathcal{O}_{3b,4a}$ only mechanisms above $\hat{\lambda}_{3b,4a} \approx 4$ TeV can be excluded and in case of $\mathcal{O}_{3a}$ the exclusion limit is even higher, reaching $\hat{\lambda}_{3a} \approx 10$ TeV. Considering searches for LNV at the LHC similar differences can be crucial, as they can decide on the possibility of observation of the associated new physics on the collider.

Impact of Field Content Although it could be naively expected that the 9-dimensional operators contribute dominantly to one of the short-range mechanisms, it turns out it is not always the case. For instance, the dominant contributions of the operators $\mathcal{O}_{5,6,7}$, which contain three Higgs doublets, are of a

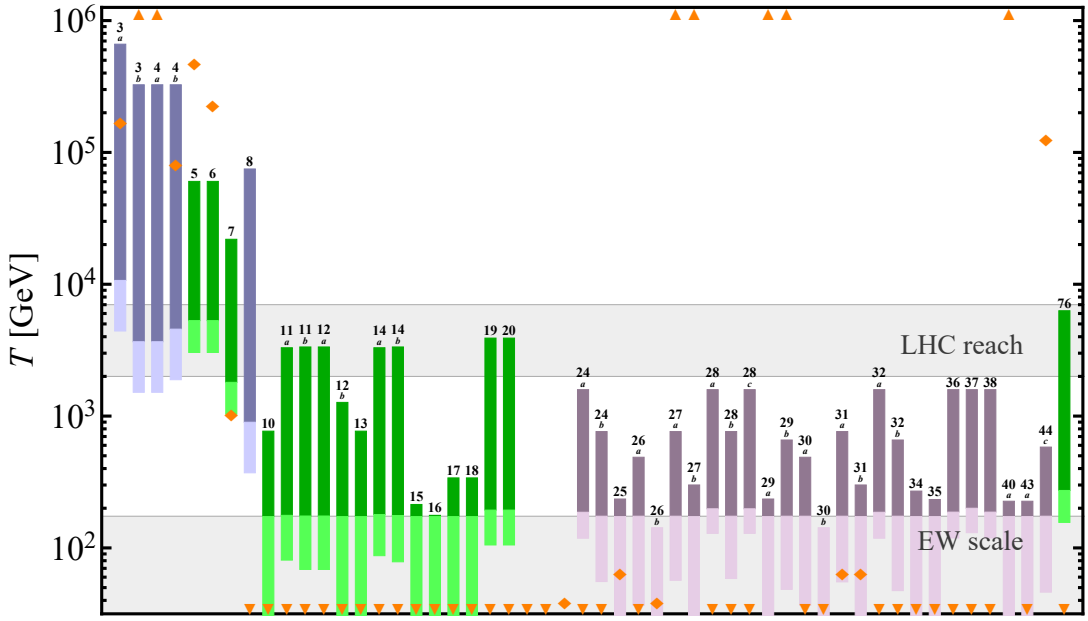

Figure 6.1: Assuming observation of $0\nu\beta\beta$ decay at $T_{1/2}^{\mathrm{Xe}} = 10^{27}$ y the washout induced by given operators is effective in the presented temperature ranges. The 7-dimensional operators are indicated in purple, 9-dimensional ones in green and 11-dimensional ones in magenta. The interval of strong washout between Λ and $\hat{\lambda}$ (see Eq. (6.21)) is represented by the darker bar segment. The lower limit of the lighter segment denoted as λ corresponds to the temperature, where $\Gamma_W/H = 1$, see Eq. (6.20). We take into account both the long-range and short-range $0\nu\beta\beta$ decay contributions of the given operator. The scale of the Weinberg operator when induced by a given higher-dimensional operator is denoted by orange symbols. While the diamond-shape marks indicate the exact value of the scale, the arrows pointing up or down denote a scale larger or smaller than the plot range. For the purpose of this plot, all the SM Yukawa couplings appearing in the $0\nu\beta\beta$ decay contributions are assigned their first generation values. The rough mass reach of the LHC searches and the temperature range below the EW scale (where sphaleron processes are inefficient) are depicted by two grey horizontal stripes.

long-range type and they read

$$\frac{G_F \epsilon_7^{5,6}}{\sqrt{2}} = \frac{v}{16\pi^2 \Lambda^3} + \frac{v^3}{\Lambda^5}, \quad \text{and} \quad \frac{G_F \epsilon_7^7}{\sqrt{2}} = \frac{v^3}{\Lambda^5}, \tag{6.24}$$

respectively. Due to different $SU(2)_L$ structures of the operators the scaling of the above contributions also differ. Unlike operator $\mathcal{O}_7 = L^i Q^j \bar{e}^c \bar{Q}_k H^k H^l H^m \epsilon_{il} \epsilon_{jm}$, the operators $\mathcal{O}_5 = L^i L^j Q^k d^c H^l H^m \bar{H}_i \epsilon_{jl} \epsilon_{km}$ and $\mathcal{O}_6 = L^i L^j \bar{Q}_k \bar{u}^c H^l H^k \bar{H}_i \epsilon_{jl}$ con-

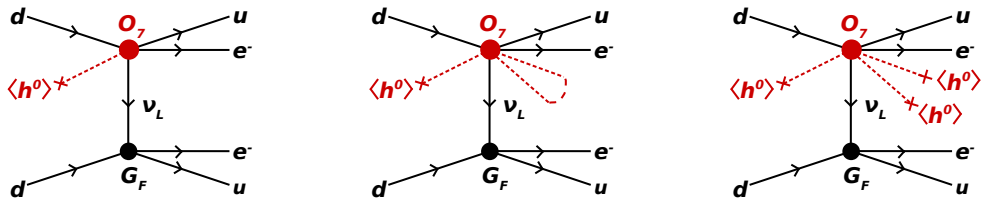

Figure 6.2: The left diagram applies to the 7-dimensional operators $\mathcal{O}_{3a}$, $\mathcal{O}_{3b}$, $\mathcal{O}_{4a}$ and $\mathcal{O}_8$ contributing to a long-range mechanism with one Higgs VEV only. The center and right diagrams show contributions of 9-dimensional operators obtained by closing a Higgs loop and by the insertion of Higgs VEVs, respectively. While the operators $\mathcal{O}_{5,6}$ allow for both these contributions, the operator $\mathcal{O}_7$ triggers only the latter one.

tain an $\bar{H}$, which can be contracted with one of the other two Higgses into a loop, and thus give an additional contribution. Hence, for operator $\mathcal{O}_7$ there is only the contribution scaling as $1/\Lambda^5$, cf. Fig. 6.2. The presence of three Higgs fields in case of all these three operators leads to a suppressed washout in comparison to other 9-dimensional operators. As a result, the corresponding limit on the scale above which baryogenesis can be excluded is higher, cf. Fig. 6.1.

6.2.2 Short-Range Contributions and their Interplay with Long-Range Contributions

Not always is it easy to decipher the dominant contribution as it was in case of the operators discussed above. As outlined in the following paragraphs, a non-trivial interplay of various features can influence the relative size of long-range and short-range contributions of particular operators.

Impact of $SU(2)_L$ Structure on Dominant Contribution We will first demonstrate the non-trivial interplay of various contributions on the comparison of operators $\mathcal{O}_{11a}$ and $\mathcal{O}_{11b}$ differing only by their $SU(2)_L$ structure. The operator $\mathcal{O}_{11b}$ triggers a tree level short-range contribution, whereas $\mathcal{O}_{11a}$ contributes only at one-loop level, cf. Fig. 6.3,

$$\frac{G_F^2 \epsilon_9^{11a}}{2m_p} = \frac{g^2}{16\pi^2 \Lambda^5}, \qquad \frac{G_F^2 \epsilon_9^{11b}}{2m_p} = \frac{1}{\Lambda^5}, \tag{6.25}$$

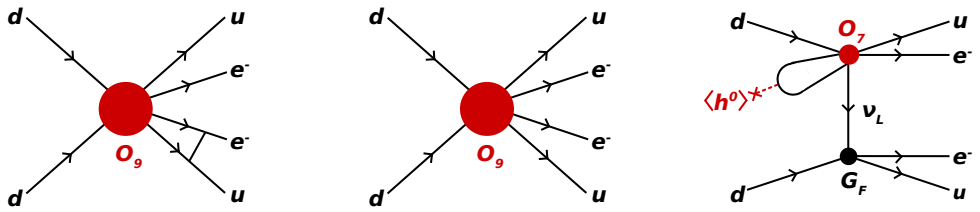

Figure 6.3: While the left diagram depicts an operator contributing only at one-loop level at short range, e.g. $\mathcal{O}_{11a}$, the center one shows a direct tree-level contribution triggered e.g. by $\mathcal{O}_{11b}$. At long range both these operators contribute with the same loop-suppression as depicted on the right.

where $\epsilon_9^{11a,b} = \epsilon_1$ and the corresponding experimental bounds can be found in Tab. 4.2. As for the long-range contribution, both operators give

$$\frac{G_F \epsilon_7^{11a,b}}{\sqrt{2}} = \frac{y_d v}{16\pi^2 \Lambda^3}. \tag{6.26}$$

The only difference is in the effective couplings of these two operators, namely $\epsilon_7^{11a} = \epsilon_{T_R}^{T_R}$ and $\epsilon_7^{11b} = \epsilon_{S+P}^{S+P}$. Hence, $\mathcal{O}_{11a}$ and $\mathcal{O}_{11b}$ can be reduced to $\mathcal{O}_{3a}$ and $\mathcal{O}_{3b}$, respectively, see Fig. 6.3.

The effects of long-range and short-range contributions and their mutual competition can be studied from Fig. 6.4, where we show separately the washout ranges obtained when considering only the operators' contribution to the long-range (upper left plot) or the short-range (lower left plot) $0\nu\beta\beta$ decay mechanisms. As mentioned above, the short-range contribution of $\mathcal{O}_{11a}$ is loop suppressed in comparison to $\mathcal{O}_{11b}$. As a result, the scale Λ_9^{11a} of the former operator is lower than the scale Λ_9^{11b} of the latter one, which means that $\mathcal{O}_{11a}$ induces a stronger washout. Both these operators give the same long-range contribution, but due to their specific $SU(2)_L$ structure they excite distinct effective couplings, ϵ_7^{11a} and ϵ_7^{11b}, which leads to different operator scales, $\Lambda_7^{11a} = 3.3$ TeV $> \Lambda_9^{11a}$ and $\Lambda_7^{11b} = 1.6$ TeV $< \Lambda_9^{11b}$, respectively. We summarize this comparison in Tab. 6.1, where the following interesting effect can be observed. On one hand, the operator $\mathcal{O}_{11b}$ behaves the expected way, i.e. the respective short-range contribution is

		$\mathcal{O}_{11a}$		$\mathcal{O}_{11b}$	
		1st gen	3rd gen	1st gen	3rd gen
long-range	$T_{1/2}^{-1}$ GeV^{-6}	$1.3 \times 10^{-6}\Lambda^{-6}$	Λ^{-6}	$1.8 \times 10^{-8}\Lambda^{-6}$	$0.01\Lambda^{-6}$
	Λ	3299	31504	1623	15501
short-range	$T_{1/2}^{-1}$ GeV^{-10}	$911\Lambda^{-10}$		$1.8 \times 10^{8}\Lambda^{-10}$	
	Λ	991		3345	
dominant $\bigcap$ non-excluded		long	long	short	long

Table 6.1: The dependence of $T_{1/2}$ [y] on the scale Λ [GeV] is shown for both operators $\mathcal{O}_{11b,b}$ and considering both first and third generation internal Yukawa couplings. In each case we also calculate the respective operator scale assuming that $0\nu\beta\beta$ decay is observed at $T_{1/2} = 10^{27}$ y. Based on their comparison the dominant and not-yet-excluded contribution is identified as the one with higher Λ. Therefore, the short-range contribution dominates only for $\mathcal{O}_{11b}$ with first generation internal Yukawa couplings.

dominant[5] and the long-range one becomes larger only for scales $\Lambda \gtrsim 9.9$ TeV. On the other hand, a similar long-range contribution of the operator $\mathcal{O}_{11a}$ dominates already above scales $\Lambda > 163$ GeV, since the corresponding short-range contribution is loop suppressed. Hence, based on this particular example one can see that different $SU(2)_L$ structures of the same operator can significantly influence the identification of the dominant contribution.

Impact of Flavour Structure on Dominant Contribution As only first generation quarks and leptons can participate in $0\nu\beta\beta$ decay, the external Yukawa couplings (i.e. those sitting in the vertices with external fermion legs in the $0\nu\beta\beta$

[5]The higher scale can be always identified with the more dominant contribution, as already argued in Sec. 5.2.3, and the reasoning is following: assuming observation of $0\nu\beta\beta$ decay at $T_{1/2}^{\mathrm{Xe}} = 10^{27}$ y the scales Λ_{long} and Λ_{short} can be independently determined. Taking the lower one of them would lead to exceeding the experimental limit for the contribution with the higher scale. Therefore, we have to choose the higher scale, as it guarantees picking the dominant contribution that is still consistent with experiment. Hence, the dominant contribution can be identified easily from Fig. 6.4 by comparing the upper row with the lower row. The washout ranges corresponding always to the dominant contribution (either long-range, or short-range) are then depicted in the final comparisons of the washout regimes for all the given operators in Figs. 6.1 and 6.5.

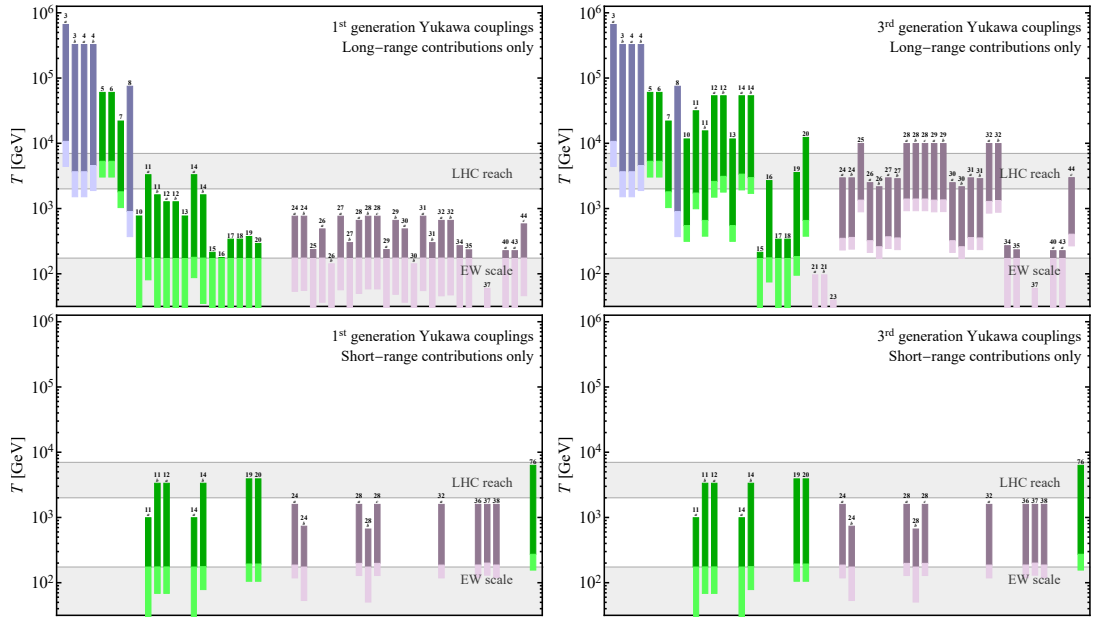

Figure 6.4: As Fig. 6.1, but here we constrain separately the operators' long-range (top row) and short range contribution (bottom row). The results are shown both for first generation internal Yukawa couplings (left column) and third generation internal Yukawa couplings (right column).

decay diagram) are fixed to the first generation. This is, however, not the case for the internal Yukawa couplings (i.e. those in vertices not attached to outer legs) in the loops, which can be summed over all flavours, e.g. in a democratic flavour structure. So far we have assumed in our calculations only first generation Yukawa couplings. To get a rough idea of the flavour dependence and to asses the potential range of the contributions we will now repeat the analysis with third generation internal Yukawa couplings (while keeping the external Yukawas fixed to the first generation). The results are presented in Fig. 6.5 taking into account all contributions, and in Fig. 6.4 (right columns) considering short-range and long-range contributions separately. These can be then compared with those obtained for first generation Yukawas only.

Let us focus again specifically on operators $\mathcal{O}_{11a}$ and $\mathcal{O}_{11b}$. Obviously, as the short-range contribution does not contain any internal Yukawas, it stays unchanged, when third generation values of internal Yukawa couplings are considered. The long-range contribution of $\mathcal{O}_{11b}$, however, gets enhanced and it dominates over the short-range one already for scales $\Lambda > 335$ GeV, cf. Fig. 6.4. Hence, while for only first generation Yukawa couplings the short-range con-

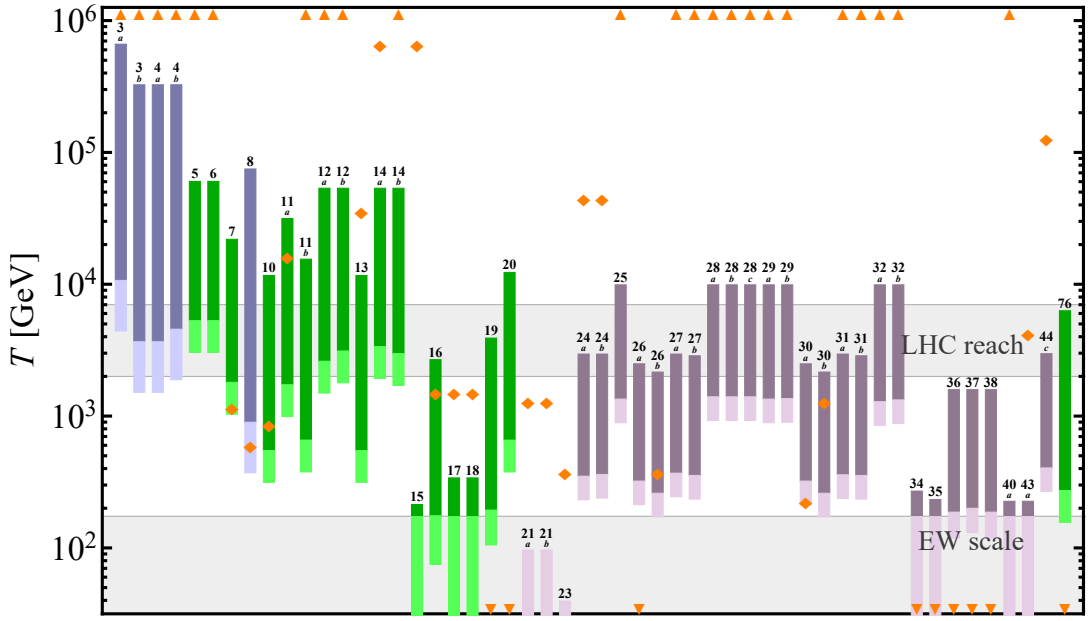

Figure 6.5: Same plot as in Fig. 6.1, but for third generation Yukawa couplings appearing at vertices not attached to the outer legs. The external Yukawa couplings are fixed at their first generation values.

tribution of $\mathcal{O}_{11b}$ was the dominant one, for third generation internal Yukawas the long-range contribution dominates. In case of $\mathcal{O}_{11a}$ the scale above which the long-range contribution dominates is fairly low already for first generation Yukawa couplings only and it is further lowered (to the limit $\Lambda > 6$ GeV) by consideration of third generation internal Yukawas.

The described swap in the dominant contribution of $\mathcal{O}_{11b}$ is induced by a change from an internal first to third generation down quark Yukawa coupling. An even stronger effect can be observed if an internal up quark Yukawa coupling is involved, which is the case e.g. for contributions of operator $\mathcal{O}_{20}$,

$$\frac{G_F^2 \epsilon_9^{20}}{2 m_p} = \frac{1}{\Lambda^5}, \qquad \frac{G_F \epsilon_7^{20}}{\sqrt{2}} = \frac{y_u v}{16\pi^2 \Lambda^3}, \tag{6.27}$$

where $\epsilon_9^{20} = 2\epsilon_5$ and $\epsilon_7^{20} = 2\epsilon_{V+A}^{V+A}$.

Although it could be naively expected that the short-range contribution will always dominate for the operators of dimension 9 and higher, the explicit examples described above demonstrate that it is not always the case. The non-trivial interplay of scales can be for all the operators inspected in Fig. 6.4. The final results are then visualized in Fig. 6.1 and Fig. 6.5.

Consequences for Washout and the Observation of LNV at Colliders If we make the assumption that the new physics responsible for the $\Delta L = 2$ SM effective operators couples to the first generation fermions only, then an experimental evidence of $0\nu\beta\beta$ decay triggered by one of the operators $\mathcal{O}_{11a}$, $\mathcal{O}_{11b}$ and $\mathcal{O}_{20}$ would imply a strong lepton number washout rate from the operator scale all the way down to the EW scale. Consequently, the scenarios of high-scale baryogenesis would be highly disfavoured. Note that if third generation internal Yukawas are used, the operator scales move upwards to higher temperatures, which may result in a window of an ineffective washout between $\hat{\lambda}$ and the EW scale (although lepton number asymmetry is still being erased at higher energy).

Not only the assumed flavour of fermions in the loops but also the specific dominant contributions (see Figs. 6.1 and 6.5) influence the theoretically predicted scale of new LNV physics, and therefore also its potential accessibility at the LHC. As follows from the previous paragraph, if only first generation Yukawa couplings are considered, resonant particles associated with operators $\mathcal{O}_{11a}$ and $\mathcal{O}_{11b}$ may be detected at the LHC, whereas for third generation internal Yukawas the corresponding scales are likely to be beyond the LHC reach.

6.2.3 Effect of Additional NMEs and QCD Running

All the above discussed results displayed in Figs. 6.1, 6.4 and 6.5 are based on the limits for low-energy effective couplings $\epsilon^{\bullet}_{\bullet}$ listed in Tab. 4.2, which were derived in Ref. [115] using only the leading order NMEs. However, in Chap. 4 we have calculated an improved set of bounds on the effective couplings corresponding to the short-range operators presented in Tab. 4.7 that take into account additional NMEs and also QCD running. Therefore, we can now employ these new limits to see how they affect the washout ranges in Figs. 6.1 and 6.5.

The resulting new plots taking into account the new short-range limits are shown in Figs. 6.6 and 6.7. As one can see in Fig. 6.6, for the case of first generation Yukawa couplings a number of washout ranges have been lifted to higher temperatures compared to those in Fig. 6.1. Logically, for all of these operators the short-range contribution now must be the dominant one (as we are using new limits only for the short-range contributions), which did not have to be the case with the old short-range limits. The enhancement of the corresponding cut-off scales is driven especially by the more stringent bounds on $\epsilon^{\bullet}_{1}$ and $\epsilon^{\bullet}_{5}$, which is a result of both the extra NMEs and QCD running, as discussed in Chap. 4. On

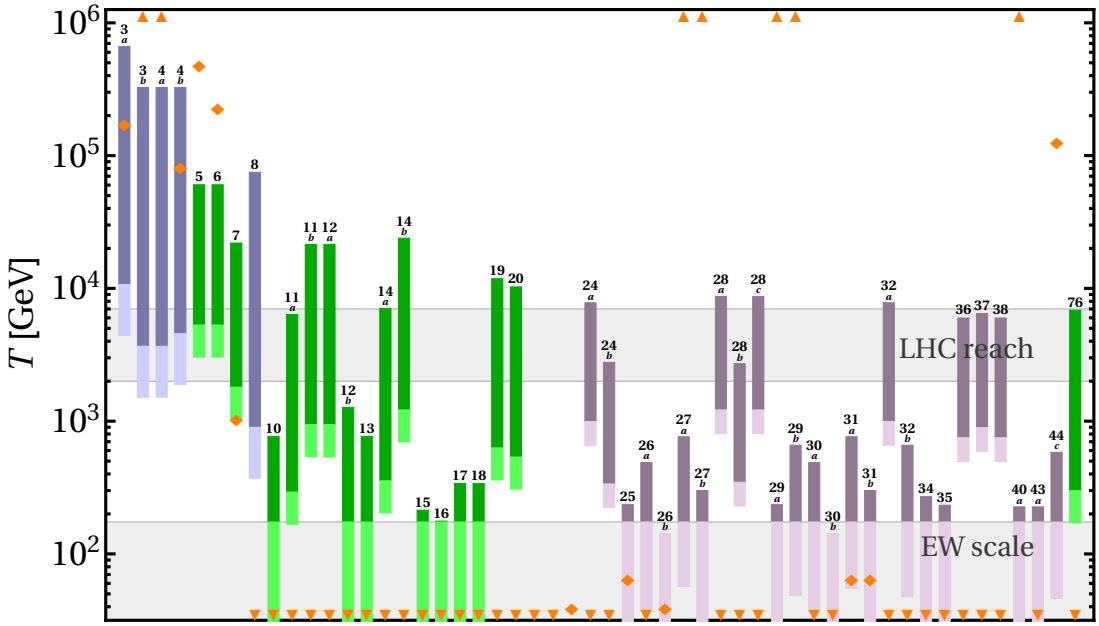

Figure 6.6: As Fig. 6.1, but using the improved bounds on the effective couplings corresponding to the short-range operators listed in Tab. 4.7 taking into account additional NMEs as well as QCD running.

the other hand, when third generation internal Yukawa couplings are considered, the new plot in Fig. 6.7 does not differ much from Fig. 6.5, as only a few washout ranges have moved upwards. This is because the third generation internal Yukawa couplings enhance significantly the long-range contributions, which then usually win the competition even when the new, more stringent bounds on the effective couplings of the short-range mechanisms are considered. Let us note that the bounds on long-range effective couplings $\epsilon^{\bullet}_{\bullet}$ are expected to change if NMEs are treated more accurately, but the effect of QCD running on these couplings is expected to be negligible, as argued in Ref. [239].

6.2.4 Comparison with Standard Mass Mechanism

In the present analysis we study primarily the non-standard mechanisms of $0\nu\beta\beta$ decay, i.e. those that originate from other lepton number violating new physics contribution than the Majorana neutrino mass mechanism. If this is assumed, then the $0\nu\beta\beta$ decay half life does not provide any direct information on effective Majorana neutrino mass, unlike it is in the standard case. Nonetheless, any interaction that violates lepton number will still induce an additional contribution to the Majorana mass at certain loop level. When deriving the washout

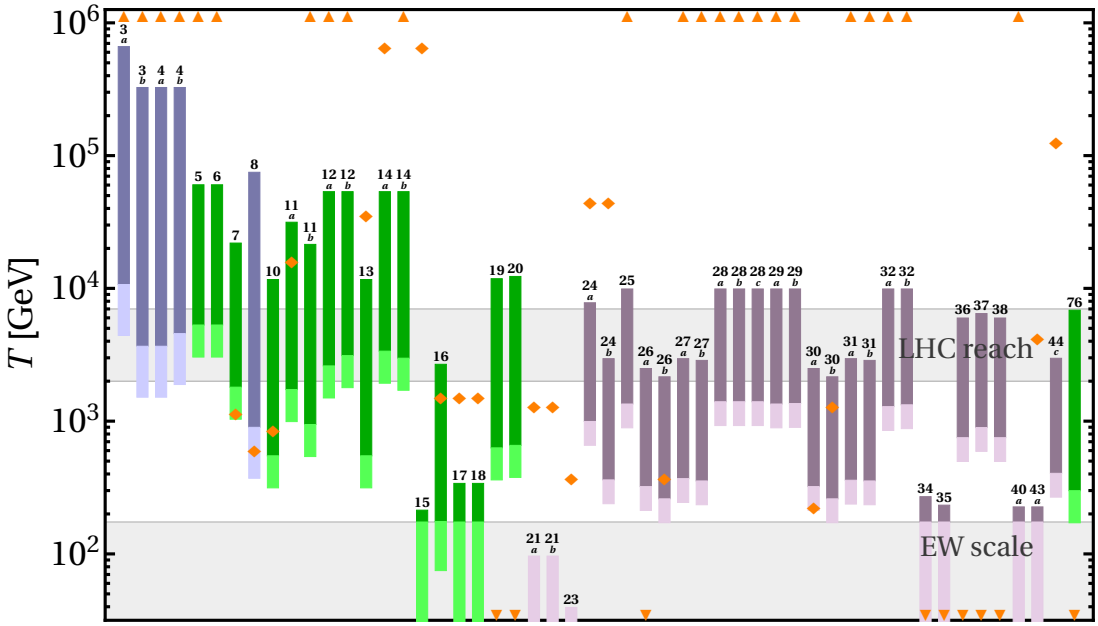

Figure 6.7: As Fig. 6.5, but employing the improved bounds on the effective couplings corresponding to the short-range operators presented in Tab. 4.7, which take into account additional NMEs as well as QCD running.

intervals, we always assumed a presence of only a single lepton number violating effective operator of dimension 7, 9 or 11, neglecting its mass contribution for calculation of the operator scale.

Besides our main focus we find it still interesting to investigate also the possibility of neutrino mass generation by one of the higher-dimensional operators at certain loop level. To this end, we reduce each operator also to the Weinberg operator and assuming this contribution to be responsible for a hypothetical $0\nu\beta\beta$ decay signal we derive the corresponding operator scale. These scales are denoted in Figs. 6.1 and 6.5 by an orange diamond, or an orange arrow pointing up or down, when the corresponding loop-induced neutrino mass scale lies outside the range of the plot.

First Generation Yukawa Couplings As can be seen in Fig. 6.1, the exotic long-range or short-range contributions are mostly dominant, if only first generation Yukawa couplings are considered. The mass mechanism dominates just for about a fifth of the operators.

Although it could be naively expected that the contribution to the mass mechanism will be dominant for operators of dimension 7 and operators of dimension

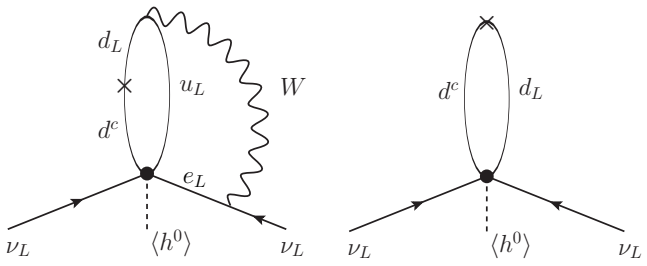

Figure 6.8: Dominant mass contribution of $\mathcal{O}_{3a}$ (left diagram) and $\mathcal{O}_{3b}$ (right diagram) to $0\nu\beta\beta$ decay.

9 containing three Higgs fields, it is not always so. For instance, operator $\mathcal{O}_{3a}$ includes the $SU(2)_L$ contraction $L_i L_j \epsilon_{ij}$, which requires a flip of one of the lepton legs (as explained earlier) suppressing the resulting mass contribution by additional loop factors. Therefore, the long-range contribution is the dominant one for $\mathcal{O}_{3a}$. In contrast, the $SU(2)_L$ structure $L_i L_j \epsilon_{ik} \epsilon_{jl}$ (or similar) present e.g. in $\mathcal{O}_{3b}$ does not lead to so significant suppression; hence, the corresponding mass contribution dominates. Both these mass contributions are given in Tab. 5.1 and illustrated in Fig. 6.8.

For operators of dimension 9 and higher the constraint given by the generated neutrino mass is expected to be generally weaker due to higher loop suppression and small Yukawa couplings. As indicated in Fig. 6.1, the corresponding scale of the loop-induced Weinberg operator is for most of these operators far too low to provide the desired light neutrino masses, and thus an additional mechanism of their generation would be needed. Hence, a potential observation of $0\nu\beta\beta$ decay would for most higher-dimensional operators hint at a dominant non-standard contribution. Nevertheless, there are a few exceptions like operator $\mathcal{O}_{44c}$, whose mass contribution is dominant, because it is proportional only to gauge couplings, see Fig. 5.4. Other operators with a similar behaviour are $\mathcal{O}_{27a}$, $\mathcal{O}_{27b}$, $\mathcal{O}_{29a}$, $\mathcal{O}_{29b}$ and $\mathcal{O}_{40a}$.

Third Generation Yukawa Couplings The interplay between the standard mass contribution and the non-standard ones becomes quite non-trivial, if third generation internal Yukawa couplings are considered. The suppression given by the loop factors can be in this case compensated or even outbalanced by the large values of Yukawa couplings. The fact that only internal Yukawas are enhanced further complicates the situation. As apparent from Fig. 6.5 approximately two thirds of the operators in question contribute dominantly to the mass mechanism,

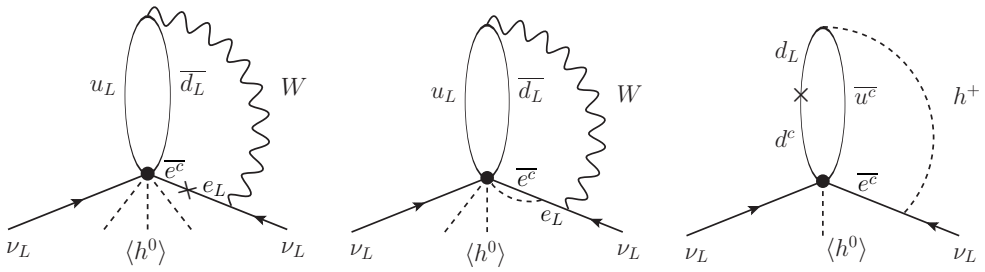

Figure 6.9: The left and center diagrams depict the dominant mass contributions ($\propto v^2/\Lambda$ and $\propto v^4/\Lambda^3$, respectively) generated by $\mathcal{O}_7$. The dominant mass contribution of $\mathcal{O}_8$ is shown on the right.

while the rest prefers an exotic $0\nu\beta\beta$ decay.

As one would expect, the mass contribution is dominant for almost all the operators of dimension 7 and dimension 9 with three Higgses. Only operators $\mathcal{O}_7$ and $\mathcal{O}_8$ contribute dominantly to a non-standard mechanism. The key difference of $\mathcal{O}_8$ is that it is the only 7-dimensional operator containing a right-handed lepton. This means that a Higgs insertion has to be used to flip the chirality and the associated small external Yukawa coupling suppresses the resulting contribution. For other operators of dimension 7 (e.g. $\mathcal{O}_{3a,3b,4a}$) such a flip is not required and an exchange of a gauge boson featuring much larger coupling can be employed. For a graphical illustration compare Fig. 6.9 with Fig. 6.8 and the relevant entries in Tab. 5.1. The reasoning is similar in case of operator $\mathcal{O}_7$, for which a more complicated loop structure including one small external Yukawa coupling is needed to trigger the mass mechanism, see Fig. 6.9. Again, this suppression is not present in mass contributions of similar operators $\mathcal{O}_{5,6}$, cf. Tab. 5.2.

In case of higher dimensional operators (dimension 9 and 11) the interplay is rather complex. It depends mostly on the external Yukawa couplings appearing in the mass contribution and on the specific properties of the non-standard contributions we compare it with. As the first example we can pick the operators $\mathcal{O}_{10}$, $\mathcal{O}_{11a}$ and $\mathcal{O}_{11b}$. Although all of them generate a similar long-range contribution, only $\mathcal{O}_{11b}$ contributes dominantly to the mass mechanism. The reason is that the other mass contributions are suppressed either by a small external Yukawa coupling ($\mathcal{O}_{10}$), or by an additional loop factor ($\mathcal{O}_{11a}$), neither of which is the case for $\mathcal{O}_{11b}$, cf. Fig. 6.10.

On the other hand, if we compare the operators $\mathcal{O}_{16}$, $\mathcal{O}_{17}$ and $\mathcal{O}_{18}$, we find the opposite behaviour. All these three operators contribute in the same way

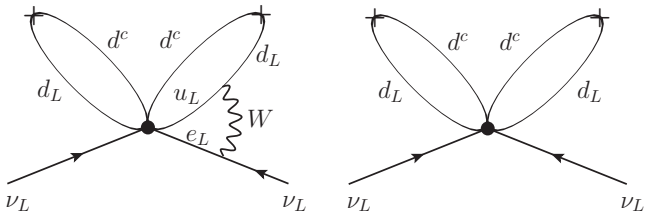

Figure 6.10: Dominant mass contribution of $\mathcal{O}_{11a}$ (left diagram) and $\mathcal{O}_{11b}$ (right diagram) to $0\nu\beta\beta$ decay.

to the mass mechanism. However, they feature different dominant long-range contributions (cf. Fig. 6.11) and only the one of $\mathcal{O}_{16}$ dominates also over the mass contribution. This is due to the fact that the long-range contribution of $\mathcal{O}_{16}$ is not, unlike those of $\mathcal{O}_{17,18}$, additionally suppressed by a loop factor or a small external Yukawa coupling.

The 9-dimensional operators $\mathcal{O}_{19}$, $\mathcal{O}_{20}$, $\mathcal{O}_{76}$ and the 11-dimensional operators $\mathcal{O}_{26a,b}$, $\mathcal{O}_{30a,b}$ and $\mathcal{O}_{34-38}$ contribute dominantly in a non-standard way, which is mostly caused by the fact that their mass contributions are suppressed by fixed external first generation Yukawa couplings.

In Tabs. 5.1, 5.2 and 5.3 we list the dominant contributions selected under the assumption of first generation Yukawa couplings only. However, all the possible ways of generation of the standard and the non-standard $0\nu\beta\beta$ decay contributions have been considered in our analysis summarized in Figs. 6.1-6.5. This approach becomes important e.g. in case of operator $\mathcal{O}_{29a}$ discussed in Sec. 5.2.2. Assuming first generation internal Yukawa couplings the dominant contribution

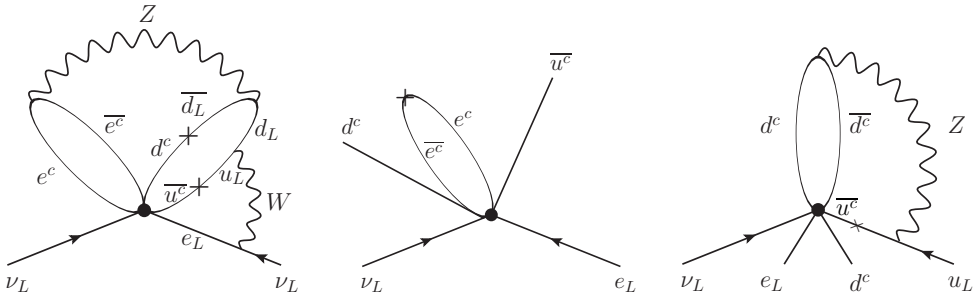

Figure 6.11: The left diagram shows the dominant mass contribution of $\mathcal{O}_{16}$ (similar for $\mathcal{O}_{17}$ and $\mathcal{O}_{18}$), whereas the other two diagrams depict the dominant long-range contributions of $\mathcal{O}_{16}$ (centre diagram) and $\mathcal{O}_{17}$ (right diagram) to $0\nu\beta\beta$ decay.

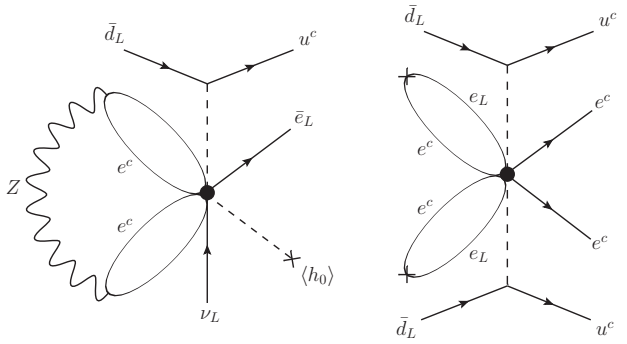

Figure 6.12: Long-range (left diagram) and short-range (right diagram) $0\nu\beta\beta$ decay contribution of $\mathcal{O}_{33}$.

of $\mathcal{O}_{29a}$ is the one in Eq. (5.32), whereas contribution in Eq. (5.33) dominates for third generation internal Yukawa couplings, cf. Fig 5.6. It is interesting to compare this behaviour with a similar operator $\mathcal{O}_{29b}$, which, due to different $SU(2)_L$ structure, induces only the contribution in Eq. (5.32).

6.2.5 An s-channel Contribution Example

Based on an example of a few 11-dimensional operators we will now discuss briefly the situations that require a heavy boson propagation to generate a $0\nu\beta\beta$ decay contribution. Specifically, we take operators $\mathcal{O}_{33}$ and $\mathcal{O}_{34}$. Although they have a structure similar to a number of other operators, there are slight differences in their particle content, which impact the possible $0\nu\beta\beta$ decay contributions.

The main issue is that the operators $\mathcal{O}_{33}$ and $\mathcal{O}_{34}$ contain more leptons than quarks; namely, the former one includes 6 leptons and no quarks, while the latter one consists of 4 leptons and 2 quarks. Hence, an exchange of at least two leptons for quarks is necessary in case of operator $\mathcal{O}_{33}$ in order to trigger $0\nu\beta\beta$ decay (via a long-range mechanism). This, however, supposes a propagation of a heavy boson as depicted in the left diagram in Fig. 6.12. The resulting long-range contribution is in consequence suppressed by a square of the heavy bosonic mass

$$\mathcal{O}_{33}^{LR} \propto \frac{y_d^{\text{ex}} g^2 v}{(16\pi^2)^3 \Lambda} \frac{1}{m_H^2}. \tag{6.28}$$

From the loop reduction shown in Fig. 6.12 it is apparent that this contribution must be subleading with respect to the standard mass mechanism. The reason is that the originally 11-dimensional operator is first reduced down to the Weinberg operator, and subsequently a Yukawa vertex is attached to it. For this reason our

analysis does not cover the operators of this type and e.g. operators $\mathcal{O}_2, \mathcal{O}_9, \mathcal{O}_{22}$ or $\mathcal{O}_{39}$ are skipped.

If we want to induce a short-range $0\nu\beta\beta$ decay contribution from operator $\mathcal{O}_{33}$, it is necessary to include a pair of the s-channel-like transitions, see the right diagram in Fig. 6.12. Clearly, this leads to even stronger suppression.

The situation is slightly better in case of operator $\mathcal{O}_{34}$ consisting of 4 leptons and 2 quarks. The long-range $0\nu\beta\beta$ decay contribution can be generated at two-loop level without any 's-channel' rule and a single heavy boson propagation providing two additional quarks is needed for the short-range mechanism.

For both operators $\mathcal{O}_{33}$ and $\mathcal{O}_{34}$ multiple long-range contributions exciting different effective couplings ϵ_α^β can be found. All of these contributions have the same form and they differ only by the type of a single external Yukawa coupling. Similarly, more distinct short-range contributions can be obtained, but they are always sub-dominant, when compared to the long-range ones.

6.3 Washout in UV-Complete Models

For the sake of generality, we have employed the model-independent effective approach to describe new lepton number violating interactions with origin at a certain high energy scale Λ. In order to test the applicability and investigate potential limits of our treatment, let us now compare the lepton number washout rate of a particular effective operator with the analogous calculation performed within an underlying UV theory. Specifically, we pick the operator $\mathcal{O}_8 = L^i \bar{e^c} \bar{u^c} d^c H^j \epsilon_{ij}$ as an example and we assume it arises from a left-right symmetric model, see Sec. 3.7, after the right-handed gauge boson W_R and the right-handed neutrino N are integrated out. To keep the calculation simple and to emphasize the impact of the resonant enhancement from on-shell W_R or N we will consider only two of all possible permutations of the particles in the initial and the final state. Namely, we will focus on washout processes $\bar{u^c} d^c \leftrightarrow \bar{L} e^c \bar{H}$ and $LH \leftrightarrow e^c u^c \bar{d^c}$, which are for the case of the LRSM illustrated in Fig. 6.13. After computing the relevant scattering amplitudes we make use of Eq. (6.6) to determine the corresponding thermal rate. At the same time, we calculate the washout rate induced by these two processes assuming they are triggered by the effective operator $\mathcal{O}_8$. We estimate the decay widths of W_R and N as

$$\Gamma_{W_R} = \frac{g_R^2 m_{W_R}}{8\pi} \quad \text{and} \quad \Gamma_N = \frac{m_N}{8\pi} \left(y_\nu^2 + \frac{g_R^4}{24\pi^2} \frac{m_N^4}{m_{W_R}^4} \right), \tag{6.29}$$

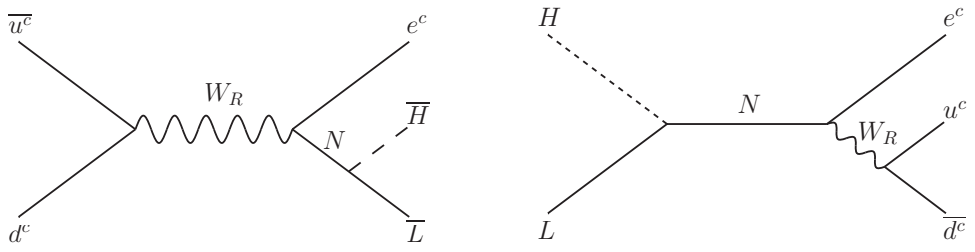

Figure 6.13: Feynman graphs of the chosen washout processes within a left-right symmetric model framework, which give rise to the effective operator $\mathcal{O}_8 = L^i \bar{e^c} \bar{u^c} d^c H^j \epsilon_{ij}$.

respectively. Here, g_R denotes the right-handed gauge coupling and y_ν stands for the neutrino Yukawa coupling. To ensure that the effective approach and the underlying UV theory yield the same result in the limit, where the transferred momentum is much smaller than m_{W_R} and m_N, we set $g_R^2 y_\nu / (m_{W_R}^2 m_N) = 1/\Lambda^3$.

The resulting interaction rates normalized with respect to the Hubble expansion rate Γ_W / H are plotted in Fig. 6.14 in dependence on temperature T. While the washout rate produced by the UV processes $\bar{u^c} d^c \leftrightarrow \bar{L} e^c \bar{H}$ and $LH \leftrightarrow e^c u^c \bar{d^c}$ is indicated by the blue and red lines, respectively, the straight purple line shows the rate of the effective operator matched to the sum of the two UV processes. Based on our previous calculation we take the value of the effective operator scale to be $\Lambda = 7 \times 10^4$ GeV (see Fig. 6.1) and it is related to the couplings and masses of the LRSM as stated earlier. In Fig. 6.14 we display two plots corresponding to two different sets of couplings, namely $(g_R, y_\nu) = (1, 1)$ (left panel) and $(g_R, y_\nu) = (1, 10^{-3})$ (right panel). As for the heavy masses, we set $m_{W_R} = 1.5\, m_N$ in both cases. Given the fixed operator scale the larger are the considered couplings, the larger become also the masses m_{W_R} and m_N and the corresponding resonance enhancement moves towards higher temperatures. Comparing the washout rates we can see that for low temperatures the results obtained from the effective operator are consistent with the UV theory. On the other hand, at temperatures much larger than the masses m_{W_R} and m_N the effective approach breaks down and becomes unphysical, whereas the rate of UV processes is proportional to T. This means that the washout becomes inefficient in the given temperature region, because the Hubble expansion rate grows with T^2. Clearly, the smaller are the values of couplings g_R and y_ν, the lower is the temperature at which the lepton number departures from thermal equilibrium.

Based on the above comparison, we can state that our conclusions regarding

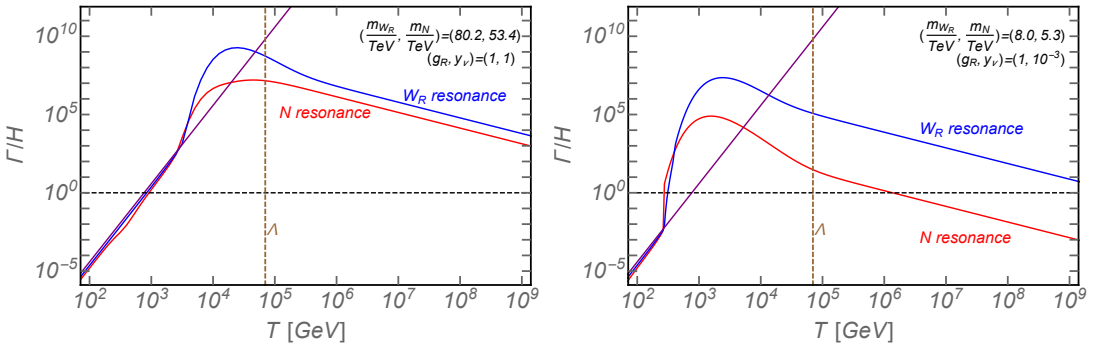

Figure 6.14: The temperature dependence of the lepton number washout rate induced by the UV processes $\bar{u^c}d^c \leftrightarrow \bar{L}e^c\bar{H}$ (blue) and $LH \leftrightarrow e^c u^c \bar{d^c}$ (*red*), and the rate given by the sum of these two processes (*purple*) when triggered by the effective operator $\mathcal{O}_8$ with the corresponding scale fixed to $\Lambda = 7 \times 10^4$ GeV. Two plots for two different sets of values of the right-handed gauge coupling g_R and the neutrino Yukawa coupling y_ν are shown. In each case we also display the chosen masses of the heavy particles.

the lepton number washout obtained using the effective operators are expected to hold even in a UV-complete model, since both the approaches should yield the same results at low energies. Therefore, unless the couplings in the UV theory are so small that the corresponding new particles have masses near or below the EW scale, a pre-existing lepton number asymmetry above the scale $\hat{\lambda}_D$ will be indeed erased, as concluded earlier. Moreover, within a UV-complete model the washout remains, in principle, effective also in the region above the cut-off scale Λ. In dependence on a particular model the resonance enhancement can in fact result in even stronger washout than the one generated within the effective approach. Note, however, that LNV can arise from spontaneous symmetry breaking - for example, in case of LRSM the $B - L$ symmetry is broken by the triplet Higgs VEVs $\langle \Delta_{L,R} \rangle$. In such case the lepton number washout processes are expected to cease to work for temperatures above the breaking scale, where the symmetry in question is restored.

6.4 Caveats and Loopholes

To complete the discussion of our study we should also comment on several limitations of the applied approach. The first of them relates to lepton flavour.

As $0\nu\beta\beta$ decay involves only electrons, our conclusions about the washout are restricted to the first generation of leptons, while the pre-existing lepton asymmetry can be stored also in the μ and τ sectors. Hence, to generalize our results to all leptons we have to make sure that the other lepton flavour asymmetries are equilibrated as well. This can be achieved e.g. by observing lepton flavour violation (LFV) effective around the same temperatures [133], or by processes violating lepton number directly in μ and τ sectors such as meson decays and direct searches at the LHC [132]. At lowest order the rare lepton flavour violating interactions are described by 6-dimensional operators of the form: $\mathcal{O}_{\ell\ell\gamma} = \mathcal{C}_{\ell\ell\gamma}\bar{L}_\ell\sigma^{\mu\nu}\bar{\ell}^c H F_{\mu\nu}$ and $\mathcal{O}_{\ell\ell qq} = \mathcal{C}_{\ell\ell qq}(\bar{\ell}\,\Pi_1\ell)(\bar{q}\,\Pi_2 q)$ (Π_i stands for possible Lorentz structures), with $\ell = e, \mu, \tau$. The corresponding operator scales can be probed by low energy LFV observables such as the following decay branching ratios (with current limits at 90% C.L.): $\mathrm{Br}_{\mu\to e\gamma} < 5.7 \times 10^{-13}$ [249], $\mathrm{Br}_{\tau\to\ell\gamma} \lesssim 4.0 \times 10^{-8}$ ($\ell = e, \mu$) [182] and the $\mu - e$ conversion rate $\mathrm{R}^{\mathrm{Au}}_{\mu\to e} < 7.0 \times 10^{-13}$ [182]. Employing these experimental limits, we can calculate the approximate bounds on the operator scales as: $\Lambda_{\mu e\gamma} \approx 3 \times 10^6$ GeV, $\Lambda_{\tau\ell\gamma} \approx 3 \times 10^4$ GeV and $\Lambda_{\mu eqq} \approx 2 \times 10^5$ GeV, respectively [133]. Using the same procedure as in the case of LNV we can then determine the temperature intervals $[\lambda_i, \Lambda_i]$, within which the individual flavour number asymmetries are equilibrated. If this interval overlaps with the temperature range of effective electron number washout derived from limit on $0\nu\beta\beta$ decay half life, then the asymmetries in muon and tauon numbers will be efficiently wiped out, too. The temperature intervals for the LFV operators were calculated in [133] and we reprint here the resulting plot, see Fig. 6.15. As can be seen, there are significant overlaps between the lepton number washout intervals corresponding to examples of higher-dimensional (dimension 7, 9 and 11) $\Delta L = 2$ SM effective operators and the ranges of LFV operators $\Lambda_{\tau\ell\gamma}$ and $\Lambda_{\mu eqq}$, if observation of $0\nu\beta\beta$ decay and LFV at near-future experimental sensitivities is assumed. The temperature interval of the operator $\Lambda_{\mu e\gamma}$ lies at higher temperatures (due to more stringent lower limit on corresponding operator scale), and thus it does not overlap with the washout ranges of most of the studied $\Delta L = 2$ operators. In Fig. 6.15 the washout range for the Weinberg operator is also shown to manifest that this standard $0\nu\beta\beta$ decay mechanism would not necessarily falsify the high-scale baryogenesis, as the lower limit for strong washout is around 10^{12} GeV.

The next limitation of our analysis is the fact that in order to keep the calculations model-independent we assume the baryon asymmetry to be generated by a mechanism unrelated to the studied washout effects. The underlying UV

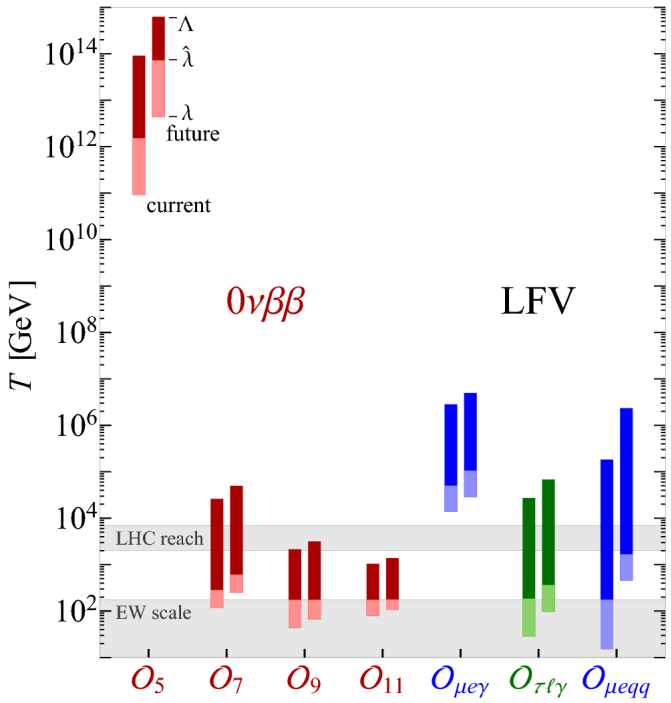

Figure 6.15: Comparison of temperature intervals in which the LNV and LFV operators are in equilibrium assuming observation of the corresponding observable at current/future (left/right bars) sensitivity; taken from Ref. [133]. The subscripts of the LNV operators denote their dimensions here. Hence, $\mathcal{O}_5$ is the Weinberg operator, while the operators $\mathcal{O}_{7,9,11}$ are examples of higher dimensional LNV operators.

theory, however, can be responsible not only for the lepton number washout but also for generation of the lepton number asymmetry. In such a scenario the implications for baryogenesis would have to be studied within the full UV-complete model. Our approach can be employed only with asymmetries created above temperatures, at which the washout becomes efficient.

Another possible loophole is a scenario pointed out in Refs. [250, 251], which assumes the existence of a decoupled sector sharing the baryon asymmetry with the visible sector. In such a case the lepton number asymmetry cannot be washed out completely in the visible sector. The reason is that during very early times, when the later decoupled sector still communicated with the visible one, it shared also a hypercharge $U(1)_Y$ asymmetry. Since the lepton number washout interactions preserve the hypercharge, they cannot washout the part of lepton number asymmetry proportional to $U(1)_Y$ asymmetry. The asymmetry from the decou-

pled sector can evade the washout effects, if it is transformed back into the visible sector after the EW phase transition, when the sphaleron transitions become ineffective. To this end, the asymmetry can be carried by long-lived particles decaying to SM particles only below the EW scale, or the efficiency of the conversion between the two sectors rises after the EW symmetry breaking as a consequence of the expansion rate scaling like $T^2/\Lambda_{\rm Pl}$.

Despite all the possible loopholes, if $0\nu\beta\beta$ decay is observed, it will open new possibilities to test not only the neutrino mass generation mechanisms but also various baryogenesis scenarios. Although the usual high-scale seesaw mechanism with origin at energies $10^9 - 10^{14}$ GeV is still the favoured scheme, other Majorana neutrino mass mechanisms close above the EW scale are of great phenomenological interest. These would clearly imply the presence of LNV at accessible energies and they would generally lead to new contributions to $0\nu\beta\beta$ decay. To use the argument regarding high-scale baryogenesis that we put forward in this work it is crucial to be able to discriminate among different $0\nu\beta\beta$ decay mechanisms, particularly, to distinguish between the standard mass mechanism and the exotic contributions. As discussed in Subsec. 3.5.3, there are several ways to do so. For instance, based on our results it is apparent that the scales as well as the washout ranges for many of the $\Delta L = 2$ operators are $\mathcal{O}$(TeV) assuming an observation of $0\nu\beta\beta$ decay in planned experiments with a sensitivity of $T_{1/2} \approx 10^{27}$ y. Hence, the underlying new physics in a number of cases lies within the reach of the LHC or future collider experiments. As a result, a potential $0\nu\beta\beta$ decay signal and non-observation of LNV at colliders could exclude some of the exotic $0\nu\beta\beta$ decay mechanisms.

7

Conclusion and Outlook

With no clear signal of new physics at the LHC[1] we are, slowly but surely, entering a new era of particle physics that will be most likely dominated by both experimental and theoretical efforts and potential discoveries in the fields of astroparticle physics, particle cosmology and undoubtedly also neutrino physics. One of the prime roles in the quest for a better understanding of neutrinos will be played by $0\nu\beta\beta$ decay searches. The consequences of its observation would be profound, as it would not only represent the first evidence of lepton number violation, but it could also help to unveil the origin of light neutrino masses and possibly open a pathway towards new physics beyond the SM.

At the same time, $0\nu\beta\beta$ decay could have interesting implications beyond light neutrinos. The reason is that lepton number violation can be related to another aspect of BSM physics; namely, to the baryon asymmetry of the Universe. As the $(B+L)$ symmetry is violated in the SM by sphaleron effects, generation of a primordial asymmetry in $(B-L)$ number is necessary for explanation of the baryon asymmetry that we observe today. However, an experimental evidence of $0\nu\beta\beta$ decay would imply some underlying $\Delta L = 2$ processes to be in equilibrium at a certain energy scale, where they would washout any net lepton number. Moreover, in combination with sphalerons these could washout also the preexisting $(B-L)$ asymmetry. This connection therefore allows to relate low-energy lepton number violating phenomena with interactions non-conserving $(B-L)$ number at high scales.

In the present work we have focussed particularly on the non-standard mechanisms of $0\nu\beta\beta$ decay. At the nuclear physics scale ~ 100 MeV, these mechanisms can be described in a model-independent way by a general low-energy $0\nu\beta\beta$ decay Lagrangian. Generally, there are two types of these mechanisms, long-range and short-range, triggered by effective operators of dimension 6 and 9, respectively, associated with effective couplings $\epsilon_{\rm LR} \approx \left(\frac{100\ \rm GeV}{\Lambda_{\rm NP}}\right)^3$ and $\epsilon_{\rm SR} \approx \left(\frac{40\ \rm GeV}{\Lambda_{\rm NP}}\right)^5$

[1] Although recently, the observation of lepton flavour anomalies challenging the lepton universality predicted by the SM has attracted a lot of attention [76].

with $\Lambda_{\rm NP}$ denoting the new physics scale. After reviewing briefly the long-range mechanisms, we concentrate in Chapter 4 primarily on the short-range operators developing a general formalism of their microscopic description. We derive the decay rate of these mechanisms and specify the involved nuclear matrix elements and phase space factors. The numerical values of the phase space factors have been computed and we also present the single electron energy distributions as well as the angular correlation distributions of the two emitted electrons. Further, we have provided a systematic derivation of short-range nuclear matrix elements taking into account the effect of the enhanced pseudoscalar form factors in all relevant nucleon current products. Employing the experimental limits on $0\nu\beta\beta$ decay half life we have estimated the numerical bounds on the effective couplings characterizing the involved particle physics in case of each short-range operator. We have also discussed the effect of QCD-running on these bounds assuming the new physics to lie around scale $\Lambda_{\rm NP} = 1$ TeV.

The numerical limits on the effective new physics parameters ϵ_I corresponding to individual short-range mechanisms range between $\epsilon_I \approx 10^{-10}$ to 10^{-7}. Since the couplings relate to the typical scale of the 9-dimensional effective operators as $\epsilon_I \propto 1/\Lambda^5_{\rm NP}$, these values correspond to probing new physics in the phenomenologically highly interesting multi-TeV region. This is why a systematic treatment as above is crucial. We have also found that the angular correlations differ for two groups of short-range mechanisms, which would potentially allow to distinguish them experimentally in certain $0\nu\beta\beta$ decay searches, e.g. SuperNEMO [112]. Another possibility to discriminate the $0\nu\beta\beta$ decay mechanism favoured by Nature is to measure the single electron energy distribution (also possible by SuperNEMO) and compare it with the obtained theoretical predictions, although this would require a solid energy resolution of the experiment. All these aspects then could lead to a better understanding of the mechanism of neutrino mass generation.

After describing the low-energy effective operators in Chapter 5 we study lepton number violation at the SM level, where it can be described by the SM-invariant $\Delta L = 2$ effective operators containing SM fermions and Higgs boson. Interestingly, operators violating lepton number appear only at odd dimensions in Standard Model Effective Field Theory. We concentrate on operators of dimensions 7, 9 and a representative selection of 11-dimensional operators, which are collected in Tabs. 5.1, 5.2 and 5.3, respectively. We have also used the Hilbert Series method [78, 215] to check the completeness of operators identifying small discrepancies.

Considering each of these operators individually we have performed a detailed analysis of their contributions to $0\nu\beta\beta$ decay. Some of the operators that have the right particle content trigger $0\nu\beta\beta$ decay directly at tree level, while others induce it only at a certain loop level. As it would have been clearly overwhelming to derive all the possible contributions manually, we have addressed the issue algorithmically developing a code scanning through all possible loop contractions and recognizing the radiative corrections that trigger $0\nu\beta\beta$ decay. For all the studied operators we have determined dominant contributions to the mass, long-range and short-range mechanisms, which are all displayed in Tabs. 5.1 - 5.3. As we have discussed in detail for particular examples, the involved phenomenology is very rich and there are a number of features influencing the dominance of different contributions. The radiatively generated neutrino mass scales have been compared with the results in Ref. [214] and a few differences have been pointed out and explained. Employing the dominant long-range and short-range contributions and assuming a hypothetical observation of $0\nu\beta\beta$ decay at the expected future sensitivity $T_{1/2}^{\mathrm{Xe}} = 10^{27}$ y we have calculated the cut-off scales associated with the $\Delta L = 2$ SM effective operators. These scales range from the electroweak scale to 10^6 GeV and are generally lower for higher-dimensional operators (dimensions 9 and 11). The internal Yukawa couplings, i.e. those that are not attached to any of the external legs, are free in flavour and should be summed over. In our approach we estimate this possible enhancement by calculating the washout in two cases: for first and third generation internal Yukawa couplings. While the consideration of third generation internal Yukawa couplings does not affect the scales of dimension-7 operators, it enhances the rather low scales of most of the higher-dimensional operators. Nonetheless, the third generation internal Yukawas increase importantly also the contributions to the standard mass mechanism, which then in many cases become dominant.

Subsequently, using the operator scales we have computed in Chapter 6 the washout rate of lepton number asymmetry in the early Universe for every operator by solving the corresponding Boltzmann equation. We assume $\mathcal{O}(1)$ lepton number asymmetry to be injected at a certain scale, from which point on only the washout from a single $\Delta L = 2$ SM effective operator on top of the usual SM interactions (including sphaleron transitions) is taken into account. Each operator can trigger a variety of different lepton number violating interactions; therefore, all permutations of particles in the initial and final states corresponding to physically distinctive processes have been accounted for in the washout calculation. As

a result, we have determined the temperature intervals of efficient lepton number asymmetry washout for each of the $\Delta L = 2$ SM effective operators. While the upper limit of these ranges is simply given by the operator scale Λ, two different lower bounds were always determined: first, scale λ was calculated by imposing the cosmological condition that the washout rate overbalances the Hubble rate and second, scale $\hat{\lambda}$ was obtained by solving the Boltzmann equation exactly assuming the primordial lepton asymmetry to be of order one and requiring the surviving asymmetry to match the observed value of baryon asymmetry. The latter lower limit is always slightly higher restricting the interval of strong washout. Based on these results the scale above which any pre-existing lepton and baryon asymmetry will be erased by the given operator can be inferred. Assuming the observation of $0\nu\beta\beta$ decay at $T_{1/2} = 10^{27}$ y, the strong washout for 7-dimensional operators can be as high as $[\hat{\lambda}, \Lambda] \approx [2\times10^3, 3\times10^5]$ GeV, whereas the operators of dimension 9 and 11 usually washout the asymmetry between 100 GeV and 1 TeV provided that first generation Yukawas are considered. As we have discussed, the 7-dimensional operators are therefore generally restricted more stringently from the mass contribution and the requirement of tiny neutrino mass, which is typically not the case for the higher-dimensional operators.

Based on the results summarized in Figs. 6.1 and 6.5 we have concluded that a signal of non-standard $0\nu\beta\beta$ decay at upcoming experimental sensitivity would imply a washout of primordial baryon and lepton asymmetry, and therefore falsify mechanisms of high-scale ($\gtrsim$ TeV) baryogenesis. On the other hand, if the mass contribution to $0\nu\beta\beta$ decay is dominant, then the origin of neutrino mass lies most likely at high energies favouring the standard leptogenesis mechanism of baryon asymmetry generation. The crucial aspect of discriminating different $0\nu\beta\beta$ decay mechanisms could be managed either by some of the $0\nu\beta\beta$ decay experiments, or by probing lepton number violation in other observables (colliders). The former possibility could, for instance, rely on the angular correlation of the emitted electrons, which can differ for distinct exotic contributions, as we have shown explicitly when analysing the short-range mechanisms in Chapter 4. In fact, for our argument the important thing is to distinguish the standard mass mechanism from any non-standard one. In this regard, observation of lepton number violation at the LHC or in meson decays would be decisive, pointing to exotic $0\nu\beta\beta$ decay.

Generally, our analysis clearly proves the importance of connecting effects of BSM physics in laboratory experiments and in early universe cosmology. A similar approach could be employed to study lepton flavour violating operators,

which, as they have the potential to equilibrate flavours at a certain scale, could affect the mechanisms of flavoured leptogenesis [252, 253]. It is also possible to develop similar connections in other contexts. An example is an analogous interplay between Dark Matter thermalization and detection at the LHC [254]. The contribution of our study can be summarized by stating that not only would the observation of $0\nu\beta\beta$ decay teach us a lot about neutrinos, but it could also help to explain the origin of matter in the Universe. Consequently, we do not necessarily exaggerate if we conclude that $0\nu\beta\beta$ decay could play an important role in unveiling the secrets of our existence.

Bibliography

[1] S. L. Glashow, Nucl. Phys. **22**, 579 (1961).

[2] S. Weinberg, Phys. Rev. Lett. **19**, 1264 (1967).

[3] A. Salam, Conf. Proc. **C680519**, 367 (1968).

[4] R. P. Feynman, Phys. Rev. Lett. **23**, 1415 (1969).

[5] J. D. Bjorken and E. A. Paschos, Phys. Rev. **185**, 1975 (1969).

[6] D. J. Gross and F. Wilczek, Phys. Rev. Lett. **30**, 1343 (1973).

[7] H. D. Politzer, Phys. Rev. Lett. **30**, 1346 (1973).

[8] Super-Kamiokande collaboration, Y. Fukuda *et al.*, Phys. Rev. Lett. **81**, 1562 (1998), [hep-ex/9807003].

[9] SNO collaboration, Q. R. Ahmad *et al.*, Phys. Rev. Lett. **87**, 071301 (2001), [nucl-ex/0106015].

[10] M. C. Gonzalez-Garcia, M. Maltoni and T. Schwetz, Nucl. Phys. **B908**, 199 (2016), [1512.06856].

[11] F. Couchot *et al.*, Astron. Astrophys. **606**, A104 (2017), [1703.10829].

[12] KATRIN collaboration, A. Osipowicz *et al.*, hep-ex/0109033.

[13] S. Weinberg, Phys.Rev.Lett. **43**, 1566 (1979).

[14] P. Minkowski, Phys.Lett. **B67**, 421 (1977).

[15] R. N. Mohapatra and G. Senjanovic, Phys. Rev. Lett. **44**, 912 (1980).

[16] T. Yanagida, Conf. Proc. **C7902131**, 95 (1979).

[17] M. Gell-Mann, P. Ramond and R. Slansky, Conf.Proc. **C790927**, 315 (1979), [1306.4669].

[18] J. Schechter and J. W. F. Valle, Phys. Rev. **D22**, 2227 (1980).

[19] S. L. Adler, Phys.Rev. **177**, 2426 (1969).

[20] J. S. Bell and R. Jackiw, Nuovo Cim. **A60**, 47 (1969).

[21] Planck Collaboration, P. A. R. Ade *et al.*, Astron.Astrophys. **571**, A16 (2014), [1303.5076].

[22] M. Fukugita and T. Yanagida, Phys. Lett. **B174**, 45 (1986).

[23] F. Reines and C. L. Cowan, Phys. Rev. **113**, 273 (1959).

[24] E. Fermi, Zeitschrift für Physik **88**, 161 (1934).

[25] C. S. Wu, E. Ambler, R. W. Hayward, D. D. Hoppes and R. P. Hudson, Phys. Rev. **105**, 1413 (1957).

[26] H. Weyl, Zeitschrift für Physik **56**, 330 (1929).

[27] R. P. Feynman and M. Gell-Mann, Phys. Rev. **109**, 193 (1958).

[28] N. Cabibbo, Phys. Rev. Lett. **10**, 531 (1963).

[29] G. 't Hooft and M. J. G. Veltman, Nucl. Phys. **B44**, 189 (1972).

[30] J. C. Maxwell, Phil. Trans. Roy. Soc. Lond. **155**, 459 (1865).

[31] P. A. M. Dirac, Proc. Roy. Soc. Lond. **A114**, 243 (1927).

[32] C. N. Yang and R. L. Mills, Phys. Rev. **96**, 191 (1954).

[33] P. W. Anderson, Phys. Rev. **130**, 439 (1963).

[34] P. W. Higgs, Phys. Rev. Lett. **13**, 508 (1964).

[35] F. Englert and R. Brout, Phys. Rev. Lett. **13**, 321 (1964).

[36] G. S. Guralnik, C. R. Hagen and T. W. B. Kibble, Phys. Rev. Lett. **13**, 585 (1964).

[37] A. A. Migdal and A. M. Polyakov, Sov. Phys. JETP **24**, 91 (1967), [Zh. Eksp. Teor. Fiz.51,135(1966)].

[38] Y. Nambu, Phys. Rev. **117**, 648 (1960).

[39] J. Goldstone, Nuovo Cim. **19**, 154 (1961).

[40] N. Cabibbo, Phys. Rev. Lett. **10**, 531 (1963).

[41] M. Kobayashi and T. Maskawa, Prog. Theor. Phys. **49**, 652 (1973).

[42] UA1, G. Arnison *et al.*, Phys. Lett. **B126**, 398 (1983).

[43] UA1, G. Arnison *et al.*, Phys. Lett. **B122**, 103 (1983).

[44] UA2, P. Bagnaia *et al.*, Phys. Lett. **B129**, 130 (1983).

[45] UA2, M. Banner *et al.*, Phys. Lett. **B122**, 476 (1983).

[46] M. Gell-Mann, Phys. Rev. **125**, 1067 (1962).

[47] PLUTO, C. Berger *et al.*, Phys. Lett. **82B**, 449 (1979).

[48] PLUTO, C. Berger *et al.*, Z. Phys. **C8**, 101 (1981).

[49] S. L. Glashow, J. Iliopoulos and L. Maiani, Phys. Rev. D **2**, 1285 (1970).

[50] M. Kobayashi and T. Maskawa, Progress of Theoretical Physics **49**, 652 (1973).

[51] J. E. Augustin *et al.*, Phys. Rev. Lett. **33**, 1406 (1974).

[52] J. J. Aubert *et al.*, Phys. Rev. Lett. **33**, 1404 (1974).

[53] S. W. Herb *et al.*, Phys. Rev. Lett. **39**, 252 (1977).

[54] CDF Collaboration, F. Abe *et al.*, Phys. Rev. Lett. **74**, 2626 (1995).

[55] D0 Collaboration, S. Abachi *et al.*, Phys. Rev. Lett. **74**, 2422 (1995).

[56] ATLAS Collaboration, G. Aad *et al.*, Phys.Lett. **B716**, 1 (2012), [1207.7214].

[57] CMS Collaboration, S. Chatrchyan *et al.*, Phys.Lett. **B716**, 30 (2012), [1207.7235].

[58] T. Aoyama, T. Kinoshita and M. Nio, Phys. Rev. **D97**, 036001 (2018), [1712.06060].

[59] D. Hanneke, S. Fogwell and G. Gabrielse, Phys. Rev. Lett. **100**, 120801 (2008), [0801.1134].

[60] D. Hanneke, S. F. Hoogerheide and G. Gabrielse, Phys. Rev. **A83**, 052122 (2011), [1009.4831].

[61] S. Weinberg, Phys. Rev. **D13**, 974 (1976), [Addendum: Phys. Rev.D19,1277(1979)].

[62] A. D. Sakharov, Pisma Zh. Eksp. Teor. Fiz. **5**, 32 (1967).

[63] Supernova Search Team, A. G. Riess *et al.*, Astron. J. **116**, 1009 (1998), [astro-ph/9805201].

[64] Supernova Cosmology Project, S. Perlmutter *et al.*, Astrophys. J. **517**, 565 (1999), [astro-ph/9812133].

[65] R. D. Peccei and H. R. Quinn, Phys. Rev. Lett. **38**, 1440 (1977).

[66] R. D. Peccei and H. R. Quinn, Phys. Rev. **D16**, 1791 (1977).

[67] A. Kusenko, Phys. Rept. **481**, 1 (2009), [0906.2968].

[68] J. Ellis and K. A. Olive, 1001.3651.

[69] R. H. Dicke, *Gravitation and the Universe* (Amer Philosophical Society, 1970).

[70] W. Rindler, Gen. Rel. Grav. **34**, 133 (2002), [Mon. Not. Roy. Astron. Soc.116,662(1956)].

[71] A. R. Liddle, *An introduction to modern cosmology* (Chichester, UK: Wiley (1998) 129 p, 1998).

[72] A. H. Guth, Phys. Rev. **D23**, 347 (1981).

[73] A. D. Linde, Phys. Lett. **108B**, 389 (1982).

[74] A. Albrecht and P. J. Steinhardt, Phys. Rev. Lett. **48**, 1220 (1982).

[75] Muon g-2, W. Gohn, 1801.00084.

[76] ATLAS, LHCb, CMS, E. Graverini, Conf. Proc. **C18-06-17** (2018), [1807.11373].

[77] I. Brivio and M. Trott, 1706.08945.

[78] B. Henning, X. Lu, T. Melia and H. Murayama, JHEP **08**, 016 (2017), [1512.03433].

[79] A. Kobach, Phys. Lett. **B758**, 455 (2016), [1604.05726].

[80] H. K. Dreiner, H. E. Haber and S. P. Martin, Phys. Rept. **494**, 1 (2010), [0812.1594].

[81] C. Giganti, S. Lavignac and M. Zito, Prog. Part. Nucl. Phys. **98**, 1 (2018), [1710.00715].

[82] S. Mikheev and A. Smirnov, Sov.J.Nucl.Phys. **42**, 913 (1985).

[83] L. Wolfenstein, Phys.Rev. **D17**, 2369 (1978).

[84] Particle Data Group, C. Patrignani *et al.*, Chin. Phys. **C40**, 100001 (2016).

[85] KM3Net, S. Adrian-Martinez *et al.*, J. Phys. **G43**, 084001 (2016), [1601.07459].

[86] MiniBooNE, A. A. Aguilar-Arevalo *et al.*, Phys. Rev. Lett. **121**, 221801 (2018), [1805.12028].

[87] LSND collaboration, A. Aguilar *et al.*, Phys. Rev. **D64**, 112007 (2001), [hep-ex/0104049].

[88] Planck, M. Lattanzi, J. Phys. Conf. Ser. **718**, 032008 (2016).

[89] E. W. Otten and C. Weinheimer, Rept. Prog. Phys. **71**, 086201 (2008), [0909.2104].

[90] Planck Collaboration, P. A. R. Ade *et al.*, Astron. Astrophys. **594**, A13 (2016), [1502.01589].

[91] GERDA, M. Agostini *et al.*, J. Phys. **G40**, 035110 (2013), [1212.3210].

[92] CUORE, C. Alduino *et al.*, Eur. Phys. J. **C77**, 13 (2017), [1609.01666].

[93] NEMO-3, R. Arnold *et al.*, Phys. Rev. **D93**, 112008 (2016), [1604.01710].

[94] W. Furry, Phys.Rev. **56**, 1184 (1939).

[95] J. Gomez-Cadenas, J. Martin-Albo, M. Mezzetto, F. Monrabal and M. Sorel, Riv.Nuovo Cim. **35**, 29 (2012), [1109.5515].

[96] W. Rodejohann, Int.J.Mod.Phys. **E20**, 1833 (2011), [1106.1334].

[97] J. J. Gomez-Cadenas *et al.*, JCAP **1106**, 007 (2011), [1010.5112].

[98] R. Henning, Rev. Phys. **1**, 29 (2016).

[99] K. Ackermann, Eur. J. Phys., C **73**, 2330 (2013).

[100] Majorana, N. Abgrall *et al.*, Adv. High Energy Phys. **2014**, 365432 (2014), [1308.1633].

[101] LEGEND, N. Abgrall *et al.*, AIP Conf. Proc. **1894**, 020027 (2017), [1709.01980].

[102] CUORE, C. Arnaboldi *et al.*, Nucl. Instrum. Meth. **A518**, 775 (2004), [hep-ex/0212053].

[103] M. Chen, Nuclear Physics B - Proceedings Supplements **145**, 65 (2005), NOW 2004.

[104] SNO+, J. Dunger, PoS **EPS-HEP2017**, 104 (2017).

[105] SNO+, E. Caden, Conf. Proc. **C17-07-24** (2017), [1711.11094].

[106] KamLAND-Zen, A. Gando *et al.*, Phys. Rev. **C85**, 045504 (2012), [1201.4664].

[107] KamLAND-Zen, J. Shirai, PoS **NEUTEL2017**, 027 (2018).

[108] M. Auger *et al.*, JINST **7**, P05010 (2012), [1202.2192].

[109] nEXO, B. Mong, PoS **HQL2016**, 074 (2017).

[110] M. Agostini, G. Benato and J. Detwiler, Phys. Rev. **D96**, 053001 (2017), [1705.02996].

[111] NEXT, V. Alvarez *et al.*, JINST **7**, T06001 (2012), [1202.0721].

[112] SuperNEMO, R. Arnold *et al.*, Eur. Phys. J. **C70**, 927 (2010), [1005.1241].

[113] GERDA, M. Agostini *et al.*, Nature **544**, 47 (2017), [1703.00570].

[114] KamLAND-Zen, A. Gando *et al.*, Phys. Rev. Lett. **117**, 082503 (2016), [1605.02889], [Addendum: Phys. Rev. Lett.117, no.10, 109903 (2016)].

[115] F. F. Deppisch, M. Hirsch and H. Päs, J.Phys. **G39**, 124007 (2012), [1208.0727].

[116] J. Schechter and J. Valle, Phys.Rev. **D25**, 2951 (1982).

[117] J. F. Nieves, Phys.Lett. **B147**, 375 (1984).

[118] E. Takasugi, Phys.Lett. **B149**, 372 (1984).

[119] M. Doi, T. Kotani, H. Nishiura and E. Takasugi, Prog.Theor.Phys. **69**, 602 (1983).

[120] M. Doi, T. Kotani and E. Takasugi, Prog. Theor. Phys. Suppl. **83**, 1 (1985).

[121] T. Tomoda, A. Faessler, K. Schmid and F. Grummer, Nucl.Phys. **A452**, 591 (1986).

[122] H. Päs, M. Hirsch, H. Klapdor-Kleingrothaus and S. Kovalenko, Phys.Lett. **B453**, 194 (1999).

[123] A. Ali, A. Borisov and D. Zhuridov, hep-ph/0606072.

[124] A. Ali, A. V. Borisov and D. V. Zhuridov, Phys. Rev. **D76**, 093009 (2007), [0706.4165].

[125] F. Deppisch, C. Jackson, I. Nasteva and S. Soldner-Rembold, Prog.Part.Nucl.Phys. **64**, 278 (2010).

[126] S. Bilenky and S. Petcov, hep-ph/0405237.

[127] F. Deppisch and H. Päs, Phys.Rev.Lett. **98**, 232501 (2007), [hep-ph/0612165].

[128] V. Gehman and S. Elliott, J.Phys.G **G34**, 667 (2007), [hep-ph/0701099].

[129] M. Hirsch, K. Muto, T. Oda and H. Klapdor-Kleingrothaus, Z.Phys. **A347**, 151 (1994).

[130] F. Simkovic, M. Nowak, W. Kaminski, A. Raduta and A. Faessler, Phys.Rev. **C64**, 035501 (2001), [nucl-th/0107016].

[131] F. Deppisch, H. Päs and J. Suhonen, Phys. Rev. **D72**, 033012 (2005), [hep-ph/0409306].

[132] F. F. Deppisch, J. Harz and M. Hirsch, Phys.Rev.Lett. **112**, 221601 (2014), [1312.4447].

[133] F. F. Deppisch, J. Harz, M. Hirsch, W.-C. Huang and H. Päs, Phys. Rev. **D92**, 036005 (2015), [1503.04825].

[134] J. Kotila and F. Iachello, Phys. Rev. **C85**, 034316 (2012), [1209.5722].

[135] J. Barea, J. Kotila and F. Iachello, Phys. Rev. **C87**, 014315 (2013), [1301.4203].

[136] J. Barea and F. Iachello, Phys. Rev. **C79**, 044301 (2009).

[137] J. Barea, J. Kotila and F. Iachello, Phys. Rev. **C91**, 034304 (2015), [1506.08530].

[138] F. Simkovic, A. Faessler, V. Rodin, P. Vogel and J. Engel, Phys. Rev. **C77**, 045503 (2008), [0710.2055].

[139] F. Simkovic, V. Rodin, A. Faessler and P. Vogel, Phys. Rev. **C87**, 045501 (2013), [1302.1509].

[140] J. Suhonen, J. Phys. **G19**, 139 (1993).

[141] J. Suhonen, AIP Conf. Proc. **1488**, 326 (2012).

[142] E. Caurier, F. Nowacki and A. Poves, Int. J. Mod. Phys. **E16**, 552 (2007).

[143] J. Menendez, A. Poves, E. Caurier and F. Nowacki, Nucl. Phys. **A818**, 139 (2009), [0801.3760].

[144] T. R. Rodriguez and G. Martinez-Pinedo, Phys. Rev. Lett. **105**, 252503 (2010), [1008.5260].

[145] L. S. Song, J. M. Yao, P. Ring and J. Meng, Phys. Rev. **C90**, 054309 (2014), [1407.1368].

[146] P. K. Rath *et al.*, Phys. Rev. **C88**, 064322 (2013), [1308.0460].

[147] J. Engel and J. Menendez, 1610.06548.

[148] S. Dell'Oro, S. Marcocci and F. Vissani, Phys. Rev. **D90**, 033005 (2014), [1404.2616].

[149] A. de Gouvea, W.-C. Huang and J. Jenkins, Phys.Rev. **D80**, 073007 (2009), [0906.1611].

[150] B. Pontecorvo, Phys. Lett. **26B**, 630 (1968).

[151] C. Giunti and M. Laveder, Phys. Rev. **D82**, 053005 (2010), [1005.4599].

[152] C. Giunti, M. Laveder, Y. F. Li and H. W. Long, Phys. Rev. **D88**, 073008 (2013), [1308.5288].

[153] J. Barry, W. Rodejohann and H. Zhang, JHEP **07**, 091 (2011), [1105.3911].

[154] J. Barea, J. Kotila and F. Iachello, Phys. Rev. **D92**, 093001 (2015), [1509.01925].

[155] M. Blennow, E. Fernandez-Martinez, J. Lopez-Pavon and J. Menendez, JHEP **07**, 096 (2010), [1005.3240].

[156] A. Faessler, M. Gonzalez, S. Kovalenko and F. Simkovic, Phys. Rev. **D90**, 096010 (2014), [1408.6077].

[157] E. Ma, Phys. Rev. Lett. **81**, 1171 (1998), [hep-ph/9805219].

[158] M. Magg and C. Wetterich, Phys.Lett. **B94**, 61 (1980).

[159] G. Lazarides, Q. Shafi and C. Wetterich, Nucl. Phys. **B181**, 287 (1981).

[160] R. N. Mohapatra and G. Senjanović, Phys. Rev. **D23**, 165 (1981).

[161] R. Foot, H. Lew, X. G. He and G. C. Joshi, Z. Phys. **C44**, 441 (1989).

[162] E. Witten, Nucl. Phys. **B258**, 75 (1985).

[163] R. N. Mohapatra and J. W. F. Valle, Phys. Rev. **D34**, 1642 (1986).

[164] M. C. Gonzalez-Garcia and J. W. F. Valle, Phys. Lett. **B216**, 360 (1989).

[165] G. 't Hooft, NATO Sci. Ser. B **59**, 135 (1980).

[166] M. Malinsky, J. C. Romao and J. W. F. Valle, Phys. Rev. Lett. **95**, 161801 (2005).

[167] M. Hirsch and J. W. F. Valle, New J. Phys. **6**, 76 (2004), [hep-ph/0405015].

[168] A. Zee, Phys. Lett. **B93**, 389 (1980), Erratum-ibid. **B95**, 461 (1980).

[169] K. S. Babu, Phys. Lett. **B203**, 132 (1988).

[170] R. N. Mohapatra and J. C. Pati, Phys.Rev. **D11**, 566 (1975).

[171] J. C. Pati and A. Salam, Phys. Rev. **D10**, 275 (1974).

[172] R. N. Mohapatra and J. C. Pati, Phys. Rev. **D11**, 2558 (1975).

[173] G. Senjanovic and R. N. Mohapatra, Phys.Rev. **D12**, 1502 (1975).

[174] R. N. Mohapatra and G. Senjanovic, Phys.Rev. **D23**, 165 (1981).

[175] C. Arbeláez, M. Hirsch, M. Malinský and J. C. Romão, Phys. Rev. **D89**, 035002 (2014), [1311.3228].

[176] E. K. Akhmedov, M. Lindner, E. Schnapka and J. W. F. Valle, Phys. Lett. **B368**, 270 (1996), [hep-ph/9507275].

[177] E. K. Akhmedov, M. Lindner, E. Schnapka and J. W. F. Valle, Phys. Rev. **D53**, 2752 (1996), [hep-ph/9509255].

[178] F. F. Deppisch *et al.*, Phys. Rev. **D93**, 013011 (2016), [1508.05940].

[179] P. Fileviez Perez, JHEP **03**, 142 (2009), [0809.1202].

[180] H. Georgi and S. L. Glashow, Phys. Rev. Lett. **32**, 438 (1974).

[181] H. Fritzsch and P. Minkowski, Annals Phys. **93**, 193 (1975).

[182] Particle Data Group, K. A. Olive *et al.*, Chin.Phys. **C38**, 090001 (2014).

[183] Super-Kamiokande, H. Nishino *et al.*, Phys. Rev. **D85**, 112001 (2012), [1203.4030].

[184] G. 't Hooft, Nucl. Phys. **B79**, 276 (1974).

[185] A. M. Polyakov, JETP Lett. **20**, 194 (1974).

[186] T. W. B. Kibble, J. Phys. **A9**, 1387 (1976).

[187] E. Ma and G. Rajasekaran, Phys. Rev. **D64**, 113012 (2001), [hep-ph/0106291].

[188] E. Ma, Mod. Phys. Lett. **A17**, 627 (2002), [hep-ph/0203238].

[189] S. F. King and M. Malinsky, Phys. Lett. **B645**, 351 (2007), [hep-ph/0610250].

[190] S. Bertolini, L. Di Luzio and M. Malinsky, Phys. Rev. **D81**, 035015 (2010), [0912.1796].

[191] S. Bertolini, L. Di Luzio and M. Malinsky, Phys. Rev. **D87**, 085020 (2013), [1302.3401].

[192] L. Gráf, M. Malinský, T. Mede and V. Susič, Phys. Rev. **D95**, 075007 (2017), [1611.01021].

[193] F. F. Deppisch, T. E. Gonzalo and L. Graf, Phys. Rev. **D96**, 055003 (2017), [1705.05416].

[194] M.-C. Chen, TASI 2006 Lectures on Leptogenesis, in *Proceedings of Theoretical Advanced Study Institute in Elementary Particle Physics : Exploring New Frontiers Using Colliders and Neutrinos (TASI 2006): Boulder, Colorado, June 4-30, 2006*, pp. 123–176, 2007, [hep-ph/0703087].

[195] M. A. Luty, Phys. Rev. **D45**, 455 (1992).

[196] W. Buchmuller and M. Plumacher, Int. J. Mod. Phys. **A15**, 5047 (2000), [hep-ph/0007176].

[197] S. Davidson and A. Ibarra, Phys. Lett. **B535**, 25 (2002), [hep-ph/0202239].

[198] S. Davidson, E. Nardi and Y. Nir, Phys.Rept. **466**, 105 (2008), [0802.2962].

[199] L. Covi, E. Roulet and F. Vissani, Phys. Lett. **B384**, 169 (1996), [hep-ph/9605319].

[200] W. Buchmuller, P. Di Bari and M. Plumacher, Nucl. Phys. **B643**, 367 (2002), [hep-ph/0205349].

[201] V. A. Kuzmin, V. A. Rubakov and M. E. Shaposhnikov, Phys. Lett. **B155**, 36 (1985).

[202] S. Y. Khlebnikov and M. E. Shaposhnikov, Nucl. Phys. **B308**, 885 (1988).

[203] A. Pilaftsis and T. E. J. Underwood, Phys.Rev. **D72**, 113001 (2005), [hep-ph/0506107].

[204] A. Pilaftsis and T. E. J. Underwood, Nucl. Phys. **B692**, 303 (2004), [hep-ph/0309342].

[205] T. Hambye, Y. Lin, A. Notari, M. Papucci and A. Strumia, Nucl. Phys. **B695**, 169 (2004), [hep-ph/0312203].

[206] M. Dine and A. Kusenko, Rev. Mod. Phys. **76**, 1 (2003), [hep-ph/0303065].

[207] E. W. Kolb and M. S. Turner, Front. Phys. **69**, 1 (1990).

[208] M. E. Shaposhnikov, JETP Lett. **44**, 465 (1986), [Pisma Zh. Eksp. Teor. Fiz.44,364(1986)].

[209] M. E. Shaposhnikov, Nucl. Phys. **B287**, 757 (1987).

[210] D. E. Morrissey and M. J. Ramsey-Musolf, New J. Phys. **14**, 125003 (2012), [1206.2942].

[211] I. Affleck and M. Dine, Nucl. Phys. **B249**, 361 (1985).

[212] L. Graf, F. F. Deppisch, F. Iachello and J. Kotila, Phys. Rev. **D98**, 095023 (2018), [1806.06058].

[213] H. Pas, M. Hirsch, H. V. Klapdor-Kleingrothaus and S. G. Kovalenko, Phys. Lett. **B498**, 35 (2001), [hep-ph/0008182].

[214] A. de Gouvea and J. Jenkins, Phys.Rev. **D77**, 013008 (2008), [0708.1344].

[215] L. Lehman, Phys. Rev. **D90**, 125023 (2014), [1410.4193].

[216] M. L. Graesser, JHEP **08**, 099 (2017), [1606.04549].

[217] G. Prezeau, M. Ramsey-Musolf and P. Vogel, Phys.Rev. **D68**, 034016 (2003), [hep-ph/0303205].

[218] T. Tomoda, Rept. Prog. Phys. **54**, 53 (1991).

[219] M. Doi *et al.*, Phys. Theor. Phys. **66**, 1739 (1983).

[220] M. Doi *et al.*, Phys. Theor. Phys. **69**, 602 (1983).

[221] S. L. Adler *et al.*, Phys. Rev. **D11**, 3309 (1975).

[222] S. Weinberg, Phys. Rev. **112**, 1375 (1958).

[223] R. Bijker and F. Iachello, Phys. Rev. **C69**, 068201 (2004), [nucl-th/0405028].

[224] Particle Data Group, W. M. Yao *et al.*, J. Phys. **G33**, 1 (2006).

[225] M. R. Schindler and S. Scherer, Eur. Phys. J. **A32**, 429 (2007), [hep-ph/0608325].

[226] F. Simkovic, G. Pantis, J. D. Vergados and A. Faessler, Phys. Rev. **C60**, 055502 (1999), [hep-ph/9905509].

[227] V. Bernard, L. Elouadrhiri and U.-G. Meissner, J. Phys. **G28**, R1 (2002), [hep-ph/0107088].

[228] MuCap, V. A. Andreev *et al.*, Phys. Rev. Lett. **110**, 012504 (2013), [1210.6545].

[229] M. Gonzalez-Alonso, O. Naviliat-Cuncic and N. Severijns, Prog. Part. Nucl. Phys. **104**, 165 (2019), [1803.08732].

[230] L. L. Foldy and S. A. Wouthuysen, Phys. Rev. **78**, 29 (1950).

[231] M. E. Rose and R. K. Osborn, Phys. Rev. **93**, 1315 (1954).

[232] F. Iachello, private communication.

[233] E. Caurier, J. Menendez, F. Nowacki and A. Poves, Phys. Rev. Lett. **100**, 052503 (2008), [0709.2137].

[234] G. A. Miller and J. E. Spencer, Annals of Physics **100**, 562 (1976).

[235] F. Simkovic, A. Faessler, H. Muther, V. Rodin and M. Stauf, Phys. Rev. **C79**, 055501 (2009), [0902.0331].

[236] KamLAND-Zen, A. Gando *et al.*, Phys. Rev. Lett. **110**, 062502 (2013), [1211.3863].

[237] GERDA, M. Agostini *et al.*, Phys. Rev. Lett. **111**, 122503 (2013), [1307.4720].

[238] CUORE, M. Martinez, Conf. Proc. **C16-06-20.4**, 112 (2017).

[239] M. González, M. Hirsch and S. G. Kovalenko, Phys. Rev. **D93**, 013017 (2016), [1511.03945].

[240] F. F. Deppisch, L. Graf, J. Harz and W.-C. Huang, 1711.10432.

[241] K. S. Babu and C. N. Leung, Nucl. Phys. **B619**, 667 (2001), [hep-ph/0106054].

[242] G. F. Giudice, in Kane, Gordon (ed.), Pierce, Aaron (ed.): Perspectives on LHC physics, 155 (2008), [0801.2562].

[243] T. Appelquist and J. Carazzone, Phys. Rev. **D11**, 2856 (1975).

[244] K. Griest and D. Seckel, Phys. Rev. **D43**, 3191 (1991).

[245] J. Edsjo and P. Gondolo, Phys. Rev. **D56**, 1879 (1997), [hep-ph/9704361].

[246] G. F. Giudice, A. Notari, M. Raidal, A. Riotto and A. Strumia, Nucl. Phys. **B685**, 89 (2004), [hep-ph/0310123].

[247] J. A. Harvey and M. S. Turner, Phys. Rev. **D42**, 3344 (1990).

[248] A. E. Nelson and S. M. Barr, Phys.Lett. **B246**, 141 (1990).

[249] MEG Collaboration, J. Adam *et al.*, Phys.Rev.Lett. **110**, 201801 (2013), [1303.0754].

[250] S. Dimopoulos and L. J. Hall, Phys. Lett. **B207**, 210 (1988).

[251] D. Aristizabal Sierra, C. S. Fong, E. Nardi and E. Peinado, JCAP **1402**, 013 (2014), [1309.4770].

[252] A. Abada *et al.*, JHEP **09**, 010 (2006), [hep-ph/0605281].

[253] P. S. B. Dev *et al.*, Int. J. Mod. Phys. **A33**, 1842001 (2018), [1711.02861].

[254] F. Kahlhoefer, Phys. Lett. **B779**, 388 (2018), [1801.07621].